Drug discovery and antimicrobial resistance for *Mycobacterium abscessus*

Jaryd R. Sullivan

Department of Microbiology & Immunology
McGill University, Montreal
November 2022

A thesis submitted to McGill University in partial fulfillment
of the requirements for the degree of Doctor of Philosophy

ABSTRACT

Mycobacterium abscessus causes pulmonary infections in patients with impaired lung function. In particular, the prevalence of lung disease caused by *M. abscessus* is increasing among patients with cystic fibrosis. *M. abscessus* is a multidrug resistant opportunistic pathogen that is notoriously difficult to treat due to a paucity of efficacious therapeutic regimens. *M. abscessus* is clinically resistant to the front-line tuberculosis regimen of isoniazid, rifampicin, pyrazinamide, and ethambutol, which achieves cure rates of 90% or greater for drug-sensitive *M. tuberculosis*. Currently, there are no standard regimens for *M. abscessus*, and treatment guidelines are based empirically on drug susceptibility testing with cure rates of 50% or less. Thus, novel antibiotics are required.

In Chapter 2, we developed and validated a robust 96-well format assay using an engineered strain of *M. abscessus* ATCC 19977 with constitutive luminescence. We then screened a library of 517 natural products purified from fermentations of bacteria/myxobacteria, fungi, and plants. Lysobactin and sorangicin A were the most promising hits and showed activity against all subspecies in the *M. abscessus* complex as well as drug resistant clinical isolates.

In Chapter 3, we identified epetraborole as a potent inhibitor of the leucyl-tRNA synthetase (LeuRS) in *M. abscessus*. Epetraborole provided protection to zebrafish embryos from lethal *M. abscessus infection* and decreased the *M. abscessus* burden in a mouse model. We mapped epetraborole resistance to the editing domain with the LeuRS^{D436H} substitution, which prevents epetraborole from binding but enables non-cognate aminoacylation with norvaline. This translated into the incorporation of norvaline across the proteome and loss of cell viability in LeuRS^{D436H} *M. abscessus* mutants when challenged with norvaline. From these data, the adjuvant nature of norvaline with epetraborole was explored, which resulted in decreased epetraborole resistance *in vitro* and improved epetraborole efficacy *in vivo*.

In Chapter 4, spontaneous *M. abscessus* mutants resistant to both epetraborole and norvaline were raised and further characterized. We excluded modified hydrophobicity of the membrane and increased efflux activity as mechanisms for norvaline resistance in the editing-deficient mutants.

Whole-genome sequencing mapped norvaline resistance to the allosteric binding site for leucine in α-isopropylmalate synthase (α-IPMS) with the α-IPMS^{A555V} substitution. α-IPMS is an enzyme in the biosynthetic pathway for leucine with negative feedback regulation. We measured increased leucine production from the α-IPMS^{A555V} mutants that rescued growth when challenged with norvaline. We showed using whole cell assays that leucine can act as a competitive inhibitor to norvaline which prevents norvaline incorporation across the proteome and therefore, increases the viability of the mutant.

Overall, these findings support a *M. abscessus*-centric approach for drug discovery and how current drug discovery efforts can be improved through creative approaches with adjuvant-like molecules. However, the data also act as a stark reminder of the antimicrobial resistant nature of *M. abscessus* and highlight the need for increased population of the *M. abscessus* drug pipeline. These observations make important contributions to the field of drug discovery and antimicrobial resistance for *M. abscessus*.

RÉSUMÉ

Mycobacterium abscessus provoque des infections pulmonaires chez les patients dont la fonction pulmonaire est altérée. En particulier, la prévalence des maladies pulmonaires causées par *M. abscessus* augmente chez les patients atteints de mucoviscidose. *M. abscessus* est un agent pathogène opportuniste multirésistant qui est difficile à traiter en raison du manque de schémas thérapeutiques efficaces. *M. abscessus* est cliniquement résistant au traitement antituberculeux de première intention à base d'isoniazide, de rifampicine, de pyrazinamide et d'éthambutol, qui permet d'obtenir des taux de guérison de 90 % ou plus pour *M. tuberculosis* sensible aux médicaments. Actuellement, il n'y a pas de schémas thérapeutiques standard pour *M. abscessus*, et les directives de traitement sont basées empiriquement sur des tests de sensibilité aux médicaments avec des taux de guérison de 50% ou moins. Ainsi, de nouveaux antibiotiques sont nécessaires.

Dans le chapitre 2, nous avons développé et validé un test de format robuste à 96 puits à l'aide d'une souche modifiée de *M. abscessus* ATCC 19977 avec luminescence constitutive. Nous avons ensuite criblé une bibliothèque de 517 produits naturels purifiés à partir de fermentations de bactéries et de plantes. La lysobactin et la sorangicin A étaient les résultats les plus prometteurs et ont montré une activité contre toutes les sous-espèces du complexe *M. abscessus* ainsi que contre les isolats cliniques résistants aux médicaments.

Au chapitre 3, nous avons identifié l'epetraborole comme un inhibiteur de la leucyl-ARNt synthétase (LeuRS) chez *M. abscessus*. L'epetraborole a fourni une protection aux embryons de poisson zèbre contre l'infection mortelle à *M. abscessus* et a diminué la charge de *M. abscessus* dans un modèle murin. Nous avons cartographié la résistance à l'epetraborole au domaine d'édition avec la substitution LeuRS^{D436H}, qui empêche l'epetraborole de se lier mais permet une aminoacylation avec norvaline. Cela s'est traduit par l'incorporation de norvaline à travers le protéome et la perte de viabilité cellulaire chez les mutants LeuRS^{D436H} *M. abscessus* lorsqu'ils sont confrontés à la norvaline. À partir de ces données, la nature adjuvante de la norvaline avec l'epetraborole a été explorée, ce qui a diminué la résistance à l'epetraborole *en vitro* et amélioré l'efficacité de l'epetraborole *en vivo*.

Dans le chapitre 4, des mutants spontanés de *M. abscessus* résistants à l'epetraborole et à la norvaline ont été élevés et caractérisés. Nous avons exclu l'hydrophobicité modifiée de la membrane et l'augmentation de l'activité d'efflux comme mécanismes de résistance à la norvaline chez les mutants déficients en édition. Le séquençage du génome entier a cartographié la résistance de la norvaline au site de liaison allostérique de la leucine dans α-isopropylmalate synthase (α-IPMS) avec la substitution A555V. α-IPMS est une enzyme biosynthétique de la leucine avec une régulation par rétroaction négative. Nous avons mesuré l'augmentation de la production de leucine à partir des mutants α-IPMS^{A555V} qui ont sauvé la croissance lorsqu'ils ont été confrontés à la norvaline. Nous avons montré à l'aide d'essais sur cellules entières que la leucine peut agir comme un inhibiteur compétitif de la norvaline, ce qui empêche l'incorporation de la norvaline à travers le protéome et, par conséquent, augmente la viabilité du mutant.

Ces résultats soutiennent une approche centrée sur *M. abscessus* pour la découverte de médicaments et comment les efforts actuels de découverte de médicaments peuvent être améliorés avec des molécules de type adjuvant. Cependant, les données agissent également comme un rappel de la nature résistante aux antimicrobiens de *M. abscessus* et soulignent la nécessité d'augmenter la population du pipeline de médicaments de *M. abscessus*. Ces observations apportent des contributions importantes au domaine de la découverte de médicaments et de la résistance antimicrobienne pour *M. abscessus*.

ACKNOWLEDGEMENTS

Graduate school is a time for training to become a scientist through a paradigm of two contrasting mantras with independent learning as the driving force amidst a foundation of collaborators and network of support. I have many colleagues, mentors, and students to thank over the past five years.

First and foremost, I would like to thank my supervisor Dr. Marcel Behr. Thank you for taking the chance on the biochemistry undergraduate student from Winnipeg with no clear project in place. Nevertheless, two weeks into September 2017, you got the phone call from Aled Edwards asking if you wanted to set up a target engagement assay in mycobacteria. In the beginning, your hands-off approach seemed daunting but that is something I will always appreciate. You instilled a complete sense of independence from day one while always being available to discuss data on a moment's notice or envision the big picture. Your knowledge of what seems like everything has been inspiring to me and your curiosity to ask 'simple' questions is infectious. This has taught me how to ask questions in the most thought-provoking manner, which helped stimulate new ideas and experiments. I understood the moment when the infectious disease attendings and residents that work with my mother at the Health Sciences Centre in Winnipeg knew who you were that I was going to be in good hands for my graduate training. I am forever grateful for my time spent in your lab and your mentorship. I wish you many happy years of sailing in the future.

I would like to thank my advisory committee members Drs. Don Sheppard and Stéphane Laporte. Thank you for being part of my training. I really enjoyed our yearly meetings especially in years 3-5. Don—thank you for your big picture perspective and critical analysis towards the project and always ensuring I had back up plans for bold experiments. Stéphane—I have enjoyed immensely our time in the trenches discussing the details of the data.

Thank you to Dr. Michael Reed for welcoming me as your Teaching Assistant for the bacterial pathogenesis course and your mentorship the past four years. I learned a lot outside of my project area when leading the journal club discussions with you.

Thank you to all the past and present Behr lab members. Your support and friendship have meant a lot to me. Thank you for the lab lunches that bring our group together, the pub lunches—probably more than we should have had—and the picnics during the lockdown period. I would like to specifically acknowledge Dr. Andréanne Lupien—thank you for your mentorship and guidance since 2019. I would not be where I am today without your support. You were instrumental in my graduate training, and I will be forever thankful. To Sarah Danchuk—my day 1 buddy. We've grown a lot since starting in the lab together September 2017 from you thinking I was an eco-hippy to not thinking we would be friends. I am thankful to have had you as a lab mate for impromptu science discussions and I am glad to call you my friend. Thank you to Ori Solomon for our coffee/smoothie dates these past few months, they were great times to take a step away from thesis writing and chat about life. Thank you to Fiona McIntosh—you are the rock of the Behr lab. Without you the lab would fall apart. You were always there with a box of culture bottles stashed away because you knew we would forget to reorder. To Dr. Jean-Yves Dube—my "NanoBro". I enjoyed our time working together on your adaptation of the target engagement assay. You were also a big influence on me in the lab when I first started with your commitment to your project. Shannon Duffy—thank you for the memories of you quietly but politely roasting Ori throughout the day. These will not be forgotten.

I need to give a special thank you to my good friend Adam Hassan from the Ward and Ndao labs. I am glad to have attended graduate school with you. You were always available to talk science and share ideas. Our passion for tennis brought our friendship closer when we could relax on the court after a long week in the lab. Whatever the future has in store for our career paths, I will always be happy to have you as a friend and will always be ready to beat you at tennis. I wish you the best of luck in medical school and look forward to ground-breaking discoveries coming out of the Hassan lab.

To my partner and cat-mom of Luna—Lisa Hennemann. I am so fortunate that you decided to pursue graduate studies at McGill in the laboratory of Dr. Dao Nguyen rather than staying in Germany. Having you by my side has made the difficulties of graduate school much easier to handle. It was also nice having the option of venting about the failures in the lab and knowing we could sympathize with each other or to ask you if I'm using the correct statistical test. Your career

pathway may be leading you away from the bench, but I know you're going to make a great consultant with Bain & Company!

Lastly, I need to thank my parents. To my stepfather Ken—thank you for being a part of my life. Your support has meant a lot throughout the years. To my mother Denielle—I owe my biggest thanks to you. You taught me to be independent and resilient, and watching you raise me while earning your degree in nursing has been one of my biggest motivations in life. I am grateful for both of your support whether it was over Facetime or during visits back home to Winnipeg.

TABLE OF CONTENTS

LIST OF TABLES AND FIGURES

CHAPTER 1

CHAPTER 2

CHAPTER 3

CHAPTER 5

LIST OF ABBREVIATIONS

1-TbAd	1-Tuberculosinyladenosine
α-IPMS	α-Isopropylmalate synthase
aaRS	Aminoacyl tRNA synthetase
ABC	ATP-binding cassette
ADC	Albumin Dextrose Catalase
AMK	Amikacin
AMP	Adenosine monophosphate
ANOVA	Analysis of variance
ATc	Anhydrotetracycline
ATS	American Thoracic Society
BCAA	Branched chain amino acid
BGC	Biosynthetic gene cluster
Bla	β-lactamase
BRET	Bioluminescence resonance energy transfer
BSL	Biosafety level
BTS	British Thoracic Society
CARD	Comprehensive Antibiotic Resource Database
CCCP	Carbonyl cyanide 3-chlorophenylhydrazone
CE	Current era
CF	Cystic fibrosis
CFTR	Cystic fibrosis transmembrane conductance regulator
CLSI	Clinical and Laboratory Standards Institute
CRISPRi	CRISPR-interference
CYP3A4	Cytochrome P450 3A4
DHFR	Dihydrofolate reductase
DMSO	Dimethyl sulfoxide
DST	Drug susceptibility testing
Eis	Enhance intracellular survival
EPT	Epetraborole
Erm	Erythromycin ribosome methyltransferase
EV	Empty vector
FAAH	Fatty acid amide hydrolase
FAD	Flavin adenine dinucleotide
FRET	Fluorescence resonance energy transfer
GLASS	Global Antimicrobial Resistance and Use Surveillance System
GMCSF	Granulocyte-monocyte colony stimulating factor
GSK	GlaxoSmithKline
HGT	Horizontal gene transfer
HPLC-MS	High performance liquid chromatography-mass spectrometry
HTS	High-throughput screening
IFN-γ	Interferon gamma
IC	Inhibitory concentration
ITC	Isothermal titration calorimetry
IV	Intravenous
LeuRS/IleRS/ValRS	Leucyl/Isoleucyl/Valyl-tRNA synthetase

LYB	Lysobactin
MABSC	*Mycobacterium abscessus* complex
MAC	*Mycobacterium avium* complex
MATE	Multidrug and toxic-compound extrusion
MDR-TB	Multidrug resistant tuberculosis
MFS	Major facilitator superfamily
MIC	Minimum inhibitory concentration
MmpL	Mycobacterial membrane protein large
MMV	Medicines for Malaria Venture
MRC	Medical Research Council
MTBC	*Mycobacterium tuberculosis* complex
Nluc	Nano luciferase
NO	Nitric oxide
NOD	Non-obese diabetic
NOS/iNOS	Nitric oxide synthase (inducible)
NRPS	Nonribosomal peptide synthase
NTM	Nontuberculous mycobacteria
OADC	Oleic acid Albumin Dextrose Catalase
OBORT	Oxaborole tRNA trapping
PARP	Poly (ADP-ribose) polymerase
PK	Pharmacokinetics
PKS	Polyketide synthase
POC	Proof of concept
PMF	Proton motive force
PROSPECT	Primary screening of strains to prioritize expanded chemistry and targets
REMA	Resazurin microtiter assay
RGM	Rapidly growing mycobacteria
RIF	Rifampicin
RiPP	Ribosomally synthesized and post translationally modified peptide
RFB	Rifabutin
RNAP	RNA polymerase
RND	Resistance nodulation cell division
ROS	Reactive oxygen species
RpoB	RNA polymerase subunit β
SAR	Structure activity relationship
SCID	Severe combined immunodeficient
SDDC	Structure-guided Drug Discovery Coalition
SGM	Slowly growing mycobacteria
SMR	Small multidrug resistance
SNP	Single nucleotide polymorphism
SOR	Sorangicin A
SSTI	Skin and soft tissue infection
TB	Tuberculosis
Tn-Seq	Transposon sequencing
TMP	Trimethoprim
VAN	Vancomycin

WCS	Whole cell screening
WGS	Whole-genome sequencing
WHO	World Health Organization
XDR-TB	Extreme drug resistant tuberculosis
zTB	Zoonotic tuberculosis

CONTRIBUTIONS OF AUTHORS

The candidate is presenting a manuscript-based thesis with three original manuscripts and is in accordance with the guidelines for thesis preparation provided by the Faculty of Graduate and Postdoctoral Studies of McGill University. The candidate, Jaryd Sullivan, is recognized as the principal author and to have performed the majority of the work presented. The specific contributions of authors are as follows:

CHAPTER 1

The introduction and literature review were written by Jaryd Sullivan and edited by Marcel Behr.

CHAPTER 2

Sullivan JR, Yao J, Courtine C, Lupien A, Herrmann J, Müller R, Behr MA. Lysobactin and sorangicin A show *in vitro* activity against *Mycobacterium abscessus* complex. *Microbiol Spectr*. **2022**, e02672-22.

This manuscript was reprinted from the journal *Microbiology Spectrum* with permissions granted by the Creative Commons Attribution (CC BY) license. JRS was involved in all aspects including experiment design, data collection and analysis, and preparation of the manuscript. JY conducted drug susceptibility testing on the clinical isolates. CC performed independent replicates of the assay validation. AL provided supervision to JY. JH and RM provided the natural product libraries. MAB supervised all experiments and was involved in the preparation of the manuscript.

CHAPTER 3

Sullivan JR, Lupien A, Kalthoff E, Hamela C, Taylor L, Munro KA, Schmeing TM, Kremer L, Behr MA. Efficacy of epetraborole against *Mycobacterium abscessus* is increased with norvaline. *PLoS Pathog*. **2021**, 17(10):e1009965.

This manuscript was reprinted from the journal PLoS Pathogens with permissions granted by the CC BY license. JRS was involved in all aspects including experiment design, data collection and analysis, and preparation of the manuscript. AL provided training to JRS and conducted experiments in the containment level 3. EK collected the crystallography data. CH performed the

zebrafish work. LT collected the proteomics data. KAM collected isothermal titration calorimetry data. TMS provided supervision to EK. LK provided supervision to CH. MAB provided supervision to JRS and was involved in the preparation of the manuscript.

CHAPTER 4

Sullivan JR, Courtine C, Taylor L, Solomon O, Behr MA. Loss of allosteric regulation of α-isopropylmalate synthase is identified as an antimicrobial resistance mechanism. *Manuscript under revisions* at npj Antimicrobials & Resistance.

JRS was involved in all aspects including experiment design, data collection and analysis, and preparation of the manuscript. CC independently the generated double mutants and provided replicates of the Congo red and efflux assays. LT collected proteomics and metabolomics data. OS created a pipeline for variant calling on whole-genome sequencing data. MAB provided supervision and was involved in the preparation of the manuscript.

CHAPTER 5

The discussion was written by Jaryd Sullivan and edited by Marcel Behr.

Figure 5.3 was reprinted from the following manuscript:
Fanti RC, Vasconcelos SNS, Catta-Preta CMC, **Sullivan JR**, Riboldi GP, dos Reis CV, Ramos PZ, Edwards AM, Behr MA, Couñago RM. A Target Engagement Assay to Assess Uptake, Potency, and Retention of Antibiotics in Living Bacteria. *ACS Infect Dis*. **2022**, 8, 1449-1467.

Figures 5.1-2, 5.4-5 are unpublished.

CONTRIBUTIONS TO ORIGINAL KNOWLEDGE

The data presented in this thesis in the format of two published manuscripts and one unpublished manuscript contributes original knowledge to the fields of drug discovery and antimicrobial resistance of *Mycobacterium abscessus*. The specific contributions are the following:

In **Chapter 2**, we engineered a strain of *M. abscessus* suitable for whole cell screening and identified lysobactin and sorangicin A as two natural products with *in vitro* activity against *M. abscessus*. We demonstrated that:

1. Luminescence is a robust readout as a proxy for bacterial burden.
2. Natural products continue to be valuable sources of antimicrobial compounds.
3. The lysobactin and sorangicin A scaffolds have whole cell activity against the *M. abscessus* complex.
4. Multidrug resistant *M. abscessus* clinical isolates remain susceptible to lysobactin and sorangicin A.

In **Chapter 3**, we identified epetraborole as a potent inhibitor against *M. abscessus* targeting LeuRS and showed that norvaline could act as an adjuvant-like molecule in combination with epetraborole. We demonstrated that:

1. Repurposed antimicrobials can be just as valuable as natural products (Natural product hit rate: 0.4%, Repurposed hit rate: 0.4%).
2. Epetraborole protected zebrafish from lethal *M. abscessus* infection and decreased the bacterial burden of *M. abscessus* in a murine model.
3. *M. abscessus* mutants resistant to epetraborole developed sensitivity to misaminoacylation with norvaline.
4. Norvaline can potentiate the efficacy of epetraborole and limit the emergence of resistance.

In **Chapter 4**, we characterised the mechanism of resistance to norvaline in *M. abscessus* in the absence of the natural editing activity of LeuRS. We demonstrated that:

1. *M. abscessus* mutants resistant to epetraborole readily develop resistance to norvaline when grown in liquid culture.
2. Modified membrane hydrophobicity and increased efflux pump activity do not mediate norvaline resistance.
3. Mutants resistant to both epetraborole and norvaline acquired a mutation in the allosteric binding site of leucine on the enzyme α-IPMS.
4. The mutation in the allosteric site leads to increased leucine production from the loss of negative feedback inhibition.
5. Leucine can outcompete norvaline as a substrate for LeuRS and limit toxic norvaline misaminoacylation.

Taken together, the data in this thesis has shown that natural products and repurposed antimicrobial libraries are valuable starting points for drug discovery against *M. abscessus* while also demonstrating the potential of unconventional combinations of molecules and highlighting the antimicrobial resistant nature of *M. abscessus*. Our drug discovery efforts have contributed compounds to the *M. abscessus* pipeline that could serve as future lead compounds for the development of effective antimicrobials for the treatment of *M. abscessus* infections.

CHAPTER 1

Literature Review & Research Objectives

1.1 MYCOBACTERIA

Mycobacteria are a diverse group of bacteria most known for causing tuberculous diseases from species belonging to the *Mycobacterium tuberculosis* complex (MTBC). However, there are non-tuberculous mycobacteria (NTM) that cause non-tuberculous disease. Unlike the MTBC which includes 13 species, NTM make up the largest diversity in the *Mycobacterium* genus with nearly 200 species identified by modern molecular techniques like 16S rRNA-sequencing and whole-genome sequencing (WGS) that have supplanted traditional semi-quantitative biochemical testing (**FIGURE 1.1**).[1,2]

1.1.1 *Mycobacterium tuberculosis* Complex

The MTBC is a group of clonally related (99.9% nucleotide identity) lineages that are pathogenic to a variety of mammalian hosts. The ancestral root of the MTBC is believed to be the smooth tubercle bacillus *M. canettii* (97.3% nucleotide identity), which is a facultative pathogen with an environmental reservoir according to epidemiological evidence.[3] The MTBC are grouped into seven human-adapted lineages and several animal-adapted lineages. Human-adapted lineages include *M. tuberculosis sensu strictu* Lineages 1-4, Lineage 7, and *M. africanum* Lineages 5 and 6. These lineages have distinct geographical patterns where Lineage 7 is exclusively in Ethiopia and Lineages 5 and 6 are restricted to West Africa, Lineages 1 and 3 show an intermediate distribution in Oceania and Central Asia while Lineages 2 (East Asian) and 4 (Euro-American) are distributed globally.[4–6]

Animal-adapted lineages are defined as not completing infection-transmission cycles in humans.[4,7] Such species include *M. bovis*, *M. orygis, M. microti*, *M. caprae*, *M. pinnipedii*, *M. mungi*, *M. suricattae*, and the dassie bacillus; these have been found in a variety of animals like cattle, voles, shrews, goats, seals, mongooses, meerkats and hyraxes.[3,8] There is significant concern regarding bovine tuberculosis (TB) for agricultural purposes but also as a proxy for measuring zoonotic

tuberculosis (zTB) in human populations. The goal of the World Health Organization (WHO) is to reduce the incidence of TB by 90% by the year 2035.[9] As such, the estimated 143 000 cases of human TB due to zTB would need to be reduced.[10] However, the definition of zTB as human infection with *M. bovis* was recently challenged and shown to be inadequate. In fact, in India, the country with the highest population of cattle, *M. orygis* was more frequently recovered than *M. bovis* from patients suspected of having TB.[11] These results urged the WHO to modify their definition of zTB to gain a more accurate estimate of zTB.

1.1.2 *Mycobacterium leprae*

M. leprae is unique among the species of mycobacteria as it is neither classified as a member of the MTBC nor as an NTM.[2] *M. leprae* is the causative agent of leprosy, or Hansen's disease, one of the oldest recorded diseases and is characterized by its unusually slow doubling time. In fact, the *M. leprae* bacillus cannot be cultured under standard laboratory conditions and requires culture in the footpad of the naturally infected nine-banded armadillo as a surrogate host where it undergoes a doubling time of 14 days.[12,13] Until the recent discovery of a methanotrophic species of mycobacteria from a biofilm with a pH of 1 in a volcanic cave that has a doubling time of 150-200 days, *M. leprae* had the longest doubling time of all known mycobacteria, which could be explained by the loss of genomic content in the genome of *M. leprae* (3.27 Mb) compared to *M. tuberculosis* (4.41 Mb).[13,14] The loss of genes and abundance of pseudogenes with intact counterparts in *M. tuberculosis* has been hypothesized to result in impaired metabolic pathways and reliance on the host metabolism for growth as an obligate intracellular parasite.[13,15]

1.1.3 Nontuberculous Mycobacteria

Other than the MTBC and *M. leprae*, all other mycobacteria are classified as NTM.[1] NTM are environmental bacteria that present as opportunistic pathogens incapable of host-to-host transmission. This contrasts to the MTBC that do not have an environmental reservoir and are transmitted exclusively between hosts as professional pathogens. In the pre-molecular era, Runyon classified NTM into four groups based on two attributes.[16] First, NTM are divided into slowly growing (SGM) and rapidly growing mycobacteria (RGM), the latter defined by whether colonies are formed before or after 7 days on solid media. Second, the SGM can be further described according to their pigmentation. Group 1 SGM are photochromogenic and become pigmented

when exposed to light, group 2 are scotochromogenic and are always pigmented, and group 3 are never or weakly pigmented.[16] Group 4 includes the RGM.

With the advent of molecular typing techniques, the number of validated *Mycobacterium* species quadrupled from 15 in the 1980's to 61 by the late 1990's. This was largely attributed to the seminal work by Carl Woese who first demonstrated the utility of phylogenetic analyses using the 16S rRNA gene.[1,17] Although 16S rRNA phylogenetics provides speciation across NTM, many NTM share nearly identical 16S rRNA sequences. Therefore, a shift from ribosomal genes to more rapidly evolving housekeeping genes like *hsp65*, encoding the 65-kDa heat shock protein is required for species discrimination. This is pertinent in hospital clinical microbiology and research laboratories where accurate speciation is required for diagnosis or culture work.

Now with WGS routinely available, over 200 species of NTM have been described. Although the majority are saprophytic, soil and water-dwelling bacteria, some species are known to cause disease in hosts ranging from humans to fish or have relevance for research purposes.[18]

The SGM *Mycobacterium avium* complex (MAC) is comprised of 12 species with certain species, such as *M. avium* more clinically relevant than others.[19] *M. intracellulare* is isolated from patients with pulmonary disease; and *M. chimaera* was recently found to be the agent responsible of a global outbreak of prosthetic valve endocarditis infections from contaminated heater-cooler units during cardiac surgery.[20–22] Within *M. avium*, there are subspecies with different reservoirs and pathogenicity. *M. avium* subsp. *avium* causes avian TB; *M. avium* subsp. *paratuberculosis* is the causative agent of Johne's disease in cattle and may have a link to Crohn's disease; *M. avium* subsp. *hominissuis* is prevalent in the cystic fibrosis (CF) community and was the cause of disseminated *M. avium* infections in patients with AIDS during the 1990s epidemic.

M. marinum is another SGM that causes tuberculous-like infections in aquatic animals and skin lesions in humans that have a close contact history of handling fish.[23] *M. marinum* is also used known as a model organism for studying host-pathogen interactions in the zebrafish (*Danio rerio*) model of TB.[24] Zebrafish are naturally susceptible to *M. marinum* infection and amenable to genetic perturbations. Additionally, zebrafish embryos are translucent making them suitable for

microscopy. Because they lack an adaptive immune system, they are used to study the early immune response following mycobacterial infection.[25–27]

M. marinum and *M. ulcerans* are genetically similar yet distinct in the diseases they cause and their epidemiology.[1] *M. ulcerans* is the causative agent of Buruli ulcer and is endemic to Western and Central Africa and regions in Australia.[28,29] Despite its genomic reduction of nearly 1 Mb of genomic material, one key feature that makes *M. ulcerans* unique in the *Mycobacterium* genus is the production of a plasmid encoded toxin.[1] This polyketide mycolactone molecule is thought to have immunosuppressive activity and to be instrumental in its pathogenesis.[30]

M. kansasii is an opportunistic pathogen that can cause lung disease in some immunocompromised individuals or people with underlying conditions like chronic obstructive pulmonary disease and silicosis.[31,32] Like *M. marinum*, recent literature on *M. kansasii* suggests its utility as a research tool to study the stepwise evolution of *M. tuberculosis*. Phylogenetic analyses of horizontal gene transfer (HGT) events predicted *M. kansasii* to be the nearest neighbour to the MTBC.[33] This study hypothesized that the *M. kansasii*-MTBC common ancestor acquired genes through HGT to become a more virulent, professional pathogen as opposed to an opportunistic pathogen. With the *M. kansasii* whole-genome sequenced, it was shown that the heterologous production of 1-tuberculosinyladenosine (1-TbAd) in *M. kansasii* from the *M. tuberculosis* operon resulted in an increased virulent phenotype in macrophages and mice.[34,35]

Of the clinically relevant RGM, *M. abscessus* is the most formidable. *M. abscessus* is second to MAC in frequency of clinical isolates but causes notoriously difficult-to-treat pulmonary infections in patients with CF and skin and soft tissue infections (SSTI) .[36] *M. abscessus* is one of the most antimicrobial resistant mycobacteria and is recalcitrant to the frontline antimicrobials used for *M. tuberculosis* infections.[37,38] This has sparked interest for new drug discovery efforts not only from an unmet clinical need but also from a basic science perspective, to uncover new mechanisms of antimicrobial resistance. Phylogenetic analyses cluster *M. abscessus* near the outgroup of the *Mycobacterium* tree which has generated debate as to whether it should be classified under its own genus. In fact, it was recently proposed to revise the *Mycobacterium* genus to better reflect the genetic and biological diversity (*Mycobacterium*, *Mycolicibacterium*,

Mycolicibacter, *Mycolicibacillus*, and *Mycobacteroides*) where *M. abscessus* is the sole bacterium in the genus *Mycobacteroides*.[39] However, traditional NCBI nomenclature using *Mycobacterium* has maintained its dominance.

M. smegmatis may not be clinically relevant but it has become established as one of the most well-known names in the *Mycobacterium* genus. *M. smegmatis* is the model organism in mycobacteria research as *Escherichia coli* (*E. coli*) is to the Gram positive/negative world.[40,41] Features that make *M. smegmatis* an attractive model to study *M. tuberculosis* include: 1) growth rate (3 hour doubling for *M. smegmatis* vs 18-24 hour doubling for *M. tuberculosis*), 2) biosafety level (BSL1-2 depending on the country for *M. smegmatis* vs BSL-3 for *M. tuberculosis* which requires a dedicated facility and staff), 3) genetic tractability and protocols available for *M. smegmatis*. Nevertheless, as with all model systems, data obtained using *M. smegmatis* must be interpreted with caution and the translation of knowledge onto *M. tuberculosis* is not straightforward nor guaranteed.

1.2 MYCOBACTERIUM ABSCESSUS COMPLEX

1.2.1 Brief History

M. abscessus is the most commonly encountered pathogenic RGM in clinical medicine where it causes pulmonary and extrapulmonary disease.[36] *M. abscessus* was first isolated in 1953 from a knee abscess after a traumatic knee injury.[42] The abscess-like lesions and tuberculoid structure earned it a new species, *Mycobacterium abscessus*. Then in 1972, *M. abscessus* lost its designation as a separate taxon when a consortium of investigators proposed that *M. abscessus* and *M. chelonae* be merged into a complex, the *M. chelonae* complex, based on a series of semi-quantitative clinical tests.[43] However, DNA hybridization experiments in 1986 and 1992 showed different annealing patterns and thus restored the status of *Mycobacterium abscessus*.[44,45]

Recent phylogenetic analyses from WGS show *M. abscessus* as a distinct clade in the *Mycobacterium* genus.[2,34,39,46] This has fueled debate as to whether *M. abscessus* should be in its own genus—most notably with the recent NCBI nomenclature amendment with *Mycobacteroides abscessus*.[39] Nevertheless, this species can be further classified into three subspecies: *M. abscessus* subsp. *abscessus*, *M. abscessus* subsp. *massiliense*, and *M. abscessus* subsp. *bolletii* to create the

M. abscessus complex (MABSC).[2,47–50] Unlike the clonal MTBC, *M. abscessus* displays a high degree of genotypic heterogeneity among the MABSC, which could be explained by its environmental reservoirs as opposed to the host-associated MTBC.[51]

1.2.2 Disease Epidemiology

The prevalence of pulmonary NTM infections is increasing worldwide with an estimated NTM disease prevalence of 1.8/100,000 in 1987 and 5 to 10/100,000 between 2006 and 2012.[52–55] However, formal epidemiological evaluation of this apparent increase in NTM prevalence had been missing until 2013 with recent updates in 2022.[54,55] Defining the epidemiology of pulmonary NTM disease is more challenging than with *M. tuberculosis* for several reasons. 1) NTM infections are thought to be acquired from their environmental soil and water sources rather than transmitted from person-to-person as is the case with *M. tuberculosis*.[54,56] Studies have identified NTM from swimming pools, hot tubs, and hot water tanks heated above 130 °F. MAC was found in nearly one third of showerheads sampled in the United States with matched isolate pairs to patient respiratory cultures, suggesting household acquisition.[57] 2) Due to their ubiquitous presence in soil and municipal water systems, exposure to NTM is likely common. Therefore, the presence of NTM in respiratory secretions may be from transient or asymptomatic colonization and might not necessarily indicate NTM pulmonary disease.[54] 3) Public health authorities in most countries do not require reporting of NTM disease unlike the global surveillance networks for *M. tuberculosis*.[54,58]

Indeed, the reporting of NTM pulmonary disease can vary based on the geographic region. One study from Ontario, Canada reported an NTM isolation prevalence of 9.1-14.1/100,000 from 1997-2003 while during a similar time period the prevalence of NTM isolation was 0.9-2.9/100,000 in regions of the United Kingdom.[59,60] These studies reflect the diversity in people colonized with NTM but do not shed light on NTM pulmonary disease.

NTM disease prevalence has been estimated across the globe. Taiwan and Australia reported a prevalence of 1.3-7.9/100,000 from 2000-2008 and 2.2-3.3/100,000 from 1999-2005, respectively.[61,62] Data from the United States is also available with NTM disease prevalence of 8.6/100,000 from 2005-2006 in Oregon, 4.1/100,000 from 2000-2008 in California, 5.5/100,000

from 2004-2006 in a multi-region study of California, Colorado, Pennsylvania, and Washington, and 47/100,00 from 1997-2007 across the United States (study population was limited to patients ≥ 65 years old).[60,63–66] NTM disease prevalence is variable across geographic regions but is increased in elderly populations. From 2008-2013 in the United States, one study reported the highest prevalence of NTM cases in the 80+ year age group, followed by the 50-80 year age group and 0-49 year age group.[67]

Globally, the prevalence of MABSC pulmonary infections is second to MAC pulmonary infections. However, the distribution of MABSC can vary across countries. In the United states, up to 13% of mycobacterial pulmonary infections are caused by MABSC while in Taiwan it can be as high as 17.2%.[68] Other studies reported up to 16% of NTM isolates were MABSC in Asia, 12% in Oceania, 5.7% in South America, 3.2% in North America and 2.9% in Europe.[69,70] Of the three subspecies in MABSC, *M. abscessus* subsp. *abscessus* is most commonly isolated, followed by *M. abscessus* subsp. *massiliense*. *M. abscessus* subsp. *bolletii* is rarely isolated (< 5% of all MABSC isolates) except for regions in France and the Netherlands where it can be found in up to 18% of MABSC isolates.[71,72]

Like MAC, household water sources could be reservoirs for MABSC infections. MABSC was shown to resist levels of chlorine typically used in water treatment facilities.[73,74] MABSC is also resistant to organic-mercurial disinfectants with its mercury-metabolising plasmid and alkaline glutaraldehyde disinfectants, possibly from the formation of biofilms.[52,75,76]

1.2.3 Clinical Aspects

NTM are ubiquitous in the environment with ecological niches of soil, and natural and engineered water supplies. Yet, relative to their abundance, NTM disease is uncommon. Therefore, it is unclear whether exposure is sufficient to cause disease. Specifically, *M. abscessus* is known to cause pulmonary, skin and soft tissue, and ocular infections.[77,78] The most common clinical presentation of MABSC infections is pulmonary disease in patients with CF, chronic lung disease, or undergoing lung transplantation.[38] Although MAC is known to be the most frequently isolated NTM from patients with CF, *M. abscessus* is becoming more common in some CF centres.[79–82]

Unlike MAC that has a higher prevalence in patients over 25 years of age, *M. abscessus* causes infections in all age groups.[83]

CF is an autosomal recessive multiorgan disorder characterized by a dysfunctional CF transmembrane conductance regulator (CFTR).[84] CFTR functions to transport chloride and bicarbonate ions across the apical surface of epithelia. In the lungs, chloride ions function to create an electrochemical gradient for sodium ion transport, followed by hydration of the mucosal surface powered by the sodium-water osmotic gradient, which is essential for proper ciliary function and antimicrobial activity. Defects in CFTR, including the ΔF508 mutation, among others, create a dehydrated airway surface which leads to mucopurulent secretions, impaired mucociliary clearance, and chronic infections.[84,85]

The importance of CFTR for *M. abscessus* infection has previously been explored in the context of zebrafish infections.[86] Like *M. marinum*, the zebrafish model has been adapted for *M. abscessus* host-pathogen interactions.[87,88] Larvae with knocked down *CFTR* showed decreased survival with enhanced proliferation and dissemination of *M. abscessus*. Although infections in CF patients are largely thought to be the result of impaired mucociliary clearance, the zebrafish evidence suggests a role for CFTR in reactive oxygen species (ROS) production to modulate bactericidal functions in macrophages and proper granuloma formation for *M. abscessus* while having no effect on infection by other NTM like *M. marinum* or *M. smegmatis*.[86]

Many CF patients undergo therapy with small molecule drugs termed CFTR modulators.[85] CFTR modulators can either improve the function of CFTR previously localized at the cell surface or assist in trafficking CFTR to the cell surface.[84] Potentiators and correctors, respectively, are powerful tools in the treatment of CF disease. However, one of the most common correctors, ivacaftor, is a substrate for the drug detoxifying enzyme cytochrome P450 3A4 (CYP3A4).[89] This poses challenges for *M. abscessus* drug discovery efforts, for example, new data suggests that clinically inactive rifampicin could be replaced with rifabutin for the treatment of *M. abscessus*, however rifamycins are known to be inducers of CYP3A4.[90,91]

1.2.4 Diagnostics

Diagnosing pulmonary *M. abscessus* disease is not trivial. Isolating *M. abscessus* from nonsterile sites like sputum does not automatically indicate disease. Pulmonary *M. abscessus* disease is diagnosed with evidence from clinical symptoms, radiographic findings, and isolation of *M. abscessus* from multiple specimens. Many of the symptoms of pulmonary NTM disease are similar to pulmonary *M. tuberculosis* infection, which can often lead to a mistaken diagnosis of TB.[92] In fact, NTM pulmonary disease is often mistaken as multidrug-resistant tuberculosis (MDR-TB) in TB-endemic areas and leads to the erroneous treatment of MDR-TB.[52,93]

1) *M. abscessus* pulmonary disease is often associated with cough, sputum production, hemoptysis, and dyspnea, and patients can experience weight loss and fever.[92] 2) Chest radiographs and computed tomography can reveal any lung cavities. 3) *M. abscessus* must be isolated from at least two separate sputum samples or one bronchial lavage. If all 3 criteria are met, the pulmonary isolate is sent for identification using 16S rRNA sequencing to distinguish MTBC vs NTM. This is followed by another molecular typing method like *hsp65* sequencing to differentiate *M. abscessus* from the closely related *M. chelonae* and determine the subspecies (*abscessus*, *massiliense*, *bolletii*).

Once the subspecies of *M. abscessus* is identified, the isolate is sent for drug susceptibility testing (DST) using the Clinical and Laboratory Standards Institute (CLSI) guidelines. RGM undergo DST using the microbroth dilution technique.[94]

1.2.5 Treatment

M. abscessus is known to cause pulmonary disease and SSTI, however, only guidelines for pulmonary disease are available. The British and American Thoracic Societies and the Canadian Tuberculosis Standards created overlapping recommendations where the biggest contrasts are with the exact number of antibiotics and length of duration.[92,95,96] The US Cystic Fibrosis Foundation and European Cystic Fibrosis Society have consensus recommendations for the management of pulmonary *M. abscessus* infections for patients with CF.[81] Because the treatment benefit/risk ratio for *M. abscessus* is poorer than for *M. tuberculosis*, treatment is performed on an individual case-

by-case basis.[92] The treatment of *M. abscessus* is difficult with its notoriously drug resistant phenotypes. *M. abscessus* is intrinsically resistant to most antitubercular agents used to treat TB.

The treatment for *M. abscessus* pulmonary disease is a long and arduous multi-drug regimen with a combination of oral and parenteral agents. Treatment regimens are designed around a macrolide backbone due to the potent activity measured *in vitro*. Although no studies have compared macrolide-containing versus macrolide-deficient regimens, numerous studies compared treatment outcomes in patients with *M. abscessus* subsp. *abscessus* or *massiliense* infections. Culture conversion ranged between 25-42% for *M. abscessus* subsp. *abscessus* and 50-96% for *massiliense*.[95] The difference in culture conversion and positive outcome was attributed to the presence of inducible macrolide resistance in *M. abscessus* subsp. *abscessus* that is missing in *M. abscessus* subsp. *massiliense*.[97] The culture conversion differences underscore the benefit of macrolides in *M. abscessus* pulmonary disease management and identifying the correct subspecies.

Treatment regimens are divided into initial and continuation phases. The British Thoracic Society (BTS) recommends an initial 4-week minimum course of intravenous amikacin, tigecycline, and imipenem, and an oral macrolide like azithromycin or clarithromycin. An antiemetic is recommended to limit the tigecycline/imipenem-induced nausea. As 3 times weekly dosing of IV amikacin can be impractical if the patient does not live near a medical centre or if IV amikacin interacts with other medications, nebulized amikacin can be used as a substitute.[98] The American Thoracic Society (ATS) recommends 2 to 5 drugs in the initial phase due to a lack of consensus among physicians.[99] If the isolate was shown to be macrolide resistant either through inducible or mutational resistance, the intravenous agents are used without a macrolide. However, the ATS recommends the continued use of azithromycin even when the isolate is macrolide resistant as it has been shown to have immunomodulatory activity.[100,101]

The BTS and ATS recommend an all-oral regimen for the 12-month-minimum continuation phase of therapy. If the isolate is macrolide sensitive, the regimen should include azithromycin or clarithromycin, nebulized amikacin, and 1 to 3 oral antibiotics (clofazimine, linezolid, moxifloxacin, doxycycline) guided by DST of the patient isolate. When isolates are macrolide resistant, patients are given 2 to 4 oral antibiotics with nebulized amikacin.

For individuals with CF and a pulmonary *M. abscessus* infection, treatment regimens are similar to non-CF patients but with an extended duration (**FIGURE 1.2**).[81] The US Cystic Fibrosis and European Cystic Fibrosis Society recommend a 3-month initial phase of IV amikacin, tigecycline, and imipenem, and oral azithromycin. Because IV amikacin is given for three months and is known to cause ototoxicity, monthly audiometry consults are required. Following this intensive phase, depending on the severity of the infection and the tolerability of the regimen, patients continue with the oral macrolide and substitute the injectable agents with all oral clofazimine, minocycline, moxifloxacin, and nebulized amikacin for 14 months.

1.3 DRUG RESISTANCE

Antibiotic resistance in mycobacteria has been known since the early clinical trials carried out by the Medical Research Council (MRC) for tuberculosis in 1946.[102] Investigators used intramuscular injection of streptomycin to treat pulmonary TB in 55 patients with 52 patients in the control group. Although some patients receiving streptomycin treatment showed improvement, isolates resistant to streptomycin could be recovered by the end of the second month of treatment. Of the 35 patients with strains for which the minimum inhibitory concentration (MIC) was > 10x higher than the reference strain, 13 patients had strains with an MIC 2,000x higher than the reference strain. The magnitude of streptomycin resistance had a statistically significant effect on treatment outcome and led to patient deterioration and even death. The streptomycin MRC trial was one of the first studies to highlight the antibiotic resistant nature of *M. tuberculosis* despite, two years previously, streptomycin showing potent *in vitro* activity against *M. tuberculosis* and having success in treating TB in an experimental guinea pig model. Overall, the investigators concluded that monotherapy should not be considered for mycobacterial infections due to the lengthy treatment durations and high rates of resistance. The adoption of combination therapy for most mycobacterial infections was largely influenced by this study.

Guidelines from the ATS, BTS, and the US and European CF Societies recommend combination therapy for *M. abscessus* pulmonary infections due to its drug resistant nature. The four-drug combination therapy of isoniazid, rifampicin, pyrazinamide, and ethambutol for drug-sensitive TB that typically achieves cure rates greater than 90% in six months is clinically inactive against *M.*

abscessus. Now termed the "new antibiotic nightmare", *M. abscessus* is resistant to most clinically useful antimycobacterial agents through a variety of intrinsic, inducible, and acquired resistance mechanisms (**FIGURE 1.3**).[37] Recently it has been shown that in addition to genotypic resistance, *M. abscessus* can also evade chemotherapeutic insult through the formation of persisters.[103] Under laboratory conditions such as low nutrient and microaerophilic environments, *M. abscessus* can form non-replicating persisters and biofilms that can withstand drug treatment. These assays could be valuable in the drug discovery assay gap, but the *in vivo* relevance remains to be determined. Today, cure rates for *M. abscessus* are on par with extreme drug-resistant *M. tuberculosis*, arguing that *M. abscessus* is one of the most antibiotic resistant bacteria.[104]

1.3.1 Intrinsic Resistance

Bacteria can often become resistant to antibiotics from *de novo* mutations or the acquisition of new genes once the antibiotic is prescribed to the patient. Besides chromosomal mutations and horizontal gene transfer, many bacteria possess an array of intrinsic mechanisms that dampen or neutralize the effect of antibiotics. For *M. abscessus* and other mycobacteria, the list includes a uniquely hydrophobic cell wall, porin channels and efflux pumps, enzymes that can modify or degrade antibiotics, and enzymes that modify the antibiotic target.[51,105]

1.3.1.1 Mycomembrane

Peptidoglycan is often used as a defining feature of bacterial cell walls. Unlike Gram-positive bacteria with cell walls largely produced of peptidoglycan or Gram-negative bacteria with cell walls that contain outer membranes, mycobacteria produce a unique cell wall. For most bacteria, peptidoglycan is composed of repeating N-acetylglucosamine-(1→4)-N-acetylmuramic acid units that are crosslinked via a pentapeptide bridge, but mycobacteria produce peptidoglycan with N-glycolylmuramic acid residues.[106] Although it is unclear as to why mycobacteria N-glycolylate their peptidoglycan, it has been speculated that N-glycolyl could strengthen the peptidoglycan structure with additional hydrogen bonding.[106] In addition to peptidoglycan, mycobacteria produce the polysaccharide arabinogalactan. The layer of arabinogalactan acts as a scaffold for covalent attachment of long-chain fatty acids termed mycolic acids.[107] The arabinosyl transferase, EmbB, responsible for the polymerization of arabinogalactan became an important front-line antitubercular target for the treatment of tuberculosis when ethambutol was shown to inhibit the

growth of *M. tuberculosis* via arabinogalactan polymerization. However, amino acid variants in the ethambutol-resistance determining region of the target gene *embB* preclude the activity of ethambutol against *M. abscessus*.[108,109]

Mycobacterial mycolic acids are high molecular weight α-alkyl, β-hydroxy fatty acids that can be esterified to the arabinogalactan layer or in the extractable form as trehalose dimycolate. Mycolic acids are not unique to mycobacteria but are distinguishable from other genera like *Corynebacterium*, *Nocardia*, and *Rhodococcus*.[106] Namely, mycobacterial mycolic acids are the largest with 70-90 carbon units in length and a 20-25 carbon unit α-branch. This inner leaflet is predicted to be in a near-crystalline state and have low fluidity due to the length of the mycolic acids.[107] To compensate for the low fluidity of the mycomembrane, double bonds and cyclopropane rings in the *cis* conformation are introduced near the arabinogalactan end of the mycolic acid to produce kinks and modulate the tight lipid packing. Mycolic acids have been a topic of mycobacterial drug discovery since the identification of the drug isoniazid (INH) in 1958.[110,111] INH has excellent *in vitro* and *in vivo* activity against *M. tuberculosis* and was shown to be far superior to other drugs used at that time such as streptomycin and *para*-aminosalicylic acid.[111,112] The mechanistic details took some time before being solved. It was shown that INH was a pro-drug that required activation by the catalase-peroxidase KatG present in mycobacteria.[113] The cellular target of activated INH proved to be controversially as there was evidence to support KasA and InhA as targets, both being part of the fatty acid synthase type II system required for mycolic acid synthesis.[113–117] Overall, the evidence pointed to InhA as the target of INH and uncovered the sensitivity of mycobacteria to inhibition of mycolic acid synthesis. *M. abscessus*, among others, carry natural variants of KatG that do not catalyze the formation of the active species of INH. Thus, *M. abscessus* and many other NTM are resistant to INH.

The outer leaflet in *M. abscessus* contains extractable mycolates like trehalose monomycolate and trehalose dimycolate, and other lipids including glycopeptidolipids.[118] Recently, the transporter, MmpL3, with flippase activity responsible for the translocation of trehalose monomycolate across the cell wall has been investigated as a potential drug target.[119,120]

All of the lipid species in the cell wall account for up to 60% by weight of the cell wall.[107] This created speculation that the mycobacteria cell wall could act as a permeability barrier to solutes like antibiotics, however, it took until 1990 for the first quantitative study to define the permeability to hydrophilic molecules.[121] In their study, Jarlier and Nikaido used *M. chelonae* (until the early 1990's, *M. abscessus* and *M. chelonae* were thought to be the same species) as a model organism. They measured permeability coefficients for small hydrophilic nutrients (glucose, glycerol, glycine, leucine) and a series of cephalosporins. Their data suggested a 10-1,000x decrease in permeability across the cell wall of *M. chelonae* relative to *E. coli* and *P. aeruginosa*. Their data also showed that the uptake of cephalosporins was not dependent on the lipophilicity of the drug or temperature, which suggests an aqueous pathway through porins. Lipophilic molecules are proposed to traverse the hydrocarbon interior of the mycolic acid bilayer, but the near-crystalline state of the lipids has been speculated to limit this process. Nevertheless, the lipophilic pathway plays a contribution to solute entry as evidenced by the studies using antibiotics. Generally, antibiotics with more lipophilic properties exert greater activity against mycobacteria. Examples include the addition of a 16 carbon fatty acyl chain to INH, the more hydrophobic tetracycline derivatives like doxycycline and minocycline, and the increased hydrophobicity of clarithromycin over erythromycin.

The mycomembrane of mycobacteria is viewed as a necessary but not a sufficient component for drug resistance. Although experiments have shown decreased permeability to solutes, the cell wall is thought to synergize with other mechanisms to create the drug resistant phenotype similar to Gram-negative bacteria. In mycobacteria, this is exemplified with β-lactamases. Mycobacteria produce β-lactamases however, their activity is minimal relative to Gram-negative bacteria.[122–124] Yet, together with the limited permeability of the cell wall, the β-lactamase activity is able to reduce the concentration of β-lactams below their minimum inhibitory concentrations.[122]

1.3.1.2 Efflux Activity

Efflux pumps are membrane bound proteins that actively transport substrates across the cell wall. Many efflux pumps mediate the translocation of endogenous substrates, but some have alternative functions as xenobiotic pumps to create drug resistant and virulent phenotypes across the *Mycobacterium* genus.[125–127] Efflux pumps are grouped into superfamilies: resistance nodulation

cell division (RND), major facilitator superfamily (MFS), ATP-binding cassette (ABC), small multidrug resistance (SMR), and multidrug and toxic-compound extrusion (MATE). RND, MFS, and SMR efflux pumps are powered by the electrochemical gradient from the proton motive force created through the electron transport chain while MATE efflux pumps require a sodium electrochemical gradient for proper function. ABC efflux pumps require the hydrolysis of ATP for active transport of substrates.

The AcrAB-TolC pump in *E. coli*, a member of the RND family, is one of the most well-studied efflux pumps. Initially, it was understood that AcrAB-TolC actively transports antibiotics out of the cell as the primary function however, newer evidence emerged that suggested AcrAB-TolC to have an alternative function to eliminate toxic bile salts produced from the host during infection.[128] This contrasts with the largest group of efflux pumps in *M. abscessus*, the RND-like mycobacterial membrane protein Large (MmpL) proteins that first emerged as modulators of the cell wall but are now understood to transport alternative substrates like antibiotics using the electrochemical proton gradient.[129] Mycobacteria display a similar range of MmpL transporters with on average 15 mmpL loci predicted. However, *M. abscessus* appears to be an outlier with 27 predicted mmpL genes whereas *M. tuberculosis* is reported to have 13. The high diversity of MmpL transporters in *M. abscessus* could be a source of unidentified multidrug efflux pumps. MmpL3 transports trehalose monomycolate across the cell wall, important for the integrity of the outer leaflet of the mycomembrane, making it the only essential *mmpL* gene in mycobacteria. *M. abscessus* is known to exist in two morphotypes: smooth or rough depending on the presence or absence of glycopeptidolipids on the surface of the cell.[130] MmpL4a and MmpL4b are the MmpL transporters responsible for exposing glycopeptidolipids to the surface. Recently, two unidentified MmpL transporters (MAB_2300-MAB_2301 and MAB_1135c-MAB_1134c) have been implicated in the cross resistance to the ATP synthase inhibitor, bedaquiline, and electron transport chain inhibitor, clofazimine, in *M. abscessus*.[131,132] Additionally, MmpL5 was shown to increase resistance to a series of thiacetazone derivatives in *M. abscessus*.[127]

Despite the drug resistant activity of efflux pumps, synthetic efflux pump inhibitors exist. Ca^{2+} channel blockers like verapamil and protonophores like carbonyl cyanide 3-chlorophenylhydrazone (CCCP) impair efflux pump activity by disrupting the transmembrane

potential. Originally thought to be a direct inhibitor of efflux pumps, new evidence suggests verapamil interacts with the lipid bilayer in the membrane to disrupt the transmembrane potential.[133] CCCP, on the other hand, acts as a protonophore that sequesters free protons thereby diminishing the proton motive force.[134] Since efflux pumps have been implicated in drug resistance, efflux pump inhibitors could prove to be successful adjuvant therapies.[135] In fact, verapamil has been shown to improve the activity of bedaquiline and moxifloxacin in a macrophage and murine model of *M. tuberculosis* infection.[136,137]

1.3.1.3 Drug Modifying Enzymes

Intrinsic resistance to antibiotics is often accomplished through enzyme-mediated modifications of the antibiotic.[138] Depending on the enzyme, modifications can range from small acetyl groups to larger ribose sugars mediated by transferases or chemical transformation by monooxygenases. *M. abscessus* is endowed with numerous antibiotic-modifying enzymes to create a complex resistome.

Although aminoglycosides like amikacin are used clinically for the treatment of *M. abscessus* pulmonary disease, its genome encodes at least two acetyltransferases (AAC) and one phosphotransferase (APH) implicated in resistance.[139] The N-acetyltransferase AAC(2') uses acetyl-CoA as a cofactor for the acetylation of the 2' amino group. As a result of the specificity for the 2' amino group, aminoglycosides like kanamycin B, gentamycin C, and tobramycin are susceptible to AAC(2').[140] *M. abscessus* encodes two Eis enzymes (Enhanced in Intracellular Survival), Eis1 and Eis2.[141] Deletion of *eis1* in *M. abscessus* was not associated with increased aminoglycoside resistance while *eis2* created a hypersusceptible phenotype to amikacin.[142] These results have since been corroborated with detailed structural analyses.[143,144] Aminoglycoside modifying enzymes are known to have selective substrate specificity.[145] Therefore, numerous modifying enzymes are required to cast a wide net of aminoglycoside resistance. Streptomycin avoids acetylation by AAC(2') and Eis2 but was shown to be susceptible to phosphorylation by a putative 3''-*O*-phosphotransferase through deletion experiments in *M. abscessus* and *M. fortuitum*.[142] The net result of acetylation and phosphorylation of aminoglycosides is impaired binding to the 30S ribosomal subunit.[145]

Rifamycins have historically been used in the treatment of tuberculosis and were pivotal in reducing the duration of treatment from 18 months to 6 months largely due to their potent *in vitro* activity against *M. tuberculosis*.[146] Because rifamycins bind to the β subunit of the bacterial RNA polymerase and prevent elongation along the DNA/RNA channel, rifamycin resistant isolates often have mutations in an 81-base pair region encoding the rifampicin resistance determining region.[147] *M. abscessus* and other NTM are clinically resistant to rifamycins despite homology between mycobacterial RNA polymerases. First shown in *M. smegmatis*, *M. abscessus* encodes an ADP-ribosyltransferase (Arr_Mab) with activity against rifamycins that confers resistance. Experiments using a series of rifamycin analogs revealed that C23 on the rifamycin backbone is prone to ADP-ribosylation.[148] This was the rationale for the low activity of rifampicin against *M. abscessus*. Recently in 2021, Dick and colleagues demonstrated that the rifampicin analog, rifabutin was active against *M. abscessus in vitro* and in a mouse model.[149,150] From these data, it was thought that rifabutin escaped ADP-ribosylation by Arr_Mab. Initial genetic experiments in *M. abscessus* showed innate resistance to rifampicin through *arr*_Mab knockout however, the activity of rifabutin also increased in this genetic background suggesting a role for ADP-ribosylation of rifabutin.[151] Promising new rifabutin analogs with ester linkages at C25 that effectively block ADP-ribosylation at position C23 have been synthesized with improved activity.[152]

Tetracyclines inhibit bacterial growth by binding to the 30S ribosomal subunit and interfering with aminoacylated tRNA delivery. Although bacteria can become resistant to tetracyclines through efflux pumps, *M. abscessus* encodes a flavin adenine dinucleotide (FAD)-dependent monooxygenase, TetX, that was shown to increase tetracycline resistance 500-fold compared to *M. tuberculosis* .[153,154] Data from UV-Vis spectroscopy and mass spectrometry suggest tetracycline and doxycycline undergo TetX-dependent monooxygenation. These authors also reported a TetR-dependent repression of TetX that is lifted during tetracycline and doxycycline replete conditions but not by tigecycline, a next-generation tetracycline approved in 2005 and used sparingly for *M. abscessus* pulmonary disease treatment.[153] Moreover, tigecycline was shown to be a poor substrate of TetX. Unfortunately, single amino acid substitutions in TetX could improve the activity against tigecycline and conferred resistance when expressed heterologously in *E. coli*. Current drug discovery efforts have identified omadacycline and eravacycline with activity against multi-drug

resistant *M. abscessus* clinical isolates.[142,155] It remains to be determined if the new tetracyclines are substrates of TetX.

1.3.1.4 Drug Degrading Enzymes

Penicillins were the first mass-produced antibiotics and are still the most widely used antibiotics today.[156,157] Despite their broad-spectrum activity, β-lactams have had limited success in the treatment of mycobacterial infections. β-lactams inhibit peptidoglycan synthesis by outcompeting the natural substrates of DD-transpeptidases. The structural mimicry of the C-terminal end native stem peptide of peptidoglycan allows β-lactams to irreversibly bind the active site of DD-transpeptidases.[124] Inhibition of DD-transpeptidase crosslinking activity results in impaired peptidoglycan scaffolding required for the structural integrity of the cell wall. Until 1974, the model of mycobacterial peptidoglycan architecture was a 4→3 linked peptide network catalyzed by DD-transpeptidases.[124] When a predominance of 3→3 linkages were discovered in the peptidoglycan of *M. tuberculosis*, it became clear that other transpeptidases were required for this type of scaffolding.[158] Specifically, LD-transpeptidases catalyze the 3→3 linkages. Studies confirmed that *M. abscessus* encodes LD-transpeptidases and DD-transpeptidases to create 4→3 and 3→3 linkages across the peptidoglycan network.[159] While most β-lactams inhibit DD-transpeptidases, only the subclasses of carbapenems and cephalosporins show some activity against LD-transpeptidases.[124,160,161] The predominant reliance on LD-transpeptidases in *M. abscessus* could explain why only imipenem (a carbapenem) and cefoxitin (a cephalosporin) show moderate activity *in vitro*.[142] Although the clinical use of imipenem and cefoxitin is hampered due to their unstable nature *in vitro*, which complicates routine drug susceptibility testing.[162]

In addition to the selectivity of β-lactams for LD- and DD-transpeptidases, *M. abscessus* has a chromosomally-encoded class A β-lactamase, Bla_{Mab}, which is thought to be the primary driver of β-lactam resistance.[163] β-lactamases hydrolyze the β-lactam ring leading to inactivation. During the characterization of Bla_{Mab}, it was shown to have a broader spectrum compared to the β-lactamase, BlaC, found in *M. tuberculosis* and to be resistant to common β-lactamase inhibitors like tazobactam, sulbactam, and clavulanate.[163,164] Avibactam was identified as the first efficient inhibitor of Bla_{Mab} with activity in a macrophage and a zebrafish infection model of *M. abscessus*.[165] Recently avibactam has proven to be instrumental in the combination of sulopenem,

tebipenem, cefuroxime, and amoxicillin to create an effective bactericidal *in vitro* regimen against *M. abscessus*.[166] This represents an important first step into creating an all-oral regimen using a combination of β-lactams with avibactam adjuvant therapy for the potential treatment of pulmonary *M. abscessus* disease. *M. abscessus* subsp. *massiliense* harbours an additional β-lactamase, Bla_{Mmas}.[123] Bla_{Mab} and Bla_{Mmas} were shown to hydrolyze penicillins and cephalosporins with similar efficiency, but Bla_{Mmas} also exhibited mild carbapenemase activity.[123] This could suggest an evolutionary step to becoming an extended spectrum β-lactamase.

1.3.1.5 Target Modifying Enzymes

The fact that macrolides like clarithromycin and azithromycin are the only consistent element in an antibiotic regimen for *M. abscessus* pulmonary infection does not underscore enough how important these drugs are for increasing the chance of a positive treatment outcome.[95,96] Macrolides are known to bind the 50S ribosomal subunit and block the nascent polypeptide exit tunnel.[142] Eventually this leads to the dissociation of the growing polypeptide prematurely and arrest of protein synthesis. Resistance to macrolides has been well-studied with the example of target modification by an erythromycin ribosome methyltransferase (Erm) enzyme. The role of Erm enzymes is to transfer a methyl group from the *S*-adenosyl methionine donor to nucleotide A2058 of the 23S rRNA.[138] A new study from 2021 performed a structural analysis of the Erm-modified 70S ribosome and proposed an alternative model for how dimethylation of A2058 prevents macrolide binding.[167] The authors identified a critical water molecule that is coordinated by A2058 and G2505 on the 23S rRNA and the dimethylamino group of the macrolide desosamine. This could pave the foundation for a new, rationally designed series of macrolides that could overcome Erm-mediated resistance.

Prior to 2009, it was believed that *M. abscessus* relied on mutations at positions A2058 and A2059 on the 23S rRNA for resistance to macrolides.[168,169] However, since then, an Erm enzyme has been implicated through inducible macrolide resistance in *M. abscessus* that is absent from the closely related *M. chelonae*. A study by Nash *et al* identified *erm*(41) as the gene responsible for conferring inducible macrolide resistance.[97] The studied examined 10 clinical isolates of *M. abscessus* subsp. *abscessus* deemed clarithromycin sensitive using standard CLSI microbroth dilution measurements. Seven isolates showed inducible resistance after pre-exposure to

macrolides for 14 days (MIC ≤ 0.5 μg/mL to MIC > 32 μg/mL), although *erm*(41) induction could be detected as early as 24 hours. In the remaining 3 isolates, a T28C single nucleotide polymorphism (SNP) was identified in *erm*(41) that resulted in a non-functional allele. Subspecies typing revealed that only *M. abscessus* subsp. *abscessus* and subsp. *bolletii* have inducible resistance to macrolides through the T28 sequevar of *erm*(41).[170] *M. abscessus* subsp. *massiliense* does not have the inducible resistance phenotype due to a 200-250bp internal deletion in *erm*(41) and therefore, requires the A2058C or A2058G mutation in the 23S rRNA for resistance. This could explain the improved outcomes for *M. abscessus* subsp. *massiliense* infections when the patient is on a macrolide-base regimen.[95] These results have since been reproduced with larger sample sizes of MABSC and *M. chelonae* clinical isolates.[171]

1.3.2 Inducible Resistance

The study by Nash *et al* identified the presence of *erm*(41) and the link to an inducible macrolide resistant phenotype in *M. abscessus*, but stopped short of describing the molecular mechanism of induction.[97] Inducible *erm* genes in bacteria are known to be predominantly regulated by translational attenuation as described for *erm*(B), *erm*(C), and others with one example of transcriptional attenuation for *erm*(K).[172–174] One prominent exception is *erm*(37) found in *M. tuberculosis*, which is regulated by WhiB7.

whiB7, found in *Streptomyces* and mycobacteria, is a conserved mycobacterial transcription factor first shown to coordinate ribosomal protection genes and multidrug efflux pumps from exposure to sub-inhibitory concentrations antibiotics.[175] The exact nature of the *whiB7* inducer is unclear since the activating agents are structurally dissimilar with Tanimoto scores < 0.7 and target different proteins. *whiB7* was induced in the presence of 50S and 30S ribosome inhibitors like clarithromycin and streptomycin, and by inhibition of DNA synthesis by fluoroquinolones but induction was absent when challenged with cell wall synthesis inhibitors.[176] The data suggests the induction of *whiB7* results from pleiotropic effects of antibiotics on cell metabolism.

Currently, it is thought that WhiB7 acts as a redox sensor that links cell metabolism, redox homeostasis, and antibiotic resistance. WhiB7 contains four conserved cysteine residues, which are thought to bind iron-sulfur clusters or form disulfide bridges.[176] By quantifying the reduced

and oxidized species of the dominant reducing agent in mycobacteria, mycothiol, after antibiotic challenge, WhiB7 was shown to become activated in a reduced intracellular environment.[176] These results were replicated using the hydroxyl radical scavenger thiourea. The leading model is that WhiB7, when in a reduced state from diverse cellular stresses, can bind WhiB7-specific promoters with SigA to modulate a protective response.[177]

In 2016, a transcriptomic analysis of *M. abscessus* under antibiotic stressed conditions revealed a *whiB7* transcriptional signature.[178] These results were followed up by a detailed study describing the induction of the *whiB7*-*erm*(41) axis of *M. abscessus in vivo*. Azithromycin and clarithromycin induced *erm*(41) expression in a *whiB7*-dependent process in zebrafish infected with a strain of *M. abscessus* carrying *tdTomato* under the control of the *erm*(41) promoter.[179] Two publications described the antibiotic landscape of *M. abscessus* through a *whiB7* lens. Hurst-Hess *et al* linked the induction of *whiB7* to clinically relevant antibiotics including macrolides, aminoglycosides, and tetracyclines, as was previously demonstrated for *M. tuberculosis*.[180] Among the genes included in the *whiB7* regulon is *eis2*, which leads to acetylation of amikacin and resistance *in vitro*.[180] Pryjma *et al* described the antagonistic effect between clarithromycin and amikacin.[181] Specifically, clarithromycin, but not amikacin, was shown to induce *whiB7* and subsequently *erm*(41) and *eis2*.[181]

Unlike for *M. tuberculosis*, the correlation between *in vitro* drug susceptibility testing and clinical outcomes for patients with *M. abscessus* infections is poor. It is now established that clarithromycin and amikacin are some of the most potent antimycobacterials against *M. abscessus in vitro* when used alone, however, the combination results in antagonism *in vitro*. One question looming in the field is if the *in vitro* antagonism is recapitulated *in vivo*. Whether this is driven by the master regulator *whiB7 in vivo* or other factors has yet to be investigated. Nevertheless, cure rates of < 50% on a macrolide-aminoglycoside-based regimen highlight the disconnect between our understanding of drug susceptibility testing and patient outcome.

1.3.3 Acquired Resistance

Drug resistance is the omnipresent enemy of players in the field of antibiotic discovery. This includes academic labs that identify novel cellular pathways to target with antibiotics, industry

partners that bring new antibiotics to the market, and clinicians that rely on antibiotics to provide a benefit to their patients. Modern medicine is grateful to the aforementioned groups for their contributions to the discovery of agents that can treat infections as simple as *otitis media* to diseases like tuberculosis that have plagued human populations for thousands of years.

The success of antibiotics can be split into two hurdles. Ideally, an antibiotic should successfully clear the first hurdle of intrinsic resistance before being brought to the clinic, although this is not always upheld and results in antibiotics with limited efficacy being used in clinical practice. The second hurdle that many antibiotics appear to clear but then stumble over is with acquired resistance. Limiting acquired resistance is essential for the continued success of that agent. However, this has proved challenging as evidenced by the limited publications describing antibiotics without detectable resistance. The most recent success story is the discovery of the bacterial cell wall inhibitor, teixobactin, from uncultured bacteria grown *in situ*.[182] Teixobactin highlights the need to expand the chemical space beyond small molecules produced by the handful of microorganisms culturable under standard laboratory conditions. Expanding the boundaries of the chemical landscape further, efforts have been made to implement machine learning for *in silico* drug discovery with the recent discovery of the repurposed halicin.[183]

The emergence of variant alleles and spread of antimicrobial resistance genes has sparked the creation of surveillance programs and resistance databases.[58,184] The earliest version of the Comprehensive Antibiotic Resource Database (CARD) was released in 2013. CARD is a curated sequence resource and informatics tool that can identify putative antibiotic resistance genes in unannotated genomes.[185] Since the 2020 update, CARD now features an enhanced statistical analysis of *in silico* predictions, 82 pathogens, and more than 100,000 genomes to better model trends in antimicrobial resistance mobility and detect new resistance variants.[186] In 2015, the World Health Organization launched the Global Antimicrobial Resistance and Use Surveillance System (GLASS) as the first global effort to standardize antimicrobial resistance surveillance using a One Health approach.[187] Namely, GLASS reports on resistance and antimicrobial use in humans, agriculture, and the environment.

It is primarily due to the cataloguing of acquired resistance mutations that drug susceptibility testing has taken a more modern approach for some bacteria. Resistance to rifampicin in *M. tuberculosis* frequently occurs from mutations in an 81bp region in the target gene, *rpoB*. This 81bp region is known as the rifampicin resistance determining region. Because rifampicin is part of the front-line regimen given for the treatment of tuberculosis and rifampicin resistance is frequently observed in patient isolates, a probe-based cartridge assay was designed by Cepheid that can detect common rifampicin resistance mutations and lead to more appropriate treatment plans in as little as 6 hours as opposed to 1-6 weeks.[188] Molecular drug susceptibility testing has recently established a niche in *M. abscessus* with a probe-based assay for easier detection of *M. abscessus* in sputum that is often difficult to acquire from children or detection of clarithromycin resistance either through the common 23S rRNA A2058C/G mutation or the T28C sequevars on *erm*(41) for non-functional inducible clarithromycin resistance.[189]

HGT is also responsible for the acquisition of antibiotic resistance in bacteria, however that role in *M. abscessus* is less understood.[190] HGT has been shown to be an important factor in the evolution of three dominant circulating clones of *M. abscessus* that have been reported across the globe.[191,192] Phylogenomics identified the acquisition of a DNA methylase DpnM that modulates the expression of 52 genes, some of which impart increased intracellular survival in macrophages, increased tolerance to nitric oxide, and decreased susceptibility to amikacin.[191]

1.4 DRUG DISCOVERY

The goal of antimicrobial drug discovery is to find new medicines to treat infectious diseases. Today, research and development are accomplished through global collaborative efforts between academic, industry, and government partners. However, some have argued that moving forward, the field should pivot away from relying on traditional ‘big pharma’ towards an open science business model, which has drawn criticism regarding the capital required for late-stage clinical trials.[193]

The history of antibiotics is documented to pre-date the antibiotic era of the 1940s.[194] The Eber’s papyrus from 1550 BC is perhaps the oldest recorded medical document that describes the use of traditional poultices of mouldy bread to treat open wounds.[195,196] Some of the first evidence of

tetracycline use was found during histological analysis of bones from the Sudanese Nubia region (350-550 CE) with fluorescence microscopy, and later confirmed with mass spectrometry.[197,198] Before Alexander Fleming and the discovery of penicillin, Paul Ehrlich hypothesized of a substance that could selectively target the disease-causing microbes over the host tissue from his work using synthetic aniline dyes that showed permeability to certain microbes. Thus, the first large-scale synthetic screening program to discover an antimicrobial agent was born. From this screening campaign, in 1910, the synthesis and evaluation of a compound marketed by Hoechst as Salvarsan was completed for the treatment of syphilis.[199,200]

This idea of screening molecules with antimicrobial activity followed by medicinal chemistry was not a one-hit-wonder. Chemists at Bayer produced Prontosil, a sulfa drug, using this platform of drug discovery but could not secure a patent as the active metabolite of Prontosil was commonly used in the dye industry.[194,195] Sulfonamide derivatives became widely available from the off-patent label and cheap production.[194,195]

Most people know Alexander Fleming as making the serendipitous discovery of penicillin in 1928.[201] However, the molecule was identified and purified by chemists at Oxford University in 1941 while Dorothy Hodgkin solved the β-lactam structure in 1945 helping establish penicillins as a dominant tool in the clinic.[202,203] By the time these collaborative efforts occurred, resistance had been documented for Salvarsan and sulfonamides.[195] In fact, resistance to penicillin had already been documented a few years before being introduced in the clinic in 1945 but these claims were disregarded as merely laboratory observations.[194,204] Thus started the on-going conflict between antibiotic discovery and the inevitable rise of antimicrobial resistance.

1.4.1 Chemical Space

The discovery of Salvarsan, Prontosil, and penicillins highlighted the chemical space available for chemists and pharmaceutical companies at the time. Salvarsan was the product of chemical modification of the toxic drug, Atoxyl, and perhaps the first attempts at what we know as structure activity relationship (SAR) studies. Prontosil demonstrated, for the first time, that libraries of small molecule compounds curated in laboratories could be screened for antimicrobial activity. On the

contrary, penicillins showed the world that biology can make excellent antimicrobials with incredible diversity in the chemical space of natural products.

1.4.1.1 Natural Products

Natural products are a proven source of antimicrobial agents with nearly two-thirds of clinically used antibiotics having a natural product scaffold.[205] The success of natural products as antimicrobial agents is largely due to their evolutionary history. Natural products are small molecules of 200-3,000 Da derived from the secondary metabolism of plants and microorganisms. These specialized molecules have undergone millions of years of evolution to create a diverse pool of signalling molecules.[206] The array of secondary metabolites from bacteria alone are enough to surpass the diversity of synthesized compounds.[205,207] Within the pool of secondary metabolites are compounds with antimicrobial properties co-opted by bacteria for defensive or predatory functions in their natural environments. The ancient evolutionary history of natural products has shaped complex scaffolds that have optimized interactions with their biological targets.[208,209]

The diversity of natural products is inherently linked to multifaceted biosynthetic pathways.[210] Biosynthetic gene clusters (BGCs) are genomic units, often up to hundreds of kb in length, that consist of the core biosynthetic genes, positive regulators, repressors, and self-resistance-conferring genes.[205,211] Currently, only 0.3% of the 400,000 predicted BGCs in public databases from 60,000 genomes have been experimentally validated, opening avenues for new chemistries to be discovered.[206] Despite the availability of predicted BCGs from metagenomic data obtained environmental samples, culturing these bacteria under standard laboratory conditions remains a challenge. Achieving the right set of conditions for growth and awakening silent BCGs might not coincide.[212] The development of an *in situ* chip-based technology has helped increase the diversity of culturable environment microorganisms under natural conditions and lead to new antimicrobial molecules.[182,213]

Natural products can be classified based on the type of BCG required for synthesis. Polyketide synthases (PKS) produce polyketides through the formation of a basal polyketide chain from acetate-derived building blocks.[205] Non-ribosomal peptide synthases (NRPS) generate metabolites with a peptide backbone, often with non-proteinogenic amino acids, and a cyclic structure. PKSs

and NRPSs share a modular and linear architecture with covalently linked catalytic domains. Each module, consisting of bundled domains, can perform one specific function such as the incorporation of one type of building block. Unlike PKSs, NRPSs can increase the diversity of intermediates through isomerization, hydroxylation, methylation, and halogenation reactions imparted by additional modifying domains. Although PKSs and NRPSs can produce distinct molecules independently, examples have been recorded of metabolites synthesized by PKS-NRPS hybrids.

Terpenes are comprised of isoprene units and synthesized from the mevalonate and deoxyxylulose phosphate pathways. Many lipid species in mycobacteria are derived from terpene metabolites including 1-tuberculosinyladenosine (1-tbad), which is synthesized from geranylgeranyl pyrophosphate in the presence of class II terpene cyclase and tuberculosinyl transferase enzymes.[214] Recent evidence suggests that the acquisition of 1-tbad-producing enzymes helped lead *M. tuberculosis* towards a intracellular lifestyle.[35] While terpenes are the largest class of natural products, there has been limited progress made towards identifying terpene-like metabolites with antimicrobial activity.[215–217] Rather than act directly as antimicrobial properties, the position of terpenes in the realm of antimicrobials may be best suited as adjuvant-like molecules.[218,219]

Ribosomally synthesized and post translationally modified peptides (RiPPs) are alternatives to peptides synthesized by NRPSs. The precursor peptide is synthesized by the ribosome and upon release is directed to a post translational modifying enzyme for modification, proteolysis, and export.[205,220] Recently, a new mechanism of RiPP synthesis has recently been identified. The precursor peptide synthesized by the ribosome undergoes amino acid extension and modification from NRPSs before the completed metabolite undergoes proteolysis to regenerate the precursor peptide for additional rounds of RiPP synthesis.[221,222]

Antimycobacterial drug discovery owes much gratitude to natural products. Rifampicin is invaluable as one of the front-line agents for tuberculosis and the injectable aminoglycosides like streptomycin and kanamycin are used for multidrug resistant tuberculosis regimens. Amikacin as the standard aminoglycoside and clarithromycin and azithromycin as the predominant macrolides

form the backbone of the multidrug regimen for pulmonary *M. abscessus* infections where it has been established that resistance to macrolides is one of the biggest risk factors for treatment failure.[78]

Looking to the future with natural products for antibiotic drug discovery, the PKS-NRPS hybrid metabolite, pyridomycin could be promising for the treatment of *M. abscessus* pulmonary infections and tuberculosis.[223] Like isoniazid, pyridomycin is an inhibitor of the well-validated target InhA in *M. tuberculosis* and recently validated target in *M. abscessus*.[224,225] However, unlike isoniazid, pyridomycin does not require pro-drug activation by the catalase-peroxidase KatG. This could lower resistance against pyridomycin in *M. tuberculosis* since $KatG_{Mtb}$ S315T mutations are the most common genotype resulting in isoniazid resistance.[226–228] Moreover, by pyridomycin bypassing pro-drug activation, InhA now becomes a tractable target by chemical inhibition in *M. abscessus* since $KatG_{Mab}$ cannot catalyze the formation of the INH:NAD adduct required for InhA inhibition.[225,229]

1.4.1.2 Synthetic small molecules

In the clinical world of antibiotics, natural products are still the dominant source while synthetic small molecules occupy only a minority of the chemical space.[230] On the contrary with respect to non-communicable diseases, synthetic small molecules are the front-line players in the field.[230] This discrepancy might be explained by the fact that natural products have had an evolutionary advantage for acquiring chemical properties required for optimal microbial biology while curated libraries of synthetic molecules have been tailored for human biology. Nevertheless, some of the most successful antimycobacterials are synthetic small molecules with the most recently approved antimycobacterial, bedaquiline, leading by example.

The last two agents of the front-line regimen for tuberculosis are isoniazid and ethambutol. Isoniazid binds to and inhibits InhA, the reductase component of the fatty acid synthase II cycle in mycobacteria that is responsible for synthesizing mycolic acids. Isoniazid has been a mainstay component of the tuberculosis regimen since the early 1950's but its demise is linked to its pro-drug nature.[112,195] Isoniazid requires activation by the catalase-peroxidase KatG to form the isoniazid-NAD adduct, which is the inhibitor of InhA. Since KatG is non-essential for *M.*

tuberculosis, mutations in KatG are acquired that lead to isoniazid resistance. Furthermore, isoniazid shows no activity against *M. abscessus* due to the absence of a functional KatG. Experiments have shown that *M. abscessus* becomes sensitive to isoniazid if $katG_{Mtb}$ is heterologously expressed.[231]

Ethambutol was discovered and introduced into the clinic in 1962.[195] The activity against arabinosyl transferase makes ethambutol an attractive antimycobacterial agent since the mycolic acids are covalently linked to peptidoglycan through an intermediate arabinogalactan layer.[106] Despite being a potent antibiotic against *M. tuberculosis*, *M. abscessus* encodes natural variants of the target EmbB, which lead to ethambutol resistance.[109]

Few synthetic antimicrobials demonstrate appreciable *in vitro* activity against *M. abscessus*. The synthetic class of fluoroquinolones established in the 1980's, although potent broad-spectrum antimicrobials, show poor *in vitro* activity against *M. abscessus*.[232] NTM resistant to fluoroquinolones contain amino acid variants in the quinolone resistance determining region of the target GyrA.[108,233] Recent drug discovery efforts identified the DNA gyrase inhibitor SPR719 with activity against *M. abscessus* and has moved into clinical trials for NTM lung disease.[234,235]

Clofazimine is a synthetic small molecule with a complicated history. First used in conjunction with rifampicin and dapsone to treat leprosy, clofazimine was recently shown to be effective in treating *M. avium* lung disease.[236] Unfortunately, regular ingestion of clofazimine results in a pink-orange pigmentation of the skin, which can further exacerbate stigmatization of patients historically treated for leprosy and has toxic side effects. Furthermore, the mechanism of action of clofazimine is unclear as multiple mechanisms have been proposed. Clofazimine is thought to inhibit the electron transport chain, bind to guanine residues of DNA, and increase the activity of bacterial phospholipase A_2.[237,238] Notwithstanding the *in vitro* activity of clofazimine against *M. abscessus*, the combination of side effects and obscurity of the mechanism has limited the development of clofazimine as a potential therapy for *M. abscessus* infections.

One of the most recent success stories for the treatment of mycobacterial infections was the discovery of bedaquiline by Johnson & Johnson in 2004.[239] Bedaquiline is a diarylquinolone with

activity against the ATP synthase of mycobacteria. Bedaquiline is unique among antibiotics since the final market-ready compound was the hit identified from the high-throughput screening campaign. Hits routinely undergo multiple rounds of medicinal chemistry for further optimization however, this was not necessary for bedaquiline as derivatives generated were less potent. The highlight of bedaquiline is the activity against multidrug resistant tuberculosis. The most recent data from the Nix-TB and ZeNix clinical trials shows promising results of a bedaquiline-pretomanid-linezolid optimized combination for multi and extreme drug resistant tuberculosis with six months of therapy over the standard 18 months with multiple oral and intravenous agents with severe side effects.[240–242] Bedaquiline maintains potent *in vitro* and *in vivo* activity against *M. abscessus* and could be valuable if included in a *M. abscessus* antibiotic regimen.[243–247]

Anacor Pharmaceuticals produced a series of benzoxaboroles in 2006 that gave rise to a potent antifungal agent for the treatment of onychomycosis.[248] The benzoxaboroles are an interesting class of compounds with boron chemistry that provide high affinity for ribose sugars.[249] It was, thus, unsurprising that the mechanism of action of the benzoxaborole antifungal agent was the inhibition of an aminoacyl tRNA synthetase (aaRS).[250] Benzoxaboroles form a unique semi-covalent tricomplex with the leucyl-tRNA synthetase (LeuRS) and $tRNA^{Leu}$. The benzoxaborole hydrogen bonds with residues in the editing domain of LeuRS and forms a covalent interaction between the boron of the oxaborole ring and the 2' and 3' ribose hydroxy groups of the terminal adenosine nucleotide of the non-aminoacylated $tRNA^{Leu}$, which is tethered through appropriate contacts with the C-terminal and anticodon binding domains of LeuRS.[250,251] The current understanding of the oxaborole tRNA trapping (OBORT) mechanism is a decrease in available aminoacylated $tRNA^{Leu}$ and thereby protein synthesis.

Unlike other aaRS inhibitors like mupirocin, which targets the aminoacylation domain of isoleucyl-tRNA synthetase (IleRS), benzoxaboroles bind to the editing domain of LeuRS. The editing domain of LeuRS is thought to reflect primordial cell biology before the standard proteinogenic amino acids evolved.[252] Current data suggests that the aminoacylation domain of LeuRS provides enough specificity for leucine over isoleucine and valine to maintain the error rate of protein synthesis below the natural rate of 1/3000.[253,254] However, the aminoacylation domain cannot distinguish leucine mimics like the non-proteinogenic amino acid norvaline. Being

structurally similar to leucine, norvaline is thought to have been an early branched chain amino acid (BCAA) but as proteins evolved more complex structures and required intricate folding primarily driven by the hydrophobic effect, the more hydrophobic leucine became the dominant amino acid.[252] Norvaline is rarely found in biology today, with few exceptions such as antifungal peptides, bacteria with mutations in regulatory components of leucine biosynthesis, or heterologous over-expression of leucine-rich proteins.[255–259] The editing domain of LeuRS can recycle $tRNA^{Leu}$ misaminoacylated with norvaline through hydrolysis. Without the editing domain of LeuRS, the error rate of norvaline misaminoacylation can be as high as 1/118, which is well above the threshold for accepted protein synthesis errors.[260]

After showing good pharmacokinetics data and no serious side-effects in a phase 1 study, the benzoxaborole epetraborole was brought to a phase 2 clinical trial to evaluate the efficacy of treatment of complicated urinary tract infections from *E. coli* but was terminated early due to the presence of epetraborole-resistant *E. coli* isolates from patients as early as day 1 post treatment.[261,262] Since those reports, epetraborole and other benzoxaboroles have found potential for mycobacterial infections namely, for *M. tuberculosis* and some NTM. The benzoxaborole compound GSK656 shown to be active against *M. tuberculosis* has since undergone iterative cycles of medicinal chemistry and passed a phase 1 safety and early bactericidal activity study and is currently being evaluated in a phase 2 study.[263–265] Epetraborole is currently in a phase 2 clinical study spearheaded by AN2 therapeutics for refractory *M. avium* pulmonary disease. With good results from the AN2 trial, there could be a *M. abscessus* clinical trial in the future.

1.4.2 Whole Cell Approaches

Whole-cell screening (WCS) has been the gold standard for antibiotic discovery since the early 1900's when the first antimicrobial compounds Salvarsan, Prontosil, and penicillin were discovered.[266,267] WCS identifies compounds that exhibit whole-cell phenotypes, which is most commonly growth inhibition (**FIGURE 1.4**). However, growth inhibition can be substituted for a number of other readouts using fluorescent or luminescent reporter systems, transcriptomics, or proteomics .[268–270] This approach of inhibitor-first and allowing biology guide us to the best cellular targets and identifying compounds with membrane permeable physicochemical properties lead to the discovery of the most clinically useful antibiotics.[266,271] Where target-based screens

focus on one target, and thus the mechanism is known, WCS can identify compounds with diverse mechanisms but resolving the mechanism is often challenging and never fully complete before the antibiotic is brought to the clinic as was the case for isoniazid.[113–117] Other downsides to WCS are compounds that act in a non-specific manner such as alkylating agents or detergents, however these can be filtered out with rigorous cheminformatics tools.[266,269]

If a drawback of the target-based approach for antimicrobials is the lack of *a priori* knowledge of cell permeable compounds, the equivalent drawback for WCS is the inherent link between the mechanism of action of the compound and its *in vivo* potency. This was highlighted in a landmark study where potent whole-cell inhibitors were identified against *M. tuberculosis* but showed no activity *in vivo*. After careful elucidation of the mechanism of action, it was determined that the compounds targeted glycerol metabolism, which is central for growth under standard laboratory conditions but is not a required carbon source for growth in the host.[272] Understanding the limitations of standard laboratory media has opened the doors to performing WCS in media with different carbon sources or under nutrient starvation to simulate an *in vivo* environment.[273]

Another major pitfall for WCS in mycobacteria is the structural and mechanistic redundancy of hits identified.[267,274–276] A series of imidazo[1,2-a]pyridine-3-carboxamides were identified from four separate screens,[277–280] tetrahydropyrazolo[1,5-a]pyrimidine-3-carboxamides were identified from three screens,[281] and adamantly urea-based compounds were identified from two screens.[282–284] Although WCS provides, in theory, the whole cell as a pool of potential targets, promiscuous targets are often the resistance determinant when followed up by forward genetic assays. DprE1, an enzyme critical for the synthesis of cell wall arabinan, has been targeted by five different structural series.[285,286] The transporter of trehalose monomycolate, MmpL3, was shown to be a common target of structurally divergent compounds.[287] Lastly, QcrB, subunit b of the cytochrome bc_1 oxidase of the electron transport chain in mycobacteria, is being explored as a drug target through different series of small molecule inhibitors.[288,289]

1.4.3 Target-Based Approaches

Drug discovery using a target-based approach has been a mainstay for the development of therapeutics for human biology including cancer but has struggled to make dividends for the field

of antimycobacterials, despite expanded efforts for *M. tuberculosis*, and antibiotics in general.[267,290,291] Antimicrobial target-based discovery leveraging the power of the genomics era uses a three step operational code.[292] First, using a bioinformatics approach from whole-genome sequencing data repositories, pathogen-specific genes without human orthologs are tabulated. Second, loss-of-function mutations either by SNPs or transposon insertions are introduced into the candidate genes to probe for essential genes. Finally, information on whether the target is druggable is gathered using bioinformatics to identify druggable motifs, structural knowledge to identify putative binding pockets, or prior enzyme kinetics data with small molecule inhibitors (**FIGURE 1.4**).

Ideally, these principals could lead to the rational design of new antibiotics but are often oversimplified or have failed to account for historical precedent.[292] i) Most successful antibiotics are derived from natural product scaffolds like macrolides and aminoglycosides or synthetic fluoroquinolones that target processes conserved across all domains of life.[293] ii) Prior to the CRISPR era, essential genes were identified using different variations of transposon insertion screening.[294–297] These assays are prone to bias based on the transposon insertion and create a dichotomous model of essential and non-essential genes. Now with the advent of CRISPR and more specifically CRISPR-interference (CRISPRi) in mycobacteria, we have a better understanding that essentiality is a spectrum and that two genes, declared essential from methods likes Tn-Seq and TraSH, are in fact, quite different along the spectrum.[298–300] Historically, we have known that genes involved in ribosome function and mycolic acid synthesis were vulnerable gene targets for small molecule inhibition. However, coenzyme A and sulfur metabolism, both essential processes in mycobacteria, are less vulnerable than previously thought and could explain why developing small molecules targeting coenzyme A metabolism has not been fruitful.[300,301] Other essential processes that were previously overlooked were tRNA synthetases and Clp proteases, which are high on the vulnerability scale.[263,300,302,303] iii) Having prior enzyme kinetics data is helpful but that pre-selects for targets with a molecular function that is well-known, potentially omitting promising targets with a more complex mechanism. *A priori* knowledge on the target may lead to being too selective but it may deconvolute the mechanism of action as the interaction between the target and small molecule has already been characterized. However, a caveat is raised

that the *in vitro* mechanism may not translate into a similar mechanism once *in cellulo* or the cellular phenotype may arise from potential polypharmacology of the small molecule.

1.4.4 Whole Cell Target-Based Hybrid Approaches

To overcome some of the limitations of whole-cell and target-based approaches, new hybrid methods using hypomorph strains are being developed that could spark new life in the field of drug discovery. The goal of hybrid approaches is to uncover new chemical scaffolds rather than redundant scaffolds using hypomorphs where each hypomorph could display a hypersusceptible profile to a small molecule. By virtue of finding new chemical scaffolds, novel targets might become available to small molecule inhibition. Hybrid assays maintain the *in cellulo* approach insomuch that cell permeable chemistry is favoured and that the observed phenotype results from the *in cellulo* milieu rather than *in vitro* conditions. In addition, hybrid methods preserve the target specificity of target-based drug discovery through the generation of gene or protein specific hypomorphs to aid in the deconvolution of the mechanism of action (**FIGURE 1.4**).

Recently, hypomorph strains generated by CRISPRi gene knockdown have shed light on the spectrum of essentiality where some genes are more vulnerable than others.[300] Although these pools of *M. tuberculosis* hypomorphs have yet to deliver new small molecules or new targets besides proof of concept work, *M. tuberculosis* hypomorphs generated using the DAS-tag proteolytic system have yielded deliverables.[304] This method, termed PROSPECT, enabled the screening of 100-150 *M. tuberculosis* proteolytic hypomorphs with a library of >50,000 compounds and identified 40 new scaffolds that target DNA gyrase, RNA polymerase, cell wall synthesis, tryptophan and folate synthesis—all well-known drug targets.[305] Surprisingly, the essential efflux pump EfpA, previously unknown as a druggable target, was discovered during this screen.

The main limitation to the hypomorph hybrid approach is the inherent link between hit identification and the hypersusceptible profile. Indeed, hypomorph strains will become more susceptible to many molecules, and that scaffolds identified might appear as weak hits from a more traditional in cellulo screening approach. This highlights the requirement for excellent structure activity relationship analysis and medicinal chemistry efforts. For these reasons, the

EfpA inhibitor, when first identified as a weak hit, underwent optimization to generate an EfpA inhibitor with wild-type *M. tuberculosis* drug-like potency.[306] In the end, the PROSPECT method was successful in uncovering new molecules against new targets that previously went undetected by conventional screening.

1.5 RATIONALE & RESEARCH OBJECTIVES

The repertoire of antibiotics used for treating pulmonary *M. abscessus* infections has relied on antibiotics from the tuberculosis world and other bacteria.[307] For many other bacteria, this repurposing process has worked in the past with broad spectrum antibiotics but most antibacterials do not exhibit activity across the MTBC-NTM spectrum.[308] Some exceptions exist like rifampicin but *M. abscessus* is an outlier with intrinsic resistance.[148,309] As a result, new antibiotics will be needed considering the increase in *M. abscessus* pulmonary infections globally and the aging population of CF patients.[55,84]

The first objective of this thesis was to construct a strain of *M. abscessus* with constitutive luminescence and screen a library of 517 natural product compounds (**Chapter 2**). The reference strain ATCC 19977 of *M. abscessus* was engineered to constitutively express the *luxCDABE* operon and generate luminescence. Next, the *M. abscessus*-*lux* strain was validated with a Z' factor > 0.7 and used in all subsequent library screening. From the 517-compound library with natural products from myxobacteria, fungi, and other diverse sources, lysobactin and sorangicin A were identified as *in vitro* growth inhibitors of *M. abscessus*. Both compounds were active against multi drug-resistant clinical isolates of *M. abscessus* and provide opportunities for the *M. abscessus* drug pipeline. Currently, the pipeline does not have compounds like lysobactin targeting lipid II of the cell wall. Additionally, sorangicin A targets the validated drug target RNA polymerase but unlike other RNA polymerase inhibitors like rifampicin and rifabutin, sorangicin A does not induce drug metabolising enzymes like cytochrome P450 that are known to interfere with the CF corrector Ivacaftor. As interesting as lysobactin and sorangicin A are, both compounds are early in the discovery phase and could benefit from iterative rounds of medicinal chemistry and formulation optimization.

Going forward, we wanted to identify compounds with a quick return on investment. From the Medicines for Malaria Venture, we screened 400 compounds active against various disease sets and 400 compounds with general antibacterial, antifungal, or antiviral activities (**Chapter 3**). We identified epetraborole as the most potent hit and characterized the *in vitro* and *in vivo* antimycobacterial activity in *M. abscessus* infected zebrafish and the recently described SCID mouse model for *M. abscessus*. Using a forward genetic approach, epetraborole resistant mutations were mapped to the editing domain of LeuRS. Keeping in mind the failed phase 2 clinical trial with epetraborole, we looked for solutions to salvage epetraborole as a therapy. Taking advantage of the lack of editing activity, we showed epetraborole mutants became sensitive to the non-proteinogenic amino acid norvaline. Norvaline challenge inhibited growth of epetraborole mutants and resulted in the misincorporation of norvaline in lieu of leucine across the proteome. When used as an adjuvant-like molecule with epetraborole, norvaline decreased resistance to epetraborole in both *M. abscessus* and *M. tuberculosis*. This highlights the potential of norvaline as an adjuvant for LeuRS editing domain inhibitors.

M. abscessus mutants with resistance to both epetraborole and norvaline were raised unintentionally and characterized (**Chapter 4**). The double mutants incorporated less norvaline in the proteome, but we note no change in the hydrophobicity of the cell wall nor increased efflux activity. WGS identified mutations in the first enzyme in the biosynthetic pathway of leucine, α-isopropylmalate synthase (α-IPMS), and were mapped to the allosteric binding site for leucine. Metabolomics showed that the double mutants had increased leucine production, but no change in isoleucine, indicating a disruption of the allosteric regulation of IPMS. Ultimately, the increased leucine production countered norvaline inhibition.

The findings in this thesis underscore a place for drug discovery tailored to *M. abscessus* and highlight the antimicrobial resistant nature of *M. abscessus*. From the work presented here and from others, epetraborole could be moved to a phase II clinical trial for *M. abscessus* pulmonary infections as was done with epetraborole for MAC.

1.6 REFERENCES

1. Turenne, C. Y. Nontuberculous mycobacteria: Insights on taxonomy and evolution. *Infect. Genet. Evol.* **72**, 159–168 (2019).
2. Tortoli, E. et al. The new phylogeny of the genus Mycobacterium: The old and the news. *Infect. Genet. Evol.* **56**, 19–25 (2017).
3. Coscolla, M. & Gagneux, S. Consequences of genomic diversity in mycobacterium tuberculosis. *Semin. Immunol.* **26**, 431–444 (2014).
4. Brites, D. & Gagneux, S. The Nature and Evolution of Genomic Diversity in the Mycobacterium tuberculosis Complex. in *Strain Variation in the Mycobacterium tuberculosis Complex: Its role in Biology, Epidemiology and Control* vol. 1019 1–26 (2017).
5. de Jong, B. C., Antonio, M. & Gagneux, S. Mycobacterium africanum-review of an important cause of human tuberculosis in West Africa. *PLoS Negl. Trop. Dis.* **4**, (2010).
6. Firdessa, R. et al. Mycobacterial lineages causing pulmonary and extrapulmonary Tuberculosis, Ethiopia. *Emerg. Infect. Dis.* **19**, 460–463 (2013).
7. Ernst, J. D. The immunological life cycle of tuberculosis. *Nat. Rev. Immunol.* **12**, 581–591 (2012).
8. Smith, N. H. et al. Ecotypes of the Mycobacterium tuberculosis complex. *J. Theor. Biol.* **239**, 220–225 (2006).
9. WHO. The end TB strategy. 2015.
10. WHO. Global tuberculosis report 2019. Geneva: World Health Organization, 2019.
11. Duffy, S. C. et al. Reconsidering Mycobacterium bovis as a proxy for zoonotic tuberculosis: a molecular epidemiological surveillance study. *The Lancet Microbe* **1**, e66–e73 (2020).
12. Kirchheimer, W. . & Storrs, E. . Attempts to establish the armadillo (Dasypus novemcinctus Linn.) as a model for the study of leprosy. I. Report of lepromatoid leprosy in an experimentally infected armadillo. *Int. J. Lepr. Other Mycobact. Dis.* **39**, 693–702 (1971).
13. Cole, S. T. et al. Massive gene decay in the leprosy bacillus. *Nature* **409**, 1007–1011 (2001).

14. Van Spanning, R. J. M. et al. Methanotrophy by a Mycobacterium species that dominates a cave microbial ecosystem. *Nat. Microbiol.* (2022) doi:10.1038/s41564-022-01252-3.
15. Sharma, R. et al. Zoonotic leprosy in the southeastern United States. *Emerg. Infect. Dis.* **21**, 2127–2134 (2015).
16. Runyon, E. . Anonymous mycobacteria in pulmonary disease. *Med. Clin. North Am.* **43**, 273–290 (1959).
17. Woese, C. R. Bacterial evolution. *Microbiol. Rev.* **51**, 221–271 (1987).
18. Prasanna, A. N. & Mehra, S. Comparative Phylogenomics of Pathogenic and Nonpathogenic Species. *PLoS One* **8**, e71248 (2013).
19. van Ingen, J., Turenne, C. Y., Tortoli, E., Wallace Jr, R. J. & Brown-Elliott, B. A. A definition of the Mycobacterium avium complex for taxonomical and clinical purposes, a review. *Int. J. Syst. Evol. Microbiol.* **68**, 3666–3677 (2018).
20. van Ingen, J. et al. Global outbreak of severe Mycobacterium chimaera disease after cardiac surgery: a molecular epidemiological study. *Lancet Infect. Dis.* **17**, 1033–1041 (2017).
21. Hermon-Taylor, J. Mycobacterium avium subspecies paratuberculosis, Crohn's disease and the Doomsday scenario. *Gut Pathog.* **1**, 15 (2009).
22. Van Ingen, J., Turenne, C. Y., Tortoli, E., Wallace, R. J. & Brown-Elliott, B. A. A definition of the Mycobacterium avium complex for taxonomical and clinical purposes, a review. *Int. J. Syst. Evol. Microbiol.* **68**, 3666–3677 (2018).
23. Aronson, J. D. Spontaneous tuberculosis in salt water fish. *J. Infect. Dis.* **39**, 315–320 (1926).
24. Renshaw, S. A. & Trede, N. S. A model 450 million years in the making: Zebrafish and vertebrate immunity. *Dis. Model. Mech.* **5**, 38–47 (2012).
25. Myllymäki, H., Bäuerlein, C. A. & Rämet, M. The zebrafish breathes new life into the study of tuberculosis. *Front. Immunol.* **7**, (2016).
26. Swaim, L. E. et al. Mycobacterium marinum infection of adult zebrafish causes caseating granulomatous tuberculosis and is moderated by adaptive immunity. *Infect. Immun.* **74**, 6108–6117 (2006).
27. Prouty, M. G., Correa, N. E., Barker, L. P., Jagadeeswaran, P. & Klose, K. E. Zebrafish-Mycobacterium marinum model for mycobacterial pathogenesis. *FEMS Microbiol. Lett.*

225, 177–182 (2003).

28. Semret, M., Koromihis, G., Maclean, J. D., Libman, M. & Ward, B. J. Mycobacterium ulcerans infection (Buruli ulcer): First reported case in a traveler. *Am. J. Trop. Med. Hyg.* **61**, 689–693 (1999).
29. Werf, T. S. Van Der, Graaf, W. T. A. Van Der, Tappero, J. W. & Asiedu, K. Mycobacterium ulcerans infection. *Lancet* **354**, 1013–1018 (1999).
30. Deshayes, C. et al. Regulation of Mycolactone, the Mycobacterium ulcerans Toxin, Depends on Nutrient Source. *PLoS Negl. Trop. Dis.* **7**, (2013).
31. Corbett, E. L. et al. Risk factors for pulmonary mycobacterial disease in south african gold miners: A case-control study. *Am. J. Respir. Crit. Care Med.* **159**, 94–99 (1999).
32. Lillo, M., Orengo, S., Cernoch, P. & R.L, H. Pulmonary and disseminated infection due to Mycobacterium kansasii: a decade of experience. *Rev. Infect. Dis.* **12**, 760–767 (1990).
33. Veyrier, F., Pletzer, D., Turenne, C. & Behr, M. A. Phylogenetic detection of horizontal gene transfer during the step-wise genesis of Mycobacterium tuberculosis. *BMC Evol. Biol.* **9**, 1–14 (2009).
34. Wang, J. et al. Insights on the emergence of Mycobacterium tuberculosis from the analysis of Mycobacterium kansasii. *Genome Biol. Evol.* **7**, 856–870 (2015).
35. Ghanem, M. et al. Heterologous production of 1-tuberculosinyladenosine in mycobacterium kansasii models pathoevolution towards the transcellular lifestyle of mycobacterium tuberculosis. *MBio* **11**, 1–15 (2020).
36. Wolinsky, E. Mycobacterial Diseases Other Than Tuberculosis. *Clin. Infect. Dis.* **15**, 1–12 (1998).
37. Nessar, R., Cambau, E., Reyrat, J. M., Murray, A. & Gicquel, B. Mycobacterium abscessus: A new antibiotic nightmare. *J. Antimicrob. Chemother.* **67**, 810–818 (2012).
38. Byrd, T. F. & Ryan, K. Mycobacterium abscessus: Shapeshifter of the Mycobacterial World. *Front. Microbiol.* **9**, (2018).
39. Gupta, R. S., Lo, B. & Son, J. Phylogenomics and comparative genomic studies robustly support division of the genus Mycobacterium into an emended genus Mycobacterium and four novel genera. *Front. Microbiol.* **9**, 67 (2018).
40. Reyrat, J. M. & Kahn, D. Mycobacterium smegmatis : an absurd model for tuberculosis? *TRENDS Microbiol.* **9**, 472–473 (2001).

41. Shiloh, M. U. & DiGiuseppe Champion, P. A. To catch a killer. What can mycobacterial models teach us about Mycobacterium tuberculosis pathogenesis? *Curr. Opin. Microbiol.* **13**, 86–92 (2010).
42. Moore, M. & Frerichs, J. B. An unusual acid-fast infection of the knee with subcutaneous, abscess-like lesions of the gluteal region; report of a case with a study of the organism, Mycobacterium abscessus, n. sp. *J. Invest. Dermatol.* **20**, 133–169 (1953).
43. Kubica, G. P. et al. A co-operative numerical analysis of rapidly growing mycobacteria. *J. Gen. Microbiol.* **73**, 55–70 (1972).
44. Levy-Frebault, V., Grimont, F., Grimont, P. A. D. & David, H. L. Deoxyribonucleic acid relatedness study of the Mycobacterium fortuitum-Mycobacterium chelonae complex. *Int. J. Syst. Bacteriol.* **36**, 458–460 (1986).
45. Kusunoki, S. & Ezaki, T. and Elevation of Mycobacterium chelonae subsp . abscessus (Kubica et al .) to Species Status : Mycobacterium abscessus comb . nov . *Int. J. Syst. Bacteriol.* 240–245 (1992).
46. Tortoli, E. Microbiological features and clinical relevance of new species of the genus Mycobacterium. *Clin. Microbiol. Rev.* **27**, 727–752 (2014).
47. Tortoli, E. et al. Emended description of mycobacterium abscessus mycobacterium abscessus subsp. Abscessus and mycobacterium abscessus subsp. bolletii and designation of mycobacterium abscessus subsp. massiliense comb. nov. *Int. J. Syst. Evol. Microbiol.* **66**, 4471–4479 (2016).
48. Adékambi, T., Berger, P., Raoult, D. & Drancourt, M. rpoB gene sequence-based characterization of emerging non-tuberculous mycobacteria with descriptions of Mycobacterium bolletii sp. nov., Mycobacterium phocaicum sp. nov. and Mycobacterium aubagnense sp. nov. *Int. J. Syst. Evol. Microbiol.* **56**, 133–143 (2006).
49. Adékambi, T. et al. Amoebal coculture of 'Mycobactenum massiliense' sp. nov. from the sputum of a patient with hemoptoic pneumonia. *J. Clin. Microbiol.* **42**, 5493–5501 (2004).
50. Leao, S. C., Tortoli, E., Paul Euzé, J. & Garcia, M. J. Proposal that Mycobacterium massiliense and Mycobacterium bolletii be united and reclassified as Mycobacterium abscessus subsp. bolletii comb. nov., designation of Mycobacterium abscessus subsp. abscessus subsp. nov. and emended description of Mycobacteri. *Int. J. Syst. Evol. Microbiol.* **61**, 2311–2313 (2011).

51. Johansen, M. D., Herrmann, J.-L. & Kremer, L. Non-tuberculous mycobacteria and the rise of Mycobacterium abscessus. *Nat. Rev. Microbiol.* **18**, 392–407 (2020).
52. Victoria, L., Gupta, A., Gómez, J. L. & Robledo, J. Mycobacterium abscessus complex: A Review of Recent Developments in an Emerging Pathogen. *Front. Cell. Infect. Microbiol.* **11**, 1–8 (2021).
53. Stout, J. E., Koh, W. J. & Yew, W. W. Update on pulmonary disease due to non-tuberculous mycobacteria. *Int. J. Infect. Dis.* **45**, 123–134 (2016).
54. Kendall, B. A. & Winthrop, K. L. Update on the epidemiology of pulmonary nontuberculous mycobacterial infections. *Semin. Respir. Crit. Care Med.* **34**, 87–94 (2013).
55. Dahl, V. N. et al. Global trends of pulmonary infections with nontuberculous mycobacteria: a systematic review. *Int. J. Infect. Dis.* (2022) doi:10.1016/j.ijid.2022.10.013.
56. Waglechner, N. et al. Genomic epidemiology of Mycobacterium abscessus in a Canadian cystic fibrosis centre. *Sci. Rep.* **12**, (2022).
57. Feazel, L. M. et al. Opportunistic pathogens enriched in showerhead biofilms. *Proc. Natl. Acad. Sci. U. S. A.* **106**, 16393–16398 (2009).
58. Zignol, M. et al. Twenty Years of Global Surveillance of Antituberculosis-Drug Resistance. *N. Engl. J. Med.* **375**, 1081–1089 (2016).
59. Marras, T. K., Mendelson, D., Marchand-Austin, A., May, K. & Jamieson, F. B. Pulmonary nontuberculous mycobacterial disease, Ontario, Canada, 1998-2010. *Emerg. Infect. Dis.* **19**, 1889–1891 (2013).
60. Moore, J. E., Kruijshaar, M. E., Ormerod, L. P., Drobniewski, F. & Abubakar, I. Increasing reports of non-tuberculous mycobacteria in England, Wales and Northern Ireland, 1995-2006. *BMC Public Health* **10**, (2010).
61. Lai, C. C. et al. Increasing incidence of nontuberculous mycobacteria, Taiwan, 2000-2008. *Emerg. Infect. Dis.* **16**, 294–296 (2010).
62. Thomson, R. M. Changing epidemiology of pulmonary nontuberculous mycobacteria infections. *Emerg. Infect. Dis.* **16**, 1576–1583 (2010).
63. Winthrop, K. L. et al. Pulmonary nontuberculous mycobacterial disease prevalence and clinical features: An emerging public health disease. *Am. J. Respir. Crit. Care Med.* **182**,

977–982 (2010).

64. Prevots, D. R. et al. Nontuberculous mycobacterial lung disease prevalence at four integrated health care delivery systems. *Am. J. Respir. Crit. Care Med.* **182**, 970–976 (2010).

65. Adjemian, J., Olivier, K. N., Seitz, A. E., Holland, S. M. & Prevots, D. R. Prevalence of nontuberculous mycobacterial lung disease in U.S. medicare beneficiaries. *Am. J. Respir. Crit. Care Med.* **185**, 881–886 (2012).

66. Winthrop, K. L. et al. Mycobacterial diseases and antitumour necrosis factor therapy in USA. *Ann. Rheum. Dis.* **72**, 37–42 (2013).

67. Donohue, M. J. & Wymer, L. Increasing prevalence rate of nontuberculous mycobacteria infections in five states, 2008-2013. *Ann. Am. Thorac. Soc.* **13**, 2143–2150 (2016).

68. Lee, M. R. et al. Mycobacterium abscessus complex infections in humans. *Emerg. Infect. Dis.* **21**, 1638–1646 (2015).

69. Cassidy, P. M., Hedberg, K., Saulson, A., McNelly, E. & Winthrop, K. L. Nontuberculous Mycobacterial Disease Prevalence and Risk Factors: A Changing Epidemiology. *Clin. Infect. Dis.* **49**, e124–e129 (2009).

70. Zweijpfenning, S. M. H., Ingen, J. Van & Hoefsloot, W. Geographic Distribution of Nontuberculous Mycobacteria Isolated from Clinical Specimens: A Systematic Review. *Semin. Respir. Crit. Care Med.* **39**, 336–342 (2018).

71. Koh, W. J., Stout, J. E. & Yew, W. W. Advances in the management of pulmonary disease due to Mycobacterium abscessus complex. *Int. J. Tuberc. Lung Dis.* **18**, 1141–1148 (2014).

72. Koh, W. J. et al. Clinical significance of differentiation of Mycobacterium massiliense from Mycobacterium abscessus. *Am. J. Respir. Crit. Care Med.* **183**, 405–410 (2011).

73. Jones, R. S., Shier, K. L., Master, R. N., Bao, J. R. & Clark, R. B. Current significance of the Mycobacterium chelonae-abscessus group. *Diagn. Microbiol. Infect. Dis.* **94**, 248–254 (2019).

74. Covert, T. C., Rodgers, M. R., Reyes, A. L. & Stelma, G. N. Occurrence of nontuberculous mycobacteria in environmental samples. *Appl. Environ. Microbiol.* **65**, 2492–2496 (1999).

75. Steingrube, V. A., Wallace, R. J., Steele, L. C. & Pang, Y. Mercuric reductase activity and

evidence of broad-spectrum mercury resistance among clinical isolates of rapidly growing mycobacteria. *Antimicrob. Agents Chemother.* **35**, 819–823 (1991).

76. Brown-Elliott, B. A. & Wallace, R. J. Clinical and Taxonomic Status of Pathogenic Nonpigmented or Late-Pigmenting Rapidly Growing Mycobacteria. *Clin. Microbiol. Rev.* **15**, 716–746 (2002).
77. Girgis, D. O., Karp, C. L. & Miller, D. Ocular infections caused by non-tuberculous mycobacteria: Update on epidemiology and management. *Clin. Exp. Ophthalmol.* **40**, 467–475 (2012).
78. Sfeir, M. et al. Mycobacterium abscessus complex infections: A retrospective cohort study. *Open Forum Infect. Dis.* **5**, (2018).
79. Esther, C. R., Esserman, D. A., Gilligan, P., Kerr, A. & Noone, P. G. Chronic Mycobacterium abscessus infection and lung function decline in cystic fibrosis. *J. Cyst. Fibros.* **9**, 117–123 (2010).
80. Sermet-Gaudelus, I. et al. Mycobacterium abscessus and Children with Cystic Fibrosis. *Emerg. Infect. Dis.* **9**, 1587–1591 (2003).
81. Floto, R. A. et al. US Cystic Fibrosis Foundation and European Cystic Fibrosis Society consensus recommendations for the management of non-tuberculous mycobacteria in individuals with cystic fibrosis. *Thorax* **71**, i1–i22 (2016).
82. Bange, F. C., Kirschner, P. & Böttger, E. C. Recovery of mycobacteria from patients with cystic fibrosis. *J. Clin. Microbiol.* **37**, 3761–3763 (1999).
83. Roux, A. L. et al. Multicenter study of prevalence of nontuberculous mycobacteria in patients with cystic fibrosis in France. *J. Clin. Microbiol.* **47**, 4124–4128 (2009).
84. Shteinberg, M., Haq, I. J., Polineni, D. & Davies, J. C. Cystic fibrosis. *Lancet* **397**, 2195–2211 (2021).
85. Ratjen, F. et al. Cystic fibrosis. *Nat. Rev. Dis. Prim.* **1**, 15010 (2015).
86. Bernut, A. et al. CFTR Protects against Mycobacterium abscessus Infection by Fine-Tuning Host Oxidative Defenses. *Cell Rep.* **26**, 1828-1840.e4 (2019).
87. Bernut, A. et al. Mycobacterium abscessus cording prevents phagocytosis and promotes abscess formation. *Proc. Natl. Acad. Sci. U. S. A.* **111**, (2014).
88. Bernut, A. et al. In Vivo assessment of drug efficacy against Mycobacterium abscessus using the embryonic zebrafish test system. *Antimicrob. Agents Chemother.* **58**, 4054–4063

(2014).

89. Guimbellot, J. S., Acosta, E. P. & Rowe, S. M. Sensitivity of ivacaftor to drug-drug interactions with rifampin, a cytochrome P450 3A4 inducer. *Pediatr. Pulmonol.* **53**, E6–E8 (2018).
90. Ganapathy, U. S., Dartois, V. & Dick, T. Repositioning rifamycins for Mycobacterium abscessus lung disease. *Expert Opin. Drug Discov.* **14**, 867–878 (2019).
91. Lilic, M. et al. The antibiotic sorangicin A inhibits promoter DNA unwinding in a Mycobacterium tuberculosis rifampicin-resistant RNA polymerase. *Proc. Natl. Acad. Sci. U. S. A.* **117**, 30423–30432 (2020).
92. Behr, M., Jarand, J. & Marras, T. K. *Canadian Tuberculosis Standards Chapter 11: Nontuberculous Mycobacteria*. http://www.phac-aspc.gc.ca/tbpc-latb/pubs/tb-canada-7/assets/pdf/tb-standards-tb-normes-ch11-eng.pdf (2014).
93. Prevots, D. R. & Marras, T. K. Epidemiology of Human Pulmonary Infection with Non-Tuberculous Mycobacteria. *Clin. Chest Med.* **36**, 13–34 (2015).
94. Susceptibility Testing of Mycobacteria, Nocardiae, and Other Aerobic Actinomycetes; Approved Standard (CLSI). (2011).
95. Daley, C. L. et al. Treatment of nontuberculous mycobacterial pulmonary disease: An official ats/ers/escmid/idsa clinical practice guideline. *Clin. Infect. Dis.* **71**, E1–E36 (2020).
96. Haworth, C. S. et al. British Thoracic Society guidelines for the management of non-tuberculous mycobacterial pulmonary disease (NTM-PD). *Thorax* **72**, ii1–ii64 (2017).
97. Nash, K. A., Brown-Elliott, A. B. & Wallace, R. J. A Novel gene, erm(41), confers inducible macrolide resistance to clinical isolates of mycobacterium abscessus but is absent from mycobacterium chelonae. *Antimicrob. Agents Chemother.* **53**, 1367–1376 (2009).
98. Caimmi, D. et al. Positive Effect of Liposomal Amikacin for Inhalation on Mycobacterium abcessus in Cystic Fibrosis Patients. *Open Forum Infect. Dis.* (2018) doi:10.1093/ofid/ofy034.
99. Novosad, S. A., Beekmann, S. E., Polgreen, P. M., Mackey, K. & Winthrop, K. L. Treatment of mycobacterium abscessus infection. *Emerg. Infect. Dis.* **22**, 511–514 (2016).
100. Haworth, C. S., Bilton, D. & Elborn, J. S. Long-term macrolide maintenance therapy in

non-CF bronchiectasis: Evidence and questions. *Respir. Med.* **108**, 1397–1408 (2014).

101. Wang, D., Fu, W. & Dai, J. Meta-analysis of macrolide maintenance therapy for prevention of disease exacerbations in patients with noncystic fibrosis bronchiectasis. *Medicine (Baltimore).* **98**, (2019).
102. MRC. Streptomycin treatment of pulmonary tuberculosis. *Br. Med. J.* **2**, 769–782 (1948).
103. Yam, Y. K., Alvarez, N., Go, M. L. & Dick, T. Extreme Drug Tolerance of Mycobacterium abscessus "Persisters". *Front. Microbiol.* **11**, (2020).
104. Pasipanodya, J. G. et al. Systematic review and meta-analyses of the effect of chemotherapy on pulmonary mycobacterium abscessus outcomes and disease recurrence. *Antimicrob. Agents Chemother.* **61**, (2017).
105. Nasiri, M. J. et al. New insights in to the intrinsic and acquired drug resistance mechanisms in mycobacteria. *Front. Microbiol.* **8**, (2017).
106. Brennan, P. J. & Nikaido, H. The envelope of mycobacteria. *Annu. Rev. Biochem.* **64**, 29–63 (1995).
107. Jarlier, V. & Nikaido, H. Mycobacterial cell wall: Structure and role in natural resistance to antibiotics. *FEMS Microbiol. Lett.* **123**, 11–18 (1994).
108. Wu, M. L., Aziz, D. B., Dartois, V. & Dick, T. NTM drug discovery: status, gaps and the way forward. *Drug Discov. Today* **0**, 1–18 (2018).
109. Alcaide, F., Pfyffer, G. E. & Telenti, A. Role of embB in natural and acquired resistance to ethambutol in mycobacteria. *Antimicrob. Agents Chemother.* **41**, 2270–2273 (1997).
110. Fox, H. H. The chemical approach to the control of tuberculosis. *Science (80-.).* **116**, 129–134 (1952).
111. Long, E. R. *The Chemistry and Chemotherapy of Tuberculosis*. (Williams & Wilkins, Baltimore, 1958).
112. Chakraborty, S. & Rhee, K. Y. Tuberculosis drug development: History and evolution of the mechanism-based paradigm. *Cold Spring Harb. Perspect. Med.* **5**, 1–11 (2015).
113. Vilchèze, C. & Jacobs, W. R. The mechanism of isoniazid killing: Clarity through the scope of genetics. *Annu. Rev. Microbiol.* **61**, 35–50 (2007).
114. Vilchèze, C. et al. Transfer of a point mutation in Mycobacterium tuberculosis inhA resolves the target of isoniazid. *Nat. Med.* **12**, 1027–1029 (2006).
115. Mdluli, K. et al. Inhibition of mycobacterium tuberculosis beta-ketoacyl ACP synthase by

isoniazid. *Science (80-.).* **280**, 1607–1610 (1998).

116. Mdluli, K. et al. Biochemical and genetic data suggest that InhA is not the primary target for activated isoniazid in Mycobacterium tuberculosis. *J. Infect. Dis.* **174**, 1085–1090 (1996).
117. Slayden, R. A., Lee, R. E. & Barry, C. E. Isoniazid affects multiple components of the type II fatty acid synthase system of Mycobacterium tuberculosis. *Mol. Microbiol.* **38**, 514–525 (2000).
118. Viljoen, A., Viela, F., Kremer, L. & Dufrêne, Y. F. Fast chemical force microscopy demonstrates that glycopeptidolipids define nanodomains of varying hydrophobicity on mycobacteria. *Nanoscale Horizons* **5**, 944–953 (2020).
119. Xu, Z., Meshcheryakov, V. A., Poce, G. & Chng, S. S. MmpL3 is the flippase for mycolic acids in mycobacteria. *Proc. Natl. Acad. Sci. U. S. A.* **114**, 7993–7998 (2017).
120. Li, W. et al. Novel insights into the mechanism of inhibition of MmpL3, a target of multiple pharmacophores in Mycobacterium tuberculosis. *Antimicrob. Agents Chemother.* **58**, 6413–6423 (2014).
121. Jarlier, V. & Nikaido, H. Permeability barrier to hydrophilic solutes in Mycobacterium chelonei. *J. Bacteriol.* **172**, 1418–1423 (1990).
122. Jarlier, V., Gutmann, L. & Nikaido3, H. Interplay of Cell Wall Barrier and r-Lactamase Activity Determines High Resistance to 3-Lactam Antibiotics in Mycobacterium chelonae. *Antimicrob. Agents Chemother.* **35**, 1937–1939 (1991).
123. Ramírez, A. et al. Biochemical characterization of β-lactamases from mycobacterium abscessus complex and genetic environment of the β-lactamase-encoding gene. *Microb. Drug Resist.* **23**, 294–300 (2017).
124. Story-Roller, E., Maggioncalda, E. C., Cohen, K. A. & Lamichhane, G. Mycobacterium abscessus and β-Lactams: Emerging Insights and Potential Opportunities. *Front. Microbiol.* **9**, (2018).
125. Black, P. A. et al. Energy metabolism and drug efflux in mycobacterium tuberculosis. *Antimicrobial Agents and Chemotherapy* vol. 58 2491–2503 (2014).
126. Buroni, S. et al. Insights on Mycobacterium leprae Efflux Pumps and Their Implications in Drug Resistance and Virulence. *Front. Microbiol. | www.frontiersin.org* **9**, 3072 (2018).
127. Richard, M., Gutiérrez, A. V., Viljoen, Albertus JGhigo, E., Blaise, M. & Kremer, L.

Mechanistic and Structural Insights Into the Unique TetR-Dependent Regulation of a Drug Efflux Pump in Mycobacterium abscessus. *Front. Microbiol.* **9**, (2018).

128. Blair, J. M. & Piddock, L. J. Structure, function and inhibition of RND efflux pumps in Gram-negative bacteria: an update. *Curr. Opin. Microbiol.* **12**, (2009).
129. Viljoen, A. et al. The diverse family of MmpL transporters in mycobacteria: from regulation to antimicrobial developments. *Mol. Microbiol.* **104**, 889–904 (2017).
130. Gutiérrez, A. V. et al. Glycopeptidolipids , a Double-Edged Sword of the Mycobacterium abscessus Complex. *Front. Immunol.* **9**, 1–8 (2018).
131. Gutiérrez, A. V., Richard, M., Roquet-Banères, F., Viljoen, A. & Kremer, L. The TetR Family Transcription Factor MAB_2299c Regulates the Expression of Two Distinct MmpS-MmpL Efflux Pumps Involved in Cross-Resistance to Clofazimine and Bedaquiline in Mycobacterium abscessus. *Antimicrob. Agents Chemother.* **63**, (2019).
132. Hartkoorn, R. C., Uplekar, S. & Cole, S. T. Cross-resistance between clofazimine and bedaquiline through upregulation of mmpl5 in mycobacterium tuberculosis. *Antimicrob. Agents Chemother.* **58**, 2979–2981 (2014).
133. Chen, C. et al. Verapamil targets membrane energetics in mycobacterium tuberculosis. *Antimicrob. Agents Chemother.* **62**, (2018).
134. Pule, C. M. et al. Efflux pump inhibitors: Targeting mycobacterial efflux systems to enhance TB therapy. *J. Antimicrob. Chemother.* **71**, 17–26 (2016).
135. Szumowski, J. D., Adams, K. N., Edelstein, P. H. & Ramakrishnan, L. Antimicrobial efflux pumps and Mycobacterium tuberculosis drug tolerance: Evolutionary considerations. *Curr. Top. Microbiol. Immunol.* **374**, 81–108 (2013).
136. Adams, K. N., Szumowski, J. D. & Ramakrishnan, L. Verapamil, and its metabolite norverapamil, inhibit macrophage-induced, bacterial efflux pump-mediated tolerance to multiple anti-tubercular drugs. *J. Infect. Dis.* **210**, 456–466 (2014).
137. Xu, J. et al. Verapamil increases the bioavailability and efficacy of bedaquiline but not clofazimine in a murine model of tuberculosis. *Antimicrob. Agents Chemother.* AAC.01692-17 (2017) doi:10.1128/AAC.01692-17.
138. Egorov, A. M., Ulyashova, M. M. & Rubtsova, M. Y. Bacterial enzymes and antibiotic resistance. *Acta Naturae* **10**, 33–48 (2018).
139. Van Ingen, J., Boeree, M. J., Van Soolingen, D. & Mouton, J. W. Resistance mechanisms

and drug susceptibility testing of nontuberculous mycobacteria. *Drug Resist. Updat.* **15**, 149–161 (2012).

140. Sanz-García, F. et al. Mycobacterial Aminoglycoside Acetyltransferases: A Little of Drug Resistance, and a Lot of Other Roles. *Front. Microbiol.* **10**, (2019).
141. Ripoll, F. et al. Non mycobacterial virulence genes in the genome of the emerging pathogen Mycobacterium abscessus. *PLoS One* **4**, (2009).
142. Luthra, S., Rominski, A. & Sander, P. The Role of Antibiotic-Target-Modifying and Antibiotic-Modifying Enzymes in Mycobacterium abscessus Drug Resistance. *Front. Microbiol.* **9**, (2018).
143. Ung, K. L., Alsarraf, H. M. A. B., Olieric, V., Kremer, L. & Blaise, M. Crystal structure of the aminoglycosides N-acetyltransferase Eis2 from Mycobacterium abscessus. *FEBS J.* **286**, 4342–4355 (2019).
144. Lam Ung, K., Kremer, L. & Blaise, M. Structural analysis of the N-acetyltransferase Eis1 from Mycobacterium abscessus reveals the molecular determinants of its incapacity to modify aminoglycosides. Running title: Crystal structure of M. abscessus Eis1. *Proteins Struct. Funct. Bioinforma.* (2020) doi:10.1002/prot.25997.
145. Davies, J. & Wright, G. D. Bacterial resistance to amlnoglycoside antibiotics. *Trends Microbiol.* **5**, 234–240 (1997).
146. Rothstein, D. M. Rifamycins, alone and in combination. *Cold Spring Harb. Perspect. Med.* **6**, (2016).
147. Campbell, E. A. et al. Structural Mechanism for Rifampicin Inhibition of Bacterial RNA Polymerase. *Cell* **104**, 901–912 (2001).
148. Rominski, A., Roditscheff, A., Selchow, P., Böttger, E. C. & Sander, P. Intrinsic rifamycin resistance of Mycobacterium abscessus is mediated by ADP-ribosyltransferase MAB_0591. *J. Antimicrob. Chemother.* **72**, 376–384 (2017).
149. Aziz, D. B. et al. Rifabutin Is active against mycobacterium abscessus complex. *Antimicrob. Agents Chemother.* **61**, (2017).
150. Dick, T., Shin, S. J., Koh, W. J., Dartois, V. & Gengenbacher, M. Rifabutin is active against mycobacterium abscessus in mice. *Antimicrob. Agents Chemother.* **64**, (2020).
151. Schäfle, D. et al. Rifabutin is inactivated by mycobacterium abscessus arr. *Antimicrob. Agents Chemother.* **65**, (2021).

152. Lan, T. et al. Redesign of Rifamycin Antibiotics to Overcome ADP-Ribosylation-Mediated Resistance. *Angew. Chemie Int. Ed.* (2022) doi:10.1002/ANIE.202211498.
153. Rudra, P., Hurst-Hess, K., Lappierre, P. & Ghosha, P. High levels of intrinsic tetracycline resistance in mycobacterium abscessus are conferred by a tetracycline-modifying monooxygenase. *Antimicrob. Agents Chemother.* **62**, (2018).
154. Reeves, A. Z. et al. Aminoglycoside cross-resistance in Mycobacterium tuberculosis due to mutations in the 5′ untranslated region of whiB7. *Antimicrob. Agents Chemother.* **57**, 1857–1865 (2013).
155. Sullivan, J. R. et al. Efficacy of epetraborole against Mycobacterium abscessus is increased with norvaline. *PLoS Pathog.* **17**, 1–28 (2021).
156. The History of Antibiotics. *Microbiology Society* https://microbiologysociety.org/members-outreach-resources/outreach-resources/antibiotics-unearthed/antibiotics-and-antibiotic-resistance/the-history-of-antibiotics.html.
157. Hamad, B. The antibiotics market. *Nat. Rev. Drug Discov.* **9**, 675–676 (2010).
158. Wietzerbin, J. et al. Occurrence of D-alanyl-(D)-meso-diaminopimelic acid and meso-diaminopimelyl-meso-diaminopimelic acid interpeptide linkages in the peptidoglycan of mycobacteria. *Biochemistry* **13**, 3471–3476 (1974).
159. Lavollay, M. et al. The peptidoglycan of Mycobacterium abscessus is predominantly cross-linked by L,D-transpeptidases. *J. Bacteriol.* **193**, 778–782 (2011).
160. Kumar, P. et al. Mycobacterium abscessus L,D- Transpeptidases Are Susceptible to Inactivation by Carbapenems and Cephalosporins but Not Penicillins. *Antibiotics* **61**, (2017).
161. Kumar, P. et al. Non-classical transpeptidases yield insight into new antibacterials. *Nat. Chem. Biol.* **13**, 54–61 (2017).
162. Rominski, A., Schulthess, B., Müller, D. M., Keller, P. M. & Sander, P. Effect of β-lactamase production and β-lactam instability on MIC testing results for Mycobacterium abscessus. *J. Antimicrob. Chemother.* **72**, 3070–3078 (2017).
163. Soroka, D. et al. Characterization of broad-spectrum mycobacterium abscessus class A β-lactamase. *J. Antimicrob. Chemother.* **69**, 691–696 (2014).
164. Wang, F., Cassidy, C. & Sacchettini, J. C. Crystal structure and activity studies of the

Mycobacterium tuberculosis β-lactamase reveal its critical role in resistance to β-lactam antibiotics. *Antimicrob. Agents Chemother.* **50**, 2762–2771 (2006).

165. Dubée, V. et al. β-Lactamase inhibition by avibactam in Mycobacterium abscessus. *J. Antimicrob. Chemother.* **70**, 1051–1058 (2014).
166. Negatu, D. A., Zimmerman, M. D., Dartois, V. & Dick, T. Strongly Bactericidal All-Oral b-Lactam Combinations for the Treatment of Mycobacterium abscessus Lung Disease. *Antimicrob. Agents Chemother.* **66**, (2022).
167. Svetlov, M. S. et al. Structure of Erm-modified 70S ribosome reveals the mechanism of macrolide resistance. *Nat. Chem. Biol.* **17**, 412–420 (2021).
168. Wallace, R. J. et al. Genetic basis for clarithromycin resistance among isolates of Mycobacterium chelonae and Mycobacterium abscessus. *Antimicrob. Agents Chemother.* **40**, 1676–1681 (1996).
169. Mougari, F. et al. Selection of resistance to clarithromycin in Mycobacterium abscessus subspecies. *Antimicrob. Agents Chemother.* **61**, (2017).
170. Bronson, R. A. et al. Global phylogenomic analyses of Mycobacterium abscessus provide context for non cystic fibrosis infections and the evolution of antibiotic resistance. *Nat. Commun.* **12**, (2021).
171. Maurer, F. P., Castelberg, C., Quiblier, C., Böttger, E. C. & Somosközi, A. Erm(41)-dependent inducible resistance to azithromycin and clarithromycin in clinical isolates of mycobacterium abscessus. *J. Antimicrob. Chemother.* **69**, 1559–1563 (2014).
172. Kwak, J.-H., Choi, E.-C. & Weisblum, B. Transcriptional Attenuation Control of ermK, a Macrolide-Lincosamide-Streptogramin B Resistance Determinant from Bacillus licheniformis. *J. Bacteriol.* **173**, 4725–4735 (1991).
173. Min, Y.-H., Kwon, A.-R., Yoon, E.-J., Shim, M.-J. & Choi, E.-C. Translational Attenuation and mRNA Stabilization as Mechanisms of erm(B) Induction by Erythromycin. *Antimicrob. Agents Chemother.* **52**, 1782–1789 (2008).
174. Weisblum, B. Insights into Erythromycin Action from Studies of Its Activity as Inducer of Resistance. *Antimicrob. Agents Chemother.* **39**, 797–805 (1995).
175. Morris, R. P. et al. Ancestral antibiotic resistance in Mycobacterium tuberculosis. *Proc. Natl. Acad. Sci. U. S. A.* **102**, 12200–5 (2005).
176. Burian, J. et al. The mycobacterial transcriptional regulator whiB7 gene links redox

homeostasis and intrinsic antibiotic resistance. *J. Biol. Chem.* **287**, 299–310 (2012).

177. Burian, J. et al. The mycobacterial antibiotic resistance determinant WhiB7 acts as a transcriptional activator by binding the primary sigma factor SigA (RpoV). *Nucleic Acids Res.* **41**, 10062–10076 (2013).
178. Miranda-CasoLuengo, A. A., Staunton, P. M., Dinan, A. M., Lohan, A. J. & Loftus, B. J. Functional characterization of the Mycobacterium abscessus genome coupled with condition specific transcriptomics reveals conserved molecular strategies for host adaptation and persistence. *BMC Genomics* **17**, 1–12 (2016).
179. Richard, M., Gutiérrez, A. V. & Kremer, L. Dissecting erm(41)-mediated macrolide-inducible resistance in mycobacterium abscessus. *Antimicrob. Agents Chemother.* **64**, (2020).
180. Hurst-Hess, K., Rudra, P. & Ghosh, P. Mycobacterium abscessus WhiB7 Regulates a Species-Specific Repertoire of Genes to Confer Extreme Antibiotic Resistance. *Antimicrob. Agents Chemother.* **61**, (2017).
181. Pryjma, M., Burian, J., Kuchinski, K. & Thompson, C. J. Antagonism between Front-Line Antibiotics Clarithromycin and Amikacin in the Treatment of Mycobacterium abscessus Infections Is Mediated by the whiB7 Gene. *Antimicrob. Agents Chemother.* **61**, (2017).
182. Ling, L. L. et al. A new antibiotic kills pathogens without detectable resistance. *Nature* **517**, 455–459 (2015).
183. Stokes, J. M. et al. A Deep Learning Approach to Antibiotic Discovery. *Cell* **180**, 688-702.e13 (2020).
184. Murray, C. J. et al. Global burden of bacterial antimicrobial resistance in 2019: a systematic analysis. *Lancet* **399**, 629–655 (2022).
185. McArthur, A. G. et al. The comprehensive antibiotic resistance database. *Antimicrob. Agents Chemother.* **57**, 3348–3357 (2013).
186. Alcock, B. P. et al. CARD 2020: Antibiotic resistome surveillance with the comprehensive antibiotic resistance database. *Nucleic Acids Res.* **48**, D517–D525 (2020).
187. WHO. Global Antimicrobial Resistance and Use Surveillance System (GLASS) Report. Geneva: World Health Organization, 2020.
188. Lawn, S. D. & Nicol, M. P. Xpert MTB/RIF assay: development, evaluation and implementation of a new rapid molecular diagnostic for tuberculosis and rifampicin

resistance. *Future Microbiol.* **6**, 1067–1082 (2011).

189. Marras, S. A. E. et al. A Molecular-Beacon-Based Multiplex Real-Time PCR Assay To Distinguish Mycobacterium abscessus Subspecies and Determine Macrolide Susceptibility. *J. Clin. Microbiol.* **59**, (2021).
190. Chong, S. L., Tan, J. L. & Ngeow, Y. F. The resistomes of Mycobacteroides abscessus complex and their possible acquisition from horizontal gene transfer. *BMC Genomics* **23**, 1–11 (2022).
191. Bryant, J. M. et al. Stepwise pathogenic evolution of Mycobacterium abscessus. *Science (80-.).* **372**, (2021).
192. Ruis, C. et al. Dissemination of Mycobacterium abscessus via global transmission networks. *Nat. Microbiol.* **6**, 1279–1288 (2021).
193. Edwards, A. & Morgan, M. Canada must develop an open and equitable pharmaceutical ecosystem for the next pandemic. *The Globe and Mail* (2021).
194. Aminov, R. I. A brief history of the antibiotic era: Lessons learned and challenges for the future. *Front. Microbiol.* **1**, (2010).
195. Hutchings, M., Truman, A. & Wilkinson, B. Antibiotics: past, present and future. *Curr. Opin. Microbiol.* **51**, 72–80 (2019).
196. Haas, L. Papyrus of Ebers and Smith. *J. Neurol. Neurosurg. Psychiatry* **67**, 572–578 (1999).
197. Bassett, E. J., Keith, M. S., Armelagos, G. J., Martin, D. L. & Villanueva, A. R. Tetracycline-labeled human bone from ancient Sudanese Nubia (A.D. 350). *Science (80-.).* **209**, 1532–1534 (1980).
198. Nelson, M. L., Dinardo, A., Hochberg, J. & Armelagos, G. J. Brief communication: Mass spectroscopic characterization of tetracycline in the skeletal remains of an ancient population from Sudanese Nubia 350-550 CE. *Am. J. Phys. Anthropol.* **143**, 151–154 (2010).
199. Ehrlich, P. & Hata, S. Die Experimentelle Chemotherapie der Spirilosen. *Berlin: Julius Springer* (1910).
200. Gelpi, A., Gilbertson, A. & Tucker, J. D. Magic bullet: Paul Ehrlich, Salvarsan and the birth of venereology. *Sex. Transm. Infect.* **91**, 68–69 (2015).
201. Fleming, A. On the Antibacterial Action of Cultures of a Penicillium, with Special

Reference to their Use in the Isolation of B. influenzae. *Br. J. Exp. Pathol.* **10**, 226–236 (1929).

202. Abraham, E. P. et al. FURTHER OBSERVATIONS ON PENICILLIN. *Lancet* 177–189 (1941).
203. Hodgkin, D. C. The X-ray analysis of the structure of penicillin. *Adv. Sci.* **6**, 85–89 (1949).
204. Abraham, E. P. & Chain, E. An Enzyme from Bacteria able to Destroy Penicillin. *Nature* **146**, 837 (1940).
205. Hug, J. J., Krug, D. & Müller, R. Bacteria as genetically programmable producers of bioactive natural products. *Nature Reviews Chemistry* vol. 4 172–193 (2020).
206. Crawford, J. M., Tang, G.-L. & Herzon, S. B. Natural Products: An Era of Discovery in Organic Chemistry. *J. Org. Chem.* **86**, 10943–10945 (2021).
207. Reymond, J. L. & Awale, M. Exploring chemical space for drug discovery using the chemical universe database. *ACS Chem. Neurosci.* **3**, 649–657 (2012).
208. Schneider, P. & Schneider, G. Privileged Structures Revisited. *Angew. Chemie - Int. Ed.* **56**, 7971–7974 (2017).
209. Rodrigues, T., Reker, D., Schneider, P. & Schneider, G. Counting on natural products for drug design. *Nat. Chem.* **8**, 531–541 (2016).
210. Hoffmann, T. et al. Correlating chemical diversity with taxonomic distance for discovery of natural products in myxobacteria. *Nat. Commun.* **9**, (2018).
211. Nützmann, H. W. et al. Active and repressed biosynthetic gene clusters have spatially distinct chromosome states. *Proc. Natl. Acad. Sci. U. S. A.* **117**, 13800–13809 (2020).
212. Wright, G. D. Opportunities for natural products in 21 st century antibiotic discovery. *Nat. Prod. Rep.* **34**, 694–701 (2017).
213. Nichols, D. et al. Use of ichip for high-throughput in situ cultivation of "uncultivable microbial species▽. *Appl. Environ. Microbiol.* **76**, 2445–2450 (2010).
214. Layre, E. et al. Molecular profiling of Mycobacterium tuberculosis identifies tuberculosinyl nucleoside products of the virulence-associated enzyme Rv3378c. *Proc. Natl. Acad. Sci. U. S. A.* **111**, 2978–2983 (2014).
215. Guimarães, A. C. et al. Antibacterial activity of terpenes and terpenoids present in essential oils. *Molecules* **24**, (2019).

216. Amirah Mahizan, N. et al. Terpene Derivatives as a Potential Agent against Antimicrobial Resistance (AMR) Pathogens. *Molecules* **24**, (2019).
217. Jefté, K. et al. Terpenes as bacterial efflux pump inhibitors : A systematic review. *Front. Pharmacol.* **13:953982**, (2022).
218. Davies, M. J. Terpenes boost antibiotic action. *Trends Biotechnol.* **19**, 488 (2001).
219. Sieniawska, E., Swatko-Ossor, M., Sawicki, R., Skalicka-Woźniak, K. & Ginalska, G. Natural Terpenes Influence the Activity of Antibiotics against Isolated Mycobacterium tuberculosis. *Med. Princ. Pract.* **26**, 108–112 (2017).
220. Ortega, M. A. & Van Der Donk, W. A. New Insights into the Biosynthetic Logic of Ribosomally Synthesized and Post-translationally Modified Peptide Natural Products. *Cell Chem. Biol.* **23**, 31–44 (2016).
221. Ting, C. P. et al. Use of a scaffold peptide in the biosynthesis of amino acid-derived natural products. *Science (80-.).* **365**, 280–284 (2019).
222. Jordan, P. A. & Moore, B. S. Biosynthetic Pathway Connects Cryptic Ribosomally Synthesized Posttranslationally Modified Peptide Genes with Pyrroloquinoline Alkaloids. *Cell Chem. Biol.* **23**, 1504–1514 (2016).
223. Huang, T. et al. Identification and characterization of the pyridomycin biosynthetic gene cluster of Streptomyces pyridomyceticus NRRL B-2517. *J. Biol. Chem.* **286**, 20648–20657 (2011).
224. Hartkoorn, R. C. et al. Towards a new tuberculosis drug: Pyridomycin - nature's isoniazid. *EMBO Mol. Med.* **4**, 1032–1042 (2012).
225. Alcaraz, M. et al. Efficacy and Mode of Action of a Direct Inhibitor of Mycobacterium abscessus InhA. *ACS Infect. Dis.* **8**, 2171–2186 (2022).
226. Wengenack, N. L. et al. Recombinant Mycobacterium tuberculosis KatG(S315T) is a competent catalase-peroxidase with reduced activity toward isoniazid. *J. Infect. Dis.* **176**, 722–727 (1997).
227. Mokrousov, I. et al. High prevalence of KatG Ser315Thr substitution among isoniazid-resistant Mycobacterium tuberculosis clinical isolates from northwestern Russia, 1996 to 2001. *Antimicrob. Agents Chemother.* **46**, 1417–1424 (2002).
228. Ghiladi, R. A., Medzihradszky, K. F., Rusnak, F. M. & Ortiz De Montellano, P. R. Correlation between isoniazid resistance and superoxide reactivity in Mycobacterium

tuberculosis KatG. *J. Am. Chem. Soc.* **127**, 13428–13442 (2005).

229. Reingewertz, T. H. et al. Differential sensitivity of mycobacteria to isoniazid is related to differences in katg-mediated enzymatic activation of the drug. *Antimicrob. Agents Chemother.* **64**, (2020).
230. Wright, G. D. Something old, something new: Revisiting natural products in Antibiotic drug discovery. *Can. J. Microbiol.* **60**, 147–154 (2014).
231. Gagliardi, A. et al. KatG as Counterselection Marker for Nontuberculous Mycobacteria. *Antimicrob. Agents Chemother.* **64:e02508-**, (2020).
232. Andriole, V. T. The Quinolones: Past, Present, and Future. *Clin. Infect. Dis.* **41**, 113–119 (2005).
233. Guillemin, I., Jarlier, V. & Cambau, E. Correlation between Quinolone Susceptibility Patterns and Sequences in the A and B Subunits of DNA Gyrase in Mycobacteria. *Antimicrob. Agents Chemother.* **42**, (1998).
234. Pennings, L. J., Ruth, M. M., Wertheim, H. F. L. & van Ingen, J. The benzimidazole SPR719 shows promising concentration-dependent activity and synergy against nontuberculous mycobacteria. *Antimicrob. Agents Chemother.* **65**, (2021).
235. Aragaw, W. W. et al. In Vitro Resistance against DNA Gyrase Inhibitor SPR719 in Mycobacterium avium and Mycobacterium abscessus. *Microbiol. Spectr.* **10**, (2022).
236. Jarand, J., Paul Davis, J., Cowie, R. L., Field, S. K. & Fisher, D. A. Long-term follow-up of mycobacterium avium complex lung disease in patients treated with regimens including clofazimine and/or rifampin. *Chest* **149**, 1285–1293 (2016).
237. Arbiser, J. L. & Moschella, S. L. Clofazimine: A review of its medical uses and mechanisms of action. *J. Am. Acad. Dermatol.* **32**, 241–427 (1995).
238. Yano, T. et al. Reduction of clofazimine by mycobacterial type 2 NADH: Quinone Oxidoreductase: A pathway for the generation of bactericidal levels of reactive oxygen species. *J. Biol. Chem.* **286**, 10276–10287 (2011).
239. Andries, K. et al. A Diarylquinoline Drug Active on the ATP Synthase of Mycobacterium tuberculosis. *Science (80-.).* **307**, 223–227 (2005).
240. Diacon, A. H. et al. The Diarylquinoline TMC207 for Multidrug-Resistant Tuberculosis. *N. Engl. J. Med.* **360**, 2397–2405 (2009).
241. Conradie, F. et al. Treatment of Highly Drug-Resistant Pulmonary Tuberculosis. *N. Engl.*

J. Med. **382**, 893–902 (2020).

242. Conradie, F. et al. Bedaquiline–Pretomanid–Linezolid Regimens for Drug-Resistant Tuberculosis. *N. Engl. J. Med.* **387**, 810–823 (2022).
243. Obregón-Henao, A. et al. Susceptibility of mycobacterium abscessus to antimycobacterial drugs in preclinical models. *Antimicrob. Agents Chemother.* **59**, 6904–6912 (2015).
244. Viljoen, A. et al. Improved activity of bedaquiline by verapamil against Mycobacterium abscessus in vitro and in macrophages. *Antimicrob. Agents Chemother.* (2019) doi:10.1128/aac.00705-19.
245. Brown-Elliott, B. A. & Wallace, R. J. In Vitro Susceptibility Testing of Bedaquiline against Mycobacterium abscessus Complex. *Antimicrob. Agents Chemother.* **63**, (2019).
246. Vesenbeckh, S. et al. Bedaquiline as a potential agent in the treatment of Mycobacterium abscessus infections. *Eur. Respir. J.* **49:1700083**, (2017).
247. Sarathy, J. P. et al. TBAJ-876, a 3,5-dialkoxypyridine analogue of bedaquiline, is active against Mycobacterium abscessus. *Antimicrob. Agents Chemother.* **64**, (2020).
248. Baker, S. J. et al. Discovery of a new boron-containing antifungal agent, 5-fluoro-1,3-dihydro- 1-hydroxy-2,1-benzoxaborole (AN2690), for the potential treatment of onychomycosis. *J. Med. Chem.* **49**, 4447–4450 (2006).
249. Liu, C. T., Tomsho, J. W. & Benkovic, S. J. The unique chemistry of benzoxaboroles: Current and emerging applications in biotechnology and therapeutic treatments. *Bioorganic Med. Chem.* **22**, 4462–4473 (2014).
250. Rock, F. L. et al. An antifungal agent inhibits an aminoacyl-tRNA synthetase by trapping tRNA in the editing site. *Science (80-.).* **316**, 1759–1761 (2007).
251. Palencia, A. et al. Structural dynamics of the aminoacylation and proofreading functional cycle of bacterial leucyl-tRNA synthetase. (2012) doi:10.1038/nsmb.2317.
252. Alvarez-Carreño, C., Becerra, A. & Lazcano, A. Norvaline and Norleucine May Have Been More Abundant Protein Components during Early Stages of Cell Evolution. *Orig. Life Evol. Biosph.* **43**, 363–375 (2013).
253. Ji, Q. Q., Fang, Z. P., Ye, Q., Chi, C. W. & Wang, E. D. Self-protective responses to norvaline-induced stress in a leucyl-tRNA synthetase editing-deficient yeast strain. *Nucleic Acids Res.* **45**, 7367–7381 (2017).
254. Loftfield, R. B. & Vanderjagt, D. The frequency of errors in protein biosynthesis.

Biochem. J. **128**, 1353–1356 (1972).

255. Nandi, P. & Sen, G. . An Antifungal Substance from a Strain of B. subtilis. *Nature* **172**, 871–872 (1953).
256. Soini, J. et al. Norvaline is accumulated after a down-shift of oxygen in Escherichia coli W3110. *Microb. Cell Fact.* **7**, (2008).
257. Apostol, I. et al. Incorporation of norvaline at leucine positions in recombinant human hemoglobin expressed in Escherichia coli. *J. Biol. Chem.* **272**, 28980–28988 (1997).
258. Kisumi, M., Sugiura, M. & Chibata, I. Biosynthesis of norvaline, norleucine, and homoisoleucine in Serratia marcescens. *J. Biochem.* **80**, 333–339 (1976).
259. Sycheva, E. V. et al. Overproduction of noncanonical amino acids by Escherichia coli cells. *Microbiology* **76**, 712–718 (2007).
260. Cvetesic, N., Palencia, A., Halasz, I., Cusack, S. & Gruic-Sovulj, I. The physiological target for Leu RS translational quality control is norvaline. *EMBO J.* **33**, 1639–1653 (2014).
261. Tenero, D. et al. Intrapulmonary pharmacokinetics of GSK2251052 in healthy volunteers. *Antimicrob. Agents Chemother.* **57**, 3334–3339 (2013).
262. O'Dwyer, K. et al. Bacterial resistance to leucyl-tRNA synthetase inhibitor GSK2251052 develops during treatment of complicated urinary tract infections. *Antimicrob. Agents Chemother.* **59**, 289–298 (2015).
263. Palencia, A. et al. Discovery of novel oral protein synthesis inhibitors of mycobacterium tuberculosis that target leucyl-tRNA synthetase. *Antimicrob. Agents Chemother.* **60**, 6271–6280 (2016).
264. Li, X. et al. Discovery of a Potent and Specific M. tuberculosis Leucyl-tRNA Synthetase Inhibitor: (S)-3-(Aminomethyl)-4-chloro-7-(2-hydroxyethoxy)benzo[c][1,2]oxaborol-1(3H)-ol (GSK656). *J. Med. Chem.* **60**, 8011–8026 (2017).
265. Tenero, D. et al. First-time-in-human study and prediction of early bactericidal activity for GSK3036656, a potent leucyl-tRNA synthetase inhibitor for tuberculosis treatment. *Antimicrob. Agents Chemother.* **63**, (2019).
266. Schnappinger, D. Genetic approaches to facilitate antibacterial drug development. *Cold Spring Harb. Perspect. Med.* **5**, (2015).
267. Mdluli, K., Kaneko, T. & Upton, A. The Tuberculosis Drug Discovery and Development

Pipeline and Emerging Drug Targets. *Cold Spring Harb. Perspect. Med.* **5**, a021154–a021154 (2015).

268. Klobucar, K. et al. Chemical Screen for Vancomycin Antagonism Uncovers Probes of the Gram-Negative Outer Membrane. *ACS Chem. Biol.* **16**, 929–942 (2021).
269. Janzen, W. P. Screening technologies for small molecule discovery: The state of the art. *Chem. Biol.* **21**, 1162–1170 (2014).
270. Warrier, T., Romano, K. P., Clatworthy, A. E. & Hung, D. T. Integrated genomics and chemical biology herald an era of sophisticated antibacterial discovery, from defining essential genes to target elucidation. *Cell Chem. Biol.* **29**, 716–729 (2022).
271. Brotz-Oesterhelt, H. & Sass, P. Postgenomic strategies in antibacterial drug discovery. *Future Microbiol.* **5**, 1553–1579 (2010).
272. Pethe, K. et al. A chemical genetic screen in Mycobacterium tuberculosis identifies carbon-source-dependent growth inhibitors devoid of in vivo efficacy. *Nat. Commun.* **1**, 57 (2010).
273. Zlitni, S., Ferruccio, L. F. & Brown, E. D. Metabolic suppression identifies new antibacterial inhibitors under nutrient limitation. *Nat. Chem. Biol.* **9**, 796–804 (2013).
274. Lee, B. S. & Pethe, K. Therapeutic potential of promiscuous targets in Mycobacterium tuberculosis. *Curr. Opin. Pharmacol.* **42**, 22–26 (2018).
275. Wellington, S. & Hung, D. T. The Expanding Diversity of Mycobacterium tuberculosis Drug Targets. *ACS Infect. Dis.* **4**, 696–714 (2018).
276. Cole, S. T. Inhibiting mycobacterium tuberculosis within and without. *Philos. Trans. R. Soc. B Biol. Sci.* **371**, (2016).
277. Abrahams, K. A. et al. Identification of Novel Imidazo[1,2-a]pyridine Inhibitors Targeting M. tuberculosis QcrB. *PLoS One* **7**, (2012).
278. Mak, P. A. et al. A high-throughput screen to identify inhibitors of ATP homeostasis in non-replicating mycobacterium tuberculosis. *ACS Chem. Biol.* **7**, 1190–1197 (2012).
279. Moraski, G. C. et al. Advent of imidazo[1,2-a]pyridine-3-carboxamides with potent multi- and extended drug resistant antituberculosis activity. *ACS Med. Chem. Lett.* **2**, 466–470 (2011).
280. Moraski, G. C. et al. Generation and exploration of new classes of antitubercular agents: The optimization of oxazolines, oxazoles, thiazolines, thiazoles to imidazo[1,2-a]pyridines

and isomeric 5,6-fused scaffolds. *Bioorganic Med. Chem.* **20**, 2214–2220 (2012).

281. Maddry, J. A. et al. Antituberculosis activity of the molecular libraries screening center network library. *Tuberculosis* **89**, 354–363 (2009).
282. Ananthan, S. et al. High-throughput screening for inhibitors of Mycobacterium tuberculosis H37Rv. *Tuberculosis* **89**, 334–353 (2009).
283. Brown, J. R. et al. The structure-activity relationship of urea derivatives as anti-tuberculosis agents. *Bioorganic Med. Chem.* **19**, 5585–5595 (2011).
284. Scherman, M. S. et al. Screening a library of 1600 adamantyl ureas for anti-Mycobacterium tuberculosis activity in vitro and for better physical chemical properties for bioavailability. *Bioorganic Med. Chem.* **20**, 3255–3262 (2012).
285. Batt, S. M. et al. Structural basis of inhibition of Mycobacterium tuberculosis DprE1 by benzothiazinone inhibitors. *Proc. Natl. Acad. Sci. U. S. A.* **109**, 11354–11359 (2012).
286. Lupien, A. et al. Optimized background regimen for treatment of active tuberculosis with the next-generation benzothiazinone macozinone (PBTZ169). *Antimicrob. Agents Chemother.* **62**, (2018).
287. Grzegorzewicz, A. E. et al. Inhibition of mycolic acid transport across the Mycobacterium tuberculosis plasma membrane. *Nat. Chem. Biol.* **8**, 334–341 (2012).
288. Pethe, K. et al. Discovery of Q203, a potent clinical candidate for the treatment of tuberculosis. *Nat. Med.* **19**, 1157–1160 (2013).
289. Foo, C. S. et al. Arylvinylpiperazine amides, a new class of potent inhibitors targeting QcrB of mycobacterium tuberculosis. *MBio* **9**, (2018).
290. Payne, D. J., Gwynn, M. N., Holmes, D. J. & Pompliano, D. L. Drugs for bad bugs: Confronting the challenges of antibacterial discovery. *Nat. Rev. Drug Discov.* **6**, 29–40 (2007).
291. Sams-Dodd, F. Target-based drug discovery: is something wrong? *Drug Discov. Today* **10**, 139–147 (2005).
292. Roemer, T. & Boone, C. Systems-level antimicrobial drug and drug synergy discovery. *Nat. Chem. Biol.* **9**, 222–231 (2013).
293. Fischbach, M. A. & Walsh, C. T. Antibiotics for Emerging Pathogens. *Science (80-.).* **325**, 1089–1093 (2009).
294. Pawelczyk, J., Viljoen, A., Kremer, L. & Dziadek, J. The influence of AccD5 on AccD6

carboxyltransferase essentiality in pathogenic and non-pathogenic Mycobacterium. *Sci. Rep.* **7**, (2017).

295. Pecsi, I. et al. Essentiality of succinate Dehydrogenase in Mycobacterium smegmatis and its role in the generation of the membrane potential under hypoxia. *MBio* **5**, 1093–1107 (2014).
296. Sassetti, C. M., Boyd, D. H. & Rubin, E. J. Comprehensive identification of conditionally essential genes in mycobacteria. *Proc. Natl. Acad. Sci. U. S. A.* **98**, 12712–12717 (2001).
297. Sassetti, C. M. & Rubin, E. J. Genetic requirements for mycobacterial survival during infection. *Proc. Natl. Acad. Sci. U. S. A.* **100**, 12989–12994 (2003).
298. Rock, J. M. et al. Programmable transcriptional repression in mycobacteria using an orthogonal CRISPR interference platform. *Nat. Microbiol.* **2**, 16274 (2017).
299. Rock, J. Tuberculosis drug discovery in the CRISPR era. *PLoS Pathog.* **15**, (2019).
300. Bosch, B. et al. Genome-wide gene expression tuning reveals diverse vulnerabilities of M. tuberculosis. *Cell* **184**, 4579-4592.e24 (2021).
301. Ballinger, E. et al. Opposing reactions in coenzyme A metabolism sensitize Mycobacterium tuberculosis to enzyme inhibition. *Science (80-.).* **363**, (2019).
302. Vaubourgeix, J. et al. Stressed mycobacteria use the chaperone ClpB to sequester irreversibly oxidized proteins asymmetrically within and between cells. *Cell Host Microbe* **17**, 178–190 (2015).
303. Raju, R. M. et al. Post-Translational Regulation via Clp Protease Is Critical for Survival of Mycobacterium tuberculosis. *PLoS Pathog* **10**, (2014).
304. Johnson, eachan O. et al. Large-scale chemical–genetics yields new M. tuberculosis inhibitor classes. *Nature* **571**, 72–78 (2019).
305. Wellington, S. et al. Asmall-molecule allosteric inhibitor of Mycobacterium tuberculosis tryptophan synthase. *Nat. Chem. Biol.* **13**, 943–950 (2017).
306. Johnson, E. O., Office, E., Kawate, T., Orzechowski, M. & Hung, D. T. Large-Scale Chemical-Genetic Strategy Enables the Design of Antimicrobial Combination Chemotherapy in Mycobacteria. *ACS Infect. Dis.* **6**, 56–63 (2020).
307. Low, J. L., Wu, M. L., Aziz, D. B., Laleu, B. & Dick, T. Screening of TB actives for activity against nontuberculous mycobacteria delivers high hit rates. *Front. Microbiol.* **8**, 1–9 (2017).

308. Malin, J. J., Winter, S., Edeltraud, van G., Plum, G. & Rybniker, J. Extremely Low Hit Rate in a Diverse Chemical Drug Screen Targeting Mycobacterium abscessus. *Antimicrob. Agents Chemother.* **63**, (2019).
309. Schön, T. & Chryssanthou, E. Minimum inhibitory concentration distributions for Mycobacterium avium complex—towards evidence-based susceptibility breakpoints. *Int. J. Infect. Dis.* **55**, 122–124 (2017).

1.7 FIGURES

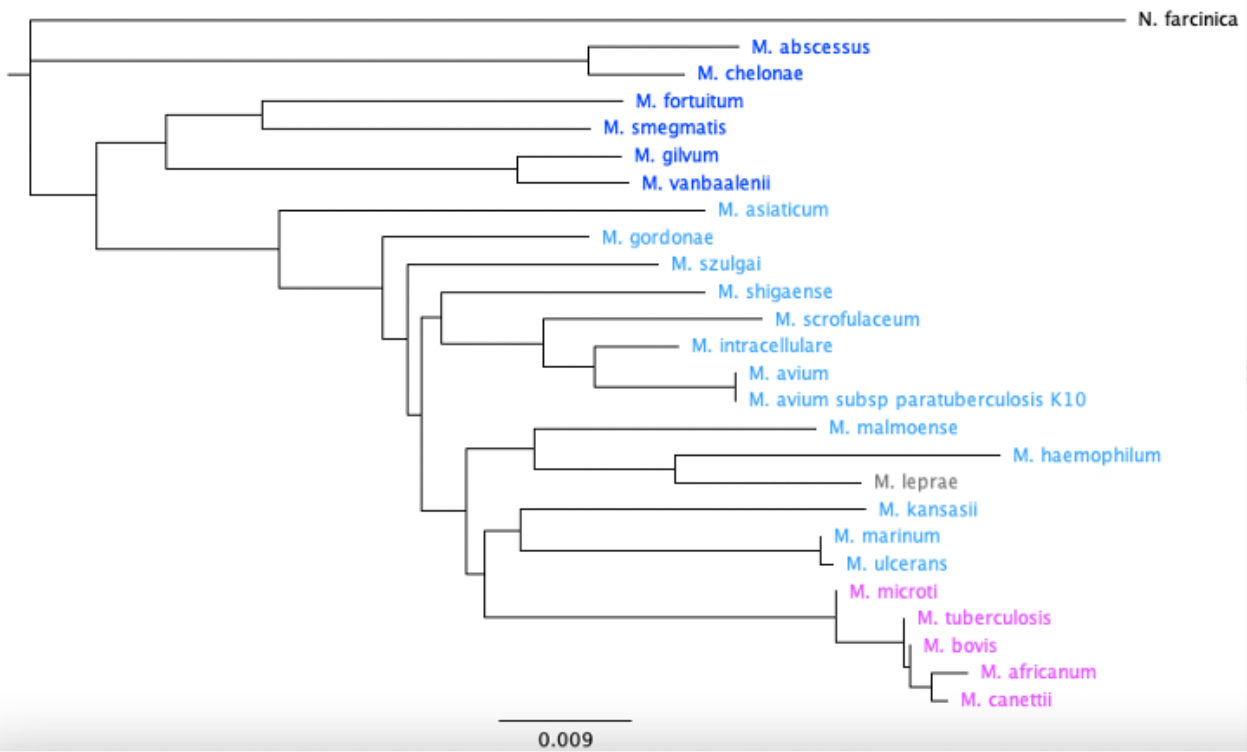

FIGURE 1.1. Diversity of the *Mycobacterium* genus. Phylogeny of the *Mycobacterium* genus using *rpoB* from a Neighbour-Joining tree built with the Jukes-Cantor distance model. Bar represents 0.009 substitutions per nucleotide position. The *Mycobacterium tuberculosis* Complex (MTBC) is highlighted in pink, and the non-tuberculous mycobacteria (NTM) are highlighted in blues. NTM are divided into slow growing (light blue) and rapid growing (dark blue). *Mycobacterium leprae* (grey) is located in between the MTBC and NTM. *Nocardia farcinica* (black) was used as the outgroup.

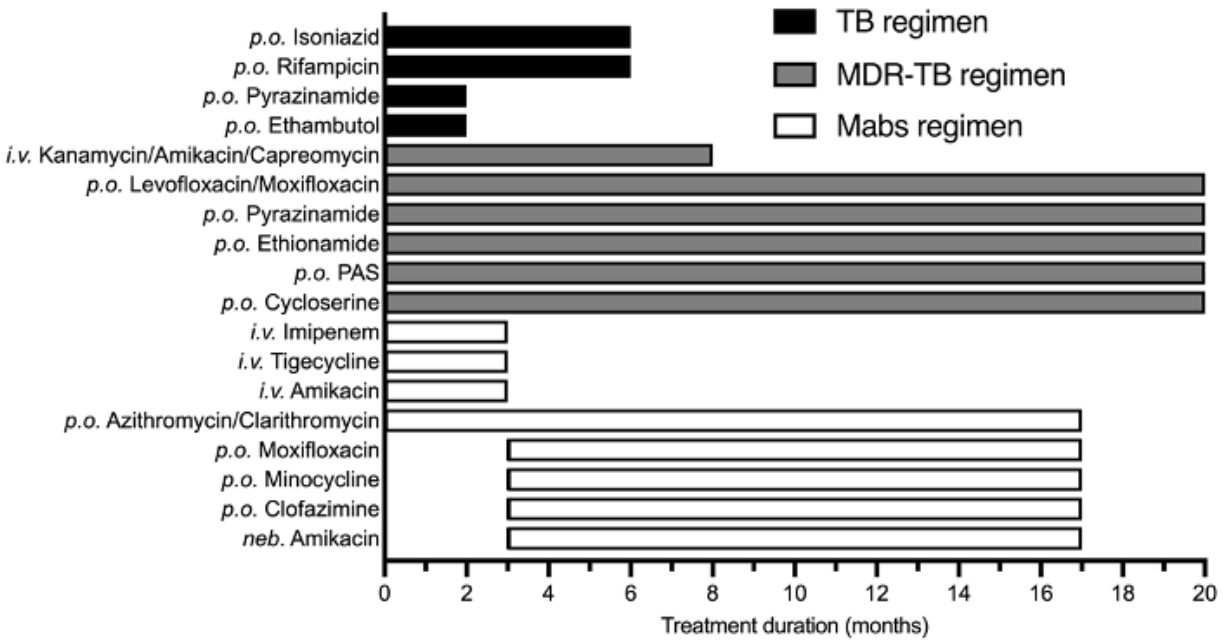

FIGURE 1.2. Treatment schedules for mycobacterial pulmonary infections. Pulmonary infection with drug sensitive (black bars) or multidrug resistant (grey bars) *M. tuberculosis*. Pulmonary infection with *M. abscessus* in a patient with CF (white bars). The *M. abscessus* regimen is implemented in two phases: an intensive phase with parenterally administered amikacin, tigecycline, and imipenem and an oral macrolide; after three months, an all-oral regimen of three antibiotics plus a macrolide and nebulized amikacin are used for the continuation phase up to 17 months. Adapted from Floto *et al*.[81]

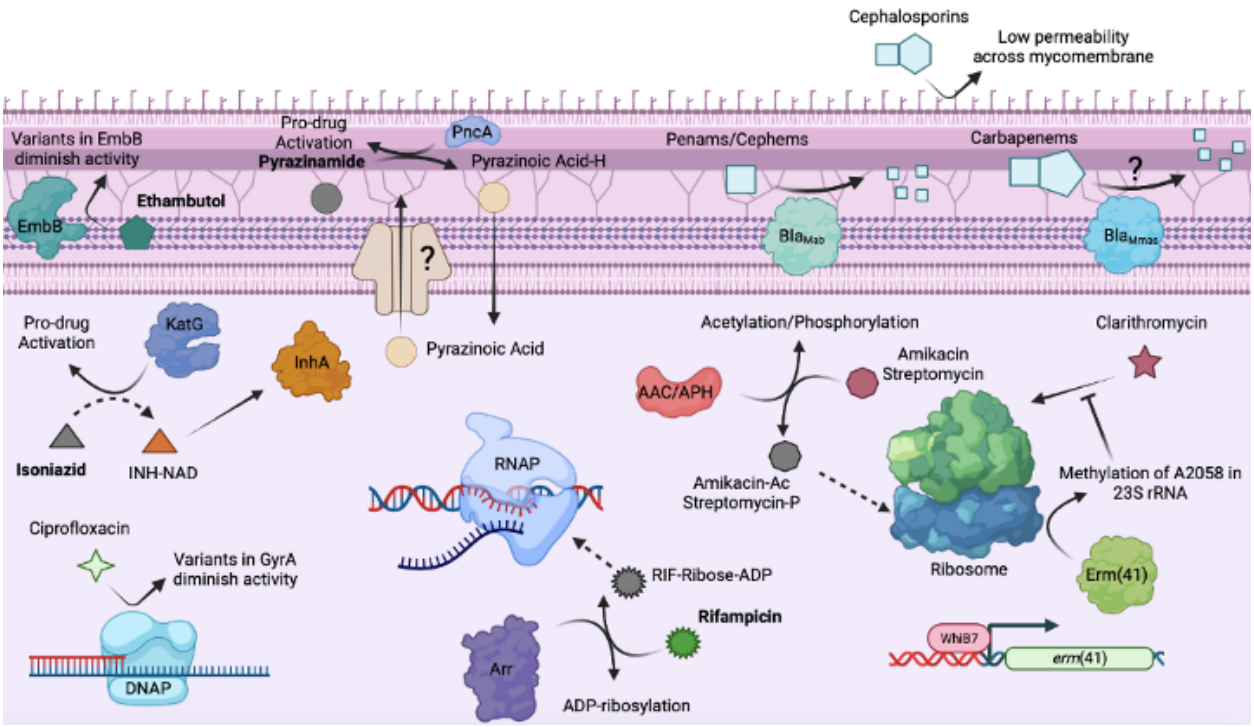

FIGURE 1.3. Antimicrobial resistance mechanisms in *M. abscessus*. Compounds highlighted in bold represent the front-line regimen for TB (Isoniazid, Rifampicin, Pyrazinamide, Ethambutol). Hashed arrow represents a process/pathway that no longer occurs in *M. abscessus*. *M. abscessus* encodes a variant of KatG that does not catalyze the formation of the isoniazid-NAD adduct, which is required for inhibition of InhA. Drug modifying enzymes such as acetyltransferases (AAC), phosphotransferases (APH), and ADP-ribosyltransferases (Arr) impart resistance to aminoglycosides and rifamycins. *M. abscessus* expresses one β-lactamase (Bla_{Mab}) with activity against the penam and cephem family of β-lactams, and one β-lactamase (Bla_{Mmas}) with putative carbapenem activity. Macrolides trigger inducible resistance through the transcription factor WhiB7 that upregulates the target modifying enzyme Erm(41) and provides macrolide resistance. NTM do encode the enzyme responsible for converting pyrazinamide into the active species pyrazinoic acid (PncA), however, current evidence suggests pyrazinoic acid is effluxed from the cell before inhibition of the putative target aspartate decarboxylase occurs. Non-enzymatic-mediated resistance in *M. abscessus* includes target variants that preclude binding of certain fluoroquinolones to gyrase A of the DNA polymerase complex and binding of ethambutol to the arabinosyltransferase EmbB.

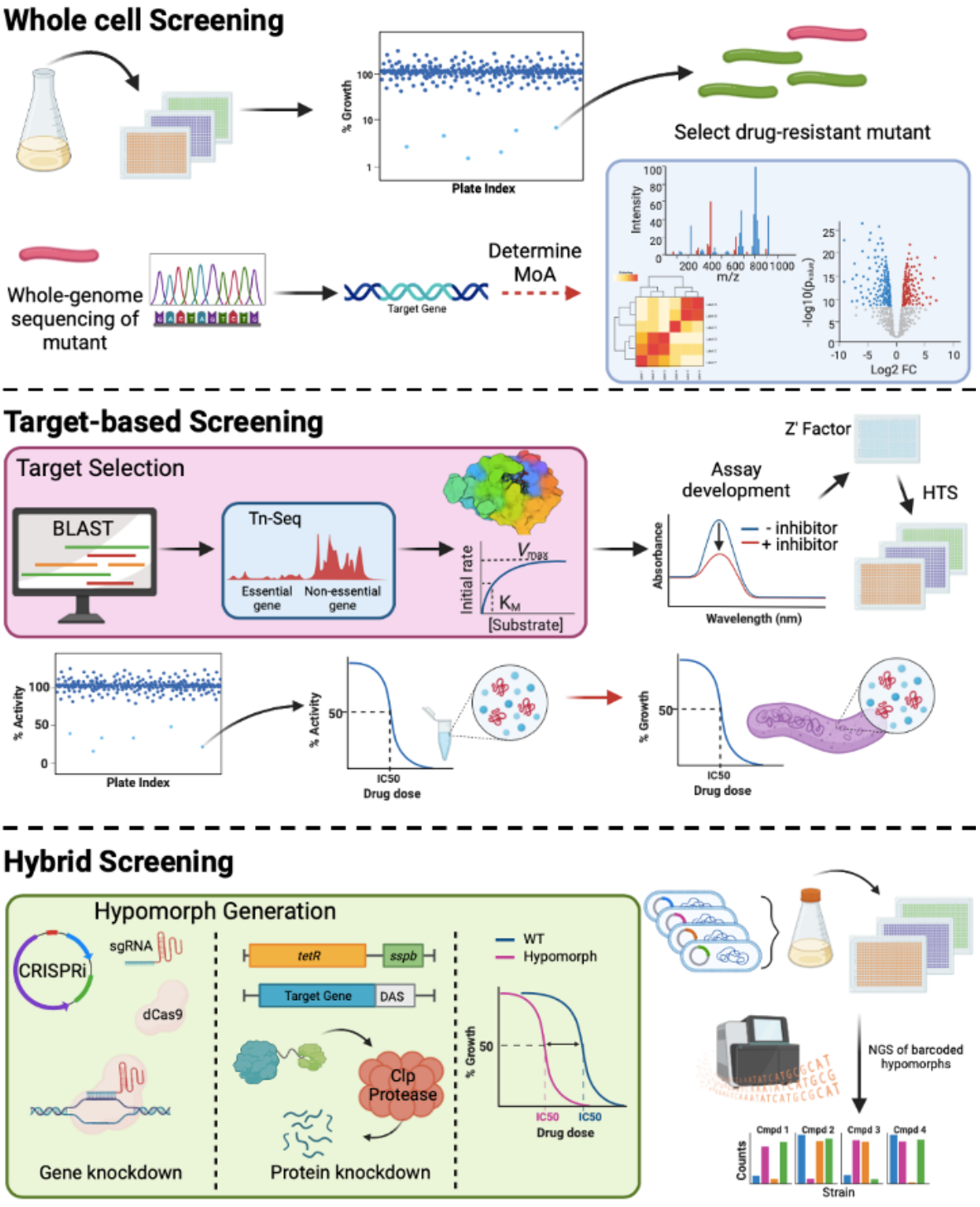

FIGURE 1.4. Pathways for antimicrobial discovery. Drug discovery for antimicrobials is carried out classically by the WCS method. Compounds are screened for activity against whole cell bacteria most commonly through growth inhibition. Bacterial mutants are raised on high concentrations of the hit compound and sent for WGS. Sequencing results can identify the target gene, which is followed up with extensive experimental approaches to determine the mechanism

of action. Target-based screening has yet to produce clinically useful antimicrobials. Starting with a bioinformatics approach, essential genes that have prior structural or kinetic data available are prioritized. Once a target has been selected, an *in vitro* assay is validated and used to screen for inhibitors of the target. Hit compounds are then assayed for dose response activity and other pharmacological parameters *in vitro* followed by a phenotypic assay that tests for cell permeability and whole cell activity. Hybrid screening is a newer approach that combines aspects of whole cell and target-based screening. Examples of hybrid screens use hypomorphic strains to gain insight on the target while probing for compounds with cell permeability. Barcoded-hypomorphs can be generated with CRISPRi or the DAS-tag proteolysis system. Compounds are screened against the pool of hypomorphs followed by next generation sequencing of the barcode to determine which hypomorphs were depleted. Depleted hypomorphs provide insight on the putative target and mechanism of action of the compound. The red arrow indicates the step where that method typically fails. Hybrid methods require more trial-and-error to determine which step is the chokepoint.

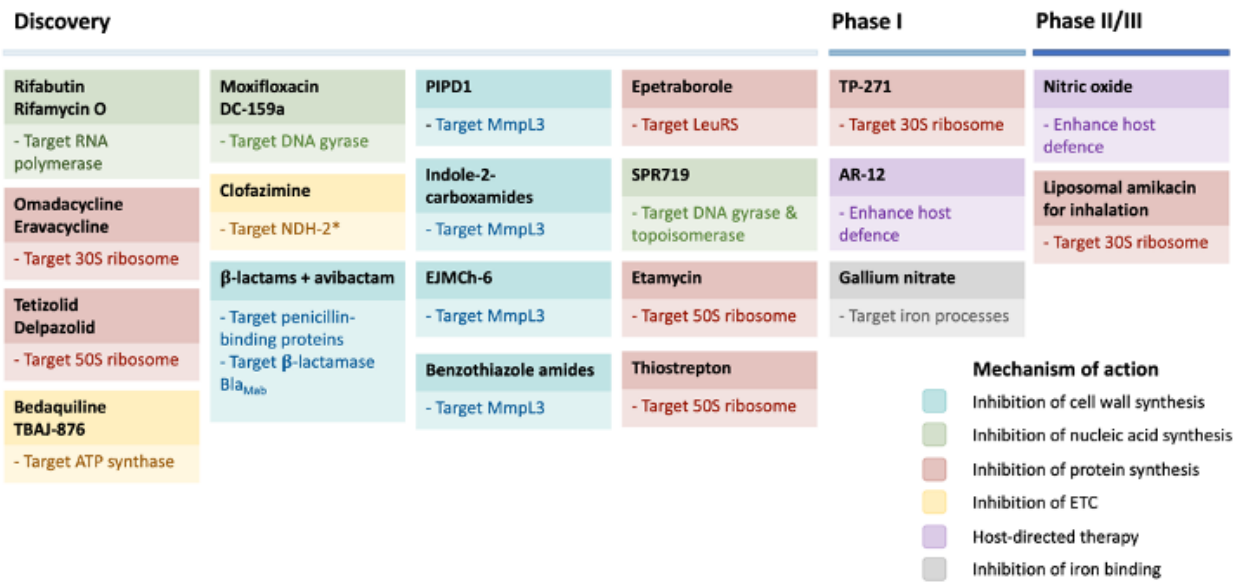

FIGURE 1.5. Antimicrobial pipeline for *M. abscessus*. The main drawback to the *M. abscessus* pipeline is the lack of target diversity and the limited number of compounds past the discovery phase. Mechanism of action denoted by colour. NDH-2, type II NADH-quinone oxidoreductase; MmpL3, mycobacterial membrane protein large 3; LeuRS, leucyl-tRNA synthetase. The asterisk (*) indicates putative drug target. Adapted from Wu et al.[107]

PREFACE TO CHAPTER 2

M. abscessus is known to cause chronic pulmonary infections in patients with impaired lung function such as CF. Current antimycobacterials that are used to treat infections caused by *M. tuberculosis* are not effective against *M. abscessus* due to a myriad of resistance mechanisms. The antibiotics that do demonstrate *in vitro* activity against *M. abscessus* are inadequate for clinical use with treatment success rates near 30-50%. We rationalized that since natural products make up a majority of the clinically useful antibiotics today, the natural product chemical space could be a valuable place to begin our drug discovery efforts. Known for its work in mycobacterial genetics, the Behr lab's first foray into antimicrobial drug discovery started with the construction of a constitutively producing luminescence strain of *M. abscessus*. The luminescence readout was correlated with the biomass of a growing culture and validated with a Z' factor. Starting with a small pilot library of natural products, lysobactin and sorangicin showed promising activity against *M. abscessus* and clinical isolates, which suggests that no prior resistance to these novel scaffolds has developed.

This chapter was adapted from the manuscript: Natural products lysobactin and sorangicin A show *in vitro* activity against *Mycobacterium abscessus* complex. Sullivan *et al*. *Microbiol Spectr.* 2022

CHAPTER 2

Natural products lysobactin and sorangicin A show *in vitro* activity against *Mycobacterium abscessus* complex

Jaryd R. Sullivan[1,2,3], Jacqueline Yao[2], Christophe Courtine[1,2], Andréanne Lupien[2,3], Jennifer Herrmann[4], Rolf Müller[4,5], Marcel A. Behr[1,2,3,6#]

[1]Department of Microbiology & Immunology, McGill University, Montréal, Québec, Canada.

[2]Infectious Diseases and Immunity in Global Health Program, Research Institute of the McGill University Health Centre, Montréal, Québec, Canada.

[3]McGill International TB Centre, Montréal, Québec, Canada.

[4]Department of Microbial Natural Products, Helmholtz-Institute for Pharmaceutical Research Saarland (HIPS), Helmholtz Centre for Infection Research (HZI), Saarland University, Campus E8 1, 66123 Saarbrücken, Germany

Department of Pharmacy, Saarland University, Campus E8 1, 66123 Saarbrücken, Germany

[6]Department of Medicine, McGill University Health Centre, Montréal, Québec, Canada.

Microbiol Spectr. 2022

2.1 ABSTRACT

The prevalence of lung disease caused by *Mycobacterium abscessus* is increasing among patients with cystic fibrosis. *M. abscessus* is a multidrug resistant opportunistic pathogen that is notoriously difficult to treat due to a lack of efficacious therapeutic regimens. Currently, there are no standard regimens, and treatment guidelines are based empirically on drug susceptibility testing. Thus, novel antibiotics are required. Natural products represent a vast pool of biologically active compounds that have a history of being a good source of antibiotics. Here, we screened a library of 517 natural products purified from fermentations of various bacteria, fungi and plants against *M. abscessus* ATCC 19977. Lysobactin and sorangicin A were active against the *M. abscessus* complex and drug resistant clinical isolates. These natural products merit further consideration to be included in the *M. abscessus* drug pipeline.

2.2 IMPORTANCE

The many thousands of people living with cystic fibrosis are at a greater risk of developing a chronic lung infection caused by *Mycobacterium abscessus*. Since *M. abscessus* is clinically resistant to most anti-TB drugs available, treatment options are limited to macrolides. Despite macrolide-based therapies, cure rates for *M. abscessus* lung infections are 50%. Using an in-house library of curated natural products, we identified lysobactin and sorangicin A as novel scaffolds for the future development of antimicrobials for patients with *M. abscessus* infections.

2.3 INTRODUCTION

Mycobacterium abscessus (*M. abscessus*) complex consists of three subspecies (*M. abscessus* subsp. *abscessus*, *M. abscessus* subsp. *massiliense*, *M. abscessus* subsp. *bolletii*) that causes disease in immunocompromised and immunocompetent hosts.[1–5] Although *M. abscessus* was first isolated from a knee abscess in 1953, the most common clinical presentation is pulmonary disease in patients with cystic fibrosis (CF), chronic lung disease, or undergoing lung transplantation and is becoming more frequent.[6–8] In some instances, extrapulmonary disease can result from dissemination or surgical site infections that lead to skin and soft tissue infections.[6,9]

Clinical management of *M. abscessus* pulmonary disease is challenged by notoriously drug resistant phenotypes and a lack of effective antimicrobials. *M. abscessus* is intrinsically resistant to most antitubercular agents used to treat tuberculosis despite having a homolog of the target.[10] The treatment for *M. abscessus* pulmonary disease in a patient with CF includes an intensive phase of an oral macrolide like clarithromycin or azithromycin, intravenous amikacin, and an additional intravenous agent like cefoxitin or imipenem.[11] The intensive phase of treatment lasts for up to three months depending on the severity of the infection and the tolerability of the regimen. Subsequently, patients continue with the oral macrolide and substitute the injectable agents with oral clofazimine, minocycline, moxifloxacin, and nebulized amikacin for 14 months.[11]

Treatment regimens can be further complicated by varying susceptibilities among the subspecies where *M. abscessus* subsp. *abscessus* and *bolletii* display inducible resistance to macrolides conferred by the ribosomal methyltransferase encoded by *erm*(41), resulting in worse treatment outcomes. Comparatively, *M. abscessus* subsp. *massiliense* has a truncated *erm*(41) and higher treatment success rates.[12–14] Consequently, the intrinsic resistance mechanisms of the bacteria and the lack of effective antimicrobials against *M. Abscessus* necessitate additional drug discovery efforts to identify novel antimicrobials.

Natural products are a reservoir of genetically encoded microbial metabolites with vast chemical diversity.[15,16] These metabolites have been crafted by evolution to mediate chemical signaling roles and thus, possess the required properties for microbial penetration and an affinity for biological targets.[17,18] Considering that two-thirds of antibiotics used in the clinic are natural products or

derived from a natural product scaffold, they are a proven source for antimicrobial discovery.[19,20] Here, we screened an in house HZI/HIPS library of 517 natural products purified from fermentations of various bacteria (mostly myxobacteria) and fungi against *M. abscessus* ATCC 19977. We discovered that the cyclic depsipeptide lysobactin (LYB) and the macrolide sorangicin A (SOR) have activity against the reference strain and against a panel of drug resistant clinical isolates from CF patients.

2.4 METHODS

2.4.1 Compounds

Myxobacteria and fungi are prolific sources of structurally diverse metabolites displaying innovative modes-of-action.[21,22] The labs at HZI/HIPS focus on exploring understudied sources and expanding the natural product space in biodiversity-driven approaches.[15] Production and isolation procedures are being developed and adapted to match compound properties, and we typically aim at isolating compounds at > 90% purity. The library plates and master stocks are stored at -80°C and undergo routine quality control via HPLC-MS/UV. For hit confirmation and dose-response, independent powder stocks are provided which are typically at 95% purity. An in-house collection of 517 natural products were included in the screen. The library includes 176 compounds isolated from diverse sources, 88 compounds isolated from fungi, and 253 compounds isolated from myxobacterial fermentation. The natural products were prepared at 1 mM in 100% dimethyl sulfoxide (DMSO). Amikacin (AMK) was resuspended in distilled H_2O (dH_2O). Vancomycin (VAN) was resuspended in dH_2O while lysobactin (LYB), rifampicin (RIF) and rifabutin (RFB) were resuspended in 100% DMSO. Sorangicin A (SOR) was prepared in-house and resuspended in 100% DMSO. For Sorangicin A, fermentation and downstream processing is described elsewhere and the provided sample was > 95% purity. All drugs were purchased from Sigma-Aldrich unless otherwise stated.

2.4.2 Bacterial Strains

Mycobacterium abscessus ATCC 19977 reference strain was used to create a constitutively luminescent strain by integration of the *luxCDABE* operon (*M. abscessus lux*) for screening assays. The integration was accomplished by electroporating the plasmid plux that targets the attP site of the mycobacterial genome and selecting on 7H10 plates containing 250 µg/mL of kanamycin. *M. abscessus lux* cultures were grown in 100 µg/mL kanamycin for plasmid maintenance. Cultures were passaged in antibiotic-free media one night prior to the primary screen assay. Clinical isolates of *M. abscessus* subsp. *abscessus* and subsp. *massiliense* from patients with cystic fibrosis were obtained from an epidemiologic study of *M. abscessus* transmission on the island of Montreal. Isolates were characterized by Illumina Mi-Seq whole-genome sequencing. *M. abscessus* subsp. *bolletii* clinical isolate was obtained from France. Single nucleotide polymorphisms (SNPs) in *erm*(41), *rpoB*, and *rrl* were detected using Galaxy. Briefly, whole-genome sequence qualities

were checked with FASTQC, and adapter sequences were trimmed with Trimmomatic. Snippy was used to map whole-genome sequences to *erm*(41), *rpoB*, and *rrl* from ATCC 19977 reference (GenBank accession: CU458896.1) with a minimum mapping quality of 60 and minimum coverage of 40. SNPs in *erm*(41), *rpoB*, and *rrl* were confirmed with Sanger sequencing. *erm*(41) primers: P_F GTGTCCGGCCAACGGTCGCGA; P_R TCAGCGCCGCCTGATCACCAGC. *rpoB* primers: P_F TGTCGCAGTTCATGGACCAGAA; P_R GTCGTGCTCGAGGAACGGGAT. *Rrl* primers: P_F GACGATGTATACGGACTGACGC; P_R CGTCCAGGTTGAGGGAACCTT. Phenotypic clarithromycin resistance was confirmed genotypically by *erm*(41) sequevar (T28 for active *erm*(41) or C28 for inactive *erm*(41)) or A2058/2059 polymorphisms in *rrl*.

2.4.3 Culture Conditions

M. abscessus strains were grown in rolling liquid culture at 37 °C in Middlebrook 7H9 broth (BD Difco) supplemented with 10% (v/v) albumin dextrose catalase enrichment (ADC), 0.2% (v/v) glycerol, and 0.05% (v/v) Tween 80 (7H9 complete) or on 7H10 agar plates supplemented with 10% (v/v) oleic acid ADC enrichment and 0.5% (v/v) glycerol at 37 °C unless otherwise stated. 7H9 broth supplemented with 10% (v/v) ADC enrichment, 0.2% (v/v) sodium acetate, and 0.05% (v/v) Tween 80 was used as an alternative carbon source. Cation-adjusted Mueller Hinton broth (BD Difco) with 10% (v/v) ADC enrichment, 0.2% (v/v) glycerol, and 0.05% (v/v) Tween 80 was used as an alternative media and bacteria were grown at 30°C. Sauton's minimal media was used as a defined minimal media (0.5 g/L monobasic potassium phosphate, 4.0 g/L L-asparagine monohydrate, 2.0 g/L citric acid monohydrate, 0.05 g/L ferric ammonium citrate, 0.1 mL of 1% zinc sulfate, 0.5 g/L magnesium sulfate heptahydrate, 60mL of 100% glycerol, 2.5 mL of 20% Tween 80, pH 7).

2.4.4 Screening assay

The natural product library was screened against *M. abscessus lux* at a single-point concentration of 10 μM in duplicate in 96-well flat-bottom white plates in 7H9 complete media. The culture was grown to log phase (OD_{600} 0.4-0.8) and diluted to an OD_{600} of 0.005 ($5x10^6$ CFU/mL). 90 μL of culture was mixed with 10 μL of 100 μM compound diluted in a mixture of 10% DMSO/90% 7H9. The final concentration of DMSO in each well was 1%. Plates were sealed with parafilm and incubated at 37 °C for 48 hours. The last column of each plate had 1% DMSO as negative control

in quadruplicate (drug-free conditions) and 110 μM of AMK as positive control in quadruplicate. Luminescence was measured with an Infinite F200 Tecan plate reader. Percentage of luminescence relative to DMSO control was plotted using GraphPad Prism version 9. Compounds that decreased the luminescence to ≤ 10% or ≤ 50% of the drug-free conditions were classified as strong or moderate hits, respectively.

2.4.5 Determination of minimum inhibitory concentrations (MIC)

MIC values were determined using the resazurin microtiter assay (REMA). Cultures were grown to log phase (OD_{600} of 0.4-0.8) and diluted to OD_{600} of 0.005 ($5x10^6$ CFU/mL). Drugs were prepared in two-fold serial dilutions in 96-well plates with 90 μL of bacteria per well to a final volume of 100 μL. 96-well clear, flat bottom plates were incubated at 37 °C until drug-free wells were turbid (48 hours for *M. abscessus*). Ten μL of resazurin (0.025% wt/vol) was added to each well. Once the drug-free wells turned pink (3-4 hours), the fluorescence (ex/em 560nm/590nm) was measured using an Infinite F200 Tecan plate reader. Fluorescence intensities were converted to % viable cells relative to drug-free conditions and fit to the modified Gompertz equation using GraphPad Prism version 9. MIC values at 90% growth inhibition were determined from the nonlinear regression Gompertz equation.[23] To compare MICs across media or clinical isolates, MIC values were log transformed. (pMIC = -log(MIC).

2.5 RESULTS

2.5.1 Validation of M. abscessus lux for phenotypic screening

To identify new antimicrobial agents against the difficult-to-treat pulmonary pathogen *M. abscessus*, we investigated the feasibility of *M. abscessus* constitutively expressing luciferase from the *luxCDABE* operon as a primary screening strain (*M. abscessus lux*). We showed that expression of *luxCDABE* did not interfere with the growth kinetics of *M. abscessus lux* when compared to *M. abscessus* ATCC 19977 by CFU/mL over 72 hours, and that *luxCDABE* provided 1000-fold more luminescence than background (**FIGURE 2.1A**). More importantly, luminescence production had a positive correlation (Pearson $r^2 = 0.9887$) with growth kinetics (**FIGURE 2.1B**). Therefore, we substituted the luminescence readout as a proxy for bacterial growth.

Primary screens of chemical libraries often include false positives that later prove to be inactive against the microorganism of interest and thus, incur additional time and resources on screening campaigns. Conversely, compounds with *bona fide* activity may be missed as false negatives. To limit both scenarios, screening conditions are subjected to a Z' factor measurement to determine the robustness of a particular readout. We compared the Z' factor of our *M. abscessus lux* to three other readouts of bacterial growth, namely: optical density at 600nm (OD_{600nm})[24,25], resazurin microtiter assay (REMA)[26–28], and Bactiter Glo[29,30]. *M. abscessus* ATCC 19977 and *M. abscessus lux* were grown until mid-log phase, diluted to OD_{600nm} of 0.005 ($5x10^6$ CFU/mL) and incubated with 1% DMSO or 100 µM amikacin in a 96 well plate format for 48 hours. We measured the highest Z' factor of 0.70 [95% CI, 0.65-0.82] using luminescence from *M. abscessus lux* while luminescence from the commercial Bactiter Glo kit generated the lowest Z' factor of 0.51 [95% CI, 0.13-0.50] (**FIGURE 2.1C**). Importantly, the reproducibility between Z' factors was highest with *M. abscessus lux* as measured by the 95% CI range (*M. abscessus lux* = 0.17, REMA = 0.23, Bactiter Glo = 0.38, OD = 0.39). The high Z' factor and its reproducibility for the *M. abscessus lux* readout gave us confidence to use it in our primary screening assays (**FIGURE 2.1C**).

2.5.2 Lysobactin and sorangicin A are identified as inhibitors of M. abscessus ATCC 19977 from a natural product library

To identify novel antimicrobials against *M. abscessus*, we carried out a phenotypic screen with an in house HZI/HIPS library of 517 natural products against *M. abscessus lux*. The natural products

originated from the fermentation of various biological sources, fungi, and myxobacteria. Fermentations were fractionated into single compounds at 1 mM in DMSO. We screened the natural products at 10 μM (1% DMSO) and applied a threshold of 90% and 50% reduction in luminescence compared to drug free controls (1% DMSO). These criteria provided us with compounds with MIC_{90} and $MIC_{50} \leq 10$ μM, respectively. The last column of each plate contained drug free wells and 100 μM AMK wells as negative and positive controls, respectively. After screening in duplicate, we identified 12 compounds that met our threshold of 90% loss of viability and 20 compounds at 50% loss of viability at 10 μM (**FIGURE 2.2, TABLE S2.1**). Many of the compounds identified are known DNA intercalators and were flagged as potentially cytotoxic. Telithromycin was omitted through de-replication as it shares a similar mechanism of action to CLR. Two compounds identified with specific targets were LYB (**FIGURE 2.3**) and SOR (**FIGURE 2.4**). LYB was a compound of interest since there are currently no lead compounds that target lipid II in the cell wall in the *M. abscessus* drug pipeline.[31] Although traditional cyclic peptides like vancomycin (VAN) do exhibit *in vitro* activity against *M. abscessus,*[32] VAN is associated with an increased risk ratio for total adverse events, nephrotoxicity, and vancomycin flushing reaction.[33] SOR, a known RNA polymerase (RNAP) inhibitor, was a compound of interest since RNAP is a validated drug target in *Mycobacterium tuberculosis* targeted by the front-line drug rifampicin (RIF).[34] Relatedly, rifabutin (RFB) has been shown to be active against *M. abscessus*,[35,36] and so SOR could be added to the group of repurposed RNAP inhibitors for *M. abscessus.*

2.5.3 Lysobactin and sorangicin A maintain activity in different media compositions

To confirm the activity of LYB and SOR and determine the minimum concentration of each drug that inhibits 90% of bacterial growth (MIC_{90}), fresh LYB and SOR powder was obtained and tested against the *M. abscessus* ATCC 19977 reference strain. We observed low micromolar dose-response activity for both LYB and SOR as illustrated in **TABLE 2.1**. It was previously shown that some antimycobacterial agents have carbon dependent activities.[37] Therefore, we measured the $pMIC_{90}$ of LYB and SOR for *M. abscessus* ATCC 19977 grown in traditional Middlebrook 7H9 with glycerol, Middlebrook 7H9 with acetate, and Sauton's minimal mycobacteria medium with glycerol. Alternatively from a clinical perspective, the Clinical and Laboratory Standards Institute guidelines recommend *M. abscessus* drug susceptibility testing in cation-adjusted Mueller

Hinton (CaMH) broth.[38] LYB and SOR retained activity across glycerol and acetate as carbon sources, in a minimal media, and in media adjusted for Mg^{2+} and Ca^{2+} (**TABLE 2.1, TABLE S2.2**).

2.5.4 Lysobactin and sorangicin A are active against the *M. abscessus* complex and drug resistant clinical isolates

To compare the activity of LYB and SOR against other drugs with a similar target, we measured the $pMIC_{90}$ of *M. abscessus* ATCC 19977 S and R reference strains against VAN as a representative cyclic peptide cell wall antimicrobial, and RIF and RFB as representative RNAP inhibitors. LYB and VAN demonstrated similar potencies against both *M. abscessus* S and *M. abscessus* R reference strains while SOR and RIF exhibited lower potencies than RFB (**TABLE 2.2**, **TABLE S2.3**). To determine if LYB and SOR are active against the *M. abscessus* complex, we measured the $pMIC_{90}$ of the natural products against drug resistant clinical isolates that include *M. abscessus* subsp. *abscessus* (n = 5), *M. abscessus* subsp. *massiliense* (n = 5), and *M. abscessus* subsp. *bolletii* (n = 1). These clinical isolates are resistant to a variety of antibiotics used to treat *M. abscessus* pulmonary disease (**TABLE S2.4**).

Whole-genome sequencing of the clinical isolates identified SNPs in *erm*(41), *rrl*, and *rpoB* that were confirmed with Sanger sequencing (**TABLE 2.2**). Clinical isolates represented T28 sequevars with a functional *erm*(41) for inducible CLR resistance and C28 sequevars with a non-functional *erm*(41). Two strains possessed the A2058G (A2270G in *M. abscessus*) or A2059C (A2271C in *M. abscessus*) SNP in the *rrl* gene that conferred constitutive CLR resistance (**TABLE 2.2**). Most isolates harbored a D523E substitution in RpoB. LYB and VAN demonstrated nearly equipotent activities against the clinical isolates (Median LYB $pMIC_{90}$ = 5.3 [95% CI, 4.9-5.4], VAN $pMIC_{90}$ = 5.3 [95% CI, 5.1-5.6], P = 0.46) (**FIGURE 2.5A**). SOR and RIF were less potent compared to best-in-class RFB (Median SOR $pMIC_{90}$ = 4.9 [95% CI, 4.7-5.1], RIF $pMIC_{90}$ = 4.9 [95% CI, 4.4-5.2], RFB $pMIC_{90}$ = 5.8 [95% CI, 5.5-5.9]) (**FIGURE 2.5B**). However, to measure pre-existing resistance to the new compounds, $pMIC_{90}$ values were standardized to the ATCC 19977 S reference strain. We measured up to a 10-fold change in $pMIC_{90}$ of the clinical isolates relative to the ATCC 19977 reference strain for LYB with median LYB $\Delta pMIC_{90}$ = 0.4 [95% CI, 0.3-0.9] and VAN $\Delta pMIC_{90}$ = -0.1 [95% CI, -0.4-0.1] (**FIGURE 2.5A**). Although the $RpoB^{D523E}$

variant was commonly identified in these *M. abscessus* clinical isolates, *M. tuberculosis* naturally encodes E523 in the rifampicin resistance determining region. **FIGURE 2.5B** illustrates a similar activity spectrum to SOR, RIF, and RFB. Taken together, these data suggest a lack of acquired resistance in the clinic to LYB and SOR.

2.6 DISCUSSION

Ten hits were identified from a library of 517 natural products from fermented microorganisms. Two compounds of interest are LYB and SOR. LYB, also known as katanosin B, is a cyclic depsipeptide secondary metabolite produced by *Lysobacter ezymogenes*.[39,40] First identified in 1988, LYB was found to inhibit peptidoglycan synthesis in Gram-positive bacteria but its molecular mechanism remained undefined.[39,40] Later, it was shown that while VAN binds to the terminal D-Ala-D-Ala residue of the pentapeptide stem on N-acetylmuramic acid/N-acetylglucosamine units, LYB binds to the reducing end of the lipid-anchored peptidoglycan precursor, lipid II.[31] Cyclic peptides have recently been investigated for activity against *M. abscessus*. Teicoplanin showed synergy in combination with the glycylcycline, tigecycline and VAN synergized with the macrolide, clarithromycin.[41,42] Due to previous work showing that LYB causes moderate toxicity in mice when administered intravenously[40] but the absence of clinical resistance shown here, LYB could benefit from novel formulations to increase the oral bioavailability and limit side effects.

SOR is produced by the gliding myxobacterium *Sorangium cellulosum* and targets eubacterial but not eukaryotic RNAPs.[43,44] Like RIF and RFB, SOR inhibits bacterial transcription via binding to the RpoB subunit of wildtype RNAP but in *M. tuberculosis*, SOR was shown to prevent promoter DNA unwinding specifically in RIF^R mutants.[34,45] Importantly, SOR maintained activity against *E. coli* and *M. tuberculosis rpoB* mutants despite being resistant to RIF. This has important implications for the treatment of *M. tuberculosis* as RIF is a front-line agent and for the treatment of *M. abscessus* since the activity of RFB has recently been explored.[35,36,46] SOR could be a promising candidate for the *M. abscessus* drug pipeline as it not only retains activity against *M. tuberculosis* RIF^R mutants, but induces cytochrome P450 3A4 to a lesser degree than the classic RNAP inhibitors RIF and RFB.[34] Cytochrome P450 3A4 induction from rifampicin has been

shown to reduce the efficacy of the CFTR corrector, ivacaftor, for patients with CF through drug-drug interactions.[47]

M. abscessus drug discovery could benefit from additional library screening to identify novel scaffold/drug target pairs like the oxaboroles and tRNA synthetases, but attrition rates are high.[48–50] Alternatively, focusing on pharmacologically and clinically validated drug targets like peptidoglycan and RNAP might accelerate the drug discovery process.[51] Although inhibitors for these targets do not exert the most potent *in vitro* activity, they provide novel scaffolds with subtly different mechanism of action, whose potency and drug disposition properties can be improved through careful medicinal chemistry optimization or alternative biotechnological approaches for compound improvement.[19] Future studies should include structure activity relationship analysis and novel formulations to improve the activity and bioavailability while minimizing toxicity of the natural products LYB and SOR for the development of *M. abscessus* antibiotics.

2.7 ACKNOWLEDGEMENTS

The *luxCDABE* plasmid was kindly gifted by Jeffery S. Cox (UC. Berkeley).

2.8 AUTHORS' CONTRIBUTIONS

JRS was involved in all aspects including experiment design, data collection and analysis, and preparation of the manuscript. JY conducted drug susceptibility testing on the clinical isolates. CC performed independent replicates of the assay validation. AL provided supervision to JY. JH and RM provided the natural product libraries. MAB supervised all experiments and was involved in the preparation of the manuscript.

2.9 REFERENCES

1. Johansen, M. D., Herrmann, J.-L. & Kremer, L. Non-tuberculous mycobacteria and the rise of Mycobacterium abscessus. *Nat. Rev. Microbiol.* (2020) doi:10.1038/s41579-020-0331-1.
2. Bronson, R. A. et al. Global phylogenomic analyses of Mycobacterium abscessus provide context for non cystic fibrosis infections and the evolution of antibiotic resistance. *Nat. Commun.* **12**, (2021).
3. Tortoli, E. et al. The new phylogeny of the genus Mycobacterium: The old and the news. *Infect. Genet. Evol.* **56**, 19–25 (2017).
4. Moreno-Izquierdo, C., Zurita, J., Contreras-Yametti, F. I. & Jara-Palacios, M. A. Mycobacterium abscessus subspecies abscessus infection associated with cosmetic surgical procedures: Cases series. *IDCases* **22**, (2020).
5. Hui, S. H., Noonan, L. & Chavada, R. Post liposuction Mycobacterium abscessus surgical site infection in a returned medical tourist complicated by a paradoxical reaction during treatment. *Infect. Dis. Rep.* **7**, 87–90 (2015).
6. Byrd, T. F. & Ryan, K. Mycobacterium abscessus: Shapeshifter of the Mycobacterial World. *Front. Microbiol.* **9**, (2018).
7. Moore, M. & Frerichs, J. B. An unusual acid-fast infection of the knee with subcutaneous, abscess-like lesions of the gluteal region; report of a case with a study of the organism, Mycobacterium abscessus, n. sp. *J. Invest. Dermatol.* **20**, 133–169 (1953).
8. Cassidy, P. M., Hedberg, K., Saulson, A., McNelly, E. & Winthrop, K. L. Nontuberculous Mycobacterial Disease Prevalence and Risk Factors: A Changing Epidemiology. *Clin. Infect. Dis.* **49**, e124–e129 (2009).
9. Lee, M. R. et al. Mycobacterium abscessus complex infections in humans. *Emerg. Infect. Dis.* **21**, 1638–1646 (2015).
10. Wu, M. L., Aziz, D. B., Dartois, V. & Dick, T. NTM drug discovery: status, gaps and the way forward. *Drug Discov. Today* **0**, 1–18 (2018).
11. Floto, R. A. et al. US Cystic Fibrosis Foundation and European Cystic Fibrosis Society consensus recommendations for the management of non-tuberculous mycobacteria in individuals with cystic fibrosis. *Thorax* **71**, i1–i22 (2016).
12. Richard, M., Gutiérrez, A. V. & Kremer, L. Dissecting erm(41)-mediated macrolide-

inducible resistance in mycobacterium abscessus. *Antimicrob. Agents Chemother.* **64**, (2020).

13. Nash, K. A., Brown-Elliott, A. B. & Wallace, R. J. A Novel gene, erm(41), confers inducible macrolide resistance to clinical isolates of mycobacterium abscessus but is absent from mycobacterium chelonae. *Antimicrob. Agents Chemother.* **53**, 1367–1376 (2009).
14. Svetlov, M. S. et al. Structure of Erm-modified 70S ribosome reveals the mechanism of macrolide resistance. *Nat. Chem. Biol.* **17**, 412–420 (2021).
15. Hoffmann, T. et al. Correlating chemical diversity with taxonomic distance for discovery of natural products in myxobacteria. *Nat. Commun.* **9**, (2018).
16. Hug, J. J., Krug, D. & Müller, R. Bacteria as genetically programmable producers of bioactive natural products. *Nature Reviews Chemistry* vol. 4 172–193 (2020).
17. Wright, G. D. Something old, something new: Revisiting natural products in Antibiotic drug discovery. *Can. J. Microbiol.* **60**, 147–154 (2014).
18. Crawford, J. M., Tang, G.-L. & Herzon, S. B. Natural Products: An Era of Discovery in Organic Chemistry. *J. Org. Chem.* **86**, 10943–10945 (2021).
19. Hug, J. J., Krug, D. & Müller, R. Bacteria as genetically programmable producers of bioactive natural products. *Nat. Rev. Chem.* **4**, 172–193 (2020).
20. Fischbach, M. A. & Walsh, C. T. Antibiotics for Emerging Pathogens. *Science (80-.).* **325**, 1089–1093 (2009).
21. Herrmann, J. & Fayad, A. A. Natural products from myxobacteria: novel metabolites and bioactivities. *Nat. Prod. Rep.* **34**, 135–160 (2017).
22. Becker, K. & Stadler, M. Recent progress in biodiversity research on the Xylariales and their secondary metabolism. *J. Antibiot. (Tokyo).* **74**, 1–23 (2021).
23. Lambert, R. J. W. & Pearson, J. Susceptibility testing: Accurate and reproducible minimum inhibitory concentration (MIC) and non-inhibitory concentration (NIC) values. *J. Appl. Microbiol.* **88**, 784–790 (2000).
24. Sarathy, J. P. et al. TBAJ-876, a 3,5-dialkoxypyridine analogue of Bedaquiline, is active against Mycobacterium abscessus. *Antimicrob. Agents Chemother.* (2020) doi:10.1128/aac.02404-19.
25. Warrier, T. et al. Identification of Novel Anti-mycobacterial Compounds by Screening a

Pharmaceutical Small-Molecule Library against Nonreplicating Mycobacterium tuberculosis. *ACS Infect. Dis.* **1**, 580–585 (2015).

26. Niles, A. L., Moravec, R. A. & Riss, T. L. Update on in vitro cytotoxicity assays for drug development. *Expert Opin. Drug Discov.* **3**, 655–669 (2008).
27. Lupien, A. et al. Optimized background regimen for treatment of active tuberculosis with the next-generation benzothiazinone macozinone (PBTZ169). *Antimicrob. Agents Chemother.* **62**, (2018).
28. Malin, J. J., Winter, S., Edeltraud, van G., Plum, G. & Rybniker, J. Extremely Low Hit Rate in a Diverse Chemical Drug Screen Targeting Mycobacterium abscessus. *Antimicrob. Agents Chemother.* **63**, (2019).
29. Ballell, L. et al. Fueling Open-Source Drug Discovery: 177 Small-Molecule Leads against Tuberculosis. *ChemMedChem* **8**, 313–321 (2013).
30. Szekely, R. et al. 6,11-Dioxobenzo[f]pyrido[1,2-a]indoles kill Mycobacterium tuberculosis by targeting iron-sulfur protein Rv0338c (IspQ) a putative redox sensor. *ACS Infect. Dis.* (2020) doi:10.1021/acsinfecdis.0c00531.
31. Lee, W. et al. The Mechanism of Action of Lysobactin. *J. Am. Chem. Soc.* **138**, 100–103 (2016).
32. Chew, K. L. et al. In vitro susceptibility of Mycobacterium abscessus complex and feasibility of standardizing treatment regimens. *J. Antimicrob. Chemother.* **76**, 973–978 (2021).
33. Svetitsky, S., Leibovici, L. & Paul, M. Comparative efficacy and safety of vancomycin versus teicoplanin: Systematic review and meta-analysis. *Antimicrob. Agents Chemother.* **53**, 4069–4079 (2009).
34. Lilic, M. et al. The antibiotic sorangicin A inhibits promoter DNA unwinding in a Mycobacterium tuberculosis rifampicin-resistant RNA polymerase. *Proc. Natl. Acad. Sci. U. S. A.* **117**, 30423–30432 (2020).
35. Aziz, D. B. et al. Rifabutin Is active against mycobacterium abscessus complex. *Antimicrob. Agents Chemother.* **61**, (2017).
36. Dick, T., Shin, S. J., Koh, W. J., Dartois, V. & Gengenbacher, M. Rifabutin is active against mycobacterium abscessus in mice. *Antimicrob. Agents Chemother.* **64**, (2020).
37. Pethe, K. et al. A chemical genetic screen in Mycobacterium tuberculosis identifies

carbon-source-dependent growth inhibitors devoid of in vivo efficacy. *Nat. Commun.* **1**, 57 (2010).

38. Hatakeyama, S., Ohama, Y., Okazaki, M., Nukui, Y. & Moriya, K. Antimicrobial susceptibility testing of rapidly growing mycobacteria isolated in Japan. *BMC Infect. Dis.* **17**, (2017).
39. O'Sullivan, J. et al. Lysobactin, a novel antibacterial agent produced by lysobacter sp. I. Taxonomy, isolation and partial characterization. *J. Antibiot. (Tokyo).* **41**, 1740–1744 (1988).
40. Bonner, D. P., O'Sullivan, J., Tanaka, S. K., Clark, J. M. & Whitney, R. R. Lysobactin, a novel antibacterial agent produced by lysobacter sp. II. Biological properties. *J. Antibiot. (Tokyo).* **41**, 1745–1751 (1988).
41. Mukherjee, D., Wu, M. L., Teo, J. W. P. & Dick, T. Vancomycin and clarithromycin show synergy against Mycobacterium abscessus in vitro. *Antimicrob. Agents Chemother.* **61**, (2017).
42. Aziz, D. B., Teo, J. W. P., Dartois, V. & Dick, T. Teicoplanin - Tigecycline combination shows synergy against Mycobacterium abscessus. *Front. Microbiol.* **9**, (2018).
43. Jansen, R., Wray, V., Irschik, H., Reichenbach, H. & Höfle, G. Isolation and spectroscopic structure elucidation of sorangicin a, a new type of macrolide-polyether antibiotic from gliding bacteria - XXX. *Tetrahedron Lett.* **26**, 6031–6034 (1985).
44. Irschik, H., Gerth, K., Reichenbach, H., Jansen, R. & Hofle, G. The Sorangicins, Novel And Powerful Inhibitors Of Eubacterial Rna Polymerase Isolated From Myxobacteria. *J. Antibiot. (Tokyo).* **40**, 7–13 (1987).
45. Campbell, E. A. et al. Structural, functional, and genetic analysis of sorangicin inhibition of bacterial RNA polymerase. *EMBO J.* **24**, 674–682 (2005).
46. Ganapathy, U. S., Dartois, V. & Dick, T. Repositioning rifamycins for Mycobacterium abscessus lung disease. *Expert Opin. Drug Discov.* **14**, 867–878 (2019).
47. Guimbellot, J. S., Acosta, E. P. & Rowe, S. M. Sensitivity of ivacaftor to drug-drug interactions with rifampin, a cytochrome P450 3A4 inducer. *Pediatr. Pulmonol.* **53**, E6–E8 (2018).
48. Kim, T. et al. A screening of the mmv pandemic response box reveals epetraborole as a new potent inhibitor against mycobacterium abscessus. *Int. J. Mol. Sci.* **22**, (2021).

49. Ganapathy, U. S., Gengenbacher, M. & Dick, T. Epetraborole is active against mycobacterium abscessus. *Antimicrob. Agents Chemother.* **65**, (2021).
50. Sullivan, J. R. et al. Efficacy of epetraborole against Mycobacterium abscessus is increased with norvaline. *PLoS Pathog.* **17**, 1–28 (2021).
51. Dartois, V. & Dick, T. Drug development challenges in nontuberculous mycobacterial lung disease: TB to the rescue. *J. Exp. Med.* **219**, e20220445 (2022).
52. Hollstein, U. Actinomycin. Chemistry and mechanism of action. *Chem. Rev.* **74**, 625–652 (1974).
53. Robey, R. W. et al. Becatecarin (rebeccamycin analog, NSC 655649) is a transport substrate and induces expression of the ATP-binding cassette transporter, ABCG2, in lung carcinoma cells. *Cancer Chemother. Pharmacol.* **64**, 575–583 (2009).
54. Kong, D. et al. Echinomycin, a small-molecule inhibitor of hypoxia-inducible factor-1 DNA-binding activity. *Cancer Res.* **65**, 9047–9055 (2005).
55. Zhanel, G. G. et al. The Ketolides: A Critical Review. *Drugs* **62**, 1771–1804 (2002).
56. Surup, F. et al. Activation of the NLRP3 Inflammasome by Hyaboron, a New Asymmetric Boron-Containing Macrodiolide from the Myxobacterium Hyalangium minutum. *ACS Chem. Biol.* **13**, 2981–2988 (2018).
57. Santiago, M. et al. Genome-wide mutant profiling predicts the mechanism of a Lipid II binding antibiotic article. *Nat. Chem. Biol.* **14**, 601–608 (2018).
58. Irschik, H. & Reichenbach, H. The mechanism of action of myxovalargin a, a peptide antibiotic from myxococcus fulvus. *J. Antibiot. (Tokyo).* **38**, 1237–1245 (1985).
59. Lilic, M. et al. The antibiotic sorangicin A inhibits promoter DNA unwinding in a Mycobacterium tuberculosis rifampicin-resistant RNA polymerase. *Proc. Natl. Acad. Sci. U. S. A.* **117**, 30423–30432 (2020).
60. Müller, R. et al. Novel Sorangicin Antibiotic. (2020).
61. Flatman, R. H., Howells, A. J., Heide, L., Fiedler, H. P. & Maxwell, A. Simocyclinone D8, an inhibitor of DNA gyrase with a novel mode of action. *Antimicrob. Agents Chemother.* **49**, 1093–1100 (2005).
62. Bols, M., Binderup, L., Hansen, J. & Rasmussen, P. Inhibition of Collagenase by Aranciamycin and Aranciamycin Derivatives. *J. Med. Chem.* **35**, 2768–2771 (1992).
63. Hartkoorn, R. C. et al. Towards a new tuberculosis drug: Pyridomycin - nature's isoniazid.

EMBO Mol. Med. **4**, 1032–1042 (2012).

64. Phonkerd, N. et al. Bis-spiro-azaphilones and azaphilones from the fungi Chaetomium cochliodes VTh01 and C. cochliodes CTh05. *Tetrahedron* **64**, 9636–9645 (2008).
65. Wang, R. et al. Molecular basis of V-ATPase inhibition by bafilomycin A1. *Nat. Commun.* **12**, (2021).
66. Schummer, D., HöFle, G. & Reichenbach, H. The Tartrolons, New Boron-containing Antibiotics from a Myxobacterium, Sorangium cellulosum. *J. Antibiot. (Tokyo).* **48**, 26–30 (1995).
67. Lewer, P., Chapin, E. L., Graupner, P. R., Gilbert, J. R. & Peacock, C. Tartrolone C: A novel insecticidal macrodiolide produced by Streptomyces sp. CP1130. *J. Nat. Prod.* **66**, 143–145 (2003).

2.10 FIGURES AND TABLES

TABLE 2.1. Effect of carbon source and minimal media on potencies of natural product hits against *M. abscessus* ATCC 19977 smooth reference strain.

	pMIC$_{90}$ (M)			
Compound	**7H9[a] Glycerol**	**7H9[a] Acetate**	**CaMH[b] Glycerol**	**Sauton[c] Glycerol**
Lysobactin	5.5	5.5	5.4	5.3
Sorangicin A	4.9	4.8	4.8	4.4

[a]Middlebrook 7H9 media

[b]Cation-adjusted Mueller Hinton media

[c]Sauton mycobacteria minimal media

TABLE 2.2. Characterization of *M. abscessus* clinical isolates.

Isolate	Subspecies	Morphotype	*rpoB* AA	*rrl* SNP	*erm*(41) sequevar	Clarithromycin susceptibility
ATCC19977	abscessus	Smooth	none	none	T28	Sensitive
ATCC19977	abscessus	Rough	none	none	T28	Sensitive
MB084806	abscessus	Smooth	D523E	none	T28	Sensitive
MB092927	abscessus	Smooth	D523E	none	C28	Sensitive
MB093261	abscessus	Smooth	none	none	T28	Sensitive
L0007906	abscessus	Rough	D523E	A2270G	T28	Resistant
MB086151	abscessus	Rough	D523E	none	C28	Sensitive
MB088425	massiliense	Smooth	D523E	none	deletion	Sensitive
MB088215	massiliense	Smooth	D523E	none	deletion	Sensitive
MB092961	massiliense	Rough	D523E	none	deletion	Sensitive
L00042522	massiliense	Rough	D523E	A2271C	deletion	Resistant
AV	massiliense	Smooth	D523E	none	deletion	Sensitive
167P	bolletii	Rough	D523E	none	T28	Resistant

TABLE 2.3. Potencies of natural product hits against *M. abscessus* reference strain and clinical isolates.

Isolate	Subspecies	Morphotype	$pMIC_{90}$ (M)[a]				
			Cell Wall		RNA Polymerase		
			LYB	VAN	SOR	RIF	RFB
ATCC19977	abscessus	Smooth	5.7	5.2	5.0	4.9	5.7
ATCC19977	abscessus	Rough	5.7	5.0	4.7	4.6	5.7
MB084806	abscessus	Smooth	5.4	5.6	5.1	5.2	6.1
MB092927	abscessus	Smooth	5.1	5.5	4.7	4.8	5.8
MB093261	abscessus	Smooth	5.1	5.1	4.8	5.0	5.8
L0007906	abscessus	Rough	4.9	5.3	4.7	4.2	5.3
MB086151	abscessus	Rough	5.3	5.6	4.9	4.9	5.8
MB088425	massiliense	Smooth	5.4	5.3	5.1	5.2	5.8
MB088215	massiliense	Smooth	5.4	5.3	5.1	5.1	5.8
MB092961	massiliense	Rough	5.4	5.3	5.1	5.2	5.9
L00042522	massiliense	Rough	4.7	5.1	4.3	4.3	5.2
AV	massiliense	Smooth	4.8	5.1	4.5	4.4	5.5
167P	bolletii	Rough	5.3	5.7	5.5	5.4	6.1

[a]LYB, lysobactin; VAN, vancomycin; SOR, sorangicin A; RIF, rifampicin; RFB, rifabutin

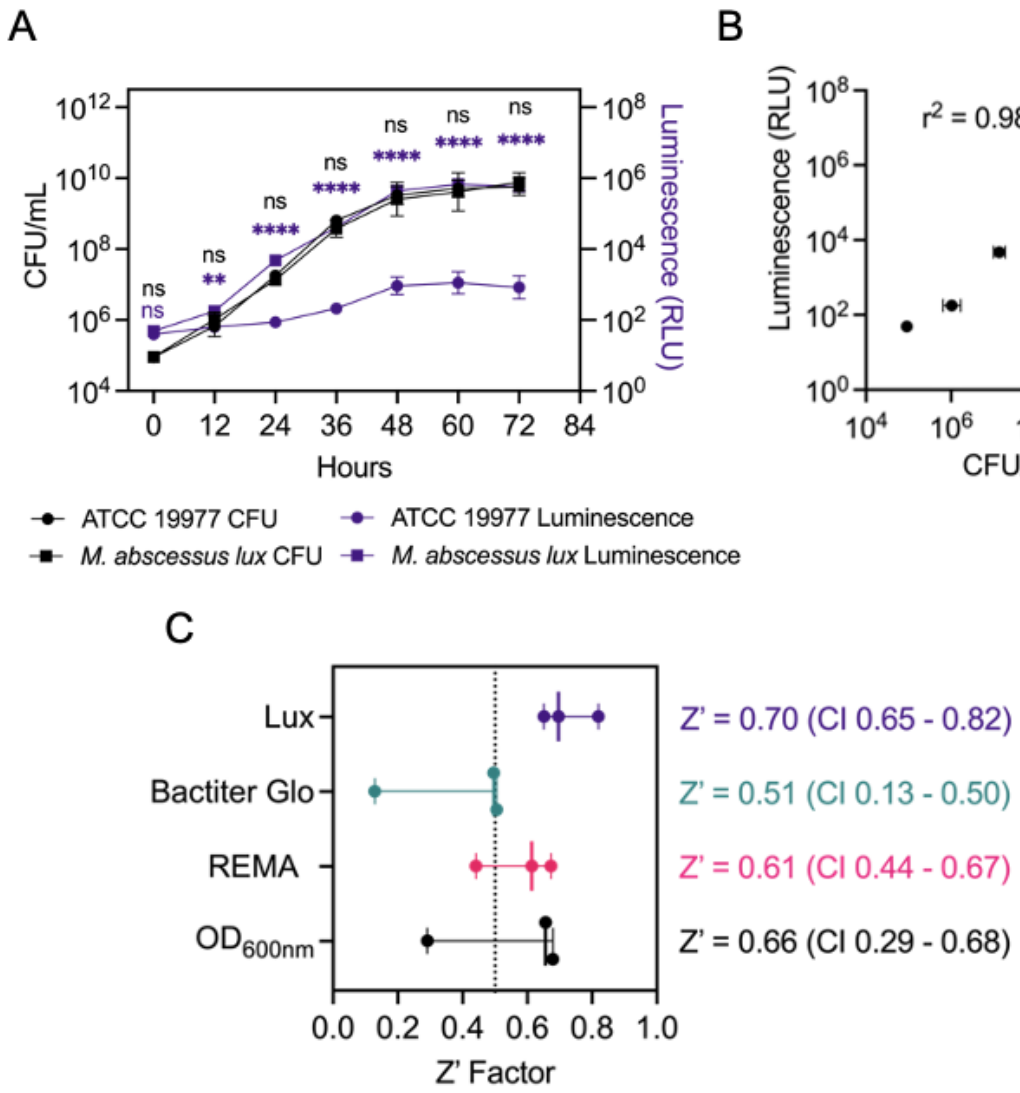

FIGURE 2.1. Validation of luminescence from *M. abscessus* constitutively expressing lux. **A** *M. abscessus* 19977 ATCC 19977 was made to constitutively express the luxCDABE operon (*M. abscessus lux*). Reference strain ATCC 19977 (circles) and *M. abscessus lux* (squares) were grown in 7H9 complete with CFU/mL (black symbols) and luminescence (purple symbols) measured at 12-hour intervals. Data shown is n = 3 with mean ± SD. P values from 2-way ANOVA with Sidak's multiple comparison test. **B** Correlation between luminescence output and bacterial growth measured with Pearson's correlation coefficient. **C** Z' Factor measured using OD_{600nm}, resazurin microtiter assay (REMA), and Bactiter Glo readouts on *M. abscessus* ATCC 19977, and luminescence readout on *M. abscessus lux*. Data shown is median with 95% CI of n = 3.

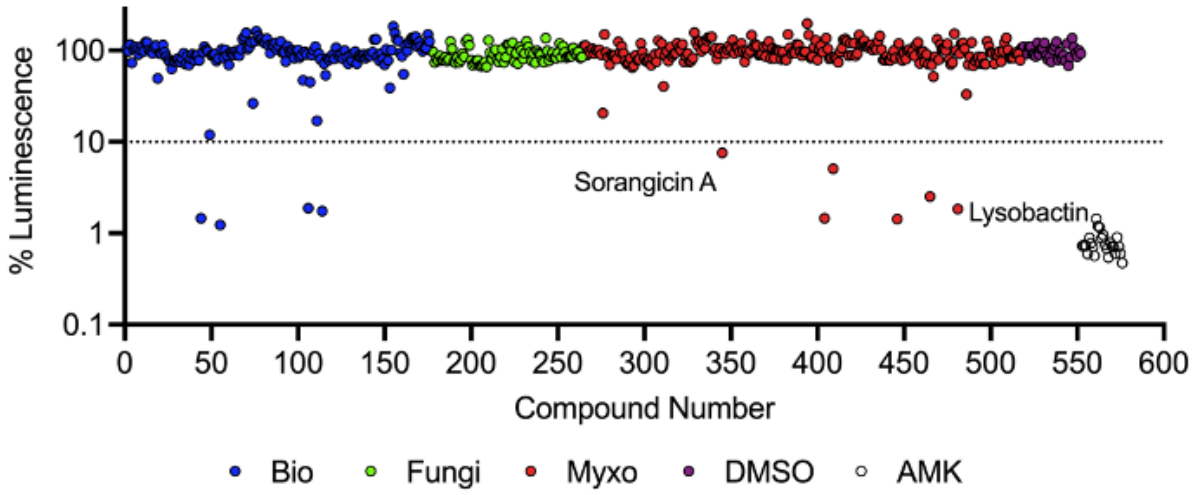

FIGURE 2.2. Natural product primary screen. A library of 517 natural products was screened against *M. abscessus lux* at a concentration of 10 µM. Dashed red line indicates 90% luminescence reduction cut off. Natural product library includes 176 compounds fractionated from diverse sources (blue, cyan), 88 compounds fractionated from fungi (green), 253 compounds fractionated from myxobacteria (red, orange, yellow), 1% DMSO as vehicle control (purple), and 100 µM amikacin as positive control (white). Data shown is mean of duplicate screening.

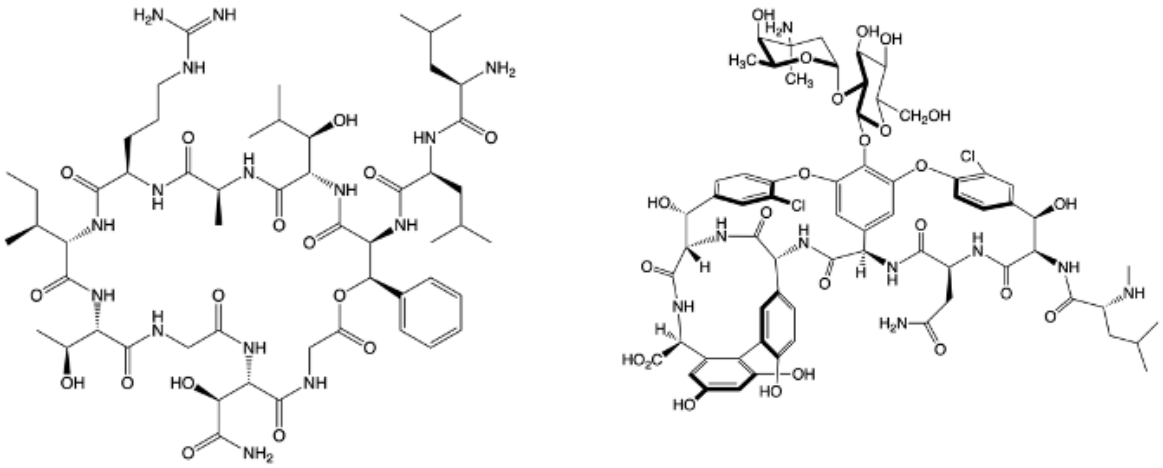

FIGURE 2.3. Structures of nonribosomal peptide synthetase-derived cyclic peptides targeting peptidoglycan biosynthesis.

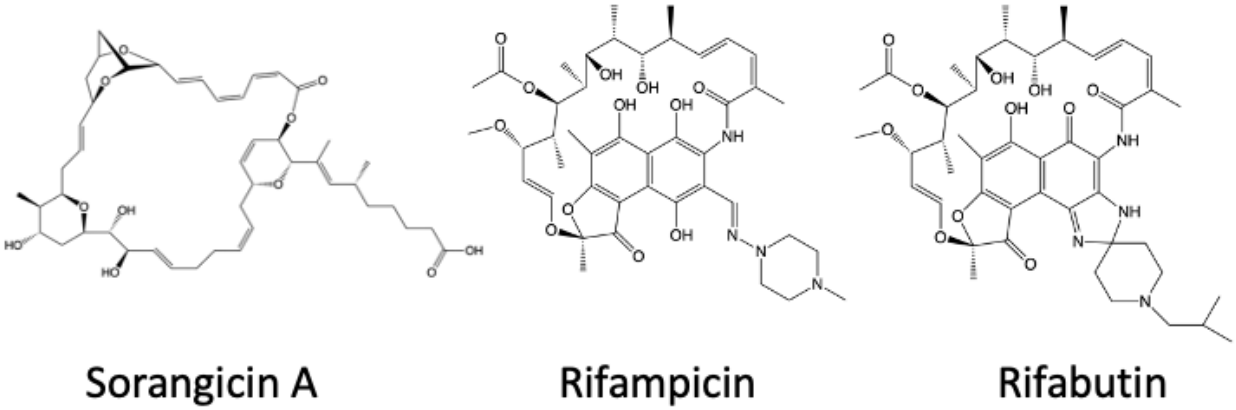

FIGURE 2.4. Structures of polyketide synthase-derived sorangicin A and semi-synthetic rifamycins targeting RNA polymerase.

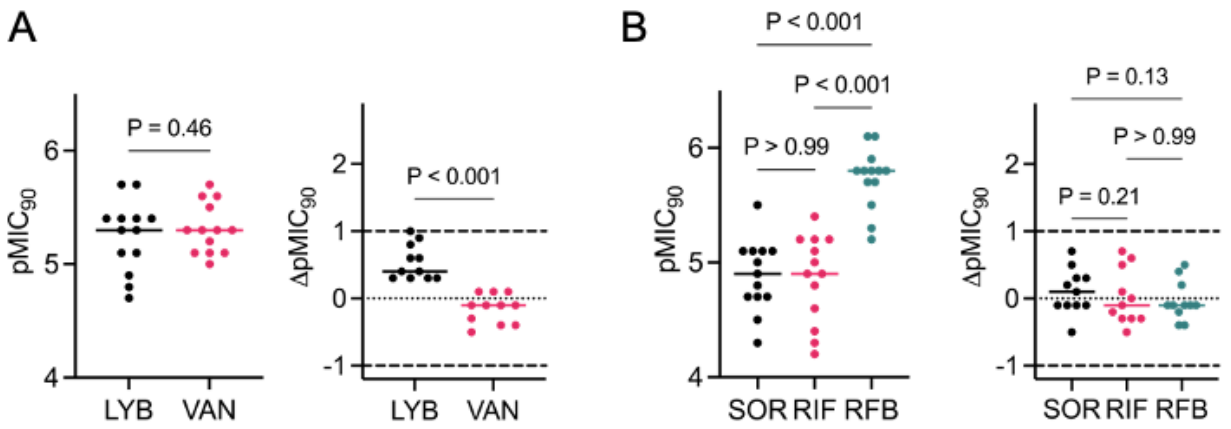

FIGURE 2.5. Potencies of natural product hits against *M. abscessus* ATCC 19977 S and R reference strains and clinical isolates. Clinical isolates comprise *M. abscessus* complex (*M. abscessus* n = 5, *M. massiliense* n = 5, *M. bolletii* n = 1). **A** MIC_{90} (μM) of LYB and VAN converted to $pMIC_{90}$ (M) (left). Change in $pMIC_{90}$ relative to *M. abscessus* ATCC 19977 ($pMIC_{90\ ATCC} - pMIC_{90\ clin\ iso}$). Values greater than 0 indicate lower potency against the clinical isolate. Dashed lines represent 10-fold change in potency. Data shown is median with P values from Wilcoxon matched-pairs rank test. **B** MIC_{90} (μM) of SOR, RIF, and RFB converted to $pMIC_{90}$ (M) (left). Change in $pMIC_{90}$ relative to *M. abscessus* ATCC 19977 ($pMIC_{90\ ATCC} - pMIC_{90\ clin\ iso}$). Values greater than 0 indicate lower potency against the clinical isolate. Dashed lines represent 10-fold change in potency. Data shown is median with P values from Friedman test with Dunn's multiple comparisons test.

2.11 SUPPLEMENTARY MATERIAL

TABLE S2.1. Compounds with *in vitro* activity against *M. abscessus* identified from natural product library.

Threshold Cut-off	Library	Compound	Source	Mechanism	Reference
10%	Bio	Actinomycin D	*Streptomyces* spp.	DNA intercalator	[52]
	Bio	Actinomycin X2	*Streptomyces* spp.	DNA intercalator	[52]
	Bio	Becatecarin	Derivative of rebeccamycin (*Nocardia* spp.)	DNA intercalator	[53]
	Bio	Echinomycin	*Streptomyces* spp.	DNA intercalator	[54]
	Bio	Telithromycin	Semisynthetic erythromycin derivative	50S ribosome inhibitor	[55]
	Myxo	Hyaboron	*Hyalangium minutum*	Putative potassium ionophore	[56]
	Myxo	Lysobactin (Katanosin B)	*Lysobacter* spp.	Lipid II inhibitor	[31]
	Myxo	Lysocin E	*Lysobacter* spp.	Lipid II/Menaquinone inhibitor	[57]
	Myxo	Lysocin I	*Lysobacter* spp.	Lipid II/Menaquinone inhibitor	[57]
	Myxo	Myxovalargin A	*Myxococcus fulvus*	Inhibitor of protein synthesis	[58]
	Myxo	Sorangicin A	*Sorangium cellulosum*	RNAP inhibitor	[59]
	Myxo	Neosorangicin A	*Sorangium cellulosum*	RNAP inhibitor	[60]
50%	Bio	Simocyclinone D4	*Streptomyces antibioticus* Tü 6040	DNA gyrase inhibitor	[61]
	Bio	Simocyclinone D8	*Streptomyces antibioticus* Tü 6040	DNA gyrase inhibitor	[61]
	Bio	Aranciamycin	*Streptomyces* spp.	Collagenase inhibitor	[62]
	Bio	Pyridomycin	*Dactylosporangium fulvum*	Enoyl-ACP reductase inhibitor	[63]
	Bio	Cochliodone A	*Chaetomium cochliodes*	N.D[a]	[64]
	Bio	Bafilomycin A1	*Streptomyces* spp.	Vacuolar-type H^+-ATPase inhibitor	[65]
	Myxo	Tartrolon B	*Sorangium cellulosum*	Disrupt K^+ gradient	[66]
	Myxo	Tartrolon C	*Streptomyces* spp.	N.D[a]	[67]

[a]Not determined

TABLE S2.2. Effect of carbon source and minimal media on potencies of natural product hits against *M. abscessus* ATCC 19977 smooth reference strain.

	MIC_{90} (μM)			
Compound	**7H9[a] Glycerol**	**7H9[a] Acetate**	**CaMH[b] Glycerol**	**Sauton[c] Glycerol**
Lysobactin	3	3	4	5
Sorangicin A	13	16	16	39

[a]Middlebrook 7H9 media with 10% ADC (albumin, dextrose, catalase), 0.05% Tween-80, 0.02% carbon source

[b]Cation-adjusted Mueller Hinton media with 10% ADC, 0.05% Tween-80, 0.02% carbon source

[c]Sauton mycobacteria minimal media with 0.05% Tween-80, 0.02% carbon source

TABLE S2.3. Potencies of natural product hits against *M. abscessus* reference strain and clinical isolates.

					MIC_{90} (μM)[a]				
					Cell Wall		RNA Polymerase		
Isolate	Subspecies	Morphotype	*erm*41 Sequevar	CLR susceptibility	LYB	VAN	SOR	RIF	RFB
ATCC19977	abscessus	Smooth	T28	Sensitive	2	7	11	13	2
ATCC19977	abscessus	Rough	T28	Sensitive	2	9	18	23	2
MB084806	abscessus	Smooth	T28	Sensitive	5	2	7	7	1
MB092927	abscessus	Smooth	C28	Sensitive	8	3	21	18	2
MB093261	abscessus	Smooth	T28	Sensitive	9	7	17	10	2
L0007906	abscessus	Rough	T28	Resistant	13	5	15	69	5
MB086151	abscessus	Rough	C28	Sensitive	5	2	13	12	1
MB088425	massiliense	Smooth	deletion	Sensitive	4	6	8	7	2
MB088215	massiliense	Smooth	deletion	Sensitive	4	5	8	7	2
MB092961	massiliense	Rough	deletion	Sensitive	4	5	8	7	1
L00042522	massiliense	Rough	deletion	Resistant	19	8	50	100	7
AV	massiliense	Smooth	deletion	Sensitive	15	8	30	46	3
167P	bolletii	Rough	T28	Resistant	5	2	3	4	1

[a]CLR, clarithromycin; LYB, lysobactin; VAN, vancomycin; SOR, sorangicin A; RIF, rifampicin; RFB, rifabutin

TABLE S2.4. Drug susceptibility profile of *M. abscessus* complex clinical isolates.

			MIC$_{90}$ (μM)[ab]									
			Protein Synthesis					DNA Synthesis		ETC		Cell Wall
Isolate	**Subspecies**	**Morphotype**	**CLR**	**AMK**	**LZD**	**TIG[c]**	**DOX**	**MOX**	**CIP**	**BDQ[c]**	**CFZ[c]**	**CFX**
MB084806	abscessus	Smooth	1	11	*36*	4	**120**	*3*	**31**	0.1	6	15
MB092927	abscessus	Smooth	0.3	3	*93*	3	**116**	*6*	**74**	1	7	28
MB093261	abscessus	Smooth	1	8	**97**	5	**120**	*4*	**33**	1	9	18
L0007906	abscessus	Rough	**>134**	**>172**	10	9	**28**	*10*	**28**	3	11	30
MB086151	abscessus	Rough	0.3	6	10	4	**107**	*3*	**29**	1	44	*38*
MB088425	massiliense	Smooth	1	11	5	9	**58**	2	*8*	1	10	17
MB088215	massiliense	Smooth	1	11	5	5	**61**	*3*	*8*	1	10	16
MB092961	massiliense	Rough	1	11	5	5	**56**	2	*7*	2	11	7
L00042522	massiliense	Rough	**>134**	*42*	*72*	>68	*13*	**13**	**41**	2	25	15
MB087124	massiliense	Rough	**>134**	*37*	*53*	10	*13*	**13**	**17**	3	24	15

[a]CLR, clarithromycin; AMK, amikacin; LZD, linezolid; TIG, tigecycline; DOX, doxycycline; MOX, moxifloxacin; CIP, ciprofloxacin; BDQ, bedaquiline; CFZ, clofazimine; CFX, cefoxitin

[b]Susceptible, *Intermediate*, **Resistant**

[c]No established critical concentration cut off

PREFACE TO CHAPTER 3

Indeed, the library of natural products from myxobacteria, other bacteria, and plants was a fruitful source for *M. abscessus* antimicrobials, however, lysobactin and sorangicin A represent hit compounds and would require extensive follow up studies before acquiring the status as a lead compound. During this time, Cystic Fibrosis Canada revised their goals in accordance with patient input and released a call for compounds near the pre-clinical stage. We therefore shifted our focus on libraries of known antimicrobials with the potential for repurposing for *M. abscessus*. GlaxoSmithKline (GSK) provided a set of 176 compounds that were pre-screened for activity against *M. tuberculosis* while MMV provided two boxes of 800 compounds with activity against various bacterial, fungal, and viral pathogens. This chapter describes the work that identified epetraborole from the Pandemic Response Box from MMV, one of three hit compounds identified (3/976). In the second half of this chapter, we describe the potential of using norvaline as an adjuvant-like molecule with epetraborole.

This chapter was adapted from the manuscript: Efficacy of epetraborole against *Mycobacterium abscessus* is increased with norvaline. Sullivan *et al*. *PLoS Pathog*. **2021**, 17(10): e1009965.

CHAPTER 3

Efficacy of epetraborole against *Mycobacterium abscessus* is increased with norvaline

Jaryd R. Sullivan[1,2,3], Andréanne Lupien[2,3], Elias Kalthoff[4,5], Claire Hamela[6], Lorne Taylor[7], Kim A. Munro[4,5], T. Martin Schmeing[4,5], Laurent Kremer[6,8], Marcel A. Behr[1,2,3,9*]

[1]Department of Microbiology & Immunology, McGill University, Montréal, Canada.

[2]Infectious Diseases and Immunity in Global Health Program, Research Institute of the McGill University Health Centre, Montréal, Canada.

[3]McGill International TB Centre, Montréal, Canada.

[4]Department of Biochemistry, McGill University, Montréal, Canada.

[5]Centre de Recherche en Biologie Structural, McGill University, Montréal, Canada.

[6]Centre National de la Recherche Scientifique UMR 9004, Institut de Recherche en Infectiologie de Montpellier (IRIM), Université de Montpellier, Montpellier, France.

[7]Clinical Proteomics Platform, Research Institute of the McGill University Health Centre, Montréal, Canada.

[8]INSERM, IRIM, Montpellier, France.

[9]Department of Medicine, McGill University Health Centre, Montréal, Canada.

PloS Pathog. 2021 October 12; 17(10) : e1009965. Doi : 10.1371/journal.ppat.1009965

3.1 ABSTRACT

Mycobacterium abscessus is the most common rapidly growing non-tuberculous mycobacteria to cause pulmonary disease in patients with impaired lung function such as cystic fibrosis. *M. abscessus* displays high intrinsic resistance to common antibiotics and inducible resistance to macrolides like clarithromycin. As such, *M. abscessus* is clinically resistant to the entire regimen of front-line *M. tuberculosis* drugs, and treatment with antibiotics that do inhibit *M. abscessus* in the lab results in cure rates of 50% or less. Here, we identified epetraborole (EPT) from the MMV pandemic response box as an inhibitor against the essential protein leucyl-tRNA synthetase (LeuRS) in *M. abscessus.* EPT protected zebrafish from lethal *M. abscessus* infection and did not induce self-resistance nor against clarithromycin. Contrary to most antimycobacterials, the whole cell activity of EPT was greater against *M. abscessus* than *M. tuberculosis*, but crystallographic and equilibrium binding data showed that EPT binds $LeuRS_{Mabs}$ and $LeuRS_{Mtb}$ with similar residues and dissociation constants. Since EPT-resistant *M. abscessus* mutants lost LeuRS editing activity, these mutants became susceptible to misaminoacylation with leucine mimics like the non-proteinogenic amino acid norvaline. Proteomic analysis revealed that when *M. abscessus* LeuRS mutants were fed norvaline, leucine residues in proteins were replaced by norvaline, inducing the unfolded protein response with temporal changes in expression of GroEL chaperonins and Clp proteases. This supports our *in vitro* data that supplementation of media with norvaline reduced the emergence of EPT mutants in both *M. Abscessus* and *M. tuberculosis*. Furthermore, the combination of EPT and norvaline had improved *in vivo* efficacy compared to EPT in a murine model of *M. abscessus* infection. Our results emphasize the effectiveness of EPT against the clinically relevant cystic fibrosis pathogen *M. abscessus,* and these findings also suggest norvaline adjunct therapy with EPT could be beneficial for *M. abscessus* and other mycobacterial infections like tuberculosis.

3.2 AUTHOR SUMMARY

Current antimycobacterial drugs are inadequate to handle the increasing number of non-tuberculous mycobacteria infections that eclipse tuberculosis infections in many developed countries. Of particular importance for cystic fibrosis patients, *Mycobacterium abscessus* is notoriously difficult to treat where patients spend extended time on antibiotics with cure rates comparable to extreme drug resistant *M. tuberculosis*. Here, we identified epetraborole (EPT) with *in vitro* and *in vivo* activities against *M. abscessus*. We showed that EPT targets the editing domain of the leucyl-tRNA synthetase (LeuRS) and that escape mutants lost LeuRS editing activity, making these mutants susceptible to misaminoacylation with leucine mimics. Most importantly, combination therapy of EPT and norvaline limited the rate of EPT resistance in both *M. abscessus* and *M. tuberculosis*, and this was the first study to demonstrate improved *in vivo* efficacy of EPT and norvaline compared to EPT in a murine model of *M. abscessus* pulmonary infection. The demonstration of norvaline adjunct therapy with EPT for *M. abscessus* infections is promising for cystic fibrosis patients and could translate to other mycobacterial infections, such as tuberculosis.

3.3 INTRODUCTION

Mycobacterium abscessus is a nontuberculous mycobacterium that commonly causes chronic lung disease, especially among patients with cystic fibrosis.[1] Treatment of pulmonary exacerbation relies on a regimen of intravenous amikacin (AMK), tigecycline, and imipenem plus an oral macrolide if the isolate is susceptible to macrolides.[2,3] Despite guideline-based treatment, combination therapy typically results in cure rates of 50% or less due to the bacterium being intrinsically resistant to many antibiotic classes.[4,5] Unfortunately, the *M. abscessus* drug-development pipeline is limited to a handful of repurposed drugs (clofazimine, rifabutin, and bedaquiline).[6] Lately, antibiotics that have shown activity in pre-clinical studies include the oxazolidinones (LCB01-0371[7] and tedizolid[8]) that target the 50S ribosomal subunit and PIPD1/indol-2-carboxamides that target the mycolic acid transporter MmpL3.[9,10]

Recently, aminoacyl-tRNA synthetases (aaRSs) became targets of interest for drug discovery when benzoxaboroles were identified as novel boron-based pharmacophores.[11,12] aaRSs are enzymes that aminoacylate tRNAs with their cognate amino acids. All aaRSs have an aminoacylation domain while some are bifunctional and contain an editing domain. The aminoacylation domain forms an aminoacyl adenylate through condensation of the amino acid with ATP, and then transfers the aminoacyl moiety to the 3' terminal adenosine of the tRNA acceptor stem. Some aaRSs, however, have evolved an editing domain to ensure the correct amino acid is ligated to its tRNA.[13,14] This domain is critical for aaRSs that must distinguish their cognate amino acid from structurally similar amino acids like branched-chain amino acids. Leucyl-tRNA synthetases (LeuRSs) are examples of aaRSs that rely on their editing domains to limit misaminoacylation of tRNA with near-cognate amino acids and maintain the fidelity of the genetic code.

Herein, we identified epetraborole (EPT) from the Medicines for Malaria Venture (MMV) Open pandemic response box as a LeuRS inhibitor in *M. abscessus* with nanomolar activity *in vitro* and activity in zebrafish embryos and NOD.SCID mice. Interestingly, EPT was more active against *M. abscessus* than *M. tuberculosis*, and this observation was not supported by structural differences in the crystal structures of the LeuRS editing domain of *M. abscessus* and *M. tuberculosis* bound

to EPT. Furthermore, we highlighted the utility of norvaline to target LeuRS editing deficient escape mutants and suppress resistance *in vitro* by misincorporation of norvaline in place of leucine residues resulting in disrupted protein folding. Importantly, we showed that EPT and norvaline combination has improved efficacy over EPT monotherapy in a murine model of *M. abscessus* infection. These data support the potential of the benzoxaborole scaffold in the antimycobacterial drug pipeline and suggest that its activity can be potentiated by supplementation with norvaline or a norvaline derivative.

3.4 METHODS

3.4.1 Ethics Statement

All protocols involving mice followed the guidelines of the Canadian Council on Animal Care (CCAC) and were approved by the ethics committees of the RI-MUHC (project identifier [ID] 2015-7656).

3.4.2 Culture Conditions

Mycobacteria strains were grown in rolling liquid culture at 37 °C in Middlebrook 7H9 (Difco) supplemented with 10% albumin dextrose catalase (ADC), 0.2% glycerol, and 0.05% Tween 80 (7H9 complete) or on 7H10 agar plates supplemented with 10% oleic acid ADC and 0.5% glycerol at 37 °C. When mentioned, the carbon source was modified from glycerol to acetate or the detergent Tween 80 was removed from the media. *Bacillus cereus* (clinical isolate), *Corynebacterium glutamicum* (ATCC 13032), *Escherichia coli*, and *Pseudomonas aeruginosa* PAO1 were grown in LB broth. HepG2 cells (ATCC HB-8065) were grown in Dulbecco's modified Eagle's medium (DMEM) with phenol red (from Gibco) supplemented with 10% fetal bovine serum at 37 °C with 5% CO_2.

3.4.3 Compound Libraries

The GSK library contains 176 small molecules with antimycobacterial activity, specifically against *Mycobacterium tuberculosis.*[15] Medicines for Malaria Venture created two compound sets: the Pathogen Box and the Pandemic Response Box. The Pathogen Box is composed of 400 molecules active against various disease sets (https://www.mmv.org/mmv-open/pathogen-box/about-pathogen-box). The Pandemic Response Box is composed of 400 diverse drug-like molecules broadly categorized as antibacterials (201 molecules), antivirals (153 molecules), and antifungals (46 molecules) (https://www.mmv.org/mmv-open/pandemic-response-box/about-pandemic-response-box).

3.4.4 Library Screening

MMV Pathogen Box, MMV Pandemic Response Box, and GSK TB-active libraries were screened against *M. abscessus* ATCC 19977 strain which constitutively expressed the *luxCDABE* operon (*M. abscessus* lux) at 10 μM in duplicate in 96-well flat-bottom plates in 7H9 complete media.

The culture was grown to log phase (OD_{600} 0.4-0.8) and diluted to OD_{600} 0.005 ($5x10^6$ CFU/mL). 90 µL of culture was mixed with 10µL of compound. Plates were sealed with parafilm and incubated at 37 °C for 48 hours. Plates had a column of 0.1% DMSO as negative controls (drug-free conditions) and 64 µg/mL of AMK as positive controls. Luminescence was measured with an Infinite F200 Tecan plate reader. % Luminescence relative to DMSO control was plotted using GraphPad Prism version 9. Compounds that decreased luminescence ≤ 10% were classified as primary hits. Primary hits were screened against *M. abscessus* ATCC 19977 at 10 µM in triplicate using REMA (see "Determination of MIC" below). Plates were setup as performed for the primary screen. Fluorescence was measured with an Infinite F200 Tecan plate reader. % bacteria viability relative to DMSO control was plotted using GraphPad Prism version 9. Compounds that decreased bacteria viability ≤ 10% were classified as confirmed hits. Confirmed hits were followed up with dose-response curves to determine the minimum inhibitory concentration (MIC).

3.4.5 Determination of minimum inhibitory concentrations (MIC)

MIC values were determined using the resazurin microtiter assay (REMA). Cultures were grown to log phase (OD_{600} of 0.4-0.8) and diluted to OD_{600} of 0.005. Drugs were prepared in two-fold serial dilutions in 96-well plates with 90 µL of bacteria per well to a final volume of 100 µL. Plates were incubated at 37 °C until drug-free wells were turbid (2 days for *M. abscessus*). Ten µL of resazurin (0.025% wt/vol) was added to each well. Once the drug-free wells turned pink (one doubling time), the fluorescence (ex/em 560nm/590nm) was measured using an Infinite F200 Tecan plate reader. Fluorescence intensities were converted to % viable cells relative to drug-free conditions and fit to the Gompertz equation using GraphPad Prism version 9. MIC values at 90% growth inhibition were determined from the nonlinear regression Gompertz equation.

3.4.6 *In vitro* cytotoxicity in HepG2 cells

Drugs were prepared in two-fold serial dilutions in 96-well plates with 45 µL of Human HepG2 cells (2,000 cells/well) to a final volume of 50 µL. Plates were incubated for 3 days at 37 °C with 5% CO_2. Five µL of resazurin (0.025% wt/vol) was added to each well and incubated for 4 hours at 37 °C. Cell viability was determined from the fluorescence intensity as done in the previous REMA assay. 50% toxic dose concentrations (TD_{50}) values were obtained using a nonlinear regression fit equation ([inhibitor] vs response, variable slope) in GraphPad Prism version 9.

3.4.7 Assessment of EPT efficacy in infected Zebrafish

Experiments in zebrafish were conducted according to the Comité d'Ethique pour l'Expérimentation Animale de la Région Languedoc Roussillon under reference 2020022815234677V3. Experiments were performed using the *golden* mutant and macrophage reporter Tg(*mpeg1:mCherry)* lines as previously described.[16] Embryos were obtained and maintained as described.[17] Embryo age is expressed as hours post fertilisation (hpf). Green fluorescent *M. abscessus* CIP104536^T (R) expressing Wasabi were prepared and microinjected in the caudal vein (2-3 nL containing ≈100 bacteria/nL) in 30 hpf embryos previously dechorionated and anesthetized with tricaine.[18] The bacterial inoculum was checked *a posteriori* by injection of 2 nL in sterile PBS^T and plating on 7H10^{OADC}. Infected embryos were transferred into 6-well plates (12 embryos/well) and incubated at 28.5°C to monitor kinetics of infection and embryo survival. Survival curves were determined by counting dead larvae daily for up to 11 days, with the experiment concluded when uninfected embryos started to die. EPT treatment of infected embryos and uninfected embryos was commenced at 24 hpi (hours post-infection) for 5 days. The drug-containing solution was renewed daily. Bacterial loads in live embryos were determined by anesthetising embryos in tricaine as previously described,[19] mounting on 3% (w/v) methylcellulose solution and taking fluorescent images using a Zeiss Axio Zoom.V16 coupled with an Axiocam 503 mono (Zeiss). Fluorescence Pixel Count (FPC) measurements were determined using the 'Analyse particles' function in ImageJ.[18] All experiments were completed at least three times independently.

3.4.8 Isolation of resistant mutants

Early log phase *M. abscessus* (OD_{600} 0.1-0.4) was cultured and resuspended to an OD_{600} of 10. Ten mL of culture was kept as a reference strain for future sequencing. One hundred µL of OD_{600} 10 (approx 1 X 10^9 CFU/100µL) was plated on solid media containing 10X, 20X, or 40X MIC_{90} of the compound of interest. AMK was used as a control antibiotic. Plates were incubated for 5 days at 37 °C. Number of colonies were counted to obtain mutation frequencies. Resistant colonies were transferred into fresh media without antibiotics (to avoid the emergence of secondary mutations). The MIC (REMA method) was measured for the mutant against the compound of interest as well as a panel of reference compounds with different targets for negative controls.

3.4.9 Sequencing resistant mutants

Genomic DNA (gDNA) was extracted from the 10 mL reference aliquot of *M. abscessus* harvested during mutant isolation and fresh cultures of mutant strains with confirmed resistance (REMA method) using the Qiagen QIAamp UCP Pathogen Mini kit with a modified mechanical lysis protocol. Pellet culture by centrifugation and resuspend in 590 µL of ATL buffer containing the Dx reagent in a low-bind tube. Add 40 µL of proteinase K (20 mg/mL) and 20 µL of lysozyme (100 mg/mL) and incubate for 30 minutes at 56 °C under agitation. Transfer into a Pathogen Lysis Tube L and vortex twice using a FastPrep-24 instrument at 6.5 m/s for 45 s with a 5-minute incubation on ice in between. Transfer supernatant into fresh 2 mL low-bind tube. Follow manufacturer's instructions for sample prep with spin protocol. gDNA was quantified with Quant-iT PicoGreen dsDNA kit. *leuS* from ATCC 19977 and EPT mutants was sequenced with Sanger Sequencing with the primers listed in S5 Table.

3.4.10 Cloning and over-expressing mutant *leuS* in *M. abscessus*

Wildtype and mutant *leuS* (D436H) were PCR amplified from gDNA using Phusion with primers 1 & 2 (see S5 Table), ligated into pMV306_hsp60 digested with EcoRV and HindIII restriction enzymes, and transformed into *E. coli* DH5α cells (Promega). Plasmids were extracted and sequenced with primers 3-12 (see S5 Table) using Sanger sequencing.

3.4.11 Protein Purification

The *M. abscessus* LeuRS editing domain (residues 303-499 of WP005112800.1) and the *M. tuberculosis* LeuRS editing domain (residues 311-512 of WP_003900794.1) were synthesized with an N-terminal polyhistidine tag and tobacco etch virus (TEV) protease recognition site, with codon optimization for *E. coli* and cloned into pET24a(+) by the company BioBasic to create pMabsED and pMtbED, respectively. *E. coli* BL21 (DE3) cells were transformed with pMabsED or pMtbED and grown overnight at 37 °C on LB-agar with 50 µg/mL kanamycin. Single colonies were transferred into 100 mL of LB media with 50 µg/mL kanamycin (LB-kan) and grown overnight at 37 °C. One liter of LB-kan was inoculated with 10 mL of the overnight culture and grown at 37°C until an optical density at 600 nm of 0.6 was reached. Protein expression was then

induced with addition of 0.5 mM IPTG and the culture further incubated for 18 h at 16 °C. The cells were harvested by centrifugation (4000 g for 20 min), resuspended in buffer A (50 mM Tris, 150 mM NaCl, 2 mM BME) plus 2 mM PMSF, lysed using sonication (55% amplitude, 30 cycles of 10s on 20s off) and the lysate clarified by ultracentrifugation (40,000 g for 30 min). The lysate was loaded onto a HiTrap FF (Cytiva) and eluted with buffer A plus 500 mM imidazole. The eluate was dialyzed in buffer A, digested with TEV protease overnight and the protease as well as non-cleaved protein separated from cleaved protein by application to the HiTrap FF column with flow-through collected. Protein was then subjected to size exclusion chromatography using a HiLoad Superdex Increase 75 colum (Cytiva), with fractions containing pure protein pooled.

3.4.12 Isothermal titration calorimetry

ITC measurements were performed at 30 °C on a VP-ITC system (Malvern Panalytical Inc). Epetraborole (100 μM) in measurement buffer (50 mM Tris, 150 mM NaCl, 2 mM BME, 10 mM AMP) was titrated with protein solution (1 mM) in measurement buffer over 29 injections of 10 μl with 300 seconds equilibration time between injections. The heat evolved after each protein injection was calculated by integrating the calorimetric signal. The binding isotherms obtained were fitted to a single-site model using Origin 7 (Microcal Inc.). Experiments were performed in triplicates.

3.4.13 Crystallography

Initial crystals of the *M. abscessus* LeuRS editing domain were obtained from sparse matrix screening in 96-well sitting drop format using a sample of 10 mg/mL protein in buffer A, and a precipitant solution of 100 mM HEPES pH 7.0 and 2 M ammonium sulfate, at room temperature. Diffraction-quality crystals were grown by mixing 2 μL of protein solution (7.5 mg/mL) and 2 μL of reservoir solution (100 mM HEPES pH 7.0 and 2.5 M ammonium sulfate) in 24-well sitting-drop format. Crystals were cryoprotected in 100 mM HEPES pH 7.0 and 3.5 M ammonium sulfate, looped and flash-vitrified in liquid nitrogen. Diffracting co-crystals of the editing domain and epetraborole were obtained by streak seeding un-liganded crystals shards into drops in 24-well sitting-drop format with a reservoir solution of 100 mM HEPES, pH 7.5, 2% PEG400, 2.1 M ammonium sulfate, 10 mM AMP, 1 mM epetraborole and 15% glycerol at room temperature.

These crystals were directly looped and flash-vitrified in liquid nitrogen for diffraction experiments.

3.4.14 Structure determination

Diffraction data for the unliganded editing domain was collected at the Advanced Photon Source (24-ID-E) and data for the epetraborole – editing domain complex at the Canadian Light Source (CMCF-08B1-1). The data sets were indexed, processed, and scaled with HKL2000[20] (for the unliganded editing domain) or DIALS[21] (for the complex). Initial phases for the *M. abscessus* LeuRS editing domain were obtained using molecular replacement with the program Phaser[22] using 5AGR[23] as a search model. Iterative rounds of refinement with Phenix[24] and manual modeling in Coot[25] yielded the final unliganded structure. The structure of the *M. abscessus* LeuRS editing domain with epetraborole bound in the active site crystallized in a different crystal form (S5 Table). Therefore, initial phases for the co-complex structure were obtained with molecular replacement using the program Phaser[22] utilizing the unliganded structure as a search model. The model for epetraborole was generated with eLBOW[26] and geometrical restraints were obtained with AceDRG[27]. Iterative rounds of refinement using Phenix[24] and manual modeling in Coot[25] yielded the final co-complex structure.

3.4.15 Time-kill assays

Log phase (OD_{600} of 0.4-0.8) *M. abscessus* was diluted to an OD_{600} of 0.0001 (10^5 CFU/mL) and incubated with drugs of interest. One hundred µL aliquots were taken and serially diluted in 7H9 complete and plated on 7H10 agar. The starting inoculum was determined from time 0 before drugs were added. CFUs were determined after 4 days of incubation at 37 °C. Bactericidal activity is defined as a 3 $\log_{10}$ decrease (99.9%) from the starting inoculum.

3.4.16 Checkerboard assays

Drug combinations were assessed for synergy, indifference, or antagonism using the standard checkerboard format followed by REMA for MIC determination. Fractional inhibitory concentrations (FICs): FIC (X+Y) = (MIC of X in combination with Y)/(MIC of X alone). The fractional inhibitory concentration index (FICI) was calculated from $FIC_X + FIC_Y$. FICI values < 0.5 are defined as synergy, FICI values ≥ 4.0 are defined as antagonism, and FICI values in

between are defined as indifferent. EPT was serially diluted two-fold from 4X MIC to 1/16 X MIC. Mycobacterial drugs were serially diluted two-fold from 8X MIC to 1/32X MIC.

3.4.17 Inducible resistance assay

To test whether *M. abscessus* has inducible resistance to EPT, we performed a preexposure assay. Briefly, log phase *M. abscessus* was diluted to 0.05 and grown overnight with ¼ X MIC_{50} of EPT (0.016 µg/mL) and CLR (0.016 µg/mL). After overnight growth, MICs were determined via REMA. Data is reported as the ratio of pre-exposed culture MIC to MIC of culture grown in drug-free conditions.

3.4.18 CRISPRi conditional knockdown of *leuS*

The PLJR962 plasmid was restriction digested with BsmBI and gel purified. Synthetic oligo primers (S4 Table) for the sgRNA with the PAM sequence for *leuS* were annealed and ligated into digested PLJR962 vector and transformed into *E. coli* DH5α. Clones were sequenced using sequencing primer (S4 Table). 500 ng of CRISPRi *leuS* vector was electroporated into *M. abscessus* ATCC 19977. Colonies were picked from 7H10 plates containing 250 µg/mL kanamycin and confirmed by PCR. *M. abscessus* CRISPRi *leuS* was grown in liquid culture to early log phase (OD_{600} 0.1-0.4) and diluted to $1x10^4$ CFU/mL. One hundred μL of culture was plated on 7H10 containing either serial dilutions of EPT or RFB as control, and 0, 0.05 µg/mL, or 0.1 µg/mL ATc, the inducer of the sgRNA and catalytically inactive Cas9 (dCas9). The MIC_{99} is the concentration of EPT or RFB that prevented growth relative to the drug free plate.

3.4.19 Norvaline suppression of mutants

Early log phase *M. abscessus* or *M. tuberculosis* (OD_{600} 0.1-0.4) was cultured and resuspended to an OD_{600} of 10 (*M. abscessus*) or OD_{600} of 1 (*M. tuberculosis*). One hundred µL of culture (approx. 1 X 10^9 CFU for *M. abscessus* and 1 x 10^6 CFU for *M. tuberculosis*) was plated on solid media containing 10X MIC_{90} EPT, 10X MIC_{90} EPT + 5 mM norvaline, or 5 mM norvaline. The experiment was repeated with 10X MIC_{90} RFB as control. *M. abscessus* plates were incubated for 5 days at 37 °C, *M. tuberculosis* plates were incubated for 5 weeks at 37 °C. Number of colonies were enumerated to obtain mutation frequencies. Since mutations are considered rare events,

mutation frequency rates between 10X MIC_{90} EPT and 10X MIC_{90} EPT + 5 mM norvaline were compared using the two Poisson rates.

The Poisson rate is defined as the number of events divided by the sample size: $\lambda = X/N$

The rates were compared using the small sample z-test:

$$z_{SR} = \frac{\sqrt{\lambda_2} - \sqrt{\lambda_1}}{\frac{1}{2}\sqrt{\frac{1}{N_1} + \frac{1}{N_2}}}$$

3.4.20 LC-MS/MS measurement of norvaline in the proteome

Wildtype, mutant, and complement *M. abscessus* strains were grown for 12 h or 3 days in 0.5 mM norvaline or 0.5 mM valine. Proteins were extracted using an optimized protocol for mass spectrometry follow-up [28]. Cells were collected, washed with ice-cold PBS, and resuspended in 1mL lysis buffer (50 mM NH_4HCO_3 pH 7.4, 10 mM $MgCl_2$, 0.1% NaN_3, 1 mM EGTA, 1 x protease inhibitors (Roche), 7 M urea, and 2 M thiourea). Cells were lysed with zirconia beads and the cell lysate was collected and filtered through a 0.22 µm membrane. Proteins were precipitated overnight at 4 ºC with TCA at 25% (v/v). The precipitate was washed with 1 mL cold acetone and 250 µL cold water. The final wash is only water. The pellet was resuspended in 200 µL resuspension buffer (50 mM NH_4HCO_3, 1 M urea). Protein extraction was quantified with the Bradford assay and the quality of proteins was examined on SDS-PAGE. Protein lysates were dissolved in SDS-PAGE reducing buffer and electrophoresed onto a single stacking gel band to remove lipids, detergents and salts. For each sample, a single gel band was reduced with DTT (Sigma), alkylated with iodoacetic acid (Sigma) and digested with LCMS grade trypsin (Promega). Extracted peptides were re-solubilized in 0.1% aqueous formic acid and loaded onto a Thermo Acclaim Pepmap (Thermo, 75 µM ID X 2 cm C18 3 µM beads) precolumn and then onto an Acclaim Pepmap Easyspray (Thermo, 75 µM X 15 cm with 2 µM C18 beads) analytical column separation using a Dionex Ultimate 3000 uHPLC at 250 nl/min with a gradient of 2-35% organic (0.1% formic acid in acetonitrile) over 2 hours. Peptides were analyzed using a Thermo Orbitrap Fusion mass spectrometer operating at 120,000 resolution for MS1 with HCD sequencing at top speed (15,000 resolution) for all peptides with a charge of 2+ or greater. The raw data were converted into *.mgf format (Mascot generic format) for searching using the Mascot 2.5.1 search engine (Matrix Science) against Mycobacterium abscessus protein sequences (Uniprot

downloaded 2020.11.30). A modification for Xle->Val was used to detect incorporation of Val into WT sequences. The database search results were loaded onto Scaffold Q+ Scaffold_4.4.8 (Proteome Sciences) for statistical treatment and data visualization.

3.4.21 Murine model of chronic *M. abscessus* infection using NOD.CB17-*Prkdc*^{scid}/NCrCrl mice

RFB (Sigma), EPT (Cayman Chemical), and norvaline (Sigma) were dissolved in 0.5% w/v sterile low viscosity carboxymethyl cellulose pH 7 (vehicle). Drugs were aliquoted and stored at -20 ºC for the duration of the 10-day treatment. 6-8 week-old female mice were ordered from Charles River Labs. Mice were intranasally infected with ~10^6 CFU (25 µL of 5x10^8 CFU/mL) of *M. abscessus* CIP 104536^T (rough morphotype). Five mice were sacrificed 4 hours post-infection to determine initial lung inoculum and on day 1 to enumerate CFU prior to drug administration. Mice were treated daily by oral gavage with 100 µL of vehicle or drug. On day 11, mice were humanely euthanized, the lungs were collected and homogenized in 1mL of 7H9 complete. Lung homogenates were plated on 7H11 agar and plates were incubated at 37 °C for 5 days. CFU data was log-transformed for one-way ANOVA with Tukey's multiple comparisons test using GraphPad Prism version 9.

3.5 RESULTS

3.5.1 Discovery of an antimycobacterial inhibitor against *M. abscessus*

To identify compounds with antimycobacterial activity, we first engineered a luminescent *M. abscessus* ATCC 19977 strain which constitutively expressed the *luxCDABE* operon (*M. abscessus lux*).[29] We then screened the 176 compound open-library provided by GlaxoSmithKline (**FIGURE S3.1 A-C**) and the 400 compound Pathogen and Pandemic Response Boxes from MMV (**FIGURE S3.1 D-F**) using a threshold ≥ 90% reduction in luminescence compared to non-treated bacteria at 10 μM. Primary hits (20 compounds) were tested in a secondary screen using the resazurin microtiter assay (REMA) at 10 μM on the *M. abscessus* ATCC 19977 strain. Secondary hits (9 compounds) were then tested in a dose-response assay on *M. abscessus* ATCC 19977 from a fresh solid compound to determine MIC_{90}. The HepG2 (human hepatocytes) cell line was used to assess the toxicity of hits. Among three compounds (0.3% positive hits of 976 compounds) from the pandemic response box that satisfied primary and secondary criteria, we identified EPT (**FIGURE 3.1A**) as having the most potent antimycobacterial activity and highest therapeutic index (**TABLE 3.1**, MIC_{90} 0.23 μM (0.063 μg/mL), TI (TD_{50}/MIC_{90}) EPT > 430). It was previously reported in *M. tuberculosis* that potent *in vitro* growth inhibitors could display carbon-source-dependent effects, which leads to a loss of activity when advanced into *in vivo* models.[30] We thus measured the MIC_{90} of EPT on different carbon sources (glycerol vs acetate), in the presence or absence of the detergent Tween-80, and in different nutrient bases (Middlebrook 7H9 vs cation-adjusted Mueller-Hinton). EPT was active in all assayed growth conditions but lost potency in cation-adjusted Mueller Hinton (CaMH) media (**TABLE S3.1**). Lower activity of EPT in CaMH media is unsurprising as it was previously shown that rifamycins[31] as well as other antimicrobials[32] lose activity in CaMH media (0.5mg/L Ca^{2+} and 0.05mg/L Mg^{2+} in 7H9; 20-25mg/L Ca^{2+} and 10-12.5mg/L Mg^{2+} in CaMH). It is thought that some antimicrobials may chelate divalent metal ions, thus limiting their uptake in cells.

Next, we tested the *in vitro* activity of EPT against a panel of *M. abscessus* clinical isolates belonging to the three subspecies of the *M. abscessus* complex (*M. abscessus*, *M. massiliense*, and *M. bolletii*) with smooth and rough colony morphologies and with different drug susceptibility profiles to various antibiotics. There was no loss in activity against clinical isolates (range of 0.014-0.046 μg/mL) nor different morphologies (**TABLE S3.2**). To determine the spectrum of activity

of EPT, we curated a panel of various mycobacteria and representative gram-positive and gram-negative bacteria. Interestingly, EPT appears to be more selective for *M. abscessus* with lower activity against *M. tuberculosis* H37Rv (**TABLE S3.3**). *In vitro* growth kill kinetics indicated that EPT is bacteriostatic against *M. abscessus* as previously demonstrated against *M. tuberculosis*,[23] while 10% of CFUs were lost at 24 hours with AMK and rifampicin (RIF) at 20X MIC_{90}. Interestingly, these two antimycobacterial agents with bactericidal action against other mycobacteria lose this ability when targeting *M. abscessus* (**FIGURE 3.1B**) [33].

3.5.2 Clinical considerations for EPT

Macrolides represent the cornerstone of *M. abscessus* therapy. However, macrolide susceptibility *in vitro* does not correlate with clinical outcome success due to point mutations at positions 2058 or 2059 in the 23S rRNA *rrl* gene (*E. coli* numbering), and inducible macrolide resistance conferred from the recently identified ribosomal methyltransferase *erm*(41).[34,35] Nash *et al* (2009) discovered that *M. abscessus* exhibited an inducible resistant phenotype to macrolides, like clarithromycin (CLR), during a 14-day incubation. To this extent, we asked if EPT induced self-resistance or cross-resistance to macrolides. To answer this question, we performed the inducible macrolide resistance assay where *M. abscessus* was cultured with a subinhibitory concentration of CLR (0.02 μM) or EPT (0.06 μM) for 14 days. At 24 hours and 14 days, aliquots of culture were collected, and the MIC_{90} of CLR and EPT was determined using REMA. Relative to drug-free conditions, *M. abscessus* cultured with CLR displayed an increased MIC_{90} to CLR while the EPT MIC_{90} for bacteria exposed to EPT remained unchanged up to 14 days (**FIGURE 3.1C**). To ensure the increased MIC_{90} resulted from inducible resistance rather than the selection of spontaneous CLR and EPT resistant mutants, the cultures were passaged in antibiotic-free media for 6 additional days and the MIC_{90} measurements were repeated. In the case of CLR resistance, the MIC_{90} returned to baseline after the antibiotics were removed (**FIGURE 3.1C**). In addition, EPT stimulation did not result in cross-resistance to CLR, and CLR induction did not result in cross-resistance to EPT. The latter is an important finding with clinical significance because CLR is known to impart resistance to aminoglycoside antibiotics.[36]

Because *M. abscessus* infections require 18-24 months of antibiotic courses, multidrug treatments are standard practice.[2,3] To ensure EPT would not hamper a multidrug regimen, we performed

checkerboard assays with common antimycobacterial drugs. In the checkerboard assays, we used RIF/CLR and CLR/AMK as the synergy and antagonism controls, respectively.[36,37] We did not observe antagonism between EPT and various antimycobacterial agents that target a range of cellular processes (**FIGURE S3.2**). Whether EPT should be included in a multidrug regimen remains to be determined.

3.5.3 EPT protects zebrafish from *M. abscessus* infection

In order to investigate the *in vivo* activity of EPT, we used the embryonic zebrafish model of *M. abscessus* infection, which has been developed to test the *in vivo* efficacy of drugs against *M. abscessus*.[17,38,39] Initial experiments indicated that EPT concentrations up to 40 µg/mL (final concentration in fish water) did not interfere with larval development and was well tolerated in embryos when treatment was applied for up to 5 days with daily drug renewal (**FIGURE 3.2A**). Green fluorescent wasabi-expressing *M. abscessus* (R variant) was microinjected in the caudal vein of embryos at 30 hours post-fertilization. EPT was directly added at 1 day post-infection to the water containing the infected embryos, with EPT-supplemented water changed on a daily basis for 5 days. Embryo survival was monitored and recorded daily for 11 days. While a slight increase in the survival rate was observed with 10 µg/mL EPT, this effect was significantly improved with 40 µg/mL EPT with a delay in larval mortality, as compared to the untreated group (**FIGURE 3.2B**). The protection provided by EPT is maintained throughout the 5-day treatment course and was correlated with decreased bacterial burdens beginning 4 dpi demonstrated by fluorescent pixel counting (**FIGURE 3.2C** and **3.2D**). These results clearly indicate that EPT protects zebrafish from *M. abscessus* infection.

3.5.4 EPT targets LeuRS in *M. abscessus*

Benzoxaboroles were shown to inhibit LeuRS in fungi, gram-negative pathogens and most recently *M. tuberculosis*.[11,23,40] To determine the target of EPT in *M. abscessus*, 10^9 CFUs were plated on solid media with 10X, 20X, or 40X MIC_{90} of EPT to select EPT-resistant mutants. Control mutants were also selected on 40X MIC_{90} of AMK. Unlike the EPT resistance frequency of 4.8×10^{-8} in *Pseudomonas aeruginosa*, the resistance frequency was 10-fold lower in *M. abscessus* (**TABLE S3.4**, 2×10^{-9}).[40] The low *in vitro* resistance frequency to EPT is highlighted when compared to the control mutants against AMK (1.3×10^{-8}). In order to confirm that isolated resistant mutants

were true mutants to EPT, we performed REMA using a panel of antimycobacterial agents on the four mutants (one selected on 10X, one on 20X, and two on 40X MIC_{90} of EPT). We also screened one AMK mutant. As illustrated in **FIGURE S3.3**, the four EPT mutants were resistant up to 2.7 µg/mL EPT, while maintaining susceptibility to AMK, bedaquiline (BDQ), and RIF. Likewise, the AMK control mutant was only resistant to AMK.

Since benzoxaboroles are known to target LeuRSs, we used a focused approach to identify the mutation(s) in *leuS* that could be responsible for the observed EPT resistance. *leuS* was PCR amplified from gDNA from the four EPT mutants, and single-nucleotide polymorphisms (SNPs) were identified using Sanger sequencing (**TABLE S3.5**). In all four mutants, a G to C transversion at position 1306 was identified, which resulted in the conserved D436 residue critical for the catalysis of editing misaminoacylated $tRNA^{Leu}$ substituted for H436 (**FIGURE 3.3A** and **3.3B**).[41] This was further supported with whole-genome sequencing of the *M. abscessus* ATCC 19977 reference strain, one mutant isolated at 20X MIC, and one mutant isolated at 40X MIC. When compared to the reference strain, five variants were identified in the 20X mutant including a T to G transition at position 1261 in *leuS* which resulted in a Y421D substitution. Furthermore, the G to C transversion at position 1306 which lead to the D436H substitution was confirmed in the 40X mutant (**TABLE S3.6**). This contrasts with LeuRS variants identified in *P. aeruginosa* such as T323P, T327P, and V429M from Hernandez *et al*. or LeuRS variants such as T322I, D326N, A414V, and R435H identified in a phase 2 clinical trial for complicated urinary tract infections caused by *E. coli* from O'Dwyer *et al*.[40,42] However, the phase 2 clinical trial did identify *E. coli* isolates with a LeuRS D436A variant. (*M. abscessus* numbering). To verify the functional significance of the D436H substitution, the *leuS* genes from *M. abscessus* ATCC 19977 wildtype (EPT sensitive) and *M. abscessus* containing the G1306C substitution (EPT-resistant) were cloned into the mycobacterial integrative vector pMV306 under the control of the constitutive *hsp60* promoter, yielding pMVhsp60_$leuS^{D}$ and pMVhsp60_$leuS^{D436H}$. EPT-sensitive *M. abscessus* was electroporated with pMVhsp60_$leuS^{D}$, pMVhsp60_$leuS^{D436H,}$ or empty vector control. Only EPT sensitive *M. abscessus* complemented with the mutant *leuS* (pMVhsp60_$leuS^{D436H}$) and not the wildtype *leuS* (pMVhsp60_$leuS^{D}$) had increased resistance to EPT (**FIGURE 3.3C**). The integrative complement system using pMVhsp60 may not have provided a complete phenocopy of the true mutant when compared to the episomal equivalent. Also, *M. abscessus* may not use the

hsp60 promoter from *M. bovis* with optimal efficiency. Lastly, the *hsp60* promoter may not operate with the same strength as the *leuS* promoter.

We showed that LeuRS^{D436H} confers high-level resistance to EPT and that complementing the resistant allele into a wildtype background imparts resistance. As a complementary means of verifying the target, we adapted a CRISPR-interference (CRISPRi) system for gene knockdown in *M. abscessus*.[43] CRISPRi facilitates gene knockdown using a guide RNA and catalytically inactive Cas9 endonuclease to sterically prevent transcription of a gene of interest when induced with anhydrotetracycline (ATc). We used CRISPRi to knockdown *leuS* which resulted in hyper susceptibility to EPT. Since *leuS* is an essential gene in *M. abscessus* (**FIGURE 3.3D**), we used 10-fold and 20-fold less ATc than required for complete growth suppression when targeting an essential gene. The EPT MIC_{99} of the strain induced with 0.1 µg/mL ATc decreased 10-fold compared to uninduced conditions, while induction did not affect the rifabutin (RFB) MIC_{99} (Fig 3E). These results provide further evidence that EPT targets LeuRS in *M. abscessus*.

3.5.5 EPT binds the editing active site of LeuRS

Although EPT is active against *M. abscessus* and *M. tuberculosis*, the MIC_{90} for *M. abscessus* whole-cell activity is 7-fold lower (MIC_{90Mabs} 0.063 µg/mL vs MIC_{90Mtb} 0.46 µg/mL). We hypothesized that EPT had a higher affinity for the *M. abscessus* LeuRS editing active site. We therefore performed binding studies between EPT and the editing domains of LeuRS from *M. abscessus* and *M. tuberculosis* using isothermal titration calorimetry (ITC) (**FIGURE S3.4**). *M. abscessus* LeuRS and *M. tuberculosis* LeuRS contain a single binding site for EPT, and we obtained similar equilibrium dissociation constants and Gibbs free energies (**TABLE 3.2**). The EPT – *M. abscessus* LeuRS binding has a higher enthalpic contribution (1.1 to 3.2 kcal mol^{-1}), while the EPT – *M. abscessus* LeuRS binding has a lower entropic contribution (5.5 to 3.3 kcal mol^{-1}).

To gain insight into the interactions between EPT and LeuRS, we solved the crystal structure of the *M. abscessus* editing domain ($LeuRS_{303-498}$). We obtained the crystal structures of the LeuRS editing domain unliganded at 2.1 Å resolution (PDB 7N11) and in complex with the adenosine monophosphate (AMP) adduct with EPT at 1.7 Å resolution (PDB 7N12, **TABLE S3.7**). AMP

acts as a surrogate for the 3' end of the tRNA acceptor stem. In concordance with the binding mode of action of benzoxaboroles,[23] we detected strong electron density in the active site corresponding to the EPT-AMP adduct formed through covalent interactions between the boron atom of EPT and the 2' and 3' hydroxyl groups on the ribose ring of AMP (**FIGURE 3.4A** and **FIGURE S3.5A**). Comparing unliganded and liganded residues in *M. abscessus* editing domain structures shows a sizable shift of residues 416-422, located around the adenosine pocket, upon drug binding, including ordering of Y421 to interact with the EPT-AMP adduct phosphate, and a decrease of B factors in the neighbouring residues (**FIGURE S3.5B**). This increase in order could explain the relatively lower entropic contribution to binding observed in ITC, although an unliganded *M. tuberculosis* structure is not available for comparison.

Once bound with benzoxaborole-AMP adduct, the active sites of *M. tuberculosis* (PDB: 5AGR)[23] and *M. abscessus* LeuRS, and mode of adduct binding are very similar (**FIGURE 3.4A** and **FIGURE S3.5C**). Both proteins make critical contacts with the primary amine side chain through D433 (D447 in *M. tuberculosis*) and the universally conserved D436 (D450 in *M. tuberculosis*) (**FIGURE 3.4A**). In addition, R435 (R449 in *M. tuberculosis*) hydrogen bonds with the ethoxy oxygen of EPT and packed with the ribose of AMP (**FIGURE 3.4A**). The packing interaction on the ribose of AMP is underscored from *E. coli* mutants with R435H variants that lead to resistance early in the phase 2 clinical trial for complicated urinary tract infections. EPT has a hydroxypropyl ether moiety, rather than the ethyl ether in the benzoxaborole bound to *M. tuberculosis* LeuRS, but the extension shows very weak electron density and likely does not contribute to binding. The only notable difference is a ~1 Å shift in phosphate group of the EPT-AMP adduct (**FIGURE 3.4B**). In both complexes, the phosphate is pinned between Y421 (Y435) and T323 (T337). The electron density indicates that there are multiple rotomeric conformations of T323, meaning its hydroxyl could hydrogen bond with the phosphate or with the 3' O and ether oxygen of the adduct (**FIGURE 3.4B**). *M. tuberculosis* LeuRS T337 is modelled in the latter position, but inspection of deposited maps also indicates multiple rotomeric conformations. Variants at T322, T323 and T327 were identified in *P. aeruginosa* and *E. coli* mutants resistant to benzoxaboroles, which supports the importance of the threonine rich region for editing activity.[44] From the structural data, we propose that EPT binds LeuRS from *M. abscessus* and *M. tuberculosis* in a similar manner with similar affinity, providing a shared pathway for future structure-activity relationship analysis.

3.5.6 Norvaline is toxic to editing-deficient EPT mutants

Since resistance to EPT was shown in a phase 2 clinical trial of complicated urinary tract infections from *E. coli*, we sought a way to minimize the emergence of resistance in *M. abscessus* pulmonary infections.[42] We hypothesized that norvaline, a non-proteinogenic amino acid absent from extant proteins,[45] would be toxic to *M. abscessus* editing-deficient mutants that acquired EPT resistance. When challenged with 0.5 mM norvaline, the D436H editing-deficient mutant was significantly reduced in growth, while the wild-type strain was not inhibited (**FIGURE 3.5A**). The mutant strain complemented with wild-type *leuS* (D436H::leuS^{D}) displayed a two-day lag before significant growth. As controls, leucine and isoleucine were not toxic to the D436H mutant. There was however a minor reduction in mutant growth in 0.5 mM valine, but no growth difference between the D436H and D436H::leuS^{D} strains. Thus, we cannot conclude that valine exerts some toxicity to editing-deficient strains. Next, we asked if norvaline toxicity could be rescued with branched-chain amino acids (BCAAs). The D436H mutant was grown in 0.5 mM norvaline with varying concentrations of BCAAs. Leucine but not isoleucine nor valine rescued growth (**FIGURE 3.5B**). These observations corroborate the results that LeuRSs contain natural selectivity with their aminoacylation site for leucine and can discriminate against isoleucine and valine, but to a lesser extent against norvaline as non-cognate amino acids.[46]

3.5.7 Norvalination of the proteome induces the heat shock response

To provide a mechanism of norvaline toxicity, we analyzed the proteomes of wild-type, D436H mutant, and D436H:leuS^{D} grown in norvaline or valine as control. We analyzed ~2500 proteins from whole-cell lysates after 12 hours or 3 days of incubation in 0.5 mM norvaline or valine using reverse-phase HPLC/MS. Proteins filtered for leucine residues 14 Da lighter (14 Da corresponds to missing methylene group on norvaline) were enumerated using spectral counting. The wild-type maintained preferential incorporation of leucine into proteins, while the D436H mutant had a median norvaline misincorporation in 6% of the proteome after 12 hours. However, the amount of norvaline misincorporation between the D436H mutant and the D436H::leuS^{D} strain was not significantly different (**FIGURE 3.6A**). Given that there was a two-day delay when the complemented strain was grown in norvaline (**FIGURE 3.5A**), we hypothesized that the effects of gene complementation would be seen at a later time point when grown in 0.5 mM norvaline.

The experiments were repeated, and the strains were incubated for 3 days. Again, the median norvalination increased in the D436H mutant relative to wildtype, but the level of misincorporated norvaline increased to 20% of the proteome. At this time point, the complemented strain partially rescued the level of norvalination after 3 days (**FIGURE 3.6B**). In all conditions tested, we measured background misaminoacylation of valine in the proteome (**FIGURE 3.6A** and **FIGURE 3.6B**).

Next, we asked how the cell responded to stress caused by norvaline misincorporation in the proteome. Using total spectral counting, we determined the fold change in protein abundance from D436H mutant relative to wildtype. There was a distinct increase in proteins when challenged with norvaline that was absent from the valine control (**FIGURE 3.6C-F**). We used the protein-protein interaction (PPI) mapping tool STRING to identify upregulated proteins with common functions. When 130 of the most highly abundant proteins after norvaline stress were mapped for PPIs (**FIGURE 3.7A**), proteins belonging to the Clp protease family (ClpP1, ClpP2, ClpX) and GroEL chaperonin family (GroEL, GroL2, GroS) were identified (False discovery rate $7.2x10^{-4}$ at 12 h, $2.1x10^{-5}$ at 3 d) (**FIGURE 3.7C**). As a control, 130 randomly selected proteins from the norvaline dataset were not enriched for chaperonins and proteases when analyzed for PPIs (**FIGURE 3.7B**). We also observed a temporal change in chaperonin and protease levels where early stress from norvaline at 12 hours upregulated chaperonins followed by protease upregulation at 3 days (**FIGURE 3.7D**). This data suggests that norvaline misincorporation into the proteome results in toxicity from misfolded proteins.[14,45,47–52]

3.5.8 Norvaline reduces resistance to EPT *in vitro* and potentiates EPT activity *in vivo*

Knowing that norvaline targets LeuRS editing domain, we asked if norvaline could prevent escape mutants to EPT *in vitro*. We observed a 23-fold reduction in escape mutant frequency when *M. abscessus* ATCC 19977 was plated on 7H10 plates containing 10X MIC_{90} EPT and 5 mM norvaline (1.89×10^{-10}) over EPT alone (4.28×10^{-9}) (**FIGURE 3.8A**); as a control, RFB did not benefit from norvaline supplementation. To test whether this effect would be observed in other mycobacteria, we repeated with *M. tuberculosis*, again observing a suppression of EPT mutants with norvaline exposure (**FIGURE 3.8A**). Next, the MIC_{90} of EPT against *M. abscessus* ATCC 19977 was measured with differing doses of norvaline (**FIGURE 3.8B**). Norvaline had no effect

on the MIC_{90} even up to 5 mM. These results suggest norvaline does not act as a traditional adjuvant to EPT.

We evaluated EPT and norvaline combination therapy for *in vivo* activity in a NOD.SCID mouse model of *M. abscessus* infection.[53] Mice were infected intranasally with a high inoculum of *M. abscessus* (~10^6 CFU). Treatment was started 1-day post-infection with once-daily oral vehicle (carboxymethylcellulose), RFB as positive control (10 mg/kg), EPT (10 mg/kg), EPT + norvaline (10 mg/kg + 3.3 mg/kg), or norvaline (3.3 mg/kg). Norvaline was dosed at 3.3 mg/kg (5 mM) which represents ~10X MIC_{90} *in vitro* against the editing deficient D436H mutant. Previously, norvaline had been shown to be an effective *in vivo* neuroprotective agent as an arginase inhibitor at 2 mM in a triple-transgenic mouse model of Alzheimer's disease.[54] Compared to vehicle-treated mice, we measured a 1 $\log_{10}$ decrease in bacterial burden in the lungs from RFB or EPT treatment. Furthermore, the addition of norvaline to the EPT group was significantly more active than EPT alone with an additional ~1 $\log_{10}$ decrease in bacterial burden in the lungs while norvaline alone had no significant effect (**FIGURE 3.8C**).

3.6 DISCUSSION

Our data and two recent publications[55,56] confirmed the activity of benzoxaboroles against mycobacteria using zebrafish and murine models of infection and we showed that benzoxaboroles can be potentiated when combined with norvaline. Specifically, we demonstrated that the combination of EPT with norvaline reduces the emergence of *M. abscessus* and *M. tuberculosis* mutants and results in increased activity *in vivo* compared to EPT. Whether norvaline can be a therapeutic adjunct for other benzoxaboroles remains to be established, but is supported by observations with tavaborole and norvaline in *E. coli*.[57] The potential for combination therapy may be of value in non-mycobacterial applications, such as the treatment of urinary tract infections, where EPT did not progress beyond phase 2 studies owing to the rapid emergence of resistance.[42]

While we documented that EPT is active against both *M. abscessus* and *M. tuberculosis in vitro*, unexpectedly, we observed that EPT is more active against *M. abscessus*, which conflicts with the standard experience in antimycobacterial drug discovery.[6,58–63] Our cocrystal structure and ITC data point to similarities and differences in the interaction of EPT with the respective LeuRS

proteins. Most notably, while the Kd values were similar, the enthalpy was greater for the EPT interaction with LeuRS of *M. abscessus*. Knowing that compounds with more enthalpically favourable binding are prioritized in hit-to-lead optimization,[64] it may be possible that the discordance in enthalpy in part explains the difference in biological activity of EPT against the two organisms (MIC_{90Mabs} 0.063 µg/mL vs MIC_{90Mtb} 0.46 µg/mL). Other possibilities explaining the difference in whole cell activity may be linked to differential expression level of *leuS* in both species, the lack of efflux pumps in *M. abscessus*, or the inability of *M. abscessus* to survive conditions that mimic leucine starvation, although these remain to be addressed. At a minimum, the current data can be used for future structure-activity relationship studies aimed at uncovering analogues with improved potency against LeuRS of *M. abscessus*, *M. tuberculosis* and other mycobacteria.

Our *in vivo* data shows the value of EPT alone in rescuing zebrafish embryos from lethal *M. abscessus* infection and that EPT + norvaline can control experimental pulmonary *M. abscessus* infection to a greater degree than the control antibiotic, RFB. Rather than acting as a traditional adjuvant like β-lactamase inhibitors for β-lactams,[65] we propose that norvaline potentiates EPT *in vitro* activity by maintaining a pharmacological pressure on *M. abscessus* to remain editing proficient and limit the toxicity induced by the unfolded protein response and thus, limiting escape mutants. However, given that our *in vivo* model of pulmonary *M. abscessus* infection in NOD.SCID mice does not exceed a bacterial burden of ~10^7 in the lungs and that the rate of resistance against EPT is ~10^{-9}, other mechanisms might better explain our findings. Since the NOD.SCID model is immunocompromised for NK cells and adaptive immunity, macrophages—the most notable front-line defence for mycobacterial pulmonary infections—would be the main immune cell responsible for controlling the *M. abscessus* infection. One of the primary mechanisms of macrophages for controlling infections is the production of reactive nitrogen species like nitric oxide (NO) from inducible nitric oxide synthase (iNOS). Because NO is produced from arginine by iNOS, macrophages must regulate arginine metabolism between iNOS and the urea cycle, which naturally metabolizes arginine through the enzyme arginase. Interestingly, norvaline was shown to be an inhibitor of arginase and this resulted in increased production of NO in activated macrophages.[66,67] This increased production of NO from arginase

inhibition might explain the lower bacterial burden observed in the NOD.SCID mouse group that received EPT + norvaline treatment.

Given that response rates to *M. abscessus* treatment are poor, resulting in chronic and potentially untreatable pulmonary and dermatologic infections, we submit that benzoxaboroles with the addition of a leucine mimic hold promise for the treatment of *M. abscessus* infections, and potentially other mycobacterial infections, such as tuberculosis.

3.7 ACKNOWLEDGEMENTS

We thank Adam Hassan (Research Institute of the McGill University Health Centre) for technical assistance with mouse experiments. We thank Medicines for Malaria Venture for providing the MMV Open pathogen box and pandemic response boxes. This research used resources of the Advanced Photon Source, a U.S. Department of Energy (DOE) Office of Science User Facility, operated for the DOE Office of Science by Argonne National Laboratory under Contract No. DE-AC02-06CH11357. Extraordinary facility operations were supported in part by the DOE Office of Science through the National Virtual Biotechnology Laboratory, a consortium of DOE national laboratories focused on the response to COVID-19, with funding provided by the Coronavirus CARES Act. Part or all of the research described in this paper was performed using beamline CMCF-BM at the Canadian Light Source, a national research facility of the University of Saskatchewan, which is supported by the Canada Foundation for Innovation (CFI), the Natural Sciences and Engineering Research Council (NSERC), the National Research Council (NRC), the Canadian Institutes of Health Research (CIHR), the Government of Saskatchewan, and the University of Saskatchewan. The *luxCDABE* plasmid was kindly gifted by Jeffery S. Cox. We are grateful to the CRBM zebrafish facility (Montpellier), P. Richard and M. Plays for zebrafish husbandry.

3.8 AUTHORS' CONTRIBUTIONS

JRS was involved in all aspects including experiment design, data collection and analysis, and preparation of the manuscript. AL provided training to JRS and conducted experiments in the containment level 3. EK collected the crystallography data. CH performed the zebrafish work. LT collected the proteomics data. KAM collected isothermal titration calorimetry data. TMS provided

supervision to EK. LK provided supervision to CH. MAB provided supervision to JRS and was involved in the preparation of the manuscript.

3.9 REFERENCES

1. Johansen, M. D., Herrmann, J.-L. & Kremer, L. Non-tuberculous mycobacteria and the rise of Mycobacterium abscessus. *Nat. Rev. Microbiol.* (2020) doi:10.1038/s41579-020-0331-1.
2. Griffith, D. E. et al. An official ATS/IDSA statement: Diagnosis, treatment, and prevention of nontuberculous mycobacterial diseases. *Am. J. Respir. Crit. Care Med.* **175**, 367–416 (2007).
3. Haworth, C. S. et al. British Thoracic Society guidelines for the management of non-tuberculous mycobacterial pulmonary disease (NTM-PD). *Thorax* **72**, ii1–ii64 (2017).
4. Lee, M. R. et al. Mycobacterium abscessus complex infections in humans. *Emerg. Infect. Dis.* **21**, 1638–1646 (2015).
5. Van Ingen, J., Boeree, M. J., Van Soolingen, D. & Mouton, J. W. Resistance mechanisms and drug susceptibility testing of nontuberculous mycobacteria. *Drug Resist. Updat.* **15**, 149–161 (2012).
6. Wu, M. L., Aziz, D. B., Dartois, V. & Dick, T. NTM drug discovery: status, gaps and the way forward. *Drug Discov. Today* **0**, 1–18 (2018).
7. Kim, T. S. et al. Activity of LCB01-0371, a novel oxazolidinone, against mycobacterium abscessus. *Antimicrob. Agents Chemother.* **61**, (2017).
8. Le Run, E., Arthur, M. & Mainardia, J. L. In Vitro and Intracellular Activity of Imipenem Combined with Tedizolid, Rifabutin, and Avibactam against Mycobacterium abscessus. *Antimicrob. Agents Chemother.* **63**, (2019).
9. Dupont, C. et al. A new piperidinol derivative targeting mycolic acid transport in Mycobacterium abscessus. *Mol. Microbiol.* **101**, 515–529 (2016).
10. Kozikowski, A. P. et al. Targeting Mycolic Acid Transport by Indole-2-carboxamides for the Treatment of Mycobacterium abscessus Infections. *J. Med. Chem.* **60**, 5876–5888 (2017).
11. Rock, F. L. et al. An antifungal agent inhibits an aminoacyl-tRNA synthetase by trapping tRNA in the editing site. *Science (80-.).* **316**, 1759–1761 (2007).
12. Baker, S. J. et al. Discovery of a new boron-containing antifungal agent, 5-fluoro-1,3-dihydro- 1-hydroxy-2,1-benzoxaborole (AN2690), for the potential treatment of

onychomycosis. *J. Med. Chem.* **49**, 4447–4450 (2006).

13. Nureki, O. et al. Enzyme structure with two catalytic sites for double-sieve selection of substrate. *Science (80-.).* **280**, 578–582 (1998).
14. Nangle, L. A., Motta, C. M. & Schimmel, P. Global Effects of Mistranslation from an Editing Defect in Mammalian Cells. *Chem. Biol.* **13**, 1091–1100 (2006).
15. Ballell, L. et al. Fueling Open-Source Drug Discovery: 177 Small-Molecule Leads against Tuberculosis. *ChemMedChem* **8**, 313–321 (2013).
16. Lamason, R. L. et al. Genetics: SLC24A5, a putative cation exchanger, affects pigmentation in zebrafish and humans. *Science (80-.).* **310**, 1782–1786 (2005).
17. Bernut, A. et al. Mycobacterium abscessus cording prevents phagocytosis and promotes abscess formation. *Proc. Natl. Acad. Sci. U. S. A.* **111**, (2014).
18. Bernut, A. et al. Deciphering and imaging pathogenesis and cording of Mycobacterium abscessus in zebrafish embryos. *J. Vis. Exp.* **2015**, 53130 (2015).
19. Bernut, A. et al. In Vivo assessment of drug efficacy against Mycobacterium abscessus using the embryonic zebrafish test system. *Antimicrob. Agents Chemother.* **58**, 4054–4063 (2014).
20. Otwinowski, Z. & Minor, W. Processing of X-ray diffraction data collected in oscillation mode. *Methods Enzymol.* **276**, 307–326 (1997).
21. Beilsten-Edmands, J. et al. Scaling diffraction data in the DIALS software package: Algorithms and new approaches for multi-crystal scaling. *Acta Crystallogr. Sect. D Struct. Biol.* **76**, 385–399 (2020).
22. Bunkóczi, G. et al. Phaser.MRage: Automated molecular replacement. *Acta Crystallogr. Sect. D Biol. Crystallogr.* **69**, 2276–2286 (2013).
23. Palencia, A. et al. Discovery of novel oral protein synthesis inhibitors of mycobacterium tuberculosis that target leucyl-tRNA synthetase. *Antimicrob. Agents Chemother.* **60**, 6271–6280 (2016).
24. Afonine, P. V et al. Real-space refinement in PHENIX for cryo-EM and crystallography. *Acta Crystallogr. Sect. D Struct. Biol.* **74**, 531–544 (2018).
25. Emsley, P., Lohkamp, B., Scott, W. G. & Cowtan, K. Features and development of Coot. *Acta Crystallogr. Sect. D Biol. Crystallogr.* **66**, 486–501 (2010).
26. Moriarty, N. W., Grosse-Kunstleve, R. W. & Adams, P. D. Electronic ligand builder and

optimization workbench (eLBOW): A tool for ligand coordinate and restraint generation. *Acta Crystallogr. Sect. D Biol. Crystallogr.* **65**, 1074–1080 (2009).

27. Long, F. et al. AceDRG: A stereochemical description generator for ligands. *Acta Crystallogr. Sect. D Struct. Biol.* **73**, 112–122 (2017).
28. Rabodoarivelo, M. S. et al. Optimizing of a protein extraction method for Mycobacterium tuberculosis proteome analysis using mass spectrometry. *J. Microbiol. Methods* **131**, 144–147 (2016).
29. Penn, B. H. et al. An Mtb-Human Protein-Protein Interaction Map Identifies a Switch between Host Antiviral and Antibacterial Responses. *Mol. Cell* **71**, 637-648.e5 (2018).
30. Pethe, K. et al. A chemical genetic screen in Mycobacterium tuberculosis identifies carbon-source-dependent growth inhibitors devoid of in vivo efficacy. *Nat. Commun.* **1**, 57 (2010).
31. Aziz, D. B. et al. Rifabutin Is active against mycobacterium abscessus complex. *Antimicrob. Agents Chemother.* **61**, (2017).
32. Fass, R. J. & Barnishan, J. Effect of divalent cation concentrations on the antibiotic susceptibilities of nonfermenters other than Pseudomonas aeruginosa. *Antimicrob. Agents Chemother.* **16**, 434–438 (1979).
33. Maurer, F. P. et al. Lack of antimicrobial bactericidal activity in Mycobacterium abscessus. *Antimicrob. Agents Chemother.* **58**, 3828–3836 (2014).
34. Richard, M., Gutiérrez, A. V. & Kremer, L. Dissecting erm(41)-mediated macrolide-inducible resistance in mycobacterium abscessus. *Antimicrob. Agents Chemother.* **64**, (2020).
35. Nash, K. A., Brown-Elliott, A. B. & Wallace, R. J. A Novel gene, erm(41), confers inducible macrolide resistance to clinical isolates of mycobacterium abscessus but is absent from mycobacterium chelonae. *Antimicrob. Agents Chemother.* **53**, 1367–1376 (2009).
36. Pryjma, M., Burian, J., Kuchinski, K. & Thompson, C. J. Antagonism between Front-Line Antibiotics Clarithromycin and Amikacin in the Treatment of Mycobacterium abscessus Infections is Mediated by the whiB7 gene. *Antimicrob. Agents Chemother.* **61**, (2017).
37. Aziz, D. B., Go, M. L. & Dick, T. Rifabutin Suppresses Inducible Clarithromycin Resistance in Mycobacterium abscessus by Blocking Induction of whiB7 and erm41.

Antibiotics **9**, (2020).

38. Bernut, A., Herrmann, J.-L., Ordway, D. & Kremer, L. The Diverse Cellular and Animal Models to Decipher the Physiopathological Traits of Mycobacterium abscessus Infection. *Front. Cell. Infect. Microbiol.* **7**, (2017).
39. Bernut, A. et al. CFTR Protects against Mycobacterium abscessus Infection by Fine-Tuning Host Oxidative Defenses. *Cell Rep.* **26**, 1828-1840.e4 (2019).
40. Hernandez, V. et al. Discovery of a novel class of boron-based antibacterials with activity against gram-negative bacteria. *Antimicrob. Agents Chemother.* **57**, 1394–1403 (2013).
41. Lincecum, T. L. et al. Structural and mechanistic basis of pre- and posttransfer editing by leucyl-tRNA synthetase. *Mol. Cell* **11**, 951–963 (2003).
42. O'Dwyer, K. et al. Bacterial resistance to leucyl-tRNA synthetase inhibitor GSK2251052 develops during treatment of complicated urinary tract infections. *Antimicrob. Agents Chemother.* **59**, 289–298 (2015).
43. Rock, J. M. et al. Programmable transcriptional repression in mycobacteria using an orthogonal CRISPR interference platform. *Nat. Microbiol.* **2**, 16274 (2017).
44. Zhai, Y. & Martinis, S. A. Two conserved threonines collaborate in the Escherichia coli Leucyl-tRNA synthetase amino acid editing mechanism. *Biochemistry* **44**, 15437–15443 (2005).
45. Alvarez-Carreño, C., Becerra, A. & Lazcano, A. Norvaline and Norleucine May Have Been More Abundant Protein Components during Early Stages of Cell Evolution. *Orig. Life Evol. Biosph.* **43**, 363–375 (2013).
46. Ji, Q. Q., Fang, Z. P., Ye, Q., Chi, C. W. & Wang, E. D. Self-protective responses to norvaline-induced stress in a leucyl-tRNA synthetase editing-deficient yeast strain. *Nucleic Acids Res.* **45**, 7367–7381 (2017).
47. Cvetesic, N., Palencia, A., Halasz, I., Cusack, S. & Gruic-Sovulj, I. The physiological target for Leu RS translational quality control is norvaline. *EMBO J.* **33**, 1639–1653 (2014).
48. Bacher, J. M. & Schimmel, P. An editing-defective aminoacyl-tRNA synthetase is mutagenic in aging bacteria via the SOS response. *Proc. Natl. Acad. Sci. U. S. A.* **104**, 1907–1912 (2007).
49. Song, Y. et al. Double mimicry evades tRNA synthetase editing by toxic vegetable-

sourced non-proteinogenic amino acid. *Nat. Commun.* **8**, (2017).

50. Lu, J., Bergert, M., Walther, A. & Suter, B. Double-sieving-defective aminoacyl-tRNA synthetase causes protein mistranslation and affects cellular physiology and development. *Nat. Commun.* **5**, (2014).
51. Lee, J. W. et al. Editing-defective tRNA synthetase causes protein misfolding and neurodegeneration. *Nature* **443**, 50–55 (2006).
52. Schimmel, P. Mistranslation and its control by tRNA synthetases. *Philos. Trans. R. Soc. B Biol. Sci.* **366**, 2965–2971 (2011).
53. Dick, T., Shin, S. J., Koh, W. J., Dartois, V. & Gengenbacher, M. Rifabutin is active against mycobacterium abscessus in mice. *Antimicrob. Agents Chemother.* **64**, (2020).
54. Polis, B., Srikanth, K. D., Gurevich, V., Gil-Henn, H. & Samson, A. O. L-Norvaline, a new therapeutic agent against Alzheimer's disease. *Neural Regen. Res.* **14**, 1562–1572 (2019).
55. Ganapathy, U. S., Gengenbacher, M. & Dick, T. Epetraborole is active against mycobacterium abscessus. *Antimicrob. Agents Chemother.* **65**, (2021).
56. Kim, T. et al. A screening of the mmv pandemic response box reveals epetraborole as a new potent inhibitor against mycobacterium abscessus. *Int. J. Mol. Sci.* **22**, (2021).
57. Melnikov, S. V et al. Exploiting evolutionary trade-offs for posttreatment management of drug-resistant populations. *Proc. Natl. Acad. Sci. U. S. A.* **117**, 17924–17931 (2020).
58. Reingewertz, T. H. et al. Differential sensitivity of mycobacteria to isoniazid is related to differences in katg-mediated enzymatic activation of the drug. *Antimicrob. Agents Chemother.* **64**, (2020).
59. Rominski, A., Roditscheff, A., Selchow, P., Böttger, E. C. & Sander, P. Intrinsic rifamycin resistance of Mycobacterium abscessus is mediated by ADP-ribosyltransferase MAB_0591. *J. Antimicrob. Chemother.* **72**, 376–384 (2017).
60. Luthra, S., Rominski, A. & Sander, P. The Role of Antibiotic-Target-Modifying and Antibiotic-Modifying Enzymes in Mycobacterium abscessus Drug Resistance. *Front. Microbiol.* **9**, (2018).
61. Alcaide, F., Pfyffer, G. E. & Telenti, A. Role of embB in natural and acquired resistance to ethambutol in mycobacteria. *Antimicrob. Agents Chemother.* **41**, 2270–2273 (1997).
62. Sun, Z., Scorpio, A. & Zhang, Y. The pncA gene from naturally pyrarinamide-resistant

Mycobacterium avium encodes pyrazinamidase and confers pyrazinamide susceptibility to resistant M. tuberculosis complex organisms. *Microbiology* **143**, 3367–3373 (1997).

63. Zhang, Y., Scorpio, A., Nikaido, H. & Sun, Z. Role of acid pH and deficient efflux of pyrazinoic acid in unique susceptibility of Mycobacterium tuberculosis to pyrazinamide. *J. Bacteriol.* **181**, 2044–2049 (1999).
64. Su, H. & Xu, Y. Application of ITC-based characterization of thermodynamic and kinetic association of ligands with proteins in drug design. *Front. Pharmacol.* **9**, 1–7 (2018).
65. Dubée, V. et al. β-Lactamase inhibition by avibactam in Mycobacterium abscessus. *J. Antimicrob. Chemother.* **70**, 1051–1058 (2014).
66. Ming, X. F., Rajapakse, A. G., Carvas, J. M., Ruffieux, J. & Yang, Z. Inhibition of S6K1 accounts partially for the anti-inflammatory effects of the arginase inhibitor L-norvaline. *BMC Cardiovasc. Disord.* **9**, (2009).
67. Chang, C.-I., Liao, J. C. & Kuo, L. Arginase modulates nitric oxide production in activated macrophages. *Am. J. Physiol.* **274**, H324–H348 (1998).

3.10 FIGURES AND TABLES

TABLE 3.1. MMV Open pandemic response box hits and reference compounds.

Parameter	Compound				
	EPT	**ERV**	**IQN**	**BDQ**	**AMK**
MIC_{90} (µg/mL)	0.063	1.9	3.3	0.67	4.0
TD_{50} (µg/mL)	>27	>63	>39	9.4[a]	18
TI (TD_{50}/MIC_{90})	>430	33	12	14	4.5
MW (g/mol)	237.06	631.52	393.40	555.51	585.60

EPT, Epetraborole; ERV, Eravacycline; IQN, Isoquinoline urea; BDQ, Bedaquiline; AMK, Amikacin; $MIC_{90,}$ concentration of drug that inhibits 90% of bacterial growth; TD_{50}, concentration of drug with 50% toxicity against HepG2 cell line. TI, therapeutic index.

[a]Data from Lupien *et al*. *Antimicrob Agents Chemother*. **2018**

TABLE 3.2. Thermodynamic analysis of EPT binding with LeuRS.

Bacteria	ΔG (kcal mol^{-1})	ΔH (kcal mol^{-1})	TΔS (kcal mol^{-1})	Kd (μM)
M. abscessus	-6.49 ± 0.07	-3.2 ± 0.4	-3.3 ± 0.3	16 ± 4
M. tuberculosis	-6.9 ± 0.2	-1.1 ± 0.3	-5.5 ± 0.5	10 ± 4

ΔG, change in Gibbs free energy; ΔH, change in enthalpy; ΔS, change in entropy; T, temperature (303K); Kd, dissociation constant

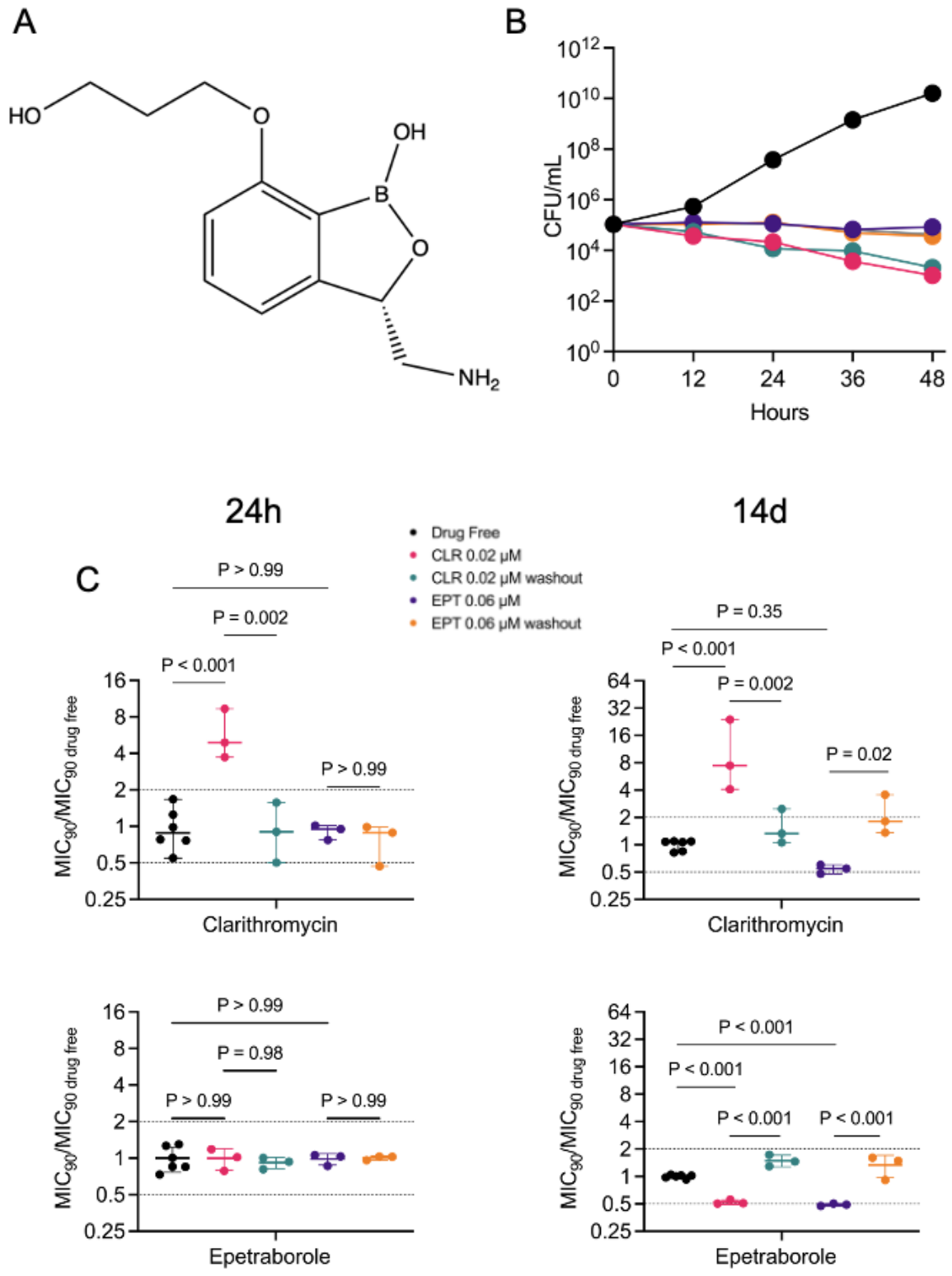

FIGURE 3.1. EPT *in vitro* activity against *M. abscessus*. **A** Structure of EPT. **B** Epetraborole kill kinetics of *M. abscessus in vitro*. Bacteria were incubated in 7H9 complete with drug-free (black circles), AMK 20X MIC_{90} (blue squares, 80 µg/mL), RIF 20X MIC_{90} (red triangles, 60

μg/mL), EPT 20X MIC_{90} (yellow hexagons, 1.6 μg/mL), EPT 40X MIC_{90} (orange diamonds, 3.2 μg/mL), or EPT 80X MIC_{90} (brown inverted triangles, 6.4 μg/mL). The dashed red line indicates 99.9% or 3 log_{10} reduction in CFU/mL threshold of a bactericidal drug. Data shown is mean ± SD of three independent experiments. **C** MIC_{90} from induced cultures relative to drug free conditions. Bacteria were grown to OD_{600} 0.05 and induced with no drug (white), 0.02 μM CLR (pink), 0.06 μM EPT (purple). After 24 hours (left) or 14 days (right) of induction, cultures were passaged for 6 days in drug free media (CLR, green; EPT, yellow). Data shown is mean ± SD from three independent experiments. Error bars for drug free data derived from MIC_{90} / MIC_{90} average from three or six replicates. P values were obtained by one-way ANOVA with Tukey's multiple comparisons test.

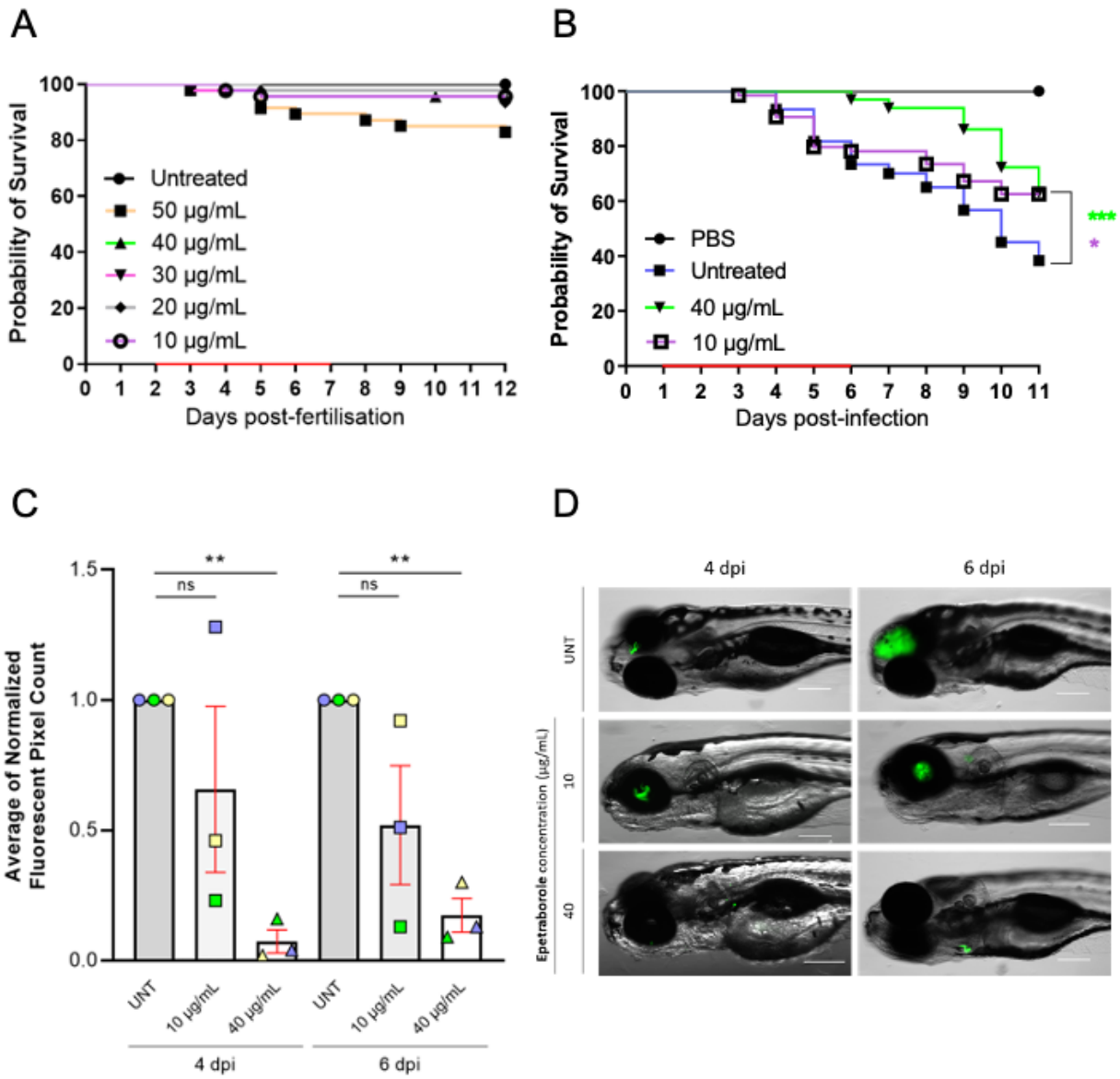

FIGURE 3.2. EPT *in vivo* activity against *M. abscessus*. A EPT toxicity against zebrafish embryos. Groups of uninfected embryos were immersed in water containing 10 to 50 µg/mL EPT for 5 days. Red bar indicates duration of treatment. Data is from two independent experiments. **B** EPT *in vivo* activity in zebrafish embryos. Zebrafish embryos at 30 h postfertilization were infected with approximately 200 CFUs of *M. abscessus* expressing green fluorescent wasabi or PBS via caudal vein injection. At 1 dpi, embryos were randomly split into approximately 20 embryos per group and exposed to increasing concentrations of EPT (10 and 40 µg/mL) in fish water. Drugs were renewed at a daily basis for 5 days (red bar) after which embryos were washed twice in fresh embryo water and maintained in fish water. Each treatment group was compared against the untreated infected group with significant differences calculated using the log-rank (Mantel-Cox)

statistical test for survival curves. Data shown are the merge of four independent experiments. *, p = 0.02; ***, p = 0.0007. **C** Fluorescent Pixel Counts (FPC) determination using the ImageJ software, reflecting the bacterial loads at 4 and 6 days post-infection (dpi). Each bar represents a pool of the average of normalized FPC from three independent experiments (n= 22 to 36 embryos). Error bars represent standard deviations. Statistical significance was determined using Welch's *t* test. **, $p \leq 0.0054$. **D** Representative whole embryos from the untreated group (upper panels) and treated group (10 or 40 µg/mL EPT; lower panels) at 4 and 6 dpi. Green overlay represents *M. abscessus* expressing wasabi. Scale bar, 200 µm.

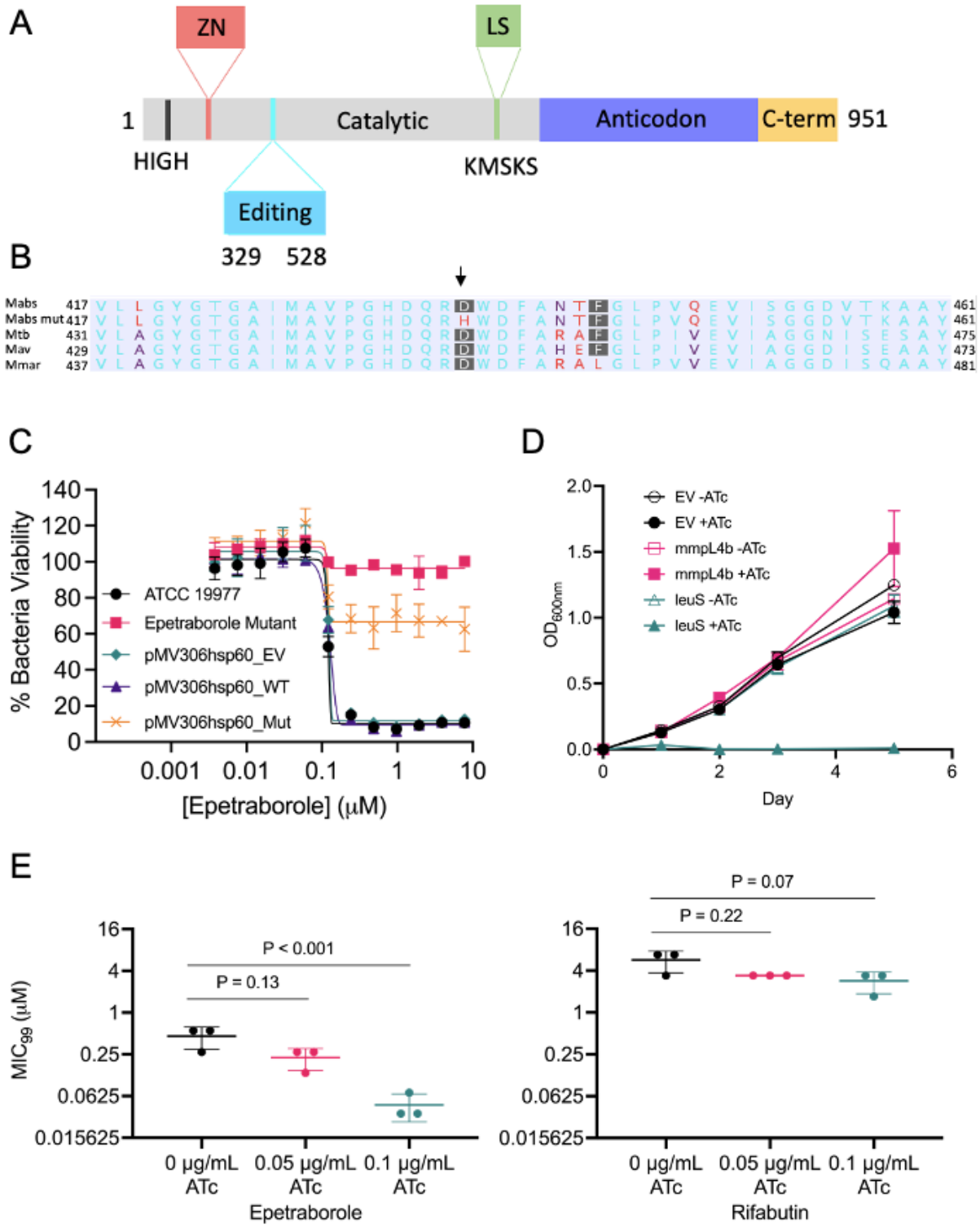

FIGURE 3.3. EPT targets the editing domain of LeuRS in *M. abscessus*. **A** Domains of *M. abscessus* LeuRS. Zinc domain, pink; editing domain, cyan; catalytic domain, grey; leucine-rich domain, green; anticodon-binding domain, purple; c-terminus, yellow. **B** Amino acid alignment of part of the editing domain of LeuRS *M. abscessus* ATCC 19977, EPT mutant, and reference

mycobacteria. Non-consensus residues are in red. Genbank accession numbers: P9WFV1.1 (*M. tuberculosis*) 11896261 (*M. avium*) 6224275 (*M. marinum*). **C** Dose-response curves of *M. abscessus* ATCC 19977 (black circles), D436H mutant (pink squares), *M. abscessus* empty vector (green diamonds), *M. abscessus* pMVhsp60_leuS_WT (purple triangles) and *M. abscessus* pMV306hsp60_leuS_Mut (yellow crosses). Data shown is mean ± SD from one experiment representative of two. **D** *leuS* is an essential gene in *M. abscessus* using CRISPRi gene knockdown. *M. abscessus* carrying integrated empty CRISPRi vector (EV, circles), CRISPRi:*mmpL4b* as a non-essential gene control (squares), or CRISPRi:*leuS* (triangles) were grown with/without 0.01 μg/mL ATc. Data is mean ± SD from biological triplicates. **E** MIC_{99} to EPT and RFB in CRISPRi knockdown of *leuS* in *M. abscessus*. P values were obtained by one-way ANOVA with Dunnett's multiple comparisons test. Data shown is mean ± SD from three biological replicates.

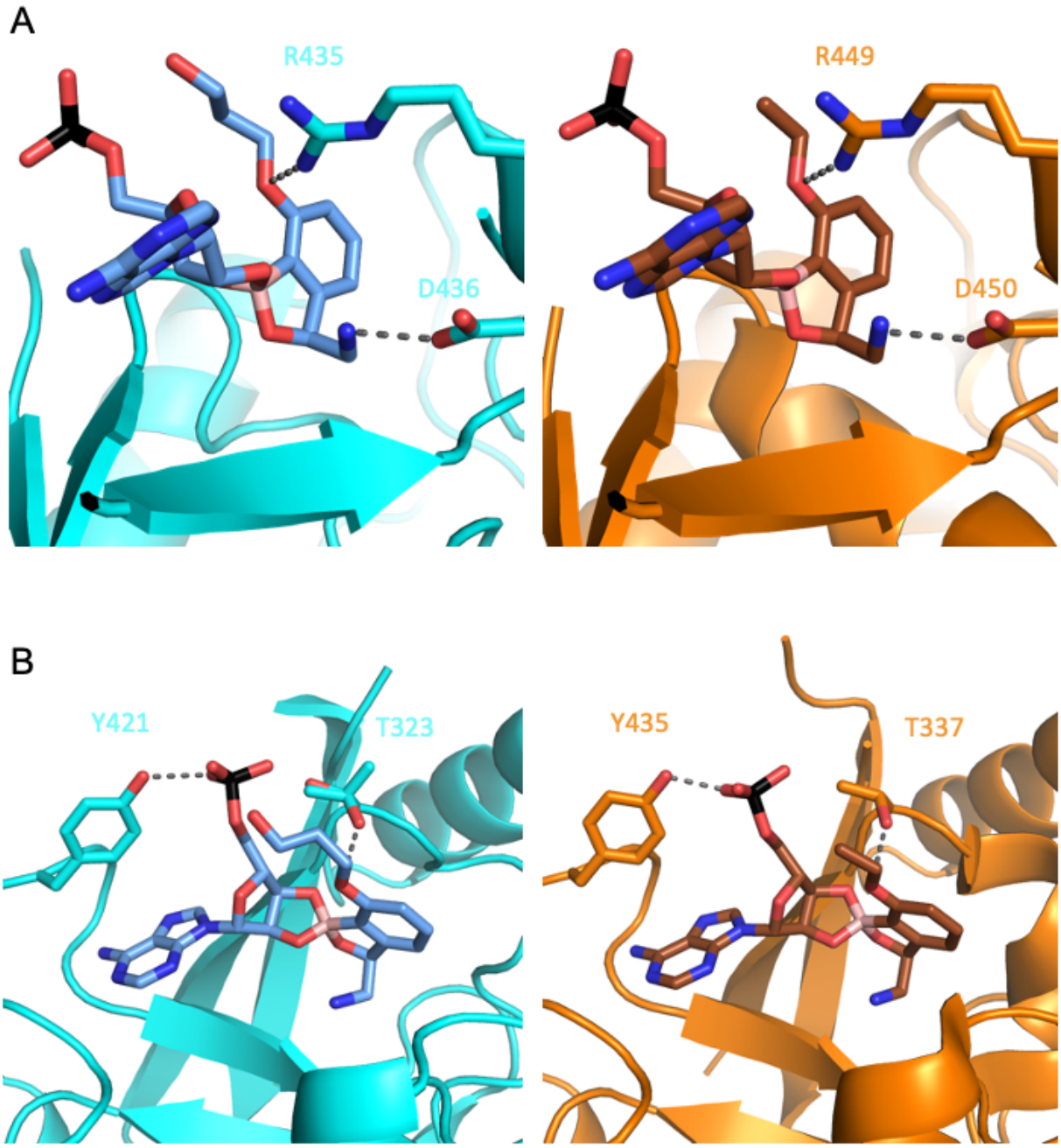

FIGURE 3.4. Similar binding of benzoxaboroles to the editing domain of LeuRS. EPT-AMP (blue) bound in the active site of *M. abscessus* LeuRS (cyan) and a similar benzoxaborole-AMP (brown) bound in active site of *M. tuberculosis* LeuRS (PDB 5AGR) (orange). **A** Critical arginine and aspartic acid residues make similar interactions with benzoxaboroles. **B** Phosphate from AMP pivots towards threonine residue in *M. abscessus* LeuRS. Conformer 1 of T323 points OH towards EPT, while conformer 2 orients OH towards the phosphate.

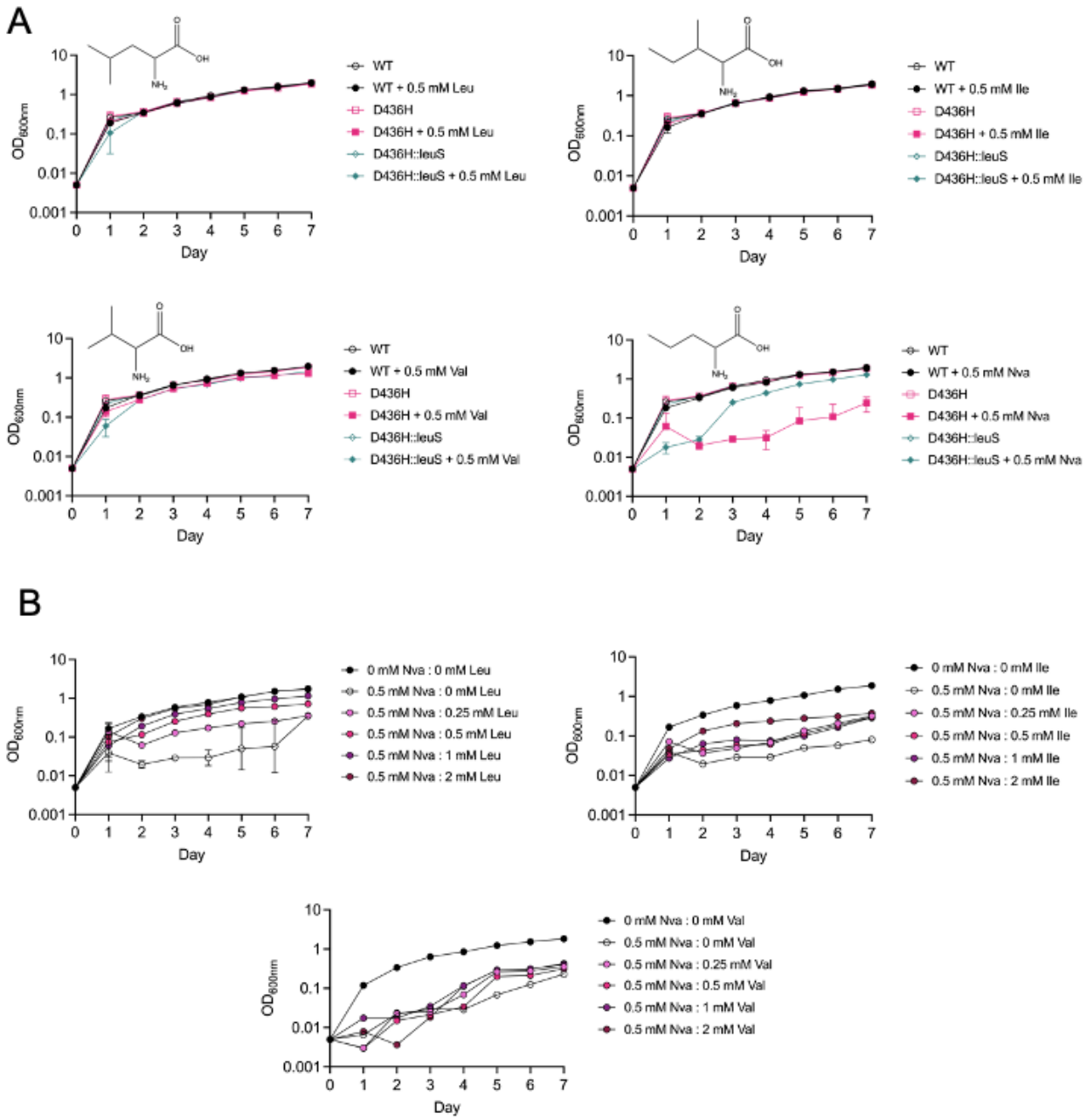

FIGURE 3.5. Norvaline is toxic to *M. abscessus* D436H editing deficient mutants. A ATCC 19977, D436H mutant, and D436H:leuS^{D} complement strains were grown in Sauton media with 0.5 mM leucine (top left), 0.5 mM isoleucine (top right), 0.5 mM valine (lower left), or 0.5 mM norvaline (lower right). Data shown is from three biological replicates. **B** D436H mutant grown in Sauton media with 0.5 mM norvaline and a range of leucine (left), isoleucine (right), or valine (bottom) concentrations. D436H mutant grown in 0 mM norvaline and 0 mM BCAA represents maximum growth control. D436H mutant grown in 0.5 mM norvaline and 0 mM BCAA represents inhibited growth control. Data shown is mean ± SD from three biological replicates.

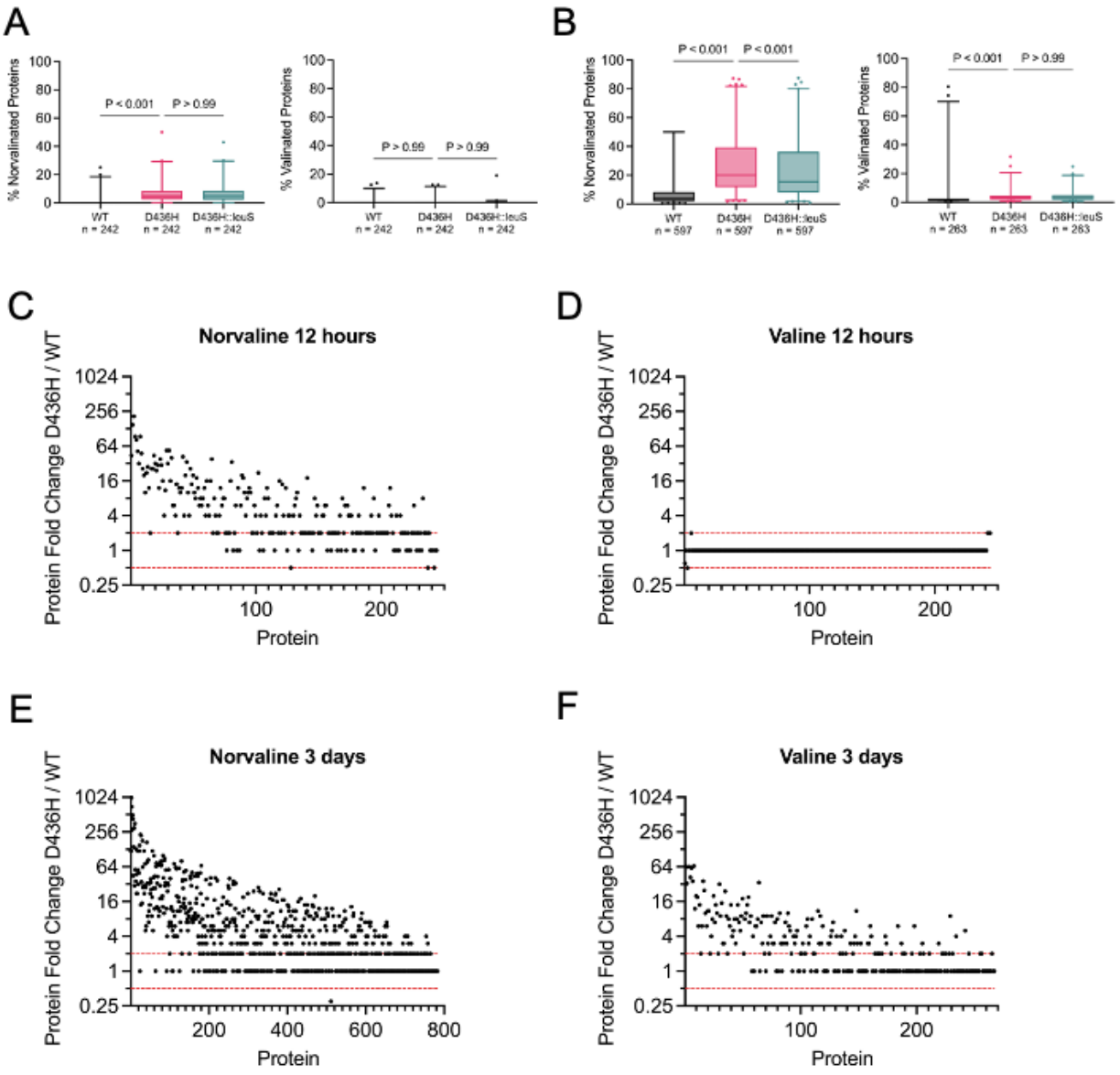

FIGURE 3.6. Norvaline misaminoacylation in editing deficient mutants alters the proteomic landscape. A,B *M. abscessus* ATCC 19977 or D436H mutant was grown in 0.5 mM norvaline or 0.5 mM valine for 12 hours or 3 days. Valine was used as a specificity control. Total cell lysate was collected. (Nor)valinated protein medians from the proteomes were compared using Friedman's test with Dunn's multiple comparisons test. **C-F** Protein fold abundance shown as D436H mutant relative to *M. abscessus* ATCC 19977. Dashed red lines indicate 0.5x and 2x fold abundance thresholds for biologically relevant changes.

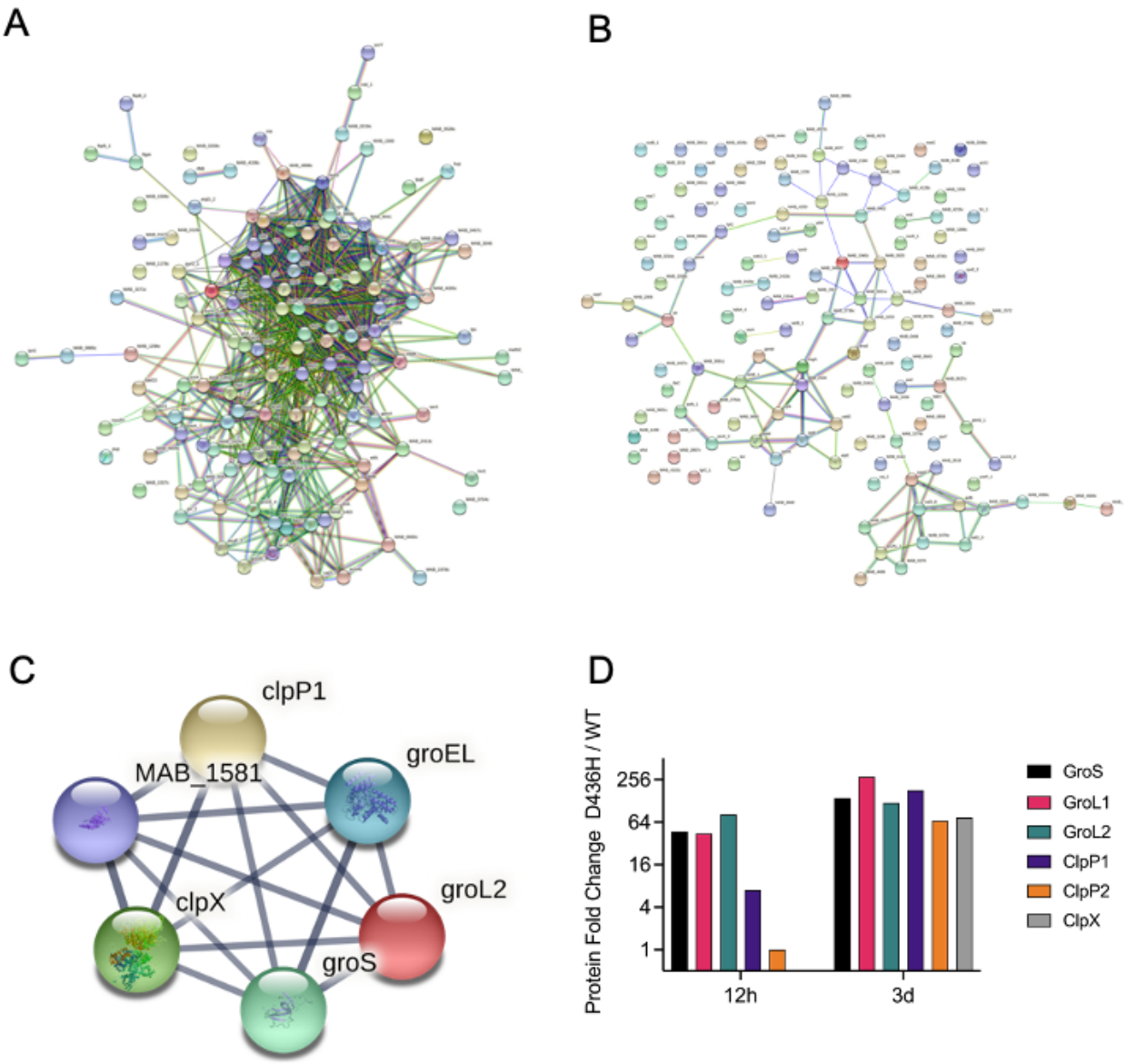

FIGURE 3.7. Norvaline stress induces the heat shock response in editing deficient mutants. **A** Protein-protein interaction network from the 130 most abundant proteins in D436H mutant when challenged with 0.5 mM norvaline for 12 hours. 942 PPIs identified with PPI enrichment p-value < $1.0x10^{-16}$. **B** PPI network from 130 randomly selected proteins in D436H mutant when challenged with 0.5 mM norvaline for 12 hours. 102 PPIs identified with PPI enrichment p-value of 0.0397. **C** Clp protease/chaperonin family local network cluster identified in **A** (false discovery rate: 0.00072). **D** Temporal signature of the heat shock response. Protein expression levels of D436H norvaline relative to WT norvaline were measured by spectral counting.

.

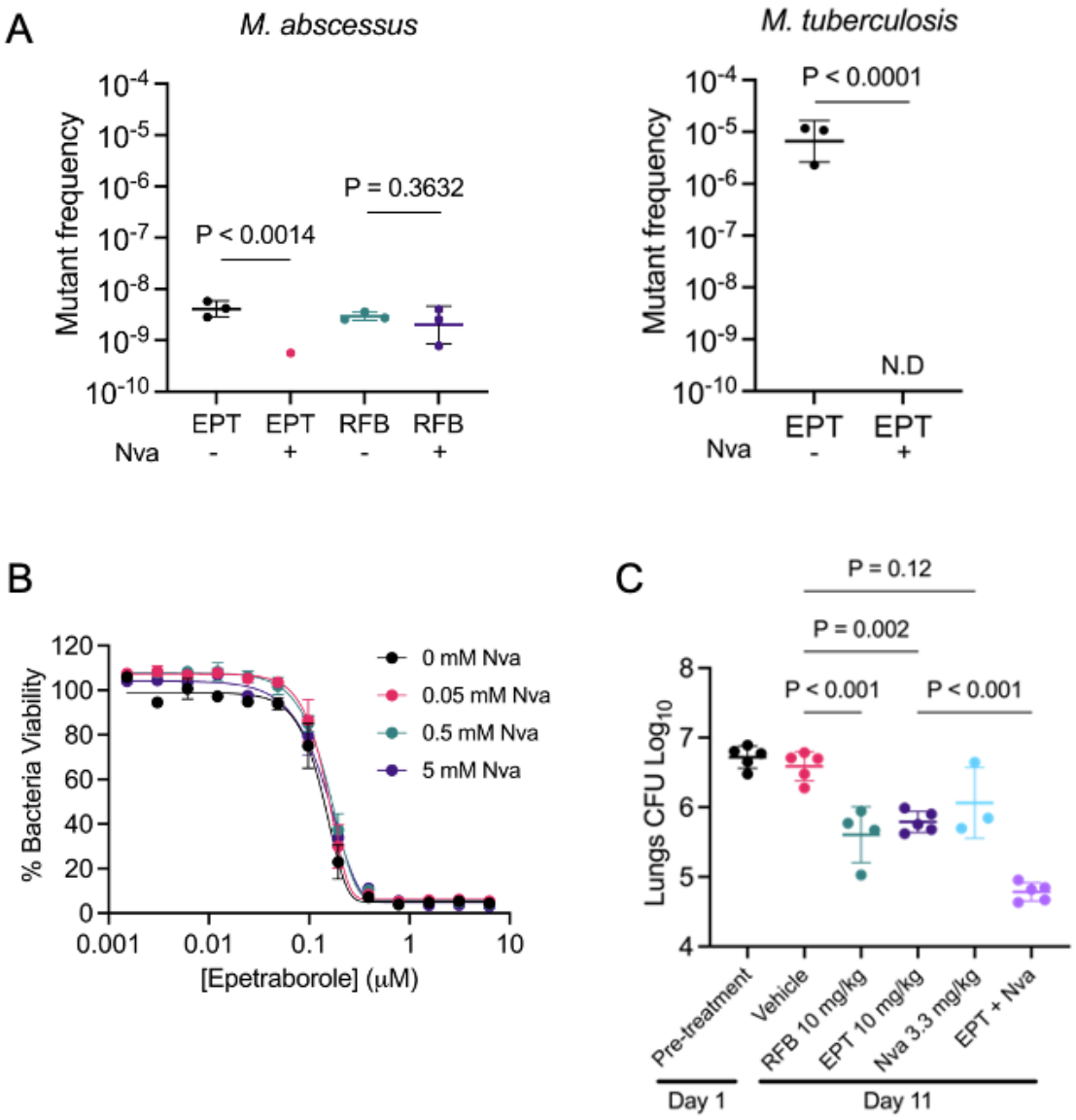

FIGURE 3.8. Norvaline improves epetraborole efficacy *in vitro* and *in vivo*. A Mutant frequency to 10X MIC_{90} EPT or 10X MIC_{90} EPT + 10X MIC_{90} norvaline in *M. abscessus* ATCC 19977 and *M. tuberculosis* H37Rv. RFB was included as specificity control. Data shown is mean ± SD from biological triplicates. Means compared using Poisson distribution. **B** *M. abscessus* susceptibility to EPT with norvaline as an adjuvant. Data shown is mean ± SD from one experiment representative of three. **C** EPT *in vivo* activity in SCID mouse model of *M. abscessus* lung infection with norvaline supplementation. RFB acts as positive control. Data shown is mean ± SD of three to five mice per treatment group. Means compared using one-way ANOVA with Tukey's multiple comparisons test.

3.11 SUPPLEMENTARY MATERIAL

TABLE S3.1. Carbon dependent variability on EPT activity.

	Media			
	7H9 G + Tw80	**7H9 G – Tw80**	**7H9 A + Tw80**	**CaMH + Tw80**
MIC_{90} (µg/mL)	0.06 ± 0.02	0.011 ± 0.008	0.016 ± 0.005	0.5 ± 0.2

G, Glycerol; A, Acetate; Tw80, Tween-80; CaMH, Cation-adjusted Muller-Hinton.

TABLE S3.2. Epetraborole *in vitro* activity against clinical isolates.

Isolate	Subspecies	Morphology[a]	MIC (µg/mL)					
			EPT	AMK	RIF	BDQ	CFX	CLR
ATCC 19977	*abscessus*	S	0.063	4.8	9.1	0.67	12	0.90
ATCC 19977	*abscessus*	R	0.11	2.4	1.8	0.27	12	0.65
MT16_1065	*abscessus*	S	0.041	2.1	>24	0.36	13	3.4
MT16_6490	*abscessus*	S	0.030	5.7	>24	0.83	13	2.9
MT15_1748	*massiliense*	R	0.022	14	9.1	0.23	26	0.068
MT15_1749	*massiliense*	R	0.014	8.8	6.7	0.40	16	0.082
Paris 167	*bolletii*	R	0.027	4.8	7.4	0.39	16	2.8
AV	*bolletii*	S	0.046	7.0	>24	1.3	15	0.15

[a]Morphology as determined by smooth (S) or rough (R) colonies on 7H10 agar. Drugs used: EPT, Epetraborole; AMK, Amikacin; RIF, Rifampicin; BDQ, Bedaquiline; CFX, Cefoxitin; CLR, Clarithromycin

TABLE S3.3. Epetraborole *in vitro* activity spectrum.

Species	Gram[a]	MIC (µg/mL)					
		EPT	**AMK**	**RIF**	**BDQ**	**CFX**	**CLR**
M. abscessus	AF	0.063	4.8	9.1	0.67	12	0.90
M. avium hominissuis	AF	2.7	5.6	0.063	0.038	4.7	0.18
M. avium intracellulaire	AF	2.7	3.8	0.063	0.014	0.42	0.014
M. tuberculosis H37Rv	AF	0.46	0.30	0.0063	0.26	>98	>1.3
M. tuberculosis Erdman	AF	0.19	0.48	0.0065	0.061	>98	>1.3
B. cereus	+	>2.7	64	<0.063	>7.8	>98	>8.2
C. glutamicum	+	2.0	0.064	<0.063	>7.8	98	>8.2
E. coli	-	5.7	0.15	3.9	>7.8	4.0	>8.2
P. aeruginosa	-	>2.7	0.22	15	>7.8	>98	>8.2

[a]Acid fast (AF); gram positive (+); gram negative (-). EPT, Epetraborole; AMK, Amikacin; RIF, Rifampicin; ERV, BDQ, Bedaquiline; CFX, Cefoxitin; CLR, Clarithromycin. Species: *Mycobacterium abscessus*, *Mycobacterium avium hominissuis*, *Mycobacterium avium intracellulaire*, *Mycobacterium tuberculosis* H37Rv, *Mycobacterium tuberculosis* Erdman, *Bacillus cereus*, *Corynebacterium glutamicum*, *Escherichia coli*, *Pseudomonas aeruginosa*

TABLE S3.4. *In vitro* resistance frequency.

	Resistance frequency[a]		
Compound[b]	**10X**	**20X**	**40X**
Amikacin	1.3×10^{-8}	N.D	N.D
Epetraborole	2×10^{-9}	1×10^{-9}	2×10^{-9}

[a]N.D: not determined. [b]MIC_{90} values on 7H10 agar used in this experiment were 4.0 µg/mL and 0.27 µg/mL for amikacin and epetraborole, respectively.

TABLE S3.5. Primers.

Primers	Function	Sequence	Source
1. pMV306hsp60_leuS_F	Cloning	GATGATCTGCAGAACCGAAACCCAGCACGACG	This study
2. pMV306hsp60_leuS_R	Cloning	GATGATAAGCTTCTAGACGACCAGGTTCACCATG	This study
3. pMV306hsp60_leuS_F1	Sequencing	GTAAGTAGCGGGGTTGCCGT	This study
4. pMV306hsp60_leuS_R1	Sequencing	GCTGCCGCTTGTAGTTGACG	This study
5. pMV306hsp60_leuS_F2	Sequencing	TGCAGACCGGCACCCATCC	This study
6. pMV306hsp60_leuS_R2	Sequencing	TTTGACCTTGTCCGGCCAGT	This study
7. pMV306hsp60_leuS_F3	Sequencing	CGCCTACTCCGACAGGTTGA	This study
8. pMV306hsp60_leuS_R3	Sequencing	CCGGCAAACCGAAGGTGTT	This study
9. pMV306hsp60_leuS_F4	Sequencing	ATGGCACCGGTGCCATCAT	This study
10. pMV306hsp60_leuS_R4	Sequencing	GCGGCATCACGTTGGTGTC	This study
11. pMV306hsp60_leuS_F5	Sequencing	AATGTCGAGCTGGACCTCGG	This study
12. pMV306hsp60_leuS_R6	Sequencing	GCAGCGTATCGGCACCATAGT	This study
13. pMV306hsp60_leuS_F6	Sequencing	GCCTCAAGAACTCGATCTCGC	This study
14. pMV306hsp60_leuS_R6	Sequencing	TGGCAGTCGATCGTACGCTAG	This study
15. CRISPRi_leuS_sgRNA_F	CRISPRi	GGGAACTCTTGTTGCACCTCTGCGCCCTG	This study
16. CRISPRi_leuS_sgRNA_R	CRISPRi	AAACCAGGGCGCAGAGGTGCAACAAGAGT	This study

TABLE S3.6. Whole-genome sequencing variants identified in EPT-resistant *M. abscessus*.

Gene	Function	Variant	
		20X	**40X**
38bp upstream MAB_2723c	3-oxoacyl-[ACP] reductase	del CCAAGGAACCGCA	
MAB_4932c	Leucyl-tRNA synthetase	T1261G (Y421D)	G1306C (D436H)
MAB_3268c	Conserved hypothetical protein	A266G (Q89R)	
MAB_4735	Putative starvation-induced DNA protecting protein	G230A (R77H)	
MAB_4814	Conserved hypothetical protein	A3576G (E1192E)	

TABLE S3.7. Crystallography collection data.

	M. abscessus LeuRS editing domain	*M. abscessus* LeuRS editing domain in complex with epetraborole-AMP adduct
Data collection		
Space group	P 2_1 2_1 2_1	C 1 2 1
Cell dimensions		
a, *b*, *c* (Å)	37.25, 51.59 116.15	113.439, 37.1074, 100.287
α, β, γ (°)	90, 90, 90	90, 112.279, 90
Resolution (Å)	1.69-50.00 (1.69-1.72) *	1.52-92.97 (1.52-1.55) *
R_{sym}	0.263 (0.824) *	0.100 (1.071) *
I / □I	4.4 (0.5) *	7.7 (0.3) *
Completeness (%)	76.8 (5.5) *	94.21 (49.23) *
Redundancy	6.8 (1.1) *	5.54 (3.08) *
Refinement		
Resolution (Å)	2.1	1.7
No. reflections	14741	109484
R_{work} / R_{free}	0.1841 / 0.2258	0.1843 / 0.2265
No. atoms	2968	5964
Protein	2822	5435
Ligand	/	126
Ion	15	5
Water	131	384
B-factors		
Protein	25.44	20.14
Ligand	/	19.98
Ion	63.20	56.13
Water	31.17	31.70
R.m.s. deviations		
Bond lengths (Å)	0.008	0.013
Bond angles (°)	0.999	1.216
PDB accession code	7N11	7N12

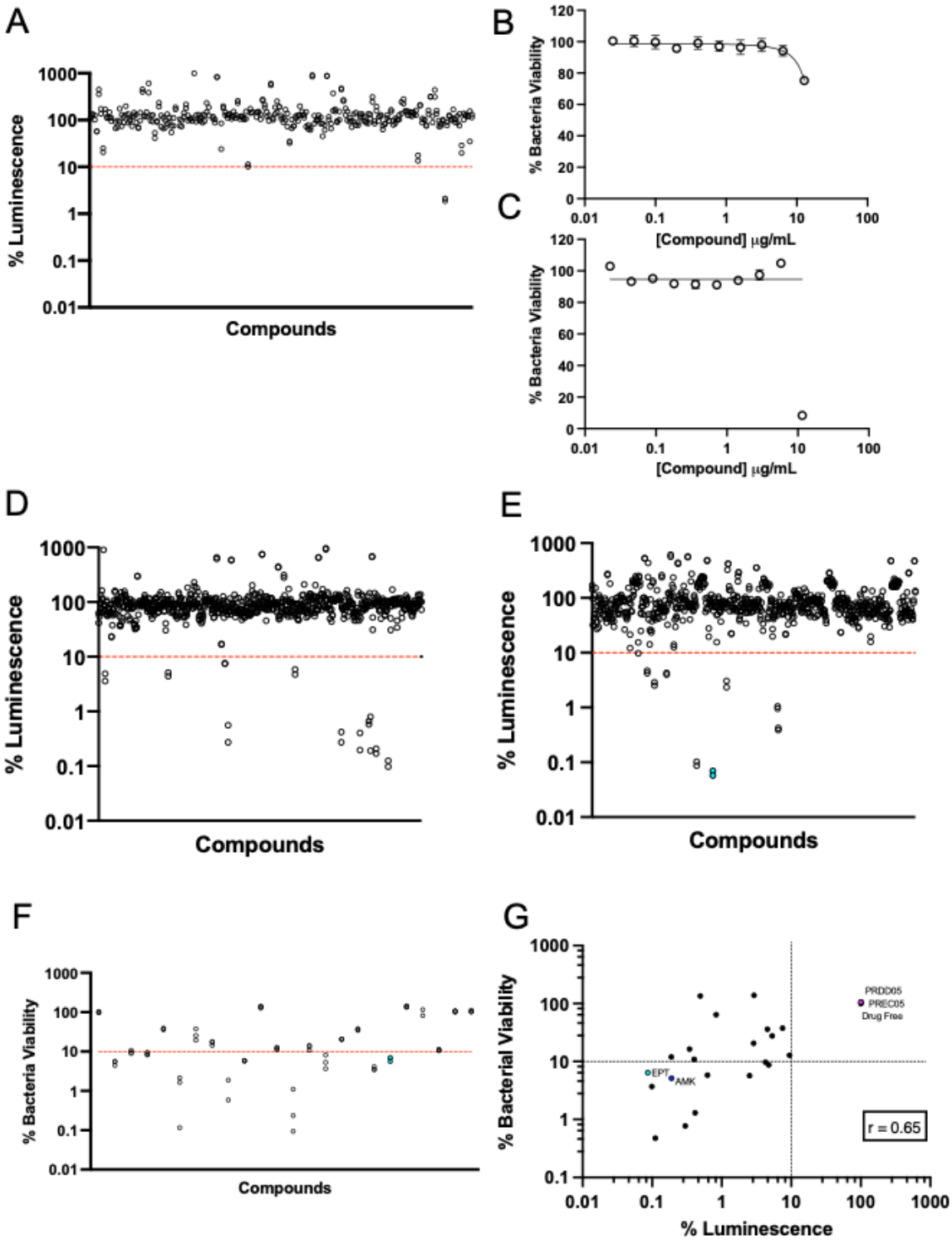

FIGURE S3.1. *M. abscessus* phenotypic screening with 176 TB-active compounds from GSK (A-C) and MMV Open pathogen and pandemic response boxes (D-F). A Luminescence relative to drug free conditions using *M. abscessus* lux. Data is shown in duplicate. **B,C** Secondary screening of primary hits using REMA on *M. abscessus* ATCC 19977. % Bacteria viability relative

to drug free conditions. Data is shown as mean ± SD from technical triplicates. Dashed red line indicates 10% viability threshold when screened at 10 μM. Three hits were identified from primary screen however, all three did not pass the secondary screen. No active compounds were identified from this library. **D** MMV Pathogen box and **E** Pandemic response box; luminescence relative to drug free conditions using *M. abscessus* lux. Data is shown in duplicate. **F** Secondary screening of primary hits using REMA on *M. abscessus* ATCC 19977. % bacteria viability relative to drug free conditions. Data is shown in technical triplicate. Dashed red line indicates 10% viability threshold when screened at 10 μM. **G** Correlation between hits from luminescence primary screen and bacterial viability secondary screen. Correlation calculated using non-parametric Spearman correlation. 20 compounds passed the primary screen and 9 passed the secondary screen. Only three compounds were still active after acquiring fresh batch and displayed dose-dependent activity (3/800). EPT in cyan. AMK in blue as positive control. Two negative hits from luminescence screen in magenta used as negative controls. Drug free in black used as media control.

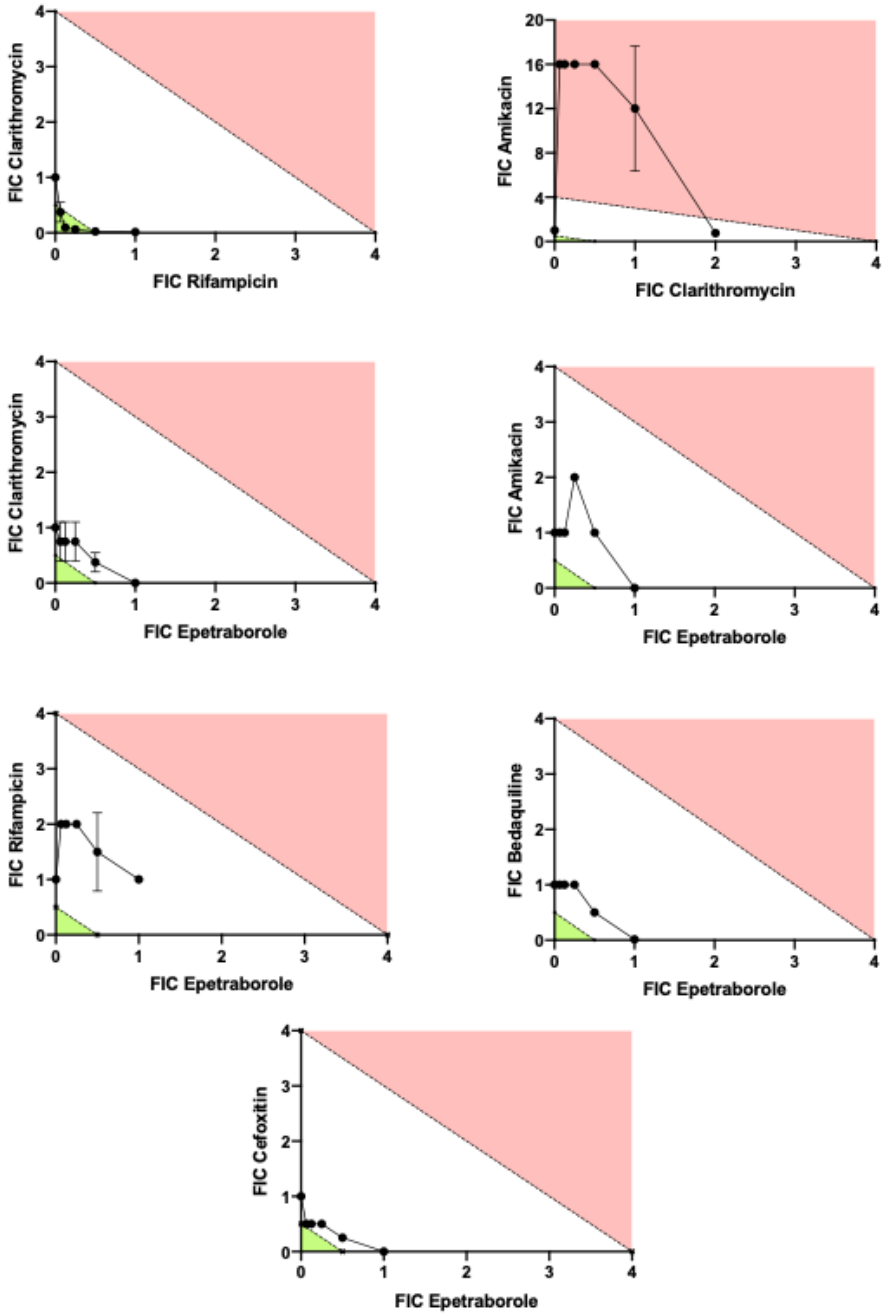

FIGURE S3.2. Isobolograms for potential combination therapy with EPT. Green area indicates synergy (FICI < 0.5); red area indicates antagonism (FICI ≥ 4.0); white area indicates indifferent. RIF and CLR, and AMK and CLR are used as synergy and antagonism controls, respectively. Data shown is from checkerboard assays done in technical duplicate.

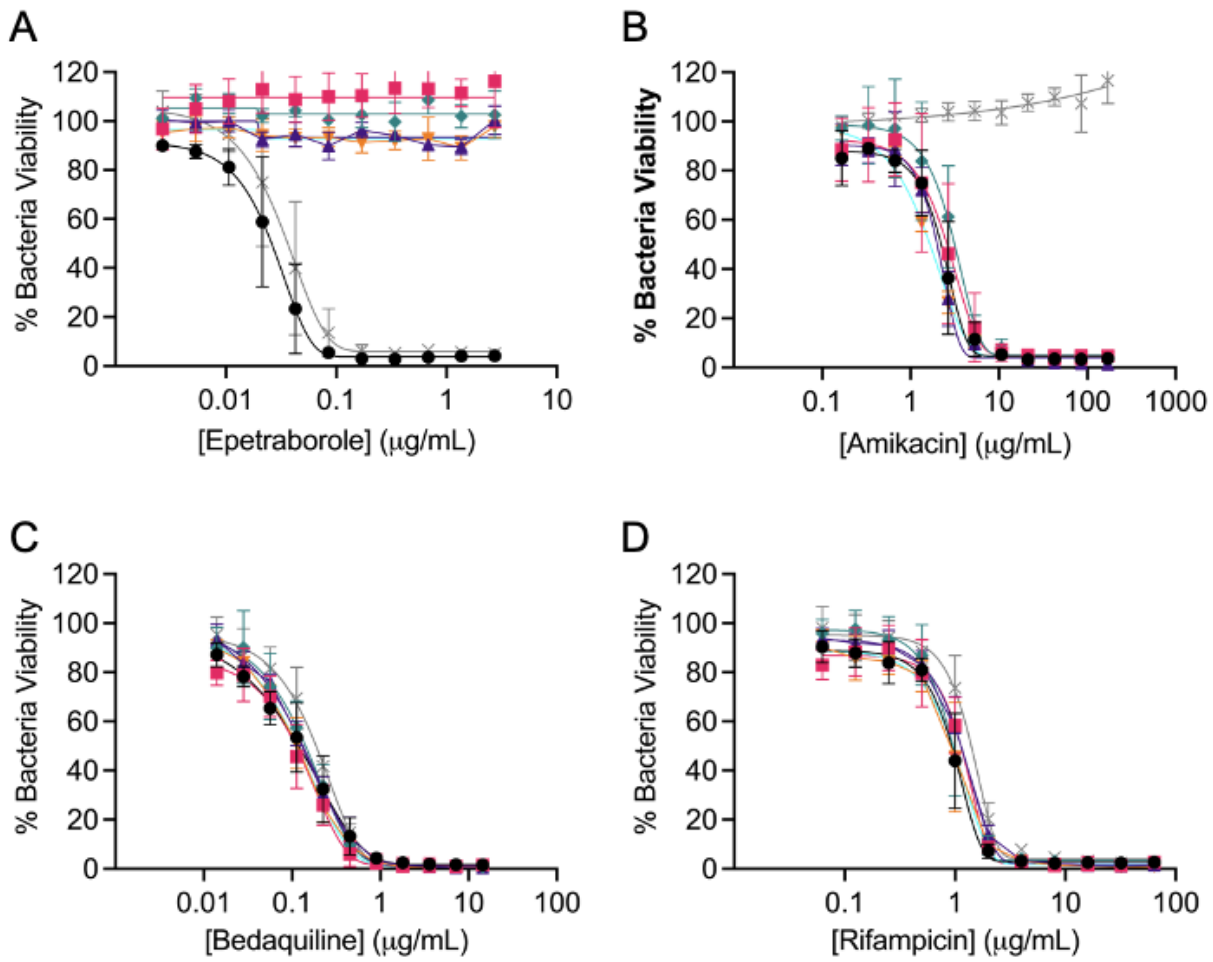

FIGURE S3.3. Drug susceptibility assessment of resistant mutants. A-D Dose-response curves of isolated EPT (10X, 20X, 40X MIC) mutants or AMK (40X MIC) mutant. AMK was used as control compound for mutant isolation. RIF and BDQ were used for cross-resistance verification. ATCC 19977 (black circles), D436H mutant-1 (pink squares), D436H mutant-2 (green diamonds), D436H mutant-3 (purple triangles), D436H mutant-4 (orange inverted triangles), AMK 40X (grey crosses). Data is mean ± SD from two independent experiments.

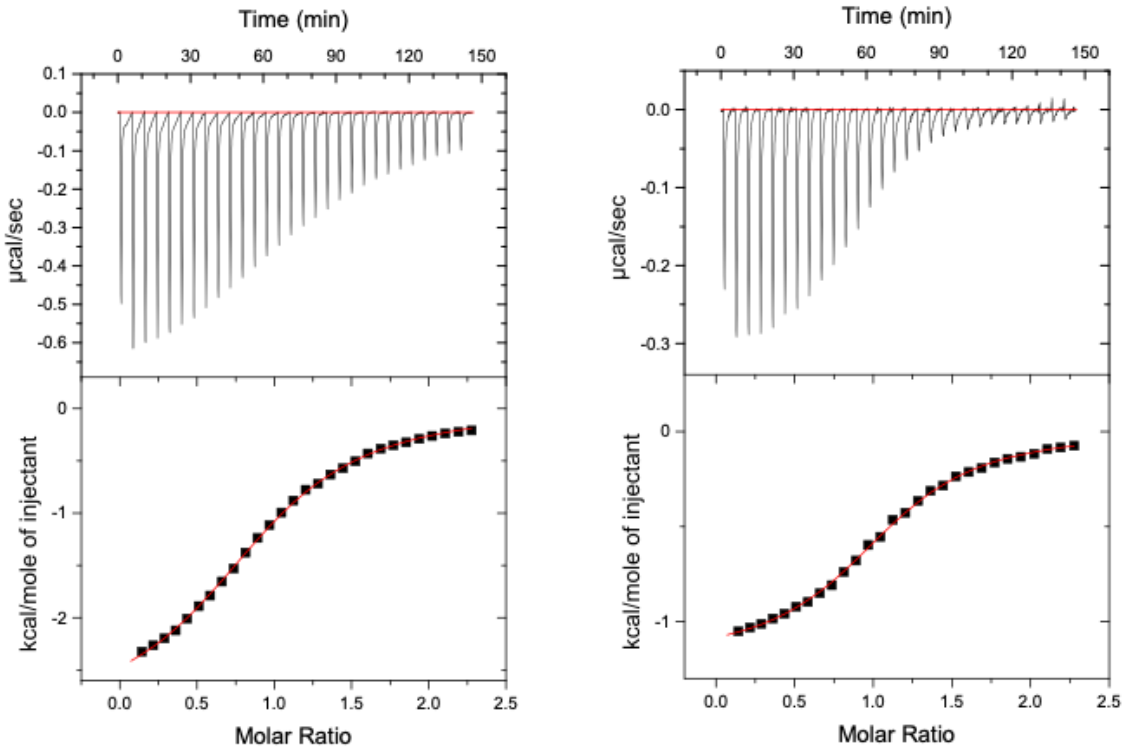

FIGURE S3.4. Thermodynamic analysis of EPT binding to LeuRS editing domain. Heat of injection (upper panel) and single-site binding model of the integrated isotherm (lower panel). *M. abscessus* LeuRS (left) or *M. tuberculosis* LeuRS (right) editing domains bound to EPT.

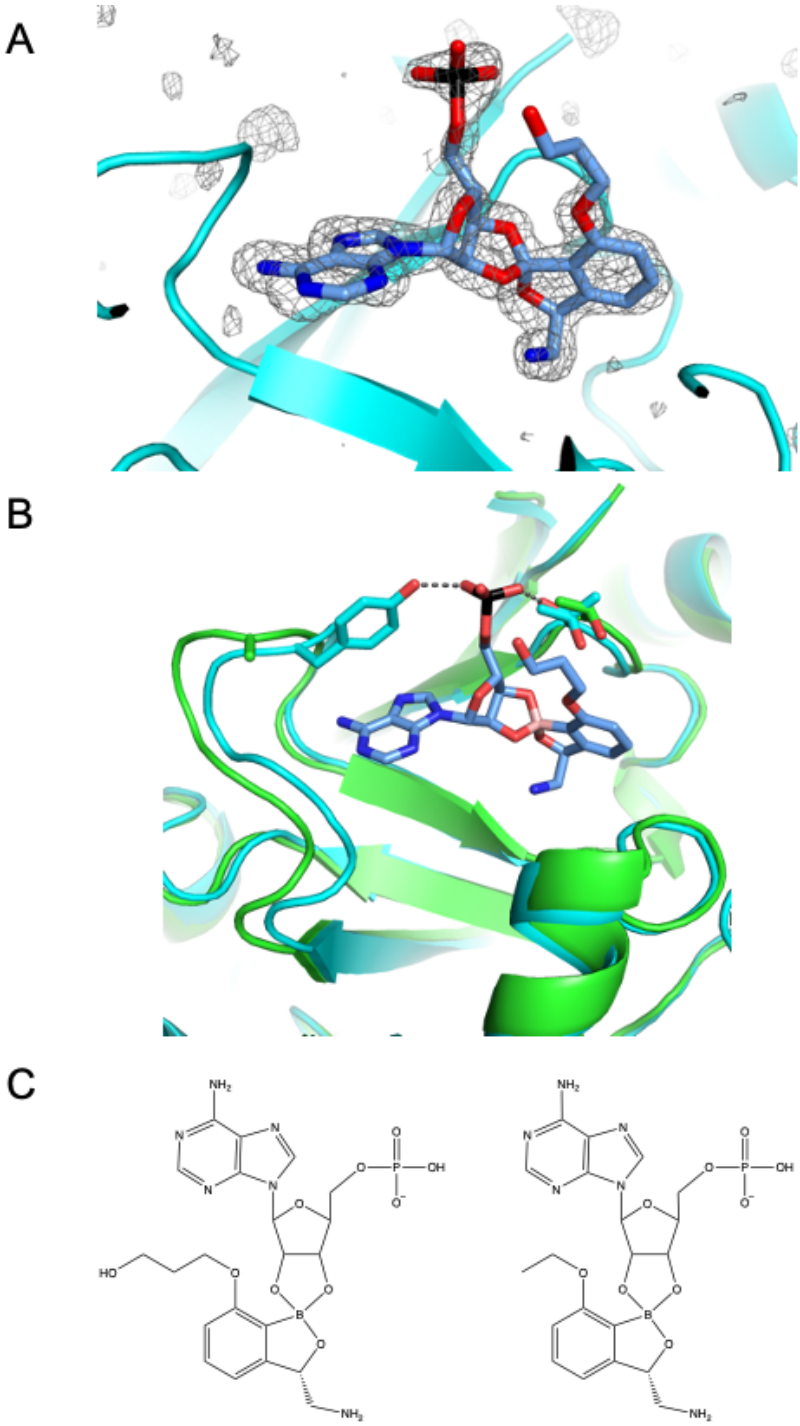

FIGURE S3.5. Co-crystal structure of LeuRS and benzoxaborole adducts. A Difference maps for the EPT-AMP adduct in 7N12. Unbiased FO-FC difference maps (2.8σ), calculated with phases from a model that never included ligand. **B** Comparison of apo (green, PDB 7N11) and co-complex (cyan, PDB 7N12) structures of *M. abscessus* LeuRS bound to EPT-AMP. **C**

Benzoxaborole inhibitors of LeuRS. (Left) EPT-AMP adduct bound to *M. abscessus* LeuRS. (Right) BNZ-AMP adduct bound to *M. tuberculosis* LeuRS.

PREFACE TO CHAPTER 4

In **Chapter 3**, we demonstrated the use of epetraborole and norvaline in combination to limit resistance to epetraborole *in vitro* and improve the efficacy *in vivo* supported by evidence of uncontrolled protein misfolding caused by the incorporation of norvaline across the proteome. Now, in **Chapter 4**, we document the unexpected resistance to norvaline through mechanistic work. Bacteria have been shown to possess intrinsic antimicrobial resistance mechanisms like drug and target modifying enzymes, efflux pumps, and drug degradation pathways. Alternatively, bacteria acquire resistance through mutations in the drug binding site that preclude binding or mutations that upregulate gene expression to minimize the effect of the drug on the physiology of the cell. Our data in **Chapter 4** suggests that *M. abscessus* developed resistance to norvaline through a LeuRS editing-independent manner. These norvaline resistant mutants over produce leucine, the natural substrate of LeuRS, and out-compete norvaline to prevent norvaline misaminoacylation.

This chapter was adapted from the manuscript: Loss of allosteric regulation in α-isopropylmalate synthase identified as an antimicrobial resistance mechanism. Sullivan *et al*. To be submitted November 2022.

CHAPTER 4

Loss of allosteric regulation in α-isopropylmalate synthase identified as an antimicrobial resistance mechanism

Jaryd R. Sullivan[a,b,c], Christophe Courtine[a,b,1], Lorne Taylor[d], Ori Solomon[a,b,c], Marcel A. Behr[a,b,c,e]

[a]Infectious Diseases and Immunity in Global Health Program, Research Institute of the McGill University Health Centre, Montreal, Canada H4A 3J1.

[b]Department of Microbiology & Immunology, McGill University, Montreal, Canada H3A 2B4.

[c]McGill International TB Centre, Montreal, Canada H4A 3S5.

[d]Clinical Proteomics Platform, Research Institute of the McGill University Health Centre, Montreal, Canada H4A 3J1.

[e]Department of Medicine, McGill University Health Centre, Montreal, Canada H3G 2M1

[1]Present address: Department of Microbiology and Immunology, Geisel School of Medicine at Dartmouth College, Hanover, NH 03755.

*Manuscript under submission.

4.1 ABSTRACT

Despite our best efforts to discover new antimicrobials, bacteria have evolved mechanisms to become resistant. Resistance to antimicrobials can be attributed to innate, inducible, and acquired mechanisms. *Mycobacterium abscessus* is one of the most antimicrobial resistant bacteria and is known to cause chronic pulmonary infections within the cystic fibrosis community. Previously, we identified epetraborole as an inhibitor against *M. abscessus* with *in vitro* and *in vivo* activities and that the efficacy of epetraborole could be improved with the combination of the non-proteinogenic amino acid norvaline. Norvaline demonstrated activity against the *M. abscessus* epetraborole resistant mutants thus, limiting resistance to epetraborole in wild type populations. Here we show *M. abscessus* mutants with resistance to epetraborole can acquire resistance to norvaline in an LeuRS editing-independent manner. After showing that the membrane hydrophobicity and efflux activity are not linked to norvaline resistance, whole-genome sequencing identified a mutation in the allosteric regulatory domain of α-IPMS. We found that mutants with the $IPMS^{A555V}$ variant incorporated less norvaline in the proteome and produced more leucine than the parental strain. Furthermore, we found that leucine can rescue growth inhibition from norvaline challenge. Our results demonstrate that *M. abscessus* can modulate its metabolism through mutations in an allosteric regulatory site to upregulate the biosynthesis of the natural LeuRS substrate and outcompete norvaline. These findings emphasize the antimicrobial resistant nature of *M. abscessus* while more broadly describe a unique mechanism of substrate and inhibitor competition.

4.2 SIGNIFICANCE STATEMENT

Cystic fibrosis patients and immunocompromised individuals are at greater risk for acquiring chronic pulmonary infections from *Mycobacterium abscessus*. Current antibiotics are not adequate and require increased drug discovery efforts to identify better treatments for these patients. The benzoxaborole, epetraborole has been shown by our group and others to be a promising candidate against *M. abscessus* but epetraborole faced issues with resistance in a clinical trial for complicated urinary tract infections. Previously, we identified the combination of epetraborole and norvaline as a potential means to limit resistance against epetraborole. Our results here demonstrate that *M. abscessus* can acquire resistance to both epetraborole and norvaline. These results call into question the utility of combining non-proteinogenic amino acids like norvaline with benzoxaborole antimicrobials.

4.3 INTRODUCTION

Antimicrobial resistance is a major public health concern and is estimated to contribute to 5 million deaths each year.[1–3] To facilitate antimicrobial research and development, the WHO created a priority pathogen list based on trends of resistance, preventability, and the status of the drug pipeline.[4,5] Arguably, when compared to *M. tuberculosis*, *M. abscessus*, is more drug resistant, more recalcitrant to treatment, and has less lead compounds in its pipeline than *M. tuberculosis*, yet it is often neglected in discussions regarding the current threat of antimicrobial resistant bacteria.[6–10]

Resistance to antimicrobials can be attributed to innate, inducible, and acquired mechanisms. *M. abscessus* uses a variety of mechanisms to overcome the antibiotic regimens clinicians have at their disposal. Besides common target mutations that alter the binding affinity for antibiotics like clarithromycin,[11] *M. abscessus* has a complex phenotypic resistome. Through its environmental reservoir, *M. abscessus* has acquired numerous bi-functional efflux pumps that transport essential lipid substrates and noxious xenobiotic agents.[12] *M. abscessus* is estimated to have 27 transporters belonging to the mycobacterial membrane protein Large (MmpL) group as opposed to 13 predicted in *M. tuberculosis.*[13] Clofazimine and bedaquiline, the most recently approved antitubercular agent, were shown to be substrates of MmpL5 in *M. abscessus.*[14]

Modification of antibiotics such as ribosylation, acetylation, and phosphorylation that disrupt key interactions between the target and antibiotic is also a common defense. *M. abscessus* encodes the ADP-ribosyltransferase arr_{Mab} that ribosylates rifamycins, and the *N*-acetyltransferase *eis2* and 3'-O-phosphotransferase *aph(3')* that inactivate aminoglycosides.[15–18] Not only can *M. abscessus* modify antibiotics, but the genome also contains β-lactamases with extended spectrum activity to limit the availability of the most widely-used antibiotic class used to treat bacterial infections.[19] The β-lactamases Bla_{Mab} and Bla_{Mmas} can hydrolyze penicillins and cephalosporins with greater efficiency than BlaC found in *M. tuberculosis* and are resistant to common BlaC β-lactamase inhibitors while Bla_{Mmas} imparts carbapenemase activity.[20,21]

Many of the mechanisms listed above are under the regulation of inducible transcription factors like WhiB7 and TetR. WhiB7 is considered the maestro of the resistome in *M. abscessus*. WhiB7

is known to be activated by ribosomal protein synthesis inhibitors like macrolides, tetracyclines, and aminoglycosides but also by molecules with pleiotropic effects on cell metabolism.[22–24] In 2009, Nash and colleagues identified an inducible *erm*(41) gene in *M. abscessus* that encodes a ribosomal methyltransferase and confers inducible macrolide resistance.[25] Later, it was shown in *M. abscessus* that inducible macrolide resistance is mediated through upregulation of *erm*(41) in a WhiB7-dependent process.[26,27] Most recently, a new explanation for how dimethylation of the 70S ribosome confers macrolide resistance was proposed that could lay the foundation for the rational design of macrolides that can overcome Erm-mediated resistance.[28] The net result of specific mechanisms combined with a hydrophobic membrane comprised of $C_{60\text{-}90}$ unit mycolic acids with significantly less permeability than other mycobacteria is a synergism against most clinically available antibiotics which results in a majority of treatment failures.[29–32]

By elucidating AMR mechanisms and leveraging the bacterial response to antimicrobial agents, novel antimicrobials and combination therapies could be developed for *M. abscessus* infections. Previously, we identified epetraborole with nanomolar whole cell activity against *M. abscessus.*[33] During this screening program, we discovered that epetraborole had failed a phase 2 clinical trial due to the rapid emergence of resistant *Escherichia coli* in complicated urinary tract infections.[34] We rationalized and then experimentally showed that epetraborole resistant *M. abscessus* mutants became sensitive to the non-proteinogenic amino acid L-norvaline. Sensitivity to L-norvaline is derived from a D436H substitution in the editing domain of leucyl-tRNA synthetase (LeuRS), which is the binding site for the epetraborole-$tRNA^{Leu}$ adduct. LeuRS activates L-leucine and subsequently transfers the activated amino acid onto the corresponding $tRNA^{Leu}$ isoacceptors. Fortunately, $tRNA^{Leu}$ with non-cognate amino acids can undergo hydrolysis in the editing domain to remove the erroneous amino acid before participating in polypeptide synthesis. However, by gaining resistance to epetraborole from $LeuRS^{D436H}$, the ability to edit misaminoacylated $tRNA^{Leu}$ is lost and the risk of translating incorrect proteins increases. Treatment of the epetraborole resistant mutants with L-norvaline caused proteome-wide misincorporation with L-norvaline at residues coding for L-leucine, and a decrease in the emergence of resistance to epetraborole when given in combination.

In this article, we show using a combination of genetics, proteomics, and small molecule analysis that overproduction of L-leucine from insensitivity to feedback inhibition can abrogate the toxicity of L-norvaline to levels similar to using the evolutionarily conserved editing domain on LeuRS. These findings demonstrate the loss of allosteric regulation as the foundation for competitive antimicrobial inhibition and highlight the propensity of *M. abscessus* to become increasingly antimicrobial resistant.

4.4 METHODS

4.4.1 Culture conditions

M. abscessus strains were grown in rolling liquid culture at 37 °C in Middlebrook 7H9 (Difco) supplemented with 10% (v/v) albumin dextrose catalase (ADC), 0.2% (v/v) glycerol, and 0.05% (v/v) Tween 80 (7H9 complete) or Sauton's defined minimal media. 7H10 agar plates supplemented with 10% (v/v) oleic acid ADC (OADC) and 0.5% (v/v) glycerol were used for growth on solid media at 37 °C.

4.4.2 Norvaline time-dependent killing

Log phase (OD_{600} of 0.4-0.8) *M. abscessus* was diluted to an OD_{600} of 0.0001 (10^5 CFU/mL) and challenged with an initial dose of L-norvaline at 4X MIC_{90} of the sensitive *M. abscessus* $LeuRS^{D436H}$ strain or norvaline at 4X MIC_{90} supplemented daily to create steady-state conditions (4XSS). One hundred µL aliquots were taken and serially diluted in 7H9 complete and plated on 7H10 agar. The starting inoculum was determined from time 0 before norvaline was added. CFUs were determined after 4 days of incubation at 37 °C. Bactericidal activity is defined as a 3 $\log_{10}$ decrease (99.9%) from the starting inoculum.

4.4.3 Minimum inhibitory concentrations (MIC)

MIC values were determined using the resazurin microtiter assay (REMA). Cultures were grown to log phase (OD_{600} of 0.4-0.8) and diluted to OD_{600} of 0.005 ($5x10^6$ CFU/mL). Compounds were prepared in two-fold serial dilutions in 96-well plates with 90 µL of bacteria per well to a final volume of 100 µL. 96-well clear, flat bottom plates were incubated at 37 °C until drug-free wells were turbid (2 days for *M. abscessus*). Ten µL of resazurin prepared at 0.025% (w/v) in distilled water was added to each well. Once the drug-free wells turned pink (3-4 hours or one doubling time), the fluorescence (Ex/Em 560/590) was measured using an Infinite F200 Tecan plate reader. Fluorescence intensities were converted to percentage of viable cells relative to drug-free conditions and fit to the modified four-parameter dose-response regression using GraphPad Prism version 9. MIC values at 90% reduction of viability were determined from the Gompertz nonlinear regression equation.[35]

4.4.4 Isolating norvaline resistant mutants

L-norvaline resistant mutants of *M. abscessus* ATCC 19977 were isolated from L-norvaline time-dependent killing assays. Single colonies were obtained from streaked 7H10 plates. Genomic DNA (gDNA) was extracted from *M. abscessus* EPT^R $LeuRS^{D436H}$ as the parental strain and two colonies of *M. abscessus* EPT^R Nva^R 4XSS mutants with confirmed norvaline resistance (REMA method) using the Qiagen QiaAMP UCP Pathogen mini kit with a modified mechanical lysis protocol. Culture was pelleted by centrifugation and resuspend in 590 µL of ATL buffer containing the Dx reagent in a low-bind tube. 40 µL of proteinase K (20 mg/mL) and 20 µL of lysozyme (100 mg/mL) were added and incubated for 30 minutes at 56 °C under agitation. Solution was transferred into a Pathogen Lysis Tube L and vortexed twice using a FastPrep-24 instrument at 6.5 m/s for 45 s with a 5-minute incubation on ice in between. Supernatant was transferred into a fresh 2 mL low-bind tube and gDNA was collected via spin protocol according to manufacturer's instructions. gDNA was quantified with Quant-iT PicoGreen dsDNA kit.

4.4.5 Sequencing and variant calling

Paired end read sequencing libraries were prepared using Illumina S4 kit. Whole genome sequencing was performed on Illumina Novaseq 6000. Raw paired end reads were adapter and quality trimmed with Trimmomatic v0.40 and aligned to the *M. abscessus* ATCC 19977 reference genome (GenBank: CU_458896.1) using Burrows-Wheeler Aligner - maximum exact matches algorithm (bwa-mem).[36,37] Aligned reads were sorted using SAMTOOLs.[38] Duplicate reads were filtered using Picard. Freebayes v1.3.6 was used for variant calling and filtering variants with mapping quality 60, minimum coverage 10, minimum allele frequency of 0.5, and QUAL >100.[39] Variants identified in parental and resistant strains were manually compared to isolate variants unique to resistant strains.

4.4.6 Growth curves

Bacteria were grown to log phase (OD_{600} of 0.4-0.8) in 7H9 complete or Sauton media and diluted to OD_{600} of 0.005 ($5x10^6$ CFU/mL). Branched-chain amino acids were added to 90 µL of bacteria to a final volume of 100 µL. Growth curves were performed in 96-well clear, flat bottom microtiter plates, incubated statically at 37 °C before measuring OD_{600} on an Infinite F200 Tecan plate reader.

Data was fit to an exponential plateau regression to determine the growth rate μ and maximum growth plateau Y_M.

4.4.7 Congo red uptake

Strains were grown on 7H10 agar plates supplemented with 10% (v/v) OADC, 0.5% (v/v) glycerol, and Congo red at 140 μM at 37 °C. After five days, cells were scraped into an Eppendorf tube and washed with water until the supernatant turned clear. Washed cells were incubated with 1 mL of DMSO for 2 hours. Supernatants were collected and measured at A_{488} using an Infinite F200 Tecan plate reader. Values were normalized to the dry weight of the pellet.

4.4.8 Ethidium bromide efflux

M. abscessus strains were grown to log phase (OD_{600} of 0.4-0.8) in Sauton media and diluted to OD_{600} of 0.2. 80 μL of bacteria was added to a black, clear bottom 96-well plate with 10 μL serially diluted ethidium bromide and 10μL of media. For efflux pump inhibition assays, media was replaced with 10 μL of verapamil or CCCP for a final concentration of 0.5 mM or 25 μM, respectively. Fluorescence (Ex/Em 525/600) was measured every 90 seconds for 2 hours at 25 °C using an Infinite F200 Tecan plate reader.

4.4.9 Cloning and over-expressing *leuA* in *M. abscessus* EPT^R $LeuRS^{D436H}$

The wildtype and mutant *leuA* gene (MAB_0337c), which encodes α-isopropylmalate synthase, including 250bp upstream to capture the native promoter were PCR amplified from gDNA using Q5 polymerase with forward primer (5' ACTGCAGAATTCTCCTTGAGAGCGCTCGCGAAG) and reverse primer (5' GATGATAAGCTTCTAGGCGCGAGCAGCACGG), ligated into pMV306_hsp60 digested with EcoRV and HindIII restriction enzymes, and transformed into *E. coli* DH5*α* cells (Promega). Plasmids were extracted and sequenced using Sanger sequencing.

4.4.10 Initial growth kinetics and data theory

M. abscessus strains were grown to log phase (OD_{600} of 0.4-0.8) in Sauton media and diluted to OD_{600} of 0.005 in 96-well clear, flat bottom microtiter plates with serial dilutions of norvaline. Each set of norvaline dose-response curves was incubated with a constant amount of L-leucine as a norvaline inhibitor. Plates were incubated statically at 37 °C and A_{600} was measured on an Infinite

F200 Tecan plate reader to monitor growth. Initial growth rates, μ_i (h^{-1}), were measured during the first 24 hours of growth. Growth rate inhibition, performed under variable norvaline concentrations and constant L-leucine concentrations (0 mM, 0.0625 mM, 0.125 mM, or 0.250 mM) were fitted to a dose-response curve

$$\mu = \mu_{min} - (\mu_{max}-\mu_{min})/[1+(I/IC_{50})^{n_H}], \quad (1)$$

where μ is the rate in the presence of inhibitor at concentration I, μ_{max} and μ_{min} are the maximum and minimum growth rates, IC_{50} is the concentration of inhibitor that inhibits the growth rate by 50%, and n_H is the Hill coefficient. IC_{50} values were used to estimate an apparent inhibition constant, K_i, using the Cheng-Prusoff equation for competitive inhibition

$$K_i = IC_{50}/(1 + L/K_s), \quad (2)$$

where K_i is the apparent inhibition constant for L-norvaline, L is the concentration of L-leucine, and K_s is the substrate affinity constant of L-leucine.

4.4.11 LC-MS/MS measurement of norvaline in the proteome

M. abscessus strains were grown to early log phase (OD_{600} of 0.1-0.2) and challenged with 0.5 mM L-norvaline in Sauton media for 24 hours. Proteins were extracted using an optimized protocol for mass spectrometry follow-up.[40] Cells were collected, washed with ice-cold PBS, and resuspended in 1mL lysis buffer (50 mM NH_4HCO_3 pH 7.4, 10 mM $MgCl_2$, 0.1% NaN_3, 1 mM EGTA, 1 x protease inhibitors (Roche), 7 M urea, and 2 M thiourea). Cells were lysed with zirconia beads and the cell lysate was collected and filtered through a 0.22 µm membrane. Proteins were precipitated overnight at 4 ºC with TCA at 25% (v/v). The precipitate was washed with 1 mL cold acetone and 250 µL cold water. The final wash is only water. The pellet was resuspended in 200 µL resuspension buffer (50 mM NH_4HCO_3, 1 M urea). Protein extraction was quantified with the Bradford assay and the quality of proteins was examined on SDS-PAGE. Protein lysates were dissolved in SDS-PAGE reducing buffer and electrophoresed onto a single stacking gel band to remove lipids, detergents and salts. For each sample, a single gel band was reduced with DTT (Sigma), alkylated with iodoacetic acid (Sigma) and digested with LCMS grade trypsin (Promega). Extracted peptides were re-solubilized in 0.1% aqueous formic acid and loaded onto a Thermo Acclaim Pepmap (Thermo, 75 µM ID X 2 cm C18 3 µM beads) precolumn and then onto an Acclaim Pepmap Easyspray (Thermo, 75 µM X 15 cm with 2 µM C18 beads) analytical column separation using a Dionex Ultimate 3000 uHPLC at 250 nl/min with a gradient of 2-35% organic

(0.1% formic acid in acetonitrile) over 2 hours. Peptides were analyzed using a Thermo Orbitrap Fusion mass spectrometer operating at 120,000 resolution for MS1 with HCD sequencing at top speed (15,000 resolution) for all peptides with a charge of 2+ or greater. The raw data were converted into *.mgf format (Mascot generic format) for searching using the Mascot 2.5.1 search engine (Matrix Science) against *M. abscessus* protein sequences (Uniprot downloaded 2020.11.30). A modification for Xle->Val was used to detect incorporation of Val into wild-type sequences. The database search results were loaded onto Scaffold Q+ Scaffold_4.4.8 (Proteome Sciences) for statistical treatment and data visualization.

4.4.12 Principal component analysis

The dataset comprised of the 1000 most abundant proteins from each strain of *M. abscessus* based on quantitative spectral counts. Spectral counts for each protein were standardized within strains. PCA was performed using R to generate the loading data and scores. PCA was visualized with the first two principal components which accounted for >95% of the variance.

4.4.13 LC-MS metabolomics of BCAAs

Samples aliquots were diluted with an internal standard (norvaline-d5) and derivatized with 6-aminoquinolyl-N-hydroxysuccinimidyl carbamate (AQC; Toronto Research Chemicals, Ontario, Canada) for analysis using reversed phase ultra performance liquid chromatography mass spectrometry (UPLC-MS). Samples were prepared and analyzed along with calibration curves containing isoleucine, leucine, norvaline and valine (Sigma-Aldrich, St. Louis, Missouri, USA) in culture media. An internal standard working solution (ISWS) containing 50 µM norvaline-d5 (CDN Isotopes, Dorval, Quebec, Canada) in water was added to the experimental and calibration samples prior to derivatization. ISWS aliquots (25 µL) were added to sample aliquots (25 µL) in microcentrifuge tubes and vortexed. Aliquots (10 µL) then were transferred into glass tubes containing 70 µL buffer solution (0.2M sodium borate pH 8.8) along with 20 µL derivatization solution (10mM AQC in acetonitrile), mixed and incubated for 10 min at 55°C. After cooling to room temperature, aliquots (5 µL) were transferred to autosampler vials containing 995 µL Type-1 water for UPLC-MS analysis. Samples were analyzed by UPLC-MS using an Agilent 6460 triple quadrupole mass spectrometer coupled with an Agilent 1290 UPLC system (Agilent, Santa Clara, California, USA). Samples (5µL) were injected onto an Agilent Eclipse Plus C18 100 x 2.1 mm

(1.8 µm) column and chromatographed with a reverse phase gradient at 0.250 mL/min using 0.1% formic acid in water and 0.1% formic acid in acetonitrile. The derivatized amino acids were detected using electrospray positive mode ionization followed by MS/MS fragmentation. Data acquisition was performed using Agilent MassHunter Data Acquisition (version B.04.01) software. Peak area measurements from selected product ions, calibration curve regression analysis and resulting sample quantification were performed using Agilent MassHunter Quantitative Analysis (version B.05.00) software.

4.4.14 Homology modeling

The models of α-IPMS$_{Mabs}$ (MAB_0337c) were generated using the SWISS-MODEL server and the crystal structures of α-IPMS$_{Mtb}$ as templates (PDB 3FIG, 3HPZ).[41,42]

4.4.15 Data analysis

Data were processed by GraphPad PRISM 9.4.1, The PyMOL Molecular Graphics System 2.3.0, R 4.1.2, and Scaffold Q+ Scaffold_4.4.8.

4.5 RESULTS

4.5.1 Spontaneous generation of L-norvaline resistance in *M. abscessus*

M. abscessus that is resistant to both epetraborole and L-norvaline was raised spontaneously during a kill kinetics experiment that sought to determine whether L-norvaline caused cell death to the epetraborole resistant *M. abscessus* LeuRS^{D436H} strain. The wild type ATCC 19977 reference strain of *M. abscessus*, the EPT^{R} LeuRS^{D436H} mutant, and the EPT^{R} LeuRS^{D436H} mutant complemented with wild type *leuS* were grown in 2.4 mM L-norvaline (4X MIC) for five days. In agreement with the editing activity of LeuRS, the wild type and complemented strain but not the editing-deficient mutant grew in 2.4 mM L-norvaline (**FIGURE. 4.1A**). In fact, L-norvaline challenge resulted in a loss of viable bacteria, congruent with the toxicity from misfolded proteins. Unexpectedly, the growth of EPT^{R} LeuRS^{D436H} mutant recovered at later timepoints. We hypothesized that L-norvaline might degrade over time and repeated the experiment where 2.4 mM L-norvaline was supplemented each day to create a steady-state (4XSS). Again, however, the EPT^{R} LeuRS^{D436H} mutant grew after day three (**FIGURE. 4.1A**). To confirm resistance to L-norvaline, aliquots of the EPT^{R} LeuRS^{D436H} mutant grown without L-norvaline and in 4XSS were taken to measure the MIC_{90} of L-norvaline using the REMA method. Indeed, the EPT^{R} LeuRS^{D436H} 4XSS strain had a MIC_{90} > 40 mM while the original strain grown without L-norvaline maintained a MIC_{90} of 0.2 mM.

Since *M. abscessus* was shown to have inducible resistance to macrolides,[28,43] we asked whether L-norvaline resistance was inducible or acquired. We previously showed that inducible macrolide resistance in *M. abscessus* can be repressed after passaging the culture in drug-free media for six days.[33] Aliquots of the EPT^{R} LeuRS^{D436H} grown in L-norvaline-free or 4XSS conditions on day five were passaged for six days in L-norvaline-free media. The MIC_{90} to L-norvaline, epetraborole, and amikacin were determined using REMA. We showed that L-norvaline resistance is not inducible since passaging the culture in L-norvaline-free media did not change the MIC_{90} (**FIGURE. 4.1A**). Alternatively, L-norvaline resistance could arise from a LeuRS^{D436H} reversion where the population regains editing activity but becomes susceptible to epetraborole. Refuting this possibility, we observed resistance to epetraborole in both strains with MIC_{90} > 0.05 mM (**FIGURE. 4.1A**). Lastly, L-norvaline resistance was not the result of a multi-drug resistant phenotype as evidenced with sensitivity to control drug amikacin.

To further characterize the new mutant resistant to both epetraborole and L-norvaline, we challenged *M. abscessus* ATCC 19977, *M. abscessus* EPT^R $LeuRS^{D436H}$, and *M. abscessus* EPT^R Nva^R 4XSS with 0.5 mM branched-chain amino acids (BCAAs) in Sauton's minimal media and fit their growth to an exponential plateau regression (**FIGURE. 4.1B**). As controls, *M. abscessus* ATCC 19977 grew in L-norvaline while *M. abscessus* EPT^R $LeuRS^{D436H}$ failed to grow. Like the wild type strain, the growth of *M. abscessus* EPT^R Nva^R 4XSS was not impeded by 0.5 mM L-norvaline. From the exponential fit, we extracted the maximum growth plateau (Y_M) and growth rate (μ). Quantitatively, we observed that L-norvaline impairs both the maximum growth and growth rate of an editing deficient strain like *M. abscessus* EPT^R $LeuRS^{D436H}$ but that *M. abscessus* EPT^R Nva^R 4XSS regained a normal growth rate with a lower plateau (**FIGURE. 4.1C**). Similar results were obtained when the experiments were repeated in nutrient rich 7H9 media (**FIGURE. S4.1**).

Growth in 0.5 mM BCAAs was repeated on solid media using 7H10 base and 100 μM amikacin as control. We observed similar results where only *M. abscessus* EPT^R $LeuRS^{D436H}$ failed to grow on 0.5 mM L-norvaline while amikacin inhibited all strains (**FIGURE. 4.1D**). These results (*i*) confirmed L-norvaline resistance and (*ii*) suggested a novel mechanism of L-norvaline resistance has been acquired by *M. abscessus* that is editing independent.

4.5.2 Membrane hydrophobicity does not drive L-norvaline resistance

Mycobacteria are recognized for their unusually hydrophobic membrane with long-chain $C_{60\text{-}90}$ mycolic acids. In 1990, Jarlier and Nikaido measured that the permeability of small nutrients and antibiotics was 10,000x lower across the cell envelope of *M. abscessus* than in *E. coli.*[30] Later in 1994, Jarlier and Nikaido repeated the permeability measurements with amino acids across the cell envelope of different mycobacteria and concluded that *M. abscessus* was less permeable to amino acids than *M. tuberculosis*.[29] It has also been established that the cell wall synergizes with the internal resistome that includes efflux pumps and drug modifying enzymes to limit the effect of toxic compounds.[6]

To examine whether the *M. abscessus* EPT^R Nva^R 4XSS mutant has a modified cell envelope, we measured the hydrophobicity via the uptake of Congo red dye. Strains were streaked onto 7H10 plates with 10% (v/v) OADC and 140 μM Congo red and incubated at 37 °C for five days (**FIGURE. 4.2A**). *M. abscessus* ATCC 19977 strains with the smooth morphotype (S) or rough morphotype (R) were used as representative hydrophilic and hydrophobic membranes, respectively. The rough morphotype contains a mutation in *mmpL4b*, which prevents the transport of glycopeptidolipids across the membrane and creates a uniform hydrophobicity across the cell envelope unlike the smooth morphotype that has clusters of hydrophobic domains.[44] Gross visualization of the colonies indicated that both the parental EPT^R LeuRS^{D436H} and EPT^R Nva^R 4XSS strains had a smooth morphotype which favors pink colonies with red borders while the rough morphotype colonies were red (**FIGURE. 4.2A**). Congo red dye retained in the membrane was extracted with DMSO and quantified at 488nm. We observed a significant increase in retained Congo red dye in *M. abscessus* R compared to S, however there was no significant change in dye retained in EPT^R Nva^R 4XSS relative to the parental strain EPT^R LeuRS^{D436H} (**FIGURE. 4.2B**). These results suggest that the cell membrane of *M. abscessus* EPT^R Nva^R 4XSS has not undergone morphotype switching that could decrease the permeability of L-norvaline.

4.5.3 L-Norvaline resistance is not mediated by efflux pump activity

Unlike the well-characterized multi-drug efflux system AcrAB-TolC of *E. coli* that facilitates efflux of xenobiotics, MmpL proteins export endogenous lipophilic molecules.[12,13] Besides being involved in the architecture of the cell envelope however, some MmpL proteins were shown to be antimycobacterial drug efflux pumps. Most notably, this was demonstrated for the recently approved drug bedaquiline.[14,45] We speculated that the large number of efflux pumps in *M. abscessus* might contribute to L-norvaline resistance. To measure efflux pump activity, we used an ethidium bromide (EtBr) accumulation assay previously used in *M. abscessus* and *M. tuberculosis* to assess drug resistance.[46,47] Initially, EtBr has limited fluorescence in aqueous solution but becomes appreciably fluorescent when intercalated with dsDNA.[48] The fluorescence (Ex/Em 525/600) of intracellular EtBr was measured over 2 hours in wild type *M. abscessus* incubated with serial dilutions of EtBr (**FIGURE. 4.3A**). Fluorescence time curves were fit with an exponential plateau regression to determine the fluorescence at equilibrium (F_{eq}) and generate a dose-response curve (**FIGURE. 4.3A** *inset*). Since EtBr fluorescence is balanced by influx and

efflux and that the *M. abscessus* EPT^{R} Nva^{R} 4XSS mutant has a similar membrane hydrophobicity to the parental strain (**FIGURE. 4.2**), we postulated that any difference observed could be attributed to efflux activity.

The fluorescence of intracellular EtBr was measured in wild type, EPT^{R} LeuRS^{D436H}, and EPT^{R} Nva^{R} 4XSS strains of *M. abscessus* at 6.25 μM EtBr. ATCC 19977 S and R morphotypes were used as controls. MmpL4b is non-functional in the rough morphotype, which resulted in impaired efflux and greater accumulation of EtBr (**FIGURE. 4.3B**). Although we measured a statistically significant difference in EtBr accumulation in the S morphotype compared to the R morphotype, the difference in F_{eq} between EPT^{R} Nva^{R} 4XSS and the parental strain was not statistically significant (**FIGURE. 4.3B**). Next, we repeated the EtBr accumulation assay with verapamil and CCCP as efflux pump inhibitors.[49] Using 0.5 mM verapamil and 25 μM CCCP, we measured a statistically significant increase in the F_{eq} for all strains except *M. abscessus* R with CCCP (**FIGURE. 4.3B and C**). To determine the effect size of verapamil and CCCP on efflux pump inhibition, ΔF_{eq} ($F_{drug} - F_{drug\ free}$) was compared between EPT^{R} Nva^{R} 4XSS and the parental strain (**FIGURE. 4.3D**). Verapamil and CCCP had similar efficacies against EPT^{R} Nva^{R} 4XSS and the parental strain, which suggests that both strains have comparable efflux phenotypes.

4.5.4 α-IPMS^{A555V} variant participates in L-norvaline resistance

To identify the putative mutation(s) underlying L-norvaline resistance, gDNA was extracted from *M. abscessus* EPT^{R} LeuRS^{D436H} as the parental strain and two *M. abscessus* EPT^{R} Nva^{R} 4XSS mutants for WGS. All strains sequenced retained the C to G transversion at position 1306 in *leuS* that translates into LeuRS^{D436H}, which confirmed that resistance was not acquired through a D436H reversion as shown with the MIC to epetraborole (**FIGURE. 4.1A**). When compared to the parental strain, both EPT^{R} Nva^{R} 4XSS mutants sequenced had a unique C to T transition at position 1664 in *leuA* (MAB_0337c) and T to C transition at position 44 in *tRNA*$^{Leu(GAG)}$ (MAB_t5031c). *leuA* codes for α-isopropylmalate synthase (α-IPMS) which catalyzes the carboxymethylation of 2-oxoisovalerate using acetyl-CoA to produce α-isopropylmalate as the first step in the L-leucine biosynthetic pathway. *tRNA*$^{Leu(GAG)}$ is one of five encoded tRNA^{Leu} isoacceptors in *M. abscessus*.

To determine which variant gene is responsible for the L-norvaline resistant phenotype, wild type and mutant *leuA* and *tRNA*$^{Leu(GAG)}$ were cloned with 250bp upstream to capture the nascent promoter into the integrative vector pMV306. These constructs, as well as an empty pMV306 vector (EV) were electroporated into *M. abscessus* EPT^{R} D436H. Next, we measured the bacterial viability of *M. abscessus* ATCC 19977, parental *M. abscessus* EPT^{R} D436H, complemented strains, and the natural double mutant *M. abscessus* EPT^{R} Nva^{R} 4XSS against L-norvaline, epetraborole, and amikacin. Only *M. abscessus* EPT^{R} D436H complemented with the mutant *leuA* but not the wild type *leuA* had increased resistance to L-norvaline (**FIGURE. S4.2A**). All strains of *M. abscessus* with LeuRS^{D436H} retained resistance to epetraborole and all strains were equally susceptible to amikacin (**FIGURE. S4.2B and C**). L-norvaline resistance was not observed when *M. abscessus* EPT^{R} D436H was complemented with wild type or mutant *tRNA*$^{Leu(GAG)}$ (**FIGURE. S4.2D-F**).

To corroborate the drug susceptibility results, we monitored the growth of *M. abscessus* ATCC 19977, *M. abscessus* EPT^{R} D436H, the *leuA* complemented strains and *M. abscessus* EPT^{R} Nva^{R} 4XSS in Sauton's minimal media with 0.5 mM BCAAs. Complementing *M. abscessus* EPT^{R} D436H with the mutant variant of *leuA* nearly completely restored the growth in 0.5 mM L-norvaline relative to L-norvaline-free media while *M. abscessus* EPT^{R} D436H with wild type *leuA* or *M. abscessus* EPT^{R} D436H still exhibited reduced growth (**FIGURE. 4.4A and FIGURE. S4.3**). These results suggest that α-IPMS^{A555V} alone is sufficient to impart the L-norvaline resistant phenotype while the role of tRNA$^{Leu(GAG)T44C}$ is yet to be determined.

Previously, we showed that in the absence of LeuRS editing activity, L-norvaline becomes misaminoacylated and incorporated into proteins at sites coding for L-leucine.[33] Therefore, we hypothesized that the *M. abscessus* EPT^{R} Nva^{R} 4XSS mutant would be lacking high levels of norvalinated proteins after L-norvaline challenge. Cell lysates were collected from *M. abscessus* ATCC 19977, *M. abscessus* EPT^{R} D436H, complemented strains, and *M. abscessus* EPT^{R} Nva^{R} 4XSS after 24 hours of growth in Sauton's minimal media with 0.5 mM L-norvaline and analyzed by reverse-phase HPLC/MS. Principal component analysis (PCA) of cell lysate proteomes identified three proteomic clusters among the five strains with PC1 and PC2 accounting for 91%

and 5% of variance, respectively (**FIGURE. 4.4B and FIGURE. S4.4A**). Cluster 1 is the naturally L-norvaline resistant strain ATCC 19977, cluster 2 is the L-norvaline sensitive strain *M. abscessus* EPT^R D436H and its complement with wild type α-$IPMS^{WT}$, and cluster 3 is the novel L-norvaline resistant strain *M. abscessus* EPT^R Nva^R 4XSS and the complement with α-$IPMS^{A555V}$. The clusters were separated based on GroEL abundance in PC1 with a small contribution from Acyl-CoA dehydrogenase FadE abundance in PC2 (**FIGURE. 4.4B and FIGURE. S4.4B**). Proteins with L-norvaline residues were identified by filtering for L-leucine residues missing the 14 Da methylene group absent on L-norvaline. As expected from the PCA results, *M. abscessus* ATCC 19977 maintained preferential incorporation of L-leucine while the editing-deficient strain *M. abscessus* EPT^R D436H had a significant increase in norvaline misincorporation (**FIGURE. 4.4C and FIGURE. S4.5A**). *M. abscessus* EPT^R Nva^R 4XSS reduced the median level of norvaline misincorporation significantly despite lacking LeuRS editing activity (**FIGURE. 4.4C and FIGURE. S4.5A**). A decrease in median norvalination was also observed in the strain complemented with mutant *leuA* while the decrease observed with wild type *leuA* was not statistically significant (**FIGURE. 4.4C**) We also measured the level of L-norvaline in the culture supernatants after 24 hours of exposure and found no evidence of L-norvaline degradation or modification (**FIGURE. S4.5B**). To measure the overall bacterial stress response to L-norvaline challenge, we compared the proteomes of *M. abscessus* EPT^R D436H, complemented strains, and *M. abscessus* EPT^R Nva^R 4XSS to the ATCC 19977 reference strain. Higher levels of L-norvaline incorporation resulted in 134 statistically significant differentially expressed proteins (DEPs) (**FIGURE. 4.4D**). While *M. abscessus* EPT^R D436H had elevated levels of heat shock proteins and Clp proteases relative to the ATCC 19977 strain, we observed a significantly attenuated stress response in *M. abscessus* EPT^R Nva^R 4XSS with 10 DEPs and in *M. abscessus* EPT^R D436H complemented with α-$IPMS^{A555V}$ with 28 DEPs (**FIGURE. 4.4D**).

4.5.5 α-$IPMS^{A555V}$ mutation located in allosteric site

To understand how the α-$IPMS^{A555V}$ substitution results in minimal norvaline misincorporation across the proteome, we modelled α-$IPMS_{Mabs}$ onto the experimentally determined structure of α-$IPMS_{Mtb}$ using Swiss-Model.[50] The current understanding is that the catalytic and regulatory domains are separated by a flexible hinge domain to accommodate conformational changes resulting from L-leucine bound in the allosteric site to elicit negative feedback inhibition.[50] As a

control, we compared the experimental structure of α-IPMS$_{Mtb}$ (PDB 3FIG) to the α-IPMS$_{Mtb}$ structure generated with Swiss-Model. We generated a homodimeric structure (QMEAN 0.87 ± 0.05) that was predicted to have the N-terminal catalytic $(\alpha/\beta)_8$ TIM barrel domain, a linker, and C-terminal regulatory domain with the βββα architecture (**FIGURE. S4.6A**). Next, we compared the overlaid structures of Swiss-Model generated α-IPMS$_{Mtb}$ and α-IPMS$_{Mabs}$ and observed substantial structural overlap with rmsd of 0.119 Å. From these results, we inferred homology between α-IPMS$_{Mtb}$ and α-IPMS$_{Mabs}$ and used the modelled α-IPMS$_{Mabs}$ structure to hypothesize the effect of α-IPMS^{A555V} substitution identified in *M. abscessus* EPT^R Nva^R 4XSS.

The experimentally determined structure of α-IPMS$_{Mtb}$ was solved as a homodimer with an N-terminal catalytic domain and a C-terminal regulatory domain (PDB 3FIG and 3HPZ). The regulatory domains contain two symmetrical pockets at the dimer interface with loops in an open conformation when unbound to L-leucine (PDB 3HPZ and **FIGURE. 4.5B**)[50] However, the loop adopts a closed conformation when L-leucine is bound in the hydrophobic pocket of the regulatory domain (PDB 3FIG, **FIGURE. 4.5C**)[50] The A555V substitution identified from WGS in *M. abscessus* EPT^R Nva^R 4XSS is located on this loop (**FIGURE. 4.5C**). We modelled the A555V substitution on α-IPMS$_{Mabs}$ and observed a deviation > 4σ from the ideal angle with D557 and S554 was identified as a rotamer outlier. Taken together with the additional electron density from A555V next to the side chain of L546, we hypothesized that A555V would prevent the loop from adopting a closed conformation when bound by L-leucine and disrupt the allosteric feedback inhibition.

4.5.6 Overproduction of L-leucine competitively inhibits norvaline

To understand the mechanism of L-norvaline resistance in the absence of LeuRS editing activity, we hypothesized that the mutation in α-IPMS would disrupt the equilibrium of the L-leucine biosynthetic pathway and confer abnormal L-leucine production through loss of allosteric regulation in α-IPMS (**FIGURE. 4.5D**). To test this hypothesis, we grew *M. abscessus* ATCC 19977, *M. abscessus* EPT^R D436H, complemented strains, and *M. abscessus* EPT^R Nva^R 4XSS in Sauton's minimal media and measured the concentration BCAAs in the culture filtrate using HPLC/MS. Indeed, *M. abscessus* strains that harbored α-IPMS^{A555V} produced higher concentrations of L-leucine relative to the ATCC 19977 reference strain while L-isoleucine

concentrations were unaffected (**FIGURE. 4.5E**). L-Valine concentrations, however, were significantly reduced in strains that produced excess L-leucine (**FIGURE. 4.5E**).

Next, we examined the rescue effect of L-leucine by growing *M. abscessus* EPT^R D436H in 0.5 mM L-norvaline with increasing L-leucine concentrations. After day 7 of growth, we observed that a 1:1 ratio of L-leucine:L-norvaine restored the growth of *M. abscessus* EPT^R D436H to 50% of the L-norvaline free conditions while L-isoleucine and L-valine had no rescue effect (**FIGURE. 4.5F**). Growth was completely restored with a 4:1 ratio of L-leucine:L-norvaline (**FIGURE. 4.5F**). Motivated by these results, we asked whether L-leucine could act as a competitive inhibitor to L-norvaline. We measured the initial growth rates from time 0 to 24 hours in serial dilutions of L-norvaline to generate a dose-response curve (**FIGURE. 4.5G**). These measurements were repeated with increasing L-leucine concentrations and required higher concentrations of norvaline to generate saturating growth inhibition. To obtain IC_{50} values for L-norvaline, the saturating curves were fit to four parameter dose-response regression. Next, IC_{50} values were used to estimate an apparent inhibition constant of L-norvaline, K_i, and an apparent substrate constant of L-leucine, K_s, using the Cheng-Prusoff theorem for competitive inhibition (**FIGURE. 4.5H**). The linear relationship between the IC_{50} of L-norvaline and the concentration of L-leucine suggests competitive inhibition between the amino acids where L-norvaline (K_i = 9 μM) is 3-4x more potent as an inhibitor than L-leucine (K_s = 32 μM) is as a substrate (**FIGURE. 4.5H**).

4.6 DISCUSSION

M. abscessus infections are notoriously difficult to treat largely due to its enhanced toolkit of antimicrobial resistance mechanisms.[6] We show that *M. abscessus* can subvert the toxicity of L-norvaline, a non-canonical amino acid shown to be an experimental adjunct agent with epetraborole.[33] Classically, *M. abscessus* is naturally resistant to L-norvaline because of the editing domain on LeuRS. LeuRS provides pre-transfer editing before the incorrect amino acid is transferred to $tRNA^{Leu}$ or post-transfer editing when the erroneous amino acid has already been transferred onto $tRNA^{Leu}$.[51] In both mechanisms, the editing activity is mediated by a conserved aspartic acid residue, D436. Our results demonstrate that a *M. abscessus* mutant can limit the incorrect use of L-norvaline in the absence of pre and post-transfer editing activity. We show that

resistance is not the result of modified membrane hydrophobicity nor increased efflux activity but stems from the loss of allosteric regulation to overproduce a metabolite and out compete the inhibitor.

The A555V mutation was found in α-IPMS, the first enzyme involved in L-leucine biosynthesis.[52] α-IPMS was previously shown to have a regulatory domain with a hydrophobic pocket where L-leucine binds with the carboxylate positioned between the partial positively charged N-terminal ends of two helices, similar to the bound chloride ion in the absence of L-leucine.[50] From the crystal structure, it was hypothesized to be a regulatory domain for feedback inhibition. Later, kinetic evidence emerged that supported intradomain communication by an allosteric mechanism with L-leucine.[53] This regulation had also been postulated in yeast where mutations were identified in the C-terminal regulatory domain that resulted in insensitivity to L-leucine feedback inhibition.[54] Other non-regulatory yeast α-IPMS mutants became resistant to Zn^{2+}-mediated inactivation by Coenzyme-A. This was later supported with kinetic data examining the effects of divalent cations on the activity of α-IPMS as a mechanism to control energy metabolism.[54,55]

In line with the allosteric mechanism of α-IPMS, our results show an increased production of L-leucine by strains harboring α-IPMS^{A555V} relative to the ATCC 19977 reference strain. We also tested L-isoleucine and observed no difference in BCAA production. L-Valine, however, was significantly reduced in strains that produced more L-leucine. Although BCAAs share structural features, the biosynthetic pathway for L-isoleucine is dependent on L-threonine production while L-leucine/L-valine are synthesized from pyruvate. The α-IPMS negative feedback mechanism is believed to be specific for L-leucine since α-IPMS catalyzes the first committed step of L-leucine biosynthesis after diverging away from the shared L-valine pathway.[52] L-Isoleucine and L-valine have also been shown to be allosteric inhibitors and activators, respectively, but towards the L-isoleucine chokepoint enzyme, threonine deaminase.[56] Unregulated α-IPMS activity that shifts the equilibrium of 2-oxoisovalerate could explain why L-valine production was stunted in strains with α-IPMS^{A555V}.

M. abscessus grown under L-norvaline challenge showed that α-IPMS^{A555V} strains were more resistant to growth inhibition than α-IPMS^{WT} strains. Strains with LeuRS^{D436H} fail to grow in 0.5

mM L-norvaline however, the natural double mutant *M. abscessus* EPT^R Nva^R 4XSS and *M. abscessus* EPT^R D436H complemented with α-IPMS^{A555V} had comparable growth to *M. abscessus* ATCC 19977. These data suggest that overproduction of L-leucine from the mutation in the loop capping the allosteric site results in resistance to L-norvaline. The growth kinetics of *M. abscessus* EPT^R D436H in L-norvaline and L-leucine shed light on the requirement for additional L-leucine and the biochemical basis for L-leucine rescue. By measuring initial growth rates, we observed increasing L-norvaline IC_{50} values proportional to the L-leucine concentration, suggestive of competitive inhibition with $K_i = 9$ μM for L-norvaline and $K_s = 32$ μM for L-leucine. The inhibition and substrate constants lend additional support to the L-leucine rescue experiments where nearly 4x more L-leucine was required to fully restore the growth of *M. abscessus* EPT^R D436H in 0.5 mM L-norvaline.

Corroborating our previous results, strains that produced higher levels of L-leucine and misincorporated less L-norvaline in the proteome had superior growth output in L-norvaline. The proteomic profiles suggest that strains with α-IPMS^{A555V} can tolerate L-norvaline as the unfolded protein response observed in *M. abscessus* EPT^R D436H, characterized by heat shock proteins and chaperonins in the dominant principal component 1, is diminished in *M. abscessus* EPT^R Nva^R 4XSS. The variance in principal component 2 is attributed to an increased FadE abundance in strains that failed to grow during norvaline challenge. FadE is predicted to be an acyl-CoA dehydrogenase involved in fatty acid β-oxidation, which suggests that *M. abscessus* EPT^R D436H and α-IPMS^{wt} complemented strain upregulated fatty acid β-oxidation to meet the metabolic requirements of misfolded protein proteolysis. Overall, the proteome of strains with α-IPMS^{A555V} clustered separately from *M. abscessus* EPT^R D436H and appeared more similar to the ATCC 19977 reference strain.

In conclusion, we describe a novel mechanism of resistance to an antimicrobial agent in the multidrug resistant pathogen, *M. abscessus*. Systematic evaluation revealed that resistance is not mediated by a cell wall phenotype nor multidrug efflux pumps, but through the loss of allosteric feedback inhibition in a biosynthetic enzyme. *M. abscessus* expressing α-IPMS^{A555V} gained the ability to produce excess quantities of L-leucine, with no deleterious consequences, to out compete L-norvaline from being used as a LeuRS substrate. This mutation reduces norvalination of the

proteome and toxicity associated with misfolded proteins. Our work here provides evidence for a mechanism of antimicrobial resistance in *M. abscessus* where an orthogonal mutation in an allosteric chokepoint enzyme rescues the bacteria through dysregulation of BCAA metabolism that limits the clinical applicability of L-norvaline as an adjuvant to benzoxaborole LeuRS inhibitors.

4.7 ACKNOWLEDGEMENTS

We thank the entire team at the Clinical Proteomics Platform of the Research Institute of the McGill University Health Centre [RI-MUHC] for discussion and their assistance with mass spectrometry. Work in MAB's laboratory was supported by a CIHR operating grant and by a doctoral studentship from the Fonds de recherche du Québec to JRS.

4.8 AUTHORS' CONTRIBUTIONS

JRS was involved in all aspects including experiment design, data collection and analysis, and preparation of the manuscript. CC independently the generated double mutants and provided replicates of the Congo red and efflux assays. LT collected proteomics and metabolomics data. OS created a pipeline for variant calling on whole-genome sequencing data. MAB provided supervision and was involved in the preparation of the manuscript.

4.9 REFERENCES

1. World Health Organisation. WHO Strategic Priorities on Antimicrobial Resistance.
2. Murray, C. J. et al. Global burden of bacterial antimicrobial resistance in 2019: a systematic analysis. *Lancet* **399**, 629–655 (2022).
3. Cassini, A. et al. Attributable deaths and disability-adjusted life-years caused by infections with antibiotic-resistant bacteria in the EU and the European Economic Area in 2015: a population-level modelling analysis. *Lancet Infect. Dis.* **19**, 56–66 (2019).
4. Geneva: World Health Organization. *Prioritization of Pathogens to Guide Discovery, Research and Development of New Antibiotics for Drug-Resistant Bacterial Infections, Including Tuberculosis*. *WHO/EMP/IAU/2017.12* https://www.researchgate.net/publication/269107473_What_is_governance/link/548173090cf22525dcb61443/download%0Ahttp://www.econ.upf.edu/~reynal/Civil wars_12December2010.pdf%0Ahttps://think-asia.org/handle/11540/8282%0Ahttps://www.jstor.org/stable/41857625 (2017).
5. Burki, T. K. Tuberculosis missing from WHO bacteria list. *Lancet Respir. Med.* **5**, 252 (2017).
6. Nessar, R., Cambau, E., Reyrat, J. M., Murray, A. & Gicquel, B. Mycobacterium abscessus: A new antibiotic nightmare. *J. Antimicrob. Chemother.* **67**, 810–818 (2012).
7. Pasipanodya, J. G. et al. Systematic review and meta-analyses of the effect of chemotherapy on pulmonary mycobacterium abscessus outcomes and disease recurrence. *Antimicrob. Agents Chemother.* **61**, (2017).
8. Dartois, V. & Dick, T. Drug development challenges in nontuberculous mycobacterial lung disease: TB to the rescue. *J. Exp. Med.* **219**, e20220445 (2022).
9. Quang, N. T. & Jang, J. Current Molecular Therapeutic Agents and Drug Candidates for Mycobacterium abscessus. *Front. Pharmacol.* **12**, (2021).
10. Dartois, V. A. & Rubin, E. J. Anti-tuberculosis treatment strategies and drug development: challenges and priorities. *Nat. Rev. Microbiol.* (2022).
11. Wallace, R. J. et al. Genetic basis for clarithromycin resistance among isolates of Mycobacterium chelonae and Mycobacterium abscessus. *Antimicrob. Agents Chemother.* **40**, 1676–1681 (1996).
12. Xu, Z., Meshcheryakov, V. A., Poce, G. & Chng, S. S. MmpL3 is the flippase for mycolic

acids in mycobacteria. *Proc. Natl. Acad. Sci. U. S. A.* **114**, 7993–7998 (2017).

13. Viljoen, A. et al. The diverse family of MmpL transporters in mycobacteria: from regulation to antimicrobial developments. *Mol. Microbiol.* **104**, 889–904 (2017).
14. Gutiérrez, A. V., Richard, M., Roquet-Banères, F., Viljoen, A. & Kremer, L. The TetR-family transcription factor MAB_2299c regulates the expression of two distinct MmpS-MmpL efflux pumps involved in cross-resistance to clofazimine and bedaquiline in Mycobacterium abscessus. *Antimicrob. Agents Chemother.* (2019) doi:10.1128/aac.01000-19.
15. Adams, R. A. et al. Rifamycin antibiotics and the mechanisms of their failure. *J. Antibiot. (Tokyo).* **74**, 786–798 (2021).
16. Schäfle, D. et al. Rifabutin is inactivated by mycobacterium abscessus arr. *Antimicrob. Agents Chemother.* **65**, (2021).
17. Ung, K. L., Alsarraf, H. M. A. B., Olieric, V., Kremer, L. & Blaise, M. Crystal structure of the aminoglycosides N-acetyltransferase Eis2 from Mycobacterium abscessus. *FEBS J.* **286**, 4342–4355 (2019).
18. Luthra, S., Rominski, A. & Sander, P. The Role of Antibiotic-Target-Modifying and Antibiotic-Modifying Enzymes in Mycobacterium abscessus Drug Resistance. *Front. Microbiol.* **9**, (2018).
19. Hamad, B. The antibiotics market. *Nat. Rev. Drug Discov.* **9**, 675–676 (2010).
20. Story-Roller, E., Maggioncalda, E. C., Cohen, K. A. & Lamichhane, G. Mycobacterium abscessus and β-Lactams: Emerging Insights and Potential Opportunities. *Front. Microbiol.* **9**, (2018).
21. Ramírez, A. et al. Biochemical characterization of β-lactamases from mycobacterium abscessus complex and genetic environment of the β-lactamase-encoding gene. *Microb. Drug Resist.* **23**, 294–300 (2017).
22. Burian, J. et al. The mycobacterial transcriptional regulator whiB7 gene links redox homeostasis and intrinsic antibiotic resistance. *J. Biol. Chem.* **287**, 299–310 (2012).
23. Burian, J. et al. The mycobacterial antibiotic resistance determinant WhiB7 acts as a transcriptional activator by binding the primary sigma factor SigA (RpoV). *Nucleic Acids Res.* **41**, 10062–10076 (2013).
24. Hurst-Hess, K., Rudra, P. & Ghosh, P. Mycobacterium abscessus WhiB7 regulates a

species-specific repertoire of genes to confer extreme antibiotic resistance. *Antimicrob. Agents Chemother.* **61**, (2017).

25. Nash, K. A., Brown-Elliott, A. B. & Wallace, R. J. A Novel gene, erm(41), confers inducible macrolide resistance to clinical isolates of mycobacterium abscessus but is absent from mycobacterium chelonae. *Antimicrob. Agents Chemother.* **53**, 1367–1376 (2009).
26. Richard, M., Gutiérrez, A. V. & Kremer, L. Dissecting erm(41)-mediated macrolide-inducible resistance in mycobacterium abscessus. *Antimicrob. Agents Chemother.* **64**, (2020).
27. Pryjma, M., Burian, J., Kuchinski, K. & Thompson, C. J. Antagonism between Front-Line Antibiotics Clarithromycin and Amikacin in the Treatment of Mycobacterium abscessus Infections is Mediated by the whiB7 gene. *Antimicrob. Agents Chemother.* **61**, (2017).
28. Svetlov, M. S. et al. Structure of Erm-modified 70S ribosome reveals the mechanism of macrolide resistance. *Nat. Chem. Biol.* **17**, 412–420 (2021).
29. Jarlier, V. & Nikaido, H. Mycobacterial cell wall: Structure and role in natural resistance to antibiotics. *FEMS Microbiol. Lett.* **123**, 11–18 (1994).
30. Jarlier, V. & Nikaido, H. Permeability barrier to hydrophilic solutes in Mycobacterium chelonei. *J. Bacteriol.* **172**, 1418–1423 (1990).
31. Brennan, P. J. Structure, function, and biogenesis of the cell wall of Mycobacterium tuberculosis. *Tuberculosis* **83**, 91–97 (2003).
32. Brennan, P. J. & Nikaido, H. The envelope of mycobacteria. *Annu. Rev. Biochem.* **64**, 29–63 (1995).
33. Sullivan, J. R. et al. Efficacy of epetraborole against Mycobacterium abscessus is increased with norvaline. *PLoS Pathog.* **17**, 1–28 (2021).
34. O'Dwyer, K. et al. Bacterial resistance to leucyl-tRNA synthetase inhibitor GSK2251052 develops during treatment of complicated urinary tract infections. *Antimicrob. Agents Chemother.* **59**, 289–298 (2015).
35. Lambert, R. J. W. & Pearson, J. Susceptibility testing: Accurate and reproducible minimum inhibitory concentration (MIC) and non-inhibitory concentration (NIC) values. *J. Appl. Microbiol.* **88**, 784–790 (2000).
36. Bolger, A. M., Lohse, M. & Usadel, B. Trimmomatic: A flexible trimmer for Illumina

sequence data. *Bioinformatics* **30**, 2114–2120 (2014).

37. Li, H. Aligning sequence reads, clone sequences and assembly contigs with BWA-MEM. *arXiv* 1–3 (2013).
38. Li, H. et al. The Sequence Alignment/Map format and SAMtools. *Bioinformatics* **25**, 2078–2079 (2009).
39. Garrison, E. & Marth, G. Haplotype-based variant detection from short-read sequencing. *arXiv* (2012).
40. Rabodoarivelo, M. S. et al. Optimizing of a protein extraction method for Mycobacterium tuberculosis proteome analysis using mass spectrometry. *J. Microbiol. Methods* **131**, 144–147 (2016).
41. Waterhouse, A. et al. SWISS-MODEL: Homology modelling of protein structures and complexes. *Nucleic Acids Res.* **46**, W296–W303 (2018).
42. Studer, G. et al. QMEANDisCo—distance constraints applied on model quality estimation. *Bioinformatics* **36**, 1765–1771 (2020).
43. Nash, K. A., Brown-Elliott, A. B. & Wallace, R. J. A Novel gene, erm(41), confers inducible macrolide resistance to clinical isolates of mycobacterium abscessus but is absent from mycobacterium chelonae. *Antimicrob. Agents Chemother.* **53**, 1367–1376 (2009).
44. Viljoen, A., Viela, F., Kremer, L. & Dufrêne, Y. F. Fast chemical force microscopy demonstrates that glycopeptidolipids define nanodomains of varying hydrophobicity on mycobacteria. *Nanoscale Horizons* **5**, 944–953 (2020).
45. Hartkoorn, R. C., Uplekar, S. & Cole, S. T. Cross-resistance between clofazimine and bedaquiline through upregulation of mmpl5 in mycobacterium tuberculosis. *Antimicrob. Agents Chemother.* **58**, 2979–2981 (2014).
46. Machado, D. et al. Efflux activity differentially modulates the levels of isoniazid and rifampicin resistance among multidrug resistant and monoresistant Mycobacterium tuberculosis strains. *Antibiotics* **7**, 1–16 (2018).
47. Vianna, J. S. et al. The contribution of efflux pumps in mycobacterium abscessus complex resistance to clarithromycin. *Antibiotics* **8**, (2019).
48. Paixão, L. et al. Fluorometric determination of ethidium bromide efflux kinetics in Escherichia coli. *J. Biol. Eng.* **3**, (2009).

49. Pule, C. M. et al. Efflux pump inhibitors: Targeting mycobacterial efflux systems to enhance TB therapy. *J. Antimicrob. Chemother.* **71**, 17–26 (2016).
50. Koon, N., Squire, C. J. & Baker, E. N. Crystal structure of LeuA from Mycobacterium tuberculosis, a key enzyme in leucine biosynthesis. *Proc. Natl. Acad. Sci. U. S. A.* **101**, 8295–8300 (2004).
51. Lincecum, T. L. et al. Structural and mechanistic basis of pre- and posttransfer editing by leucyl-tRNA synthetase. *Mol. Cell* **11**, 951–963 (2003).
52. Amorim Franco, T. M. & Blanchard, J. S. Bacterial Branched-Chain Amino Acid Biosynthesis: Structures, Mechanisms, and Drugability. *Biochemistry* **56**, 5849–5865 (2017).
53. de Carvalho, L. P. S., Frantom, P. A., Argyrou, A. & Blanchard, J. S. Kinetic evidence for interdomain communication in the allosteric regulation of α-isopropylmalate synthase from Mycobacterium tuberculosis. *Biochemistry* **48**, 1996–2004 (2009).
54. Cavalieri, D. et al. Trifluoroleucine resistance and regulation of α-isopropyl malate synthase in Saccharomyces cerevisiae. *Mol. Gen. Genet.* **261**, 152–160 (1999).
55. de Carvalho, L. P. S. & Blanchard, J. S. Kinetic analysis of the effects of monovalent cations and divalent metals on the activity of Mycobacterium tuberculosis α-isopropylmalate synthase. *Arch. Biochem. Biophys.* **451**, 141–148 (2006).
56. Eisenstein, E. Allostertic Regulation of Biosynthetic Threonine Deaminase from Escherichia coli: Effects of Isoleucine and Valine on Active-Site Ligand Binding and Catalysis. *Arch. Biochem. Biophys.* **316**, 311–318 (1995).
57. Koon, N., Squire, C. J. & Baker, E. N. *Crystal Structure of Leucine-bound LeuA from Mycobacterium tuberculosis*. (2008) doi:10.2210/pdb3fig/pdb.

4.10 FIGURES AND TABLES

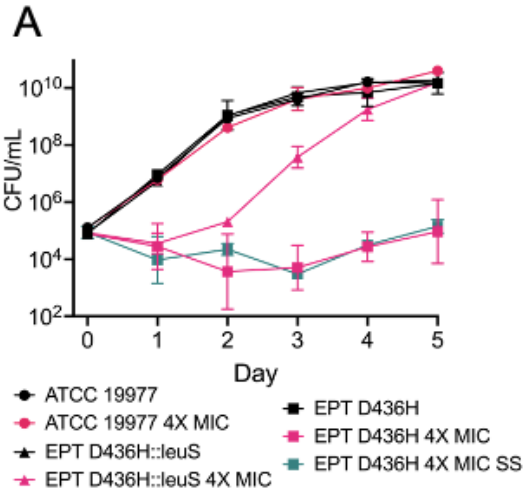

Strain	MIC_{90}			
	Day 5	+6 days passage		
	Nva (mM)	Nva (mM)	EPT (μM)	AMK (μM)
EPT D436H	0.2	0.2	>50	14
EPT D436H 4XSS	>40	>40	>50	15

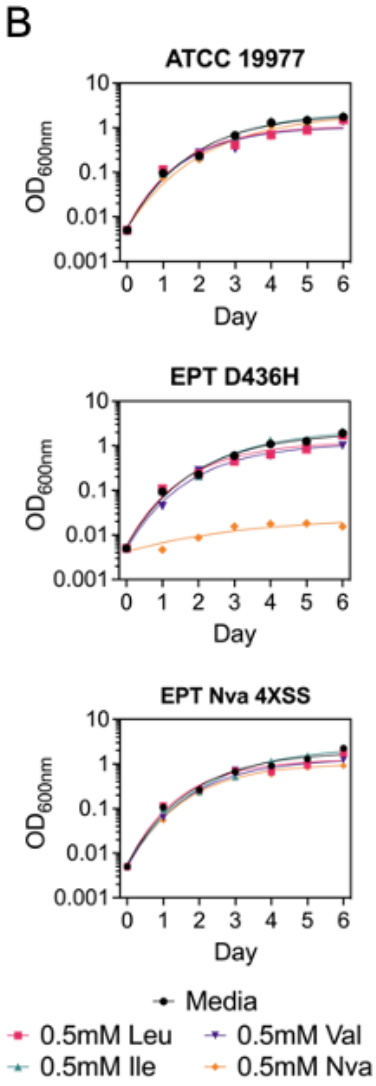

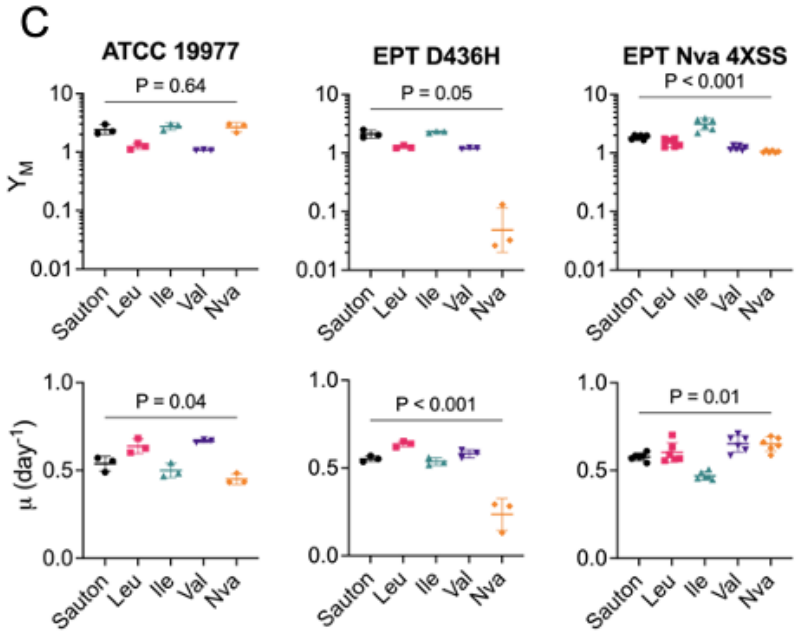

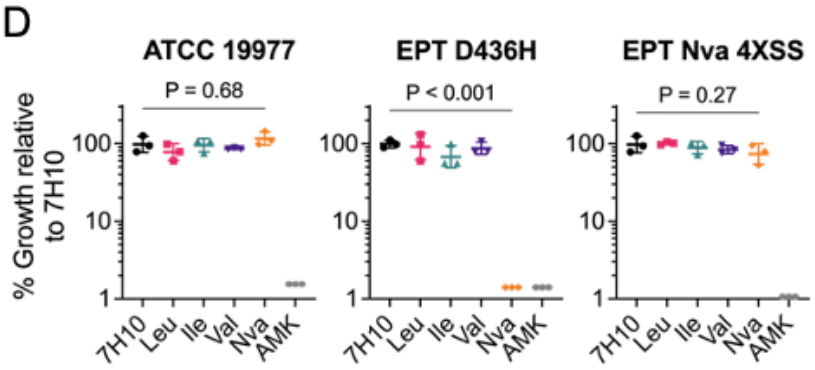

FIGURE 4.1. Editing-deficient norvaline resistance in *M. abscessus*. **A** Left, *M. abscessus* ATCC 19977, EPT^R *M. abscessus* with $LeuRS^{D436H}$, and complement strain with wild type LeuRS were grown in media free of exogenous L-norvaline, 4X MIC_{90} (MIC_{90} = 0.6 mM) of the Nva^S /EPT^R *M. abscessus* D436H strain. Alternatively, *M. abscessus* D436H strains were grown in media free of exogenous L-norvaline, with an initial inoculum of 4X MIC_{90}, or media replenished with 4X MIC_{90} daily to establish a steady-state of L-norvaline (SS). Data represents mean ± SD from n = 2-5 independent experiments. Right, Aliquots of *M. abscessus* EPT^R D436H grown in L-norvaline free media (black squares) or L-norvaline at 4XSS (teal squares) from day 5 were used to determine the MIC_{90} of L-norvaline. Cultures were passaged for six days in L-norvaline free media before measuring the MIC_{90} for L-norvaline, and control drugs epetraborole and amikacin. **B** Growth curves of *M. abscessus* ATCC 19977, *M. abscessus* EPT^R D436H, and mutant with dual EPT^R and Nva^R resistance raised at 4XSS. Strains were grown statically in 96-well plates with nutrient limited Sauton media ± BCAAs and fit with exponential plateau regression. Data is representative of n = 3 independent experiments with mean ± SD. P values were obtained by one-way ANOVA with Dunnett's multiple comparisons test. **C** Comparison of maximum growth plateau (Y_M) and growth rates (μ) in Sauton media ± BCAAs. Data is mean ± SD from n = 3 independent replicates with *M. abscessus* EPT^R Nva^R 4XSS in biological duplicates. **D** Growth on solid 7H10 media ± BCAAs. 100 μM amikacin was used as control. Data is mean ± SD from n = 3 independent experiments. P values were obtained by one-way ANOVA with Dunnett's multiple comparisons test.

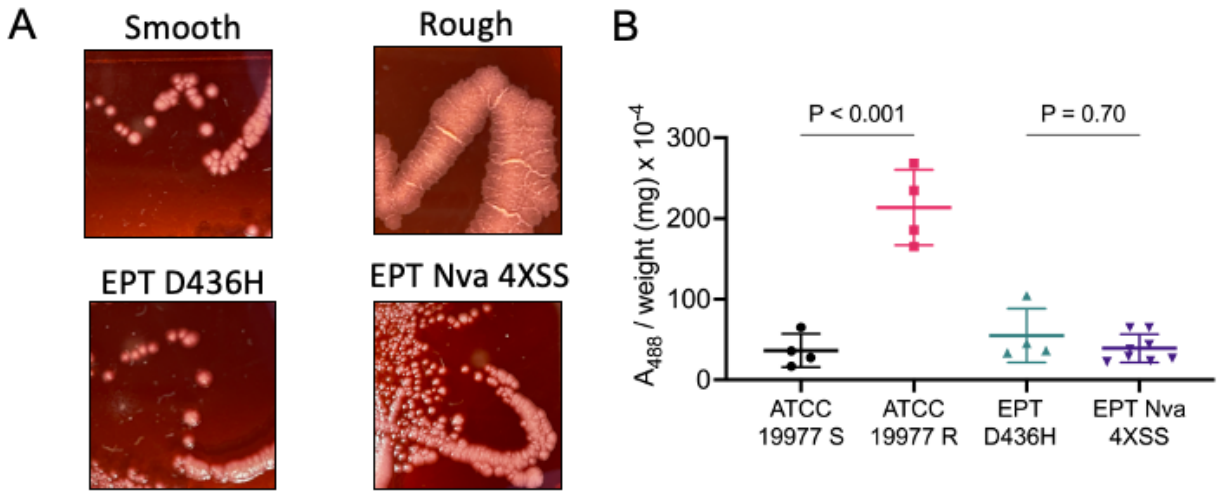

FIGURE 4.2. Membrane hydrophobicity of *M. abscessus*. A Colony morphology of ATCC 19977-S (smooth), ATCC 19977-R (rough), *M. abscessus* EPT^{R} D436H, and *M. abscessus* EPT^{R} Nva^{R} on 7H10 plates supplemented with 10% (v/v) OADC and Congo red at 140 µM. **B** Quantitative analysis of extracted Congo red dye retained in the membrane at A_{488nm}. Data represents mean ± SD of n = 4 independent experiments with *M. abscessus* EPT^{R} Nva^{R} 4XSS in biological duplicates. P values were obtained by one-way ANOVA with Tukey's multiple comparisons test.

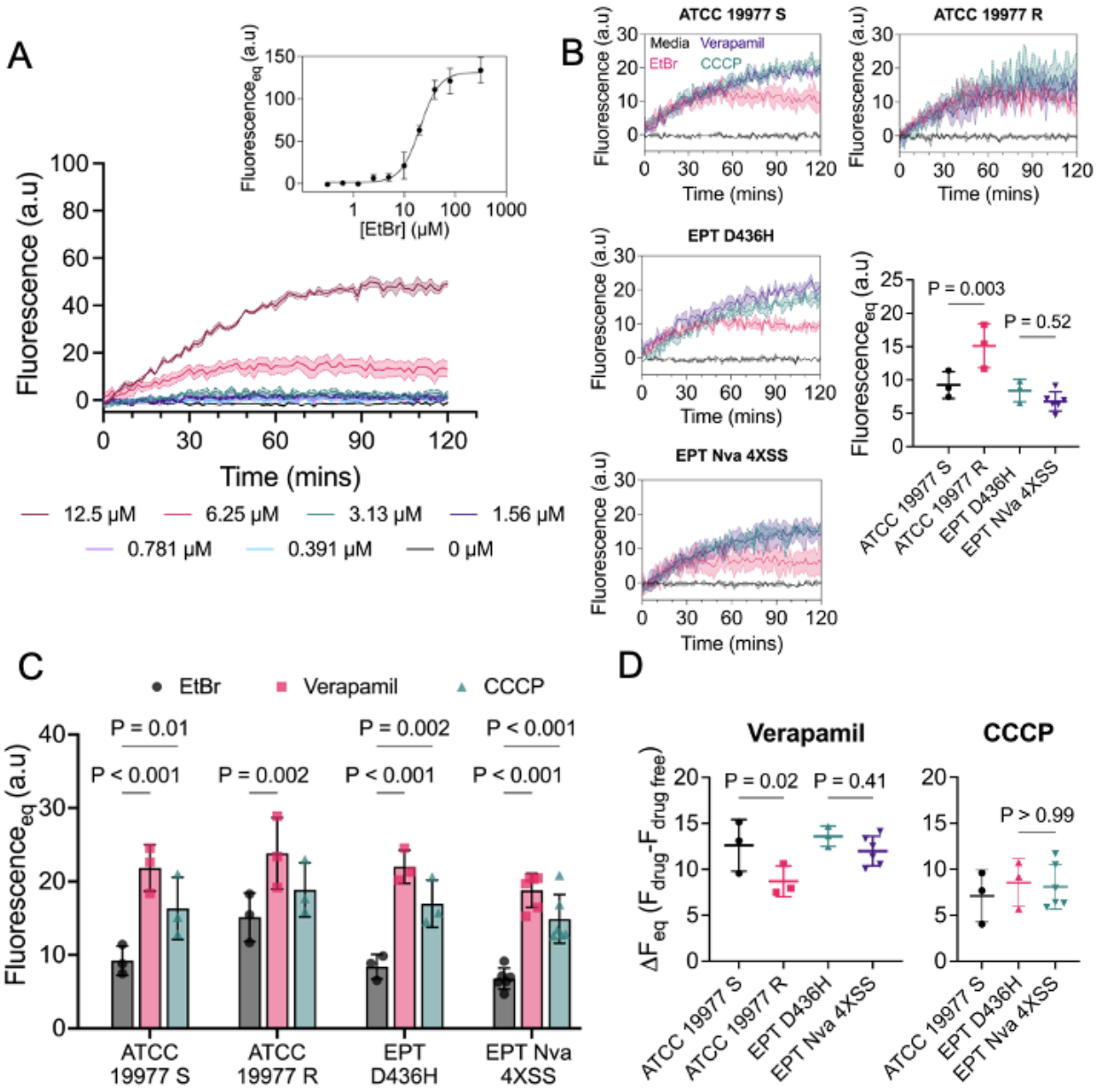

FIGURE 4.3. Efflux activity of *M. abscessus*. A Dose response curve of ethidium bromide (EtBr, Ex_{525nm}, Em_{600nm}) accumulation in *M. abscessus* ATCC 19977 S. **B** EtBr accumulation with 6.25 μM EtBr in ATCC 19977 S, ATCC 19977 R, *M. abscessus* EPT^R D436H, and *M. abscessus* EPT^R Nva^R 4XSS. 0.5 mM verapamil and 25 μM CCCP were used as efflux pump inhibitors in **B**. Data is mean ± SD of n = 3 independent replicates with *M. abscessus* EPT^R Nva^R 4XSS in biological duplicates. P values were obtained by one-way ANOVA with Sidak's multiple comparisons test. **C** Efflux pump inhibitors promote EtBr accumulation. Data is mean ± SD of n = 3 independent replicates with *M. abscessus* EPT^R Nva^R 4XSS in biological duplicates. P values were obtained by

two-way ANOVA with Dunnett's multiple comparisons test. **D** Quantification of efflux pump inhibitor effect. ATCC 19977 R was omitted from CCCP as the effect was not statistically significant. Data is mean ± SD of n = 3 independent replicates with *M. abscessus* EPT^R Nva^R 4XSS in biological duplicates. P values were obtained by one-way ANOVA with Sidak's multiple comparisons test.

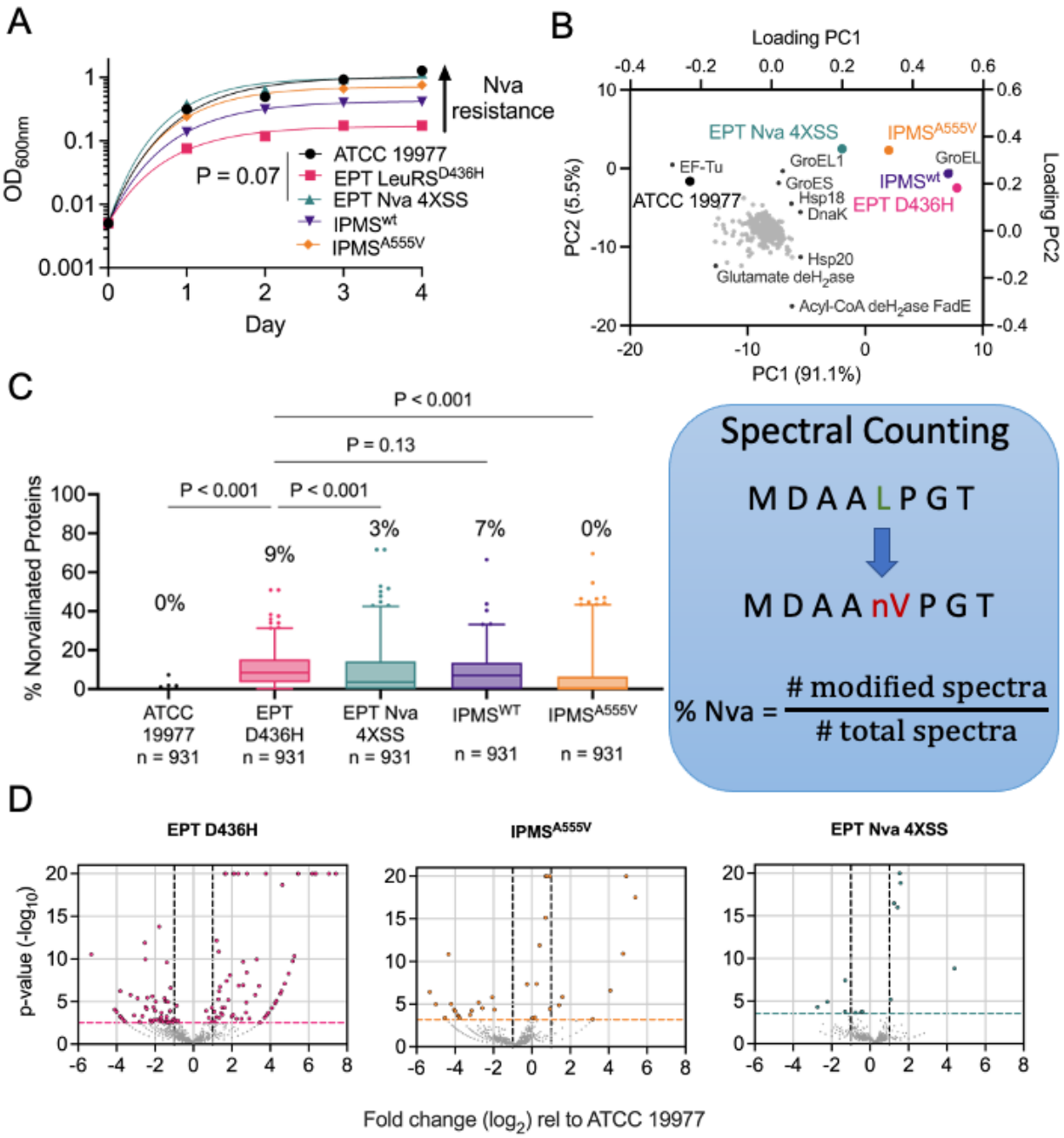

FIGURE 4.4. ***M. abscessus*** **EPT^R Nva^R mutant uses alternative mechanism to limit L-norvaline toxicity. A** Reference strain ATCC 19977 (black circles), EPT^R mutant LeuRS^{D436H} (pink squares), naturally raised EPT^R Nva^R mutant (green triangles), EPT^R mutant complemented with α-IPMS^{WT} (purple triangles) or α-IPMS^{A555V} (orange diamonds) grown in Sauton's minimal media with 0.5 mM L-norvaline and fit with exponential plateau regression. Data is representative of n = 3 independent experiments with mean ± SD of technical triplicates. P values were obtained by one-way ANOVA with Tukey's multiple comparisons test. **B** Principal component analysis of

cell lysate proteomes after 24 h of growth in Sauton's media with 0.5 mM L-norvaline. PC1 accounted for 90% of the variance, PC2 accounted for 5% of the variance. GroEL (MAB_0650) and Acyl-CoA dehydrogenase FadE (MAB_4437) had the greatest PC1 and PC2 coefficients, respectively. **C** Percentage of proteins with misincorporation of L-norvaline at leucine residues from cell lysates after 24 h of growth in Sauton's media with 0.5 mM L-norvaline. Data is median with IQR, whiskers represent 1-99 percentile from spectral counting. P values were obtained by Friedman test with Dunn's multiple comparisons test. **D** Volcano plots depict fold change (log_2) and p-value($-log_{10}$) for each protein relative to the ATCC 19977 reference strain.

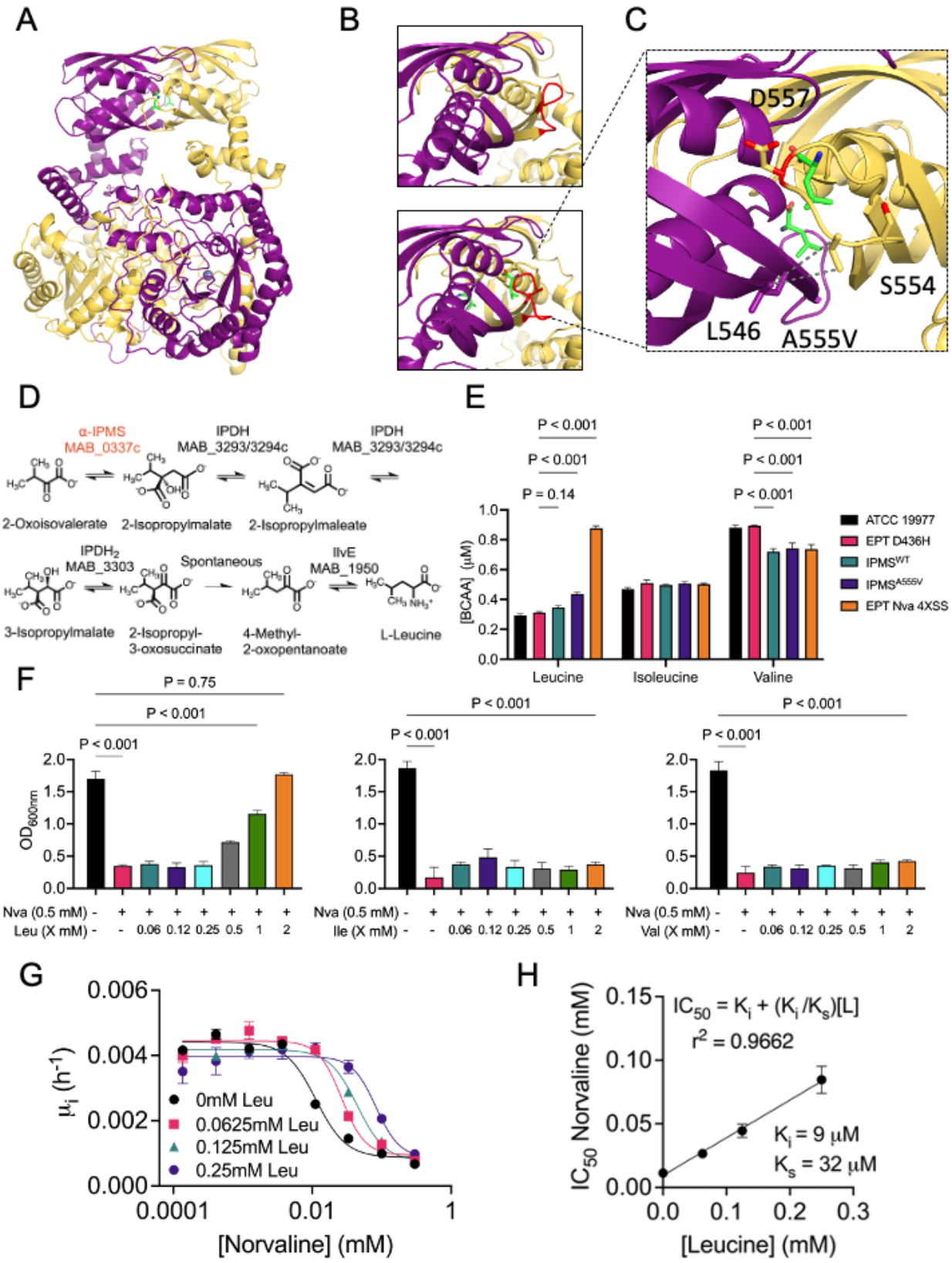
A
B
C
D557
S554
L546
A555V
D
α-IPMS
MAB_0337c
IPDH
MAB_3293/3294c
IPDH
MAB_3293/3294c
2-Oxoisovalerate
2-Isopropylmalate
2-Isopropylmaleate
IPDH2
MAB_3303
Spontaneous
IlvE
MAB_1950
3-Isopropylmalate
2-Isopropyl-
3-oxosuccinate
4-Methyl-
2-oxopentanoate
L-Leucine
E
P < 0.001
P < 0.001
P = 0.14
P < 0.001
P < 0.001
P < 0.001
[BCAA] (μM)
Leucine
Isoleucine
Valine
ATCC 19977
EPT D436H
IPMS^WT
IPMS^A555V
EPT Nva 4XSS
F
P = 0.75
P < 0.001
P < 0.001
P < 0.001
P < 0.001
P < 0.001
P < 0.001
OD600nm
Nva (0.5 mM)
Leu (X mM)
Ile (X mM)
Val (X mM)
0.06 0.12 0.25 0.5 1 2
G
μi (h-1)
0mM Leu
0.0625mM Leu
0.125mM Leu
0.25mM Leu
[Norvaline] (mM)
H
IC50 = Ki + (Ki /Ks)[L]
r2 = 0.9662
Ki = 9 μM
Ks = 32 μM
IC50 Norvaline (mM)
[Leucine] (mM)

FIGURE 4.5. α-IPMS^{A555V} variant overproduces L-leucine to outcompete L-norvaline. A Swiss-Model structure of α-IPMS$_{Mabs}$ from *M. tuberculosis* PDB 3FIG.[50] Monomers in yellow and purple, L-leucine in green, and Zn^{2+} as blue spheres. **B** (top) C-terminal regulatory domain without L-leucine bound in an open conformation (red loop). **B** (bottom) C-terminal regulatory domain with L-leucine bound in a closed conformation. **C** Effects of mutated A555V highlighted. **D** Pathway for L-leucine synthesis. **E** BCAA concentrations in culture filtrates of reference strain ATCC 19977, EPT^R mutant LeuRS^{D436H}, EPT^R mutant complemented with IPMS^{WT} or IPMS^{A555V}, and naturally raised EPT^R Nva^R mutant grown in Sauton's minimal media. Data is mean ± SD of n = 3 biological replicates. P values were obtained by one-way ANOVA with Tukey's multiple comparisons test. **F** *M. abscessus* EPT^R D436H strain grown in Sauton's minimal media ± L-norvaline and serial dilutions of L-leucine, L-isoleucine, or L-valine. Data is mean ± SD of n = 3 independent experiments. P values were obtained by one-way ANOVA with Tukey's multiple comparisons test. **G** Initial growth rates (first 24 h) of *M. abscessus* EPT^R D436H in L-norvaline supplemented with L-leucine. **H** L-norvaline inhibition fit to a model of competitive inhibition. K_i is the inhibition constant of L-norvaline. K_s is the substrate constant for L-leucine. L is the concentration of L-leucine.

4.11 SUPPLEMENTARY MATERIAL

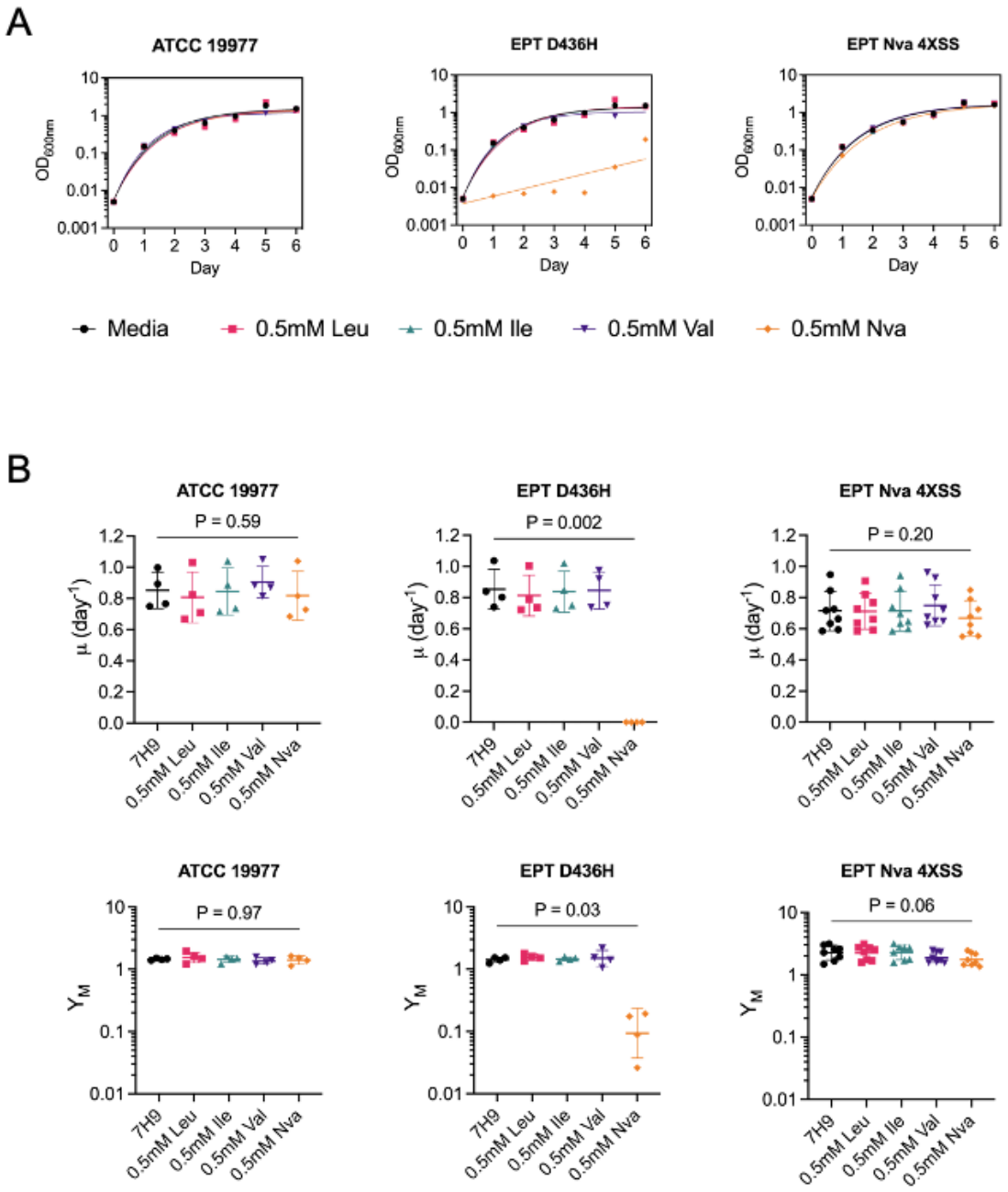

FIGURE S4.1. Growth characteristics of *M. abscessus* EPT^R Nva^R mutant in 7H9 media. A Growth curves of *M. abscessus* ATCC 19977, EPT^R *M. abscessus* with LeuRS^{D436H}, and a mutant with dual EPT^R and Nva^R resistance raised at 4X MIC_{90} SS. Strains were grown statically in 96-well plates with nutrient rich 7H9 media ± BCAAs and fit with exponential plateau regression. Data is representative of n = 4 independent experiments with mean ± SD of technical triplicates.

B Comparison of growth rates (μ) and maximum growth plateau (Y_M) in 7H9 media ± BCAAs. Data is mean ± SD from n = 4-8 independent replicates. P values were obtained by one-way ANOVA with Dunnett's multiple comparisons test.

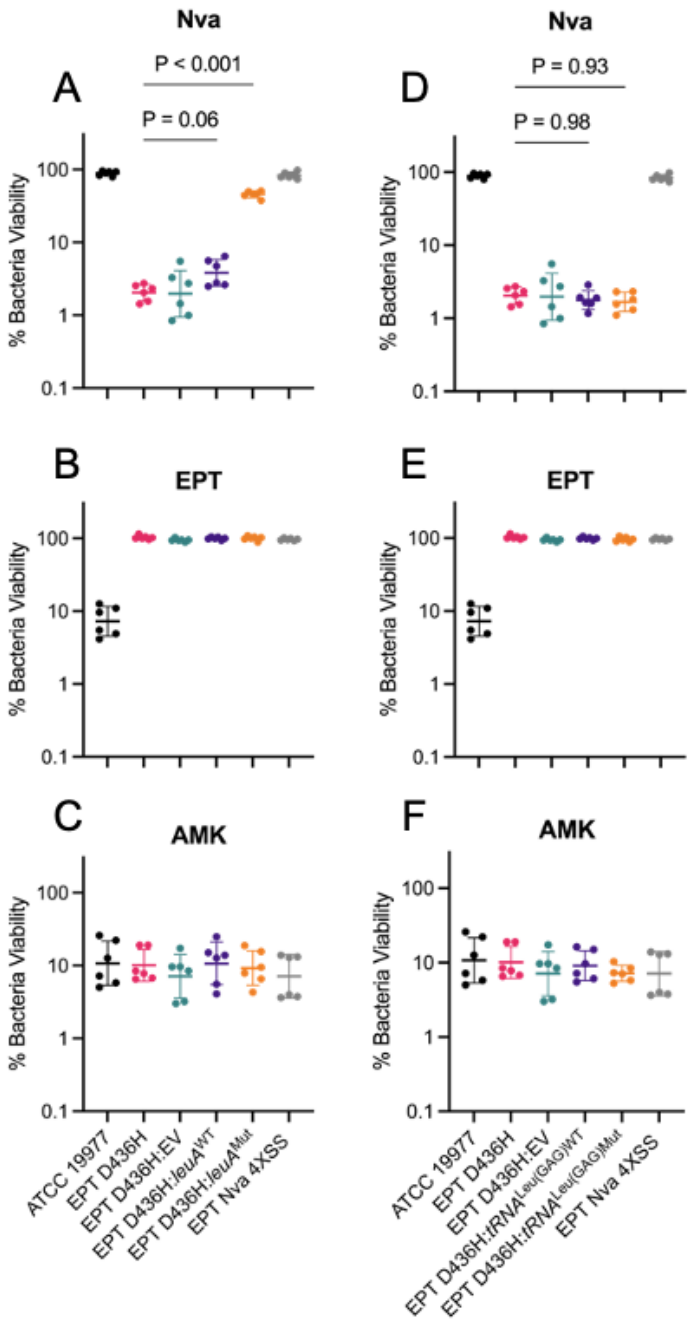

FIGURE S4.2. *M. abscessus* EPT^{R} D436H strain complemented with putative *leuA* or *tRNA*$^{Leu(GAG)}$ resistance variants. Reference strain ATCC 19977 (black), EPT^{R} mutant LeuRS^{D436H} (pink), EPT^{R} mutant complemented with empty pMV306 vector (green), EPT^{R} mutant complemented with wild type *leuA* (purple) or complemented with mutant *leuA* (orange), and naturally raised EPT^{R} Nva^{R} mutant (grey) grown in **A** L-norvaline, **B** epetraborole, or **C** amikacin. Alternatively, the EPT^{R} LeuRS^{D436H} mutant was complemented with wild type *tRNA*^{leu} (purple) or

mutant *tRNA*^{leu} (orange) and grown in **D** L-norvaline, **E** epetraborole, **F** amikacin. Data is n = 2 independent experiments with mean ± SD of technical triplicates. P values were obtained by one-way ANOVA with Tukey's multiple comparisons test.

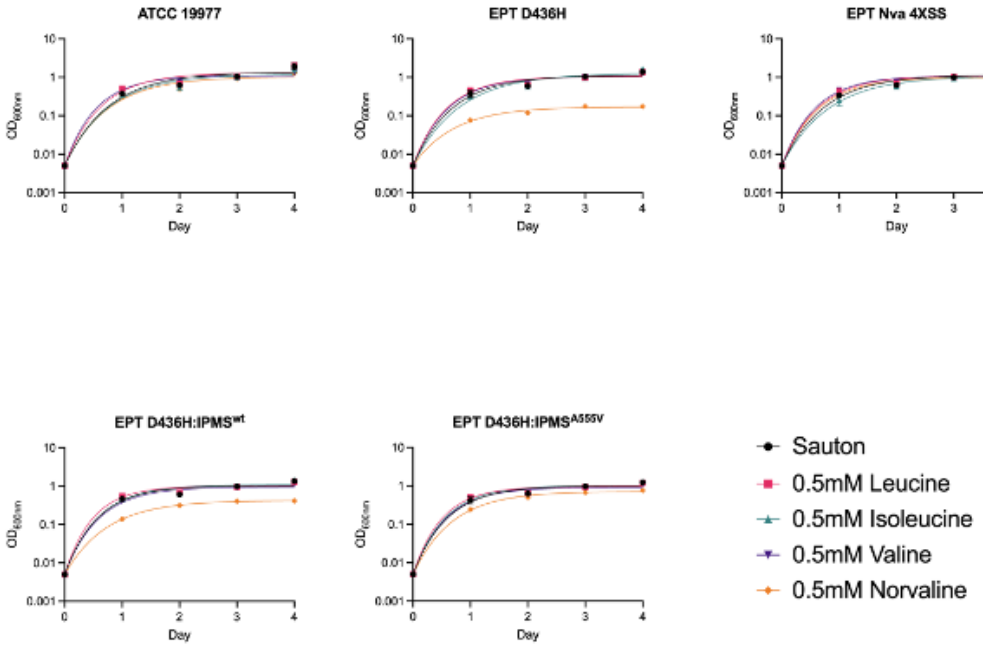

FIGURE S4.3. Growth curves of *M. abscessus* complemented with *leuA*. Reference strain ATCC 19977, EPT^{R} mutant LeuRS^{D436H}, EPT^{R} mutant complemented with wild type *leuA* or mutant *leuA*, and naturally raised EPT^{R} Nva^{R} mutant were grown statically in Sauton's minimal media ± L-leucine (pink squares), L-isoleucine (green triangles), L-valine (purple inverted triangles), or L-norvaline (orange diamonds) at 0.5 mM and fit with exponential plateau regression. Data is representative of n = 3 independent experiments with mean ± SD of technical triplicates.

A

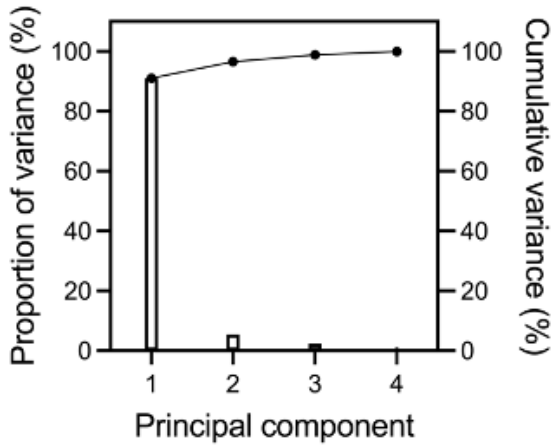

B

Strain	GroEL (MAB_0650)			Acyl-CoA deH$_2$ase (MAB_4437)		
	Counts[a]	FC[b]	P-value[c]	Counts[a]	FC[b]	P-value[c]
ATCC 19977	584	1	n.d	40	1	n.d
EPT D436H	2943	5	<0.0001	277	6.9	<0.0001
IPMS^{WT}	3002	5.1	<0.0001	135	3.4	<0.0001
IPMS^{A555V}	1123	1.9	<0.0001	28	0.7	0.19
EPT Nva 4XSS	1695	2.9	<0.0001	40	1	0.25

[a]Quantitative spectral counts; [b]Fold change relative to ATCC 19977; [c]P-value from Fisher's exact test with Benjamini-Hochberg correction; n.d, not determined.

FIGURE S4.4. Proteomic analysis of *M. abscessus*. Cell lysates were extracted from *M. abscessus* ATCC 19977, *M. abscessus* EPT^R D436H, *M. abscessus* EPT^R Nva^R 4XSS, *M. abscessus* EPT^R D436H complemented with IPMS^{WT} or IPMS^{A555V} grown in Sauton's media with 0.5 mM L-norvaline for 24 hours. **A** Variance associated with each principal component. PC1 accounted for 90% of the variance, PC2 accounted for 5% of the variance. **B** Quantification of GroEL (largest PC1 coefficient) and Acyl-CoA dehydrogenase (largest PC2 coefficient) abundance.

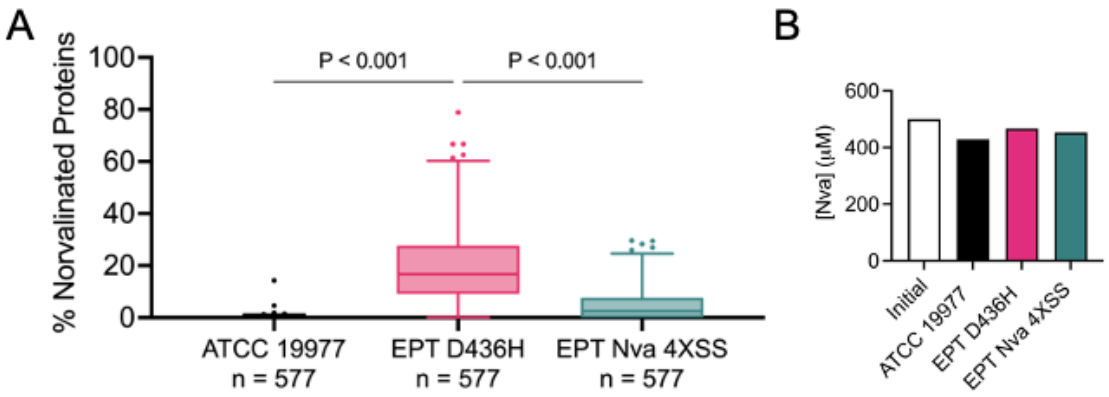

FIGURE S4.5. Norvalination of the *M. abscessus* proteome. A Percentage of proteins with misincorporation of L-norvaline at leucine residues from cell lysates after 24 h of growth in Sauton's media with 0.5 mM L-norvaline. Data is median with IQR, whiskers represent 1-99 percentile. P values were obtained by Friedman test with Dunn's multiple comparisons test. **B** Concentration of L-norvaline remaining in culture supernatants after 24 h L-norvaline challenge from **A**.

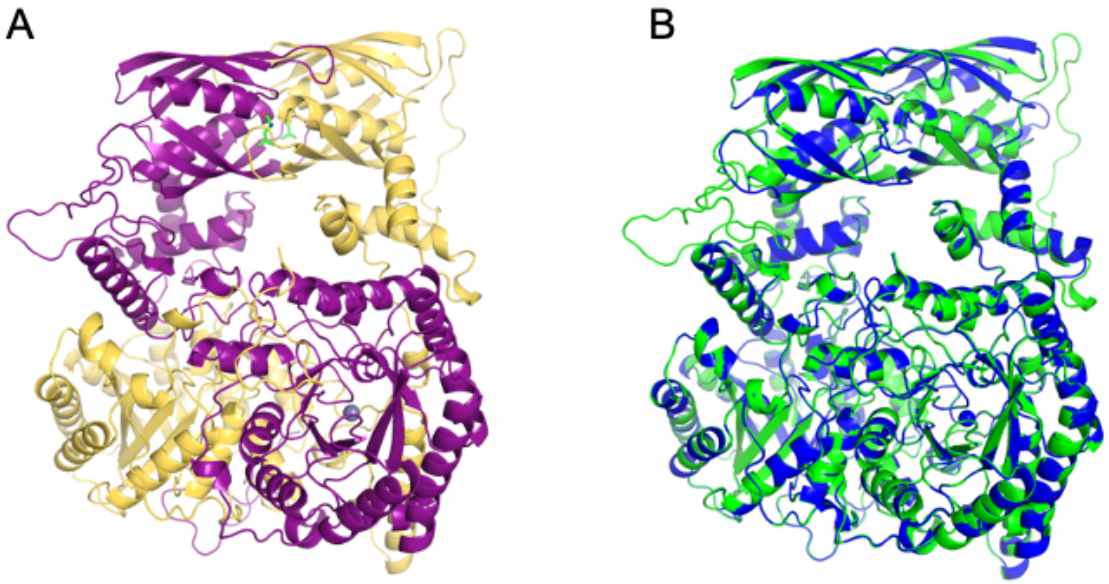

FIGURE S4.6. Predicting homology between α-IPMS$_{Mtb}$ and α-IPMS$_{Mabs}$. A α-IPMS$_{Mtb}$ model was generated using Swiss-Model and the experimentally determined structure PDB 3FIG with QMEAN global 0.87 ± 0.05.[41,42,57] **B** Overlay of α-IPMS$_{Mtb}$ (green) and Swiss-Model generated α-IPMS$_{Mabs}$ (blue) from PDB 3FIG with QMEAN global of 0.86 ± 0.05. Overlay generated rmsd of 0.199 Å.

CHAPTER 5

General Discussion

M. abscessus is an opportunistic pathogen that causes chronic pulmonary and skin and soft tissue infections.[1] This bacterium predominantly affects people with pre-existing lung conditions such as CF, chronic obstructive pulmonary disease, and bronchiectasis. Unlike TB where a positive culture demands isolation and treatment, diagnosing pulmonary *M. abscessus* infections can be challenging.[2] Many people can be colonized with *M. abscessus* but have no signs of disease and therefore, would not merit clinical intervention. Only with clinical symptoms, radiographic evidence, and speciation from a clinical isolate is a diagnosis made.[2] Current treatment regimens for pulmonary *M. abscessus* disease, however, are not adequate. A patient with CF and an *M. abscessus* pulmonary infection requires 3 months of intravenous amikacin, tigecycline, and imipenem and an oral macrolide.[3] For the following 14 months, the patient would receive an all-oral regimen of a macrolide, minocycline, moxifloxacin, and nebulized amikacin.[3] Currently, this is the standard of care for pulmonary *M. abscessus* infections with culture conversion rates of ≤ 50%. The field recognizes this problem and antibiotic drug discovery for *M. abscessus* is underway. Laboratories are discovering new chemistries against validated targets like InhA from the TB literature, repositioning rifamycins traditionally known to be active against *M. tuberculosis* but not *M. abscessus*, and identifying compounds for new cellular targets like MmpL3.[4–8] Our group joined these efforts and used the mainstay WCS method to carry out a drug discovery project for *M. abscessus*. The central goal of this thesis work was to screen new libraries against *M. abscessus* to find new compounds that could be added to the pipeline. This thesis describes two natural products and one synthetic molecule combined with an adjuvant as potential candidates for the *M. abscessus* pipeline.

5.1 MAIN FINDINGS

Drug discovery for *M. abscessus* has proven to be more challenging than for *M. tuberculosis*. Historically, WCS campaigns against *M. tuberculosis* achieve a hit rate of 0.3-1% while WCS against *M. abscessus*, on the other hand, may reach hit rates of 0.07-0.1%.[9] Therefore, the selection of libraries with appropriate chemical space is an important factor inherently linked to the success

of hit discovery. In order to achieve the best return on investment, we screened a library of natural products and three libraries of repurposed antimicrobials with drug-like properties. Natural products provide diversity in the chemical space and are a proven source of antibiotics as nearly two-thirds of clinically used antibiotics contain a natural product pharmacophore or semi-synthetic derivative.[10] Curated libraries of compounds with activity against other microorganisms relieve some of the uncertainty with novel synthetic libraries; most compounds have membrane permeable chemistry and specificity for a druggable target and non-specific cytotoxic molecules like detergents are filtered out.

In **Chapter 2**, we established our optimized screening conditions and detailed the natural product screening against *M. abscessus*. The reference strain of *M. abscessus* ATCC 19977 engineered with constitutive luminescence output was chosen for screening over standard readouts like optical density and other non-traditional readouts like cell viability and ATP production based on the correlation ($r^2 = 0.99$) between luminescence and bacterial burden, and a robust Z' factor (> 0.7). The natural product library was provided through a collaboration with Rolf Müller at the Helmholtz Institute of Pharmaceutical Science where his group provided expertise in natural product synthesis and characterization. The Müller group provided a pilot library of 517 compounds from myxobacteria, fungi, and plants. We identified two hits with scaffolds not currently in the *M. abscessus* pipeline, lysobactin and sorangicin A. Lysobactin (also known as katanosin B), like vancomycin, binds cell wall substrates rather than a defined biosynthetic target, which creates a high barrier to resistance that requires multiple genetic changes to remodel the cell envelope.[11] However, unlike vancomycin where resistance conferring alleles are circulating in the microbial community, resistance to lysobactin has not been identified. Sorangicin A is a known inhibitor of the validated RNA polymerase target in mycobacterial drug discovery but is structurally different than traditional RNA polymerase inhibitors like the rifamycins. Importantly for the patients in the CF community that receive corrector therapies, sorangicin A weakly induces drug metabolizing enzymes such as CYP3A4 that have been shown to be strongly induced by rifamycins and cause drug-drug interactions with the corrector therapy ivacaftor.[12] Both natural products displayed activity against multidrug resistant *M. abscessus* clinical isolates from CF patients in the Montreal region. Lysobactin and sorangicin A are novel scaffolds where more potent derivatives can be synthesized with novel formulations to improve oral bioavailability.

Despite the progress made with the natural products from **Chapter 2**, published in *Microbiology Spectrum* in November 2022, lysobactin and sorangicin A are still in the early discovery phase. Cystic Fibrosis Canada published a set of revised goals for research proposals making the call for pre-clinical candidates. With that goal in mind, we focused our efforts on libraries with repurposed drugs in **Chapter 3**. We screened a set of 172 compounds active against *M. tuberculosis* provided by GSK, and 800 general antimicrobials provided by Medicines for Malaria Venture (MMV). Ultimately, our three hits (hit rate 0.3 %) were identified in the Pandemic Response Box by MMV and no hits were obtained in the GSK box with compounds filtered for activity against *M. tuberculosis*. One hit had previously shown off target activity against the hERG K-channel and one had already been published for *M. abscessus*.[13,14] The remaining and most potent hit was epetraborole, a compound with the benzoxaborole pharmacophore, and at the time of these studies no group had shown interest in epetraborole for *M. abscessus*. Epetraborole is a known LeuRS inhibitor by binding in the editing site as opposed to the aminoacylation active that is observed with mupirocin and IleRS. Although no literature had described the activity of epetraborole for *M. abscessus*, GSK published a paper in 2016 discussing the potential of the benzoxaborole series for *M. tuberculosis*.[15] Throughout this work, we showed that, unlike clarithromycin, *M. abscessus* does not have inducible resistance to epetraborole and our epetraborole resistant mutants had mutations mapped to the editing site of LeuRS. The conservation of LeuRS as the target of epetraborole in *M. abscessus* was confirmed with CRISPRi knockdown of *leuS*, which generated hypomorphs that displayed hypersusceptibility to epetraborole. Through a collaboration with the group of Laurent Kremer à l'Université de Montpellier, we showed that epetraborole has a protective effect in zebrafish embryos against *M. abscessus* infection. The group of Martin Schmeing at McGill University crystallized the editing domain of LeuRS bound to EPT to help rationalize the effect of the LeuRS^{D436H} mutation we identified from whole-genome sequencing (WGS) of epetraborole resistant mutants.

While reading the literature on benzoxaboroles and tRNA synthetase inhibitors, we found a publication by GSK detailing the rapid onset of resistance to epetraborole during a failed phase II clinical trial for complicated urinary tract infections from *E. coli*.[16] These data raised the question: can we limit resistance to epetraborole and prolong its lifespan? Based on the crystal structure and

mutation of the universally conserved D436 residue, the epetraborole resistant strain of *M. abscessus* was believed to be editing deficient. The editing domain is hypothesized to safeguard against misaminoacylation of $tRNA^{Leu}$ with non-proteinogenic amino acids like norvaline. We showed that norvaline inhibited the growth of the epetraborole mutant and we found norvaline residues across the proteome. The proteomic signature suggested that protein norvalination triggers the unfolded protein response with abundant heat shock proteins and Clp proteases after norvaline challenge. Lastly, we showed that norvaline in combination with epetraborole limited *in vitro* resistance to epetraborole and improved the efficacy of epetraborole in the SCID mouse model of *M. abscessus* pulmonary infection. By the time our work in **Chapter 3** was published in *PLoS Pathogens* in October 2021, three other studies independently described the activity of benzoxaboroles as LeuRS inhibitors against *M. abscessus* between April 2021 and October 2021.[17–19] Two of these studies also identified mutations in the editing domain of LeuRS that resulted in resistance to epetraborole, however the D436H substitution was not identified.[17,18] The translation of norvaline as an adjuvant could be further supported if other editing deficient mutants were included in future experiments. Is the toxicity of norvaline reported in **Chapter 3** unique to editing deficient mutants that lost the universally conserved catalytic residue D436 or most editing deficient mutants susceptible to norvaline challenge?

The question asked in **Chapter 4** arose from an unexpected result from a seemingly trivial experiment. Initially, we asked the question does norvaline challenge of the editing deficient mutant lead to a bactericidal phenotype, which could help support our unfolded protein response mechanism for norvaline-mediated growth inhibition. After generating kill kinetic curves of different genetic backgrounds of *M. abscessus*, we observed a 1-3 $\log_{10}$ decrease in CFU of the editing deficient strain depending on the concentration of norvaline over 3 days. Unexpectedly, the editing deficient strain grew on day 4 and had become resistant to norvaline. After controlling for degradation of norvaline in the media and the reversion of *M. abscessus* $LeuRS^{D436H}$ to *M. abscessus* $LeuRS^{H436D}$, we excluded smooth-to-rough morphotype switching and increased efflux activity as possible mechanisms of norvaline resistance. WGS identified a mutation in *leuA,* which encodes α-IPMS. This mutation limited norvalination across the proteome and the proteomic signature resembled that of wild type bacteria. We mapped the A555V mutation to an allosteric binding site for leucine on α-IPMS. Since α-IPMS is an enzyme located at the branchpoint of

valine and leucine biosynthesis, we hypothesized that this mutation could interfere with leucine binding and disrupt the negative feedback loop on α-IPMS. Consistent with this hypothesis, metabolomics data revealed an increase in leucine production and a decrease in valine production while having no effect on isoleucine biosynthesis. Mechanistically, we worked out that leucine, when given together with norvaline, antagonizes the growth inhibition phenotype of norvaline through competitive inhibition as a substrate for $LeuRS^{D436H}$. This work is being submitted to PNAS, November 2022.

5.2 LIMITATIONS OF THE WORK

5.2.1 Screening Conditions

The work in this thesis demonstrates the continued success of WCS by identifying compounds with antimicrobial activity while retaining cell permeable chemistry.[20,21] Unlike target-based approaches where the focus of the assay is centred on the target of interest, whole cell approaches bias the screen with the media used in the assay. Ultimately, the metabolism of bacteria is linked to the growth media. The composition of media, such as different carbon sources, presence or absence of detergents, and pH can have an impact on gene expression and thus, determine which drug targets may or may not be available for modulation. Even if the target is produced under standard laboratory conditions, the carbon sources available *in vivo* might be different. This was emphasized in 2010 when potent growth inhibitors of glycerol metabolism in *M. tuberculosis* were identified but failed to achieve any reduction in bacterial load in the mouse model.[22] *M. tuberculosis* primarily relies on cholesterol and other lipids as its primary carbon source *ex vivo* in macrophages and *in vivo*.[23] One option to lower the attrition rate of compounds along the drug discovery pipeline is to perform the primary screen under various conditions to capture as much diversity as possible. A similar approach is being used for drug combination testing for *M. tuberculosis* where synergy/antagonism pairs are measured in a systematic manner under diverse biological conditions.[24,25]

One caveat to this approach is to include biologically relevant conditions. Because *M. abscessus* can cause pulmonary infections in patients with CF, the environment of the CF lung might be the most appropriate for identifying compounds with *in vivo* activity against *M. abscessus*. For the *P. aeruginosa* community, synthesis cystic fibrosis media (SCFM) was created to mimic the nutrients

available *in vivo*. Sputum from CF patients was analyzed my mass spectrometry to define individual components. SCFM consists of a variety of salts, 18/20 common amino acids as well as ornithine, glucose and lactose as carbon sources, and iron sulfate.[26] SCFM could be a valuable media to include in future screening programs.

5.2.2 Epetraborole resistance in *M. abscessus* vs *M. tuberculosis*

Often the limitation of WCS is identifying the target of interest. By raising mutants against epetraborole and using the power of WGS, we mapped mutations to LeuRS. Nevertheless, the phenotype of epetraborole activity on *M. abscessus* is growth inhibition and could result from polypharmacology in the complex cellular milieu. The rate of resistance to epetraborole in *M. abscessus* is ~ 10^{-9} while resistance to epetraborole is seen much more readily in *M. tuberculosis* with rates ~ 10^{-5}. The low rate of resistance for *M. abscessus* might suggest a second binding pocket on LeuRS or another target that was missed with WGS. Alternatively, one can speculate that leucine metabolism is regulated differently between *M. abscessus* and *M. tuberculosis*. One of the few studies that reported the production of norvaline was from leucine regulatory mutants in *Serratia marcescens*.[27] It could be hypothesized that if *M. abscessus* produces non-negligeable quantities of norvaline, resistance to epetraborole through mutations in the editing domain might have a higher genetic barrier.

5.2.3 SCID Mouse Model

The *in vivo* antimycobacterial activity of epetraborole was assessed in a severe combined immunodeficiency (SCID) mouse model in a NOD.CB17 background (NOD.CB17-Prkdc^{scid}/NCrCrl). This mouse model has impaired B and T lymphocytes from the SCID background as well as impaired natural killer cell functions from the non-obese diabetic background. The SCID model was first shown to be a valuable pre-clinical model for testing drug efficacy against *M. abscessus* with bedaquiline and clofazimine in 2015 and later with rifabutin in 2020.[28,29] The short duration of the SCID model used for our epetraborole study is not a model of *M. abscessus* pulmonary disease. The SCID model can help address the questions: does the antibiotic reach the site of infection and does the drug maintain activity in a complex environment?

Additional genetic backgrounds suitable for assessment of drug efficacy are the nude and granulocyte-macrophage colony-stimulating factor (GM-CSF$^{-/-}$) knockout mice where a stable and chronic infection can be observed up to 40 days.[28,30] Other immunodeficient mouse models like the beige, interferon-gamma KO (IFN-$\gamma^{-/-}$), and tumor necrosis factor receptor KO (TNFR$^{-/-}$) can clear or start to clear *M. abscessus* from the lungs by day 40 making it difficult to differentiate the decrease in bacterial burden from natural clearance or from the intervention.[28] To modify the SCID, nude, and GM-CSF$^{-/-}$ mouse models into models of disease pathogenesis, the infections should persist for 40 days to develop necrotizing and non-necrotizing granuloma-like lesions and foamy macrophages—hallmarks of pulmonary disease in patients with NTM infections.[28,31,32]

As an alternative to genetically modified immunodeficient mouse backgrounds, a corticosteroid mouse model for pulmonary *M. abscessus* infection has been developed to evaluate drug efficacy and regimens. C3HeB/FeJ mice are susceptible to *M. tuberculosis* infection but clear *M. abscessus*. To limit the clearance of *M. abscessus*, C3HeB/FeJ mice received 5 mg/kg dexamethasone daily one week prior and two weeks post *M. abscessus* aerosol infection.[33] Despite 21 consecutive days of chemical immunosuppression with dexamethasone, the burden of *M. abscessus* in the lungs is dynamic over seven weeks.[33–35] It remains to be determined if the corticosteroid model can provide advantages to other less labour-intensive and invasive traditional immunodeficient mouse models.

5.2.4 Clinically Related Models

Once the *CFTR* gene was identified, the generation of CFTR F508del mouse models thought to recapitulate disease became a focus of the CF research community.[36] The mutation was introduced in the endogenous *CFTR* gene which resulted in viable mice but no severe disease.[37] Besides intestinal blockage, mice lacked pancreatic and lung disease which are hallmarks of CF disease in humans.[37] Other iterations of CF mouse models like B6-CFTR^{tm1UNC} were introduced but did not develop chronic bacterial infections nor display spontaneous lung inflammation.[37,38] The CF community speculated that mice had alternative chloride channels or had fewer mucus glands than humans. The B6-CFTR^{1tmUNC} mouse model does, however, recapitulate CF-like manifestations in the nasal mucosa with electrophysiological defects from Na^+ hyper-absorption and impaired Cl^- secretion.[38,39] Initial infections of *CFTR* null, *CFTR* hypomorphic, and CFTR F508del mutant mice with *P. aeruginosa* resulted in acute infections followed by rapid clearance of the bacteria from

the lungs.[39] More recently, infection models of *P. aeruginosa* embedded in agar beads have gained traction but require invasive tracheotomies.[36,37] The development of a tractable CF mouse model could not only help understand CF host-pathogen interactions but also provide a valuable tool for antimicrobial discovery for many CF pathogens like *M. abscessus*, *P. aeruginosa*, and *Burkholderia cepacia*.

Although the mouse is often considered to be the most common for models, the zebrafish model has also been used to study host-pathogen interactions during *M. abscessus* infections.[40–48] Zebrafish embryos with *CFTR* knocked down by *CFTR* morpholinos showed increased susceptibility to *M. abscessus,* but not other mycobacteria, via dysfunctional host oxidative defences thus, establishing a role for *CFTR* in the control of *M. abscessus* infections.[49]

5.2.5 Pharmacokinetics

Another limitation is the lack of pharmacokinetics (PK) data throughout the epetraborole and norvaline study. We referred to the PK data generated by Ganapathy *et al* for a similar benzoxaborole.[17] The authors noted attractive PK properties with high aqueous solubility and low clearance in mouse and human microsomes. Furthermore, the drug given orally at 10 mg/kg in C57BL/6 mice maintained 100% time above the MIC for *M. abscessus*. From these data, we administered epetraborole orally at 10 mg/kg to SCID mice intranasally infected with *M. abscessus*. However, the optimal dose of epetraborole remains to be determined.[18]

There exists limited literature on the PK of norvaline. We referred to a study carried out by Polis *et al* where the effect of norvaline in drinking water of a triple-transgenic mouse model of Alzheimer's disease was examined.[50,51] The authors noted a protective benefit against Alzheimer's disease and no side-effects from norvaline dosed at 250 µg/mL (2 mM) in drinking water over 2.5 months. Therefore, we dosed norvaline in our study at 3 mM. However, going forward, a PK study should be performed with the administration of oral and intravenous norvaline at various doses to determine the proportion of free-drug available. It is uncertain whether 3 mM can achieve free-drug concentrations high enough to exert antimicrobial activity. The results of the PK study could support a hypothesis for a host-directed role for norvaline. In macrophages, the arginine pool is shared among nitric oxide synthase (NOS) and arginase.[52] Specifically in macrophages activated

by TNF-alpha, IFN-γ, or microbial factors, NOS expression is induced (iNOS) to produce nitric oxide (NO) from the catabolism of arginine as an antimicrobial response. Concomitantly, arginine can also be metabolised by arginase to produce ornithine and urea. It is known that arginase activity is inversely related to NO production by iNOS in macrophages.[52] Therefore, iNOS and arginase can be viewed as competing enzymes for the pool of arginine maintained in macrophages. Moreover, studies have shown that norvaline can inhibit arginase activity with maximum effects at 10 mM, which increased the production of NO.[52–54] These results suggest a potential role for norvaline as a host-directed antimicrobial molecule, which inhibits arginase activity thereby increasing the concentration of free arginine for iNOS metabolism and NO production.

To test this hypothesis, THP-1 macrophages were infected at MOI of 1 with smooth and rough morphotypes of *M. abscessus* ATCC 19977 expressing tdTomato. Infected monolayers were treated with PBS as the untreated control, control drugs clarithromycin and tigecycline, epetraborole and L-norvaline alone or in combination for 72 hours (**FIGURE 5.1**). From these data, we observed intracellular activity of epetraborole and the control drugs with a decrease of ≥ 1 $\log_{10}$ in viable intracellular smooth and rough bacteria relative to the untreated group. The decrease in intracellular bacteria correlates with the loss of fluorescent tdTomato signal. Treatment with L-norvaline alone, however, decreased the bacterial load of smooth *M. abscessus* by 0.5 $\log_{10}$, albeit without statistical significance, and had no effect on rough *M. abscessus*. Host-directed therapies alone often exhibit activities on a linear scale while antibiotic effects are logarithmic, which is supported by the < 1 $\log_{10}$ decrease in intracellular bacteria and 50% reduction in tdTomato fluorescence by L-norvaline.[55,56] Meanwhile, the addition of L-norvaline to epetraborole did not increase the activity of epetraborole. These data contradict the results from the mouse model but could be explained by a lack of iNOS induction in our experimental setup or the maximum effect of epetraborole alone was reached and the additional effect of L-norvaline could not be observed. Future studies are warranted to determine if there is a therapeutic benefit to using epetraborole and L-norvaline in conjunction as opposed to epetraborole alone.

5.3 FUTURE PERSPECTIVES

Hybrid methods that combine WCS and target-based assays are an underexplored space that could provide added value to the field of antibiotic discovery. The recent success with the hypomorph-

based hybrid method, PROSPECT, has created a precedent to continue exploring and innovating hybrid approaches. In the last section of this thesis, I will present preliminary data for the development of a target engagement assay for drug discovery. Initially, the assay was envisioned as a primary screening tool but other roles for the target engagement assay in the discovery phase of the pipeline will be discussed.

5.3.1 nanoBRET Target Engagement

Small molecules affect change in the cell through an interaction with a specific target. Phenotypes observed from whole cell activity can and should be linked with evidence to a drug target. Target engagement is an important step in the drug discovery pathway and limits the development of compounds with inadequate target binding or non-specific activity. Two prominent examples from the field of anticancer drug discovery illustrate the benefit of exploring target engagement early in the discovery phase.

Iniparib was shown to be a *bona fide* inhibitor of poly ADP ribose polymerase (PARP) but with a different chemical scaffold relative to other known PARP inhibitors.[57] This new drug was cytotoxic to breast cancer cell lines in preclinical models but showed no efficacy in clinical trials. Later it was confirmed that iniparib does not bind to PARP *in cellulo* but instead generates reactive oxygen species to produce an initial antiproliferative effect with no long-term phenotype.

Clinical trials of the fatty acid amide hydrolase (FAAH) inhibitor BIA 10-2474 were terminated early due to sever neurological lesions that lead to one patient fatality.[57] *Post hoc* investigation revealed that BIA 10-2474 can bind FAAH *in cellulo* and other host enzymes, which disrupted lipid synthesis and a lethal phenotype.[58]

AstraZeneca and Pfizer estimated that one fifth of failed phase II clinical trials resulted from inadequate target exposure to the small molecule.[59,60] Now target engagement assays play a prominent role in the development of cancer drugs.[61–63] Target engagement assays, however, are an under explored area for antibiotic discovery. We developed a proof-of-concept (POC) *in cellulo* target engagement assay to identify novel antimicrobials in *M. abscessus* termed nanoBRET (**FIGURE 5.2A**).[64] A fusion protein of the target of interest and a small 19 kDa nanoluciferase

(NLuc) was constructed and cloned into *M. abscessus*. NLuc was engineered to be more suitable as a fusion tag with higher luminescence intensity and a narrower bioluminescence spectrum compared to traditional fusion tags like Renilla luciferase.[65,66] A cell permeable fluorescent tracer with affinity for the target was added to the *in cellulo* system whereby the tracer will bind the target of interest bringing the fluorescent moiety in proximity of NLuc where bioluminescence resonance energy transfer (BRET) will occur. Bioluminescence generated upon the addition of the Nluc substrate is transferred to the fluorescent moiety generating measurable fluorescence. BRET shares similarities with its fluorescent counterpart, FRET, but omits the requirement for an excitation laser. Moreover, BRET has a proven track record of monitoring receptor-ligand interactions *in cellulo*.[64,67–69] Target engagement can be quantified from the ratio of fluorescence to bioluminescence ($BRET = F_{Tracer}/Lum_{Nluc}$). The purpose of the assay is to identify antimicrobial compounds with cell permeable chemistry and affinity for the target of interest. Therefore, compounds that match this description will displace the tracer and decrease the ratio of BRET.

We selected the established target dihydrofolate reductase (DHFR) with its well characterized on-target inhibitor trimethoprim (TMP) to serve as the control for the target engagement assay POC. DHFR is a small, soluble protein amenable to fusion protein engineering. Moreover, the crystal structure of TMP bound in the active site of DHFR was available. We postulated that TMP could accommodate the addition of a fluorescent BODIPY moiety via a short linker based on the perpendicular extension of the para-methoxy group (**FIGURE 5.2B**). The TMP-based tracer used for the target engagement assays is illustrated in **FIGURE 5.2C**.

5.3.2 Preliminary work with nanoBRET

First, we demonstrated target engagement with the tracer in *M. abscessus*. We showed that the TMP-based tracer is cell permeable by titrating increasing concentrations of tracer onto cultures of *M. abscessus* expressing NLuc-DHFR. The NLuc substrate NanoGlo was added after one hour of incubation and the luminescence (with 450 nm filter) and fluorescence (with 610 nm long pass filter) were sequentially measured using a Biotek Synergy plate reader. The raw BRET values were calculated as milli-BRET (mBRET) units according to eq 1:

$$\text{mBRET} = \left(\frac{\text{Fluorescence}_{\text{sample}}}{\text{Luminescence}_{\text{sample}}}\right) \text{x } 1{,}000 \qquad (1)$$

The mBRET values were transformed to % of probe occupancy according to eq 2:

$$\text{probe occupany (\%)} = \left(\frac{\text{X}-\text{Z}}{\text{Y}-\text{Z}}\right) \text{x } 100 \quad (2)$$

where X is the remaining mBRET value in the presence of a test compound and tracer, Y is the maximum mBRET with tracer only, and Z is background mBRET without test compound or tracer. Using saturation binding curves from tracer titration experiments, we estimated an *in cellulo* binding affinity with a dissociation constant (K_d) of 109 nM for the TMP-based tracer to NLuc-DHFR (**FIGURE. 5.3**). Second, we demonstrated tracer displacement in *M. abscessus*. The addition of increasing concentrations of TMP displaced the tracer, when used at 1 μM, from the NLuc-DHFR fusion protein in a dose-dependent manner. Using these displacement dose-response curves, we estimated an *in cellulo* binding affinity with an apparent K_d (K_{dA}) of 11 nM for the unlabeled ligand TMP (**FIGURE. 5.4B**). Third, we asked whether the tracer concentration influenced tracer displacement by TMP. We measured the K_{dA} of TMP across different tracer concentrations and found that even with a 10-fold increase in tracer concentration, the K_{dA} remained relatively constant with a 2-fold difference (**FIGURE 5.4A-E**). This provided evidence that potentially interesting displacing ligands will not be viewed as weak displacers from the arbitrary tracer concentration selected in future experiments. Lastly, we showed that the BRET tracer and the displacing ligand TMP undergo competitive inhibition at the binding site. From the K_{dA} values of TMP at various tracer concentrations, we calculated the respective IC_{50} (concentration of TMP that reduces probe occupancy by 50%) values using the Cheng-Prusoff theorem. A proportional increase in the IC_{50} of TMP with respect to the tracer concentration suggests competitive inhibition between the two species. Allosteric inhibition, although not observed with TMP, could also be captured with the BRET target engagement assay as the IC_{50} values of the displacing ligand would be independent of the tracer concentration for non-competitive inhibition or would exponentially decrease relative to the tracer concentration for uncompetitive inhibition. Other targets with known allostery would be valuable to expand the repertoire of targets amenable to BRET target engagement.

We demonstrated a functional BRET target engagement assay in *M. abscessus* with a TMP-based tracer and unlabeled TMP, however, the goal was to identify new chemistries other than TMP that could displace the tracer and become alternative DHFR inhibitors. In a pilot experiment to find DHFR inhibitors other than TMP, we selected four compounds from the Structure-guided Drug

Discovery Coalition (SDDC) vault with known *in vitro* activity measured through enzymatic inhibition of DHFR and used TMP as control. TMP and the four SDDC compounds displaced the tracer with varying potencies as measured by the K_{dA} (**FIGURE 5.5 A-E**). These results suggest that the tracer displacement by TMP is not an artifact derived from the similarities of TMP and the TMP-based tracer. The next question we asked was whether the on-target DHFR activity measured by K_{dA} correlated with the *M. abscessus* whole cell activity measured by the MIC_{90}. Unexpectedly, compound SDDC-1593 was an outlier among the compounds in the data set (**FIGURE 5.5F**). The compound SDDC-1593 provided an example of a compound that is cell permeable, has whole cell activity against *M. abscessus*, and inhibits DHFR activity *in vitro* but fails to show on-target activity against DHFR *in cellulo*. These data suggest that the binding and inhibition of DHFR by SDDC-1593 is an artifact of *in vitro* conditions and SDDC-1593 no longer has on-target activity in the complex cellular milieu. However, SDDC-1593 does exhibit whole cell activity against *M. abscessus* measured by the decreased cell viability. This discrepancy between target engagement and whole cell activity could suggest off-target activity or a polypharmacology profile for SDDC-1593 in *M. abscessus*.

From our preliminary results, *in cellulo* target engagement for antibiotic discovery could have two roles in the discovery pathway. One option for target engagement is upstream as a primary screening assay which provides the benefits of WCS with cell permeable compounds and the benefits of target-based screening with *a priori* knowledge of the target of interest. We acknowledge that using the target engagement assay as a primary screen might require intensive libraries that are curated by 'Big Pharma' to identify the 'magic bullet' that is cell permeable and on-target with your favourite protein of the month. Alternatively, the BRET target engagement assay could provide a useful quality control step further downstream in hit-to-lead development with SAR studies. As was shown with the apparent *M. abscessus* DHFR inhibitor SDDC-1593, our target engagement assay revealed potential polypharmacology with this compound. Since this compound came from a series of analogs with a core scaffold, target engagement might be best used to ensure compounds retain on-target activity during iterative cycles of medicinal chemistry for lead optimization.

5.4 CONCLUDING REMARKS

In the work of this thesis, we joined the drug discovery efforts for *M. abscessus* and found three promising compounds and one potential compound/adjuvant pair. Lysobactin and sorangicin A are natural products with interesting scaffolds that could lend useful for offering alternatives to similar compounds like vancomycin and the rifamycins. Epetraborole is further down the pipeline and could have a future as a potent antimycobacterial agent. The GSK derivative of epetraborole, GSK656, is currently in a phase II clinical trial for drug-sensitive *M. tuberculosis* pulmonary infection and AN2 Therapeutics recently started a phase II clinical trial with epetraborole for refractory *M. avium* pulmonary infection. Indeed, benzoxaboroles are making progress. Perhaps results from these trials could support a clinical trial for *M. abscessus*. The future for norvaline as an adjuvant-like molecule for epetraborole is more uncertain. Resistance to norvaline was shown but the clinical relevance is unclear since the experiment that generated the resistance used epetraborole and norvaline as two sequential monotherapies. More experiments are required to develop an understanding of the pharmacokinetic profile of norvaline and whether there are toxicity issues from lengthy norvaline administration. The future of drug discovery is moving away from the dichotomy of whole cell versus target-based assays. Newer hybrid approaches are becoming more widespread. We contributed a BRET-based *in cellulo* target engagement assay that proved to be useful for identifying DHFR inhibitors as a POC but could be adapted for other targets or bacteria of interest. Fortunately, progress is being made towards identifying new compounds for *M. abscessus*. This will require regimen optimization to ultimately improve treatment outcomes and the lives of patients with *M. abscessus* pulmonary infections.

5.5 REFERENCES

1. Johansen, M. D., Herrmann, J.-L. & Kremer, L. Non-tuberculous mycobacteria and the rise of Mycobacterium abscessus. *Nat. Rev. Microbiol.* **18**, 392–407 (2020).
2. Behr, M., Jarand, J. & Marras, T. K. *Canadian Tuberculosis Standards Chapter 11: Nontuberculous Mycobacteria*. http://www.phac-aspc.gc.ca/tbpc-latb/pubs/tb-canada-7/assets/pdf/tb-standards-tb-normes-ch11-eng.pdf (2014).
3. Floto, R. A. et al. US Cystic Fibrosis Foundation and European Cystic Fibrosis Society

consensus recommendations for the management of non-tuberculous mycobacteria in individuals with cystic fibrosis. *Thorax* **71**, i1–i22 (2016).

4. Hartkoorn, R. C. et al. Towards a new tuberculosis drug: Pyridomycin - nature's isoniazid. *EMBO Mol. Med.* **4**, 1032–1042 (2012).
5. Alcaraz, M. et al. Efficacy and Mode of Action of a Direct Inhibitor of Mycobacterium abscessus InhA. *ACS Infect. Dis.* **8**, 2171–2186 (2022).
6. Ganapathy, U. S., Dartois, V. & Dick, T. Repositioning rifamycins for Mycobacterium abscessus lung disease. *Expert Opin. Drug Discov.* **14**, 867–878 (2019).
7. Raynaud, C. et al. Active Benzimidazole Derivatives Targeting the MmpL3 Transporter in Mycobacterium abscessus. *ACS Infect. Dis.* **6**, 324–337 (2020).
8. Kozikowski, A. P. et al. Targeting Mycolic Acid Transport by Indole-2-carboxamides for the Treatment of Mycobacterium abscessus Infections. *J. Med. Chem.* **60**, 5876–5888 (2017).
9. Malin, J. J., Winter, S., Edeltraud, van G., Plum, G. & Rybniker, J. Extremely Low Hit Rate in a Diverse Chemical Drug Screen Targeting Mycobacterium abscessus. *Antimicrob. Agents Chemother.* **63**, (2019).
10. Fischbach, M. A. & Walsh, C. T. Antibiotics for Emerging Pathogens. *Science (80-.).* **325**, 1089–1093 (2009).
11. Lee, W. et al. The Mechanism of Action of Lysobactin. *J. Am. Chem. Soc.* **138**, 100–103 (2016).
12. Lilic, M. et al. The antibiotic sorangicin A inhibits promoter DNA unwinding in a Mycobacterium tuberculosis rifampicin-resistant RNA polymerase. *Proc. Natl. Acad. Sci. U. S. A.* **117**, 30423–30432 (2020).
13. Panchaud, P. et al. Discovery and Optimization of Isoquinoline Ethyl Ureas as Antibacterial Agents. *J. Med. Chem.* **60**, 3755–3775 (2017).
14. Kaushik, A., Ammerman, N. C., Martins, O., Parrish, N. M. & Nuermberger, E. L. In Vitro Activity of New Tetracycline Analogs Omadacycline and Eravacycline against Drug-Resistant Clinical Isolates of Mycobacterium Abscessus. *Antimicrob. Agents Chemother.* **63**, (2019).
15. Palencia, A. et al. Discovery of novel oral protein synthesis inhibitors of mycobacterium tuberculosis that target leucyl-tRNA synthetase. *Antimicrob. Agents Chemother.* **60**,

6271–6280 (2016).

16. O'Dwyer, K. et al. Bacterial resistance to leucyl-tRNA synthetase inhibitor GSK2251052 develops during treatment of complicated urinary tract infections. *Antimicrob. Agents Chemother.* **59**, 289–298 (2015).
17. Ganapathy, U. S. et al. A Leucyl-tRNA Synthetase Inhibitor with Broad-Spectrum Antimycobacterial Activity. *Antimicrob. Agents Chemother.* **65**, (2021).
18. Ganapathy, U. S., Gengenbacher, M. & Dick, T. Epetraborole is active against mycobacterium abscessus. *Antimicrob. Agents Chemother.* **65**, (2021).
19. Kim, T. et al. A screening of the mmv pandemic response box reveals epetraborole as a new potent inhibitor against mycobacterium abscessus. *Int. J. Mol. Sci.* **22**, (2021).
20. Lewis, K. Platforms for antibiotic discovery. *Nat. Rev. Drug Discov.* **12**, 371–387 (2013).
21. Schnappinger, D. Genetic approaches to facilitate antibacterial drug development. *Cold Spring Harb. Perspect. Med.* **5**, (2015).
22. Pethe, K. et al. A chemical genetic screen in Mycobacterium tuberculosis identifies carbon-source-dependent growth inhibitors devoid of in vivo efficacy. *Nat. Commun.* **1**, 57 (2010).
23. Wilburn, K. M., Fieweger, R. A. & VanderVen, B. C. Cholesterol and fatty acids grease the wheels of Mycobacterium tuberculosis pathogenesis. *Pathogens and disease* vol. 76 21 (2018).
24. Cokol, M., Kuru, N., Bicak, E., Larkins-Ford, J. & Aldridge, B. B. Efficient measurement and factorization of high-order drug interactions in Mycobacterium tuberculosis. *Sci. Adv.* **3**, (2017).
25. Larkins-Ford, J., Degefu, Y. N., Van, N., Sokolov, A. & Aldridge, B. B. Design principles to assemble drug combinations for effective tuberculosis therapy using interpretable pairwise drug response measurements. *Cell Reports Med.* **3**, (2022).
26. Palmer, K. L., Aye, L. M. & Whiteley, M. Nutritional cues control Pseudomonas aeruginosa multicellular behavior in cystic fibrosis sputum. *J. Bacteriol.* **189**, 8079–8087 (2007).
27. Kisumi, M., Sugiura, M. & Chibata, I. Biosynthesis of norvaline, norleucine, and homoisoleucine in Serratia marcescens. *J. Biochem.* **80**, 333–339 (1976).
28. Obregón-Henao, A. et al. Susceptibility of mycobacterium abscessus to antimycobacterial

drugs in preclinical models. *Antimicrob. Agents Chemother.* **59**, 6904–6912 (2015).

29. Dick, T., Shin, S. J., Koh, W. J., Dartois, V. & Gengenbacher, M. Rifabutin is active against mycobacterium abscessus in mice. *Antimicrob. Agents Chemother.* **64**, (2020).
30. De Groote, M. A. et al. GM-CSF knockout mice for preclinical testing of agents with antimicrobial activity against Mycobacterium abscessus. *J. Antimicrob. Chemother.* **69**, 1057–1064 (2014).
31. Koh, W. J., Hong, G., Kim, K., Ahn, S. & Han, J. Pulmonary sequestration infected with nontuberculous mycobacteria: A report of two cases and literature review. *Asian Pac. J. Trop. Med.* **5**, 917–919 (2012).
32. Lammas, D. A. et al. Heterogeneity in the granulomatous response to mycobacterial infection in patients with defined genetic mutations in the interleukin 12-dependent interferon-gamma production pathway. *Int. J. Exp. Pathol.* **83**, 1–20 (2002).
33. Maggioncalda, E. C. et al. A mouse model of pulmonary Mycobacteriodes abscessus infection. *Nat. Sci. Reports* (2020) doi:10.1038/s41598-020-60452-1.
34. Cain, D. W. & Cidlowski, J. A. Immune regulation by glucocorticoids. *Nat. Rev. Immunol.* **17**, 233–247 (2017).
35. Batten, J. C. & McCune, R. M. The influence of corticotrophin and cortisone with antituberculous drugs on population of Mycobacterium tuberculosis in tissues of mice. *Br. J. Exp. Pathol.* **38**, 424–437 (1957).
36. Wilke, M. et al. Mouse models of cystic fibrosis: Phenotypic analysis and research applications. *J. Cyst. Fibros.* **10**, 152–171 (2011).
37. Guilbault, C., Saeed, Z., Downey, G. P. & Radzioch, D. Cystic fibrosis mouse models. *Am. J. Respir. Cell Mol. Biol.* **36**, 1–7 (2007).
38. Mccarron, A., Parsons, D. & Donnelley, M. Animal and Cell Culture Models for Cystic Fibrosis: Which Model Is Right for Your Application? *Am. J. Pathol.* **191**, (2021).
39. Semaniakou, A., Croll, R. P. & Chappe, V. Animal Models in the Pathophysiology of Cystic Fibrosis. *Front. Pharmacol.* **9**, 1–16 (2019).
40. Prouty, M. G., Correa, N. E., Barker, L. P., Jagadeeswaran, P. & Klose, K. E. Zebrafish-Mycobacterium marinum model for mycobacterial pathogenesis. *FEMS Microbiol. Lett.* **225**, 177–182 (2003).
41. Phennicie, R. T., Sullivan, M. J., Singer, J. T., Yoder, J. A. & Kim, C. H. Specific

resistance to Pseudomonas aeruginosa infection in zebrafish is mediated by the cystic fibrosis transmembrane conductance regulator. *Infect. Immun.* **78**, 4542–4550 (2010).

42. Renshaw, S. A. & Trede, N. S. A model 450 million years in the making: Zebrafish and vertebrate immunity. *Dis. Model. Mech.* **5**, 38–47 (2012).
43. Bernut, A. et al. Mycobacterium abscessus cording prevents phagocytosis and promotes abscess formation. *Proc. Natl. Acad. Sci. U. S. A.* **111**, (2014).
44. Bernut, A. et al. In Vivo assessment of drug efficacy against Mycobacterium abscessus using the embryonic zebrafish test system. *Antimicrob. Agents Chemother.* **58**, 4054–4063 (2014).
45. Bernut, A. et al. Mycobacterium abscessus-Induced Granuloma Formation Is Strictly Dependent on TNF Signaling and Neutrophil Trafficking. *PLoS Pathog.* **12**, (2016).
46. Bernut, A. et al. Insights into the smooth-to-rough transitioning in Mycobacterium bolletii unravels a functional Tyr residue conserved in all mycobacterial MmpL family members. *Mol. Microbiol.* **99**, 866–883 (2016).
47. Myllymäki, H., Bäuerlein, C. A. & Rämet, M. The zebrafish breathes new life into the study of tuberculosis. *Front. Immunol.* **7**, (2016).
48. Bernut, A. et al. Deciphering and imaging pathogenesis and cording of Mycobacterium abscessus in zebrafish embryos. *J. Vis. Exp.* **2015**, 53130 (2015).
49. Bernut, A. et al. CFTR Protects against Mycobacterium abscessus Infection by Fine-Tuning Host Oxidative Defenses. *Cell Rep.* **26**, 1828-1840.e4 (2019).
50. Polis, B., Srikanth, K. D., Gurevich, V., Gil-Henn, H. & Samson, A. O. L-Norvaline, a new therapeutic agent against Alzheimer's disease. *Neural Regen. Res.* **14**, 1562–1572 (2019).
51. Polis, B. et al. Effects of Chronic Arginase Inhibition with Norvaline on Tau Pathology and Brain Glucose Metabolism in Alzheimer's Disease Mice. *Neurochem. Res.* **47**, 1255–1268 (2022).
52. Chang, C.-I., Liao, J. C. & Kuo, L. Arginase modulates nitric oxide production in activated macrophages. *Am. J. Physiol.* **274**, H324–H348 (1998).
53. Ming, X. F., Rajapakse, A. G., Carvas, J. M., Ruffieux, J. & Yang, Z. Inhibition of S6K1 accounts partially for the anti-inflammatory effects of the arginase inhibitor L-norvaline. *BMC Cardiovasc. Disord.* **9**, (2009).

54. Hunter, A. & Downs, C. E. The Inhibition of Arginase By Amino Acids. *J. Biol. Chem.* **157**, 427–446 (1945).
55. Tobin, D. M. Host-directed therapies for tuberculosis. *Cold Spring Harb. Perspect. Med.* **5**, (2015).
56. Poerio, N. et al. Combined Host- and Pathogen-Directed Therapy for the Control of Mycobacterium abscessus Infection. *Microbiol. Spectr.* **10**, (2022).
57. Stefaniak, J. & Huber, K. V. M. Importance of Quantifying Drug-Target Engagement in Cells. *ACS Med. Chem. Lett.* **11**, 403–406 (2020).
58. Van Esbroeck, A. C. M. et al. Activity-based protein profiling reveals off-target proteins of the FAAH inhibitor BIA 10-2474. *Science (80-.).* **356**, 1084–1087 (2017).
59. Cook, D. et al. Lessons learned from the fate of AstraZeneca's drug pipeline: a five-dimensional framework. *Nat. Rev. Drug Discov.* **13**, 419–431 (2014).
60. Bunnage, M. E., Piatnitski Chekler, E. L. & Jones, L. H. Target validation using chemical probes. *Nat. Chem. Biol.* **9**, 195–199 (2013).
61. Asquith, C. R. M. et al. SGC-GAK-1: A Chemical Probe for Cyclin G Associated Kinase (GAK). *J. Med. Chem.* **62**, 2830–2836 (2019).
62. Asquith, C. R. M. et al. Identification and Optimization of 4-Anilinoquinolines as Inhibitors of Cyclin G Associated Kinase. *ChemMedChem* **13**, 48–66 (2018).
63. Robers, M. B. et al. Target engagement and drug residence time can be observed in living cells with BRET. *Nat. Commun.* **6**, 10091 (2015).
64. Fanti, R. C. et al. A Target Engagement Assay to Assess Uptake, Potency and Retention of Antibiotics in Living Bacteria. *ACS Infect. Dis.* **8**, 1449–1467 (2022).
65. Machleidt, T. et al. NanoBRET-A Novel BRET Platform for the Analysis of Protein-Protein Interactions. *ACS Chem. Biol.* **10**, 1797–1804 (2015).
66. Soave, M., Stoddart, L. A., Brown, A., Woolard, J. & Hill, S. J. Use of a new proximity assay (NanoBRET) to investigate the ligand-binding characteristics of three fluorescent ligands to the human β1-adrenoceptor expressed in HEK-293 cells. *Pharmacol. Res. Perspect.* **4**, (2016).
67. Salahpour, A. et al. BRET biosensors to study GPCR biology, pharmacology, and signal transduction. *Front. Endocrinol. (Lausanne).* **3**, (2012).
68. Namkung, Y. et al. Quantifying biased signaling in GPCRs using BRET-based biosensors.

Methods **92**, 5–10 (2016).

69. Namkung, Y. et al. Monitoring G protein-coupled receptor and β-arrestin trafficking in live cells using enhanced bystander BRET. *Nat. Commun.* **7**, 12178 (2016).

5.6 FIGURES

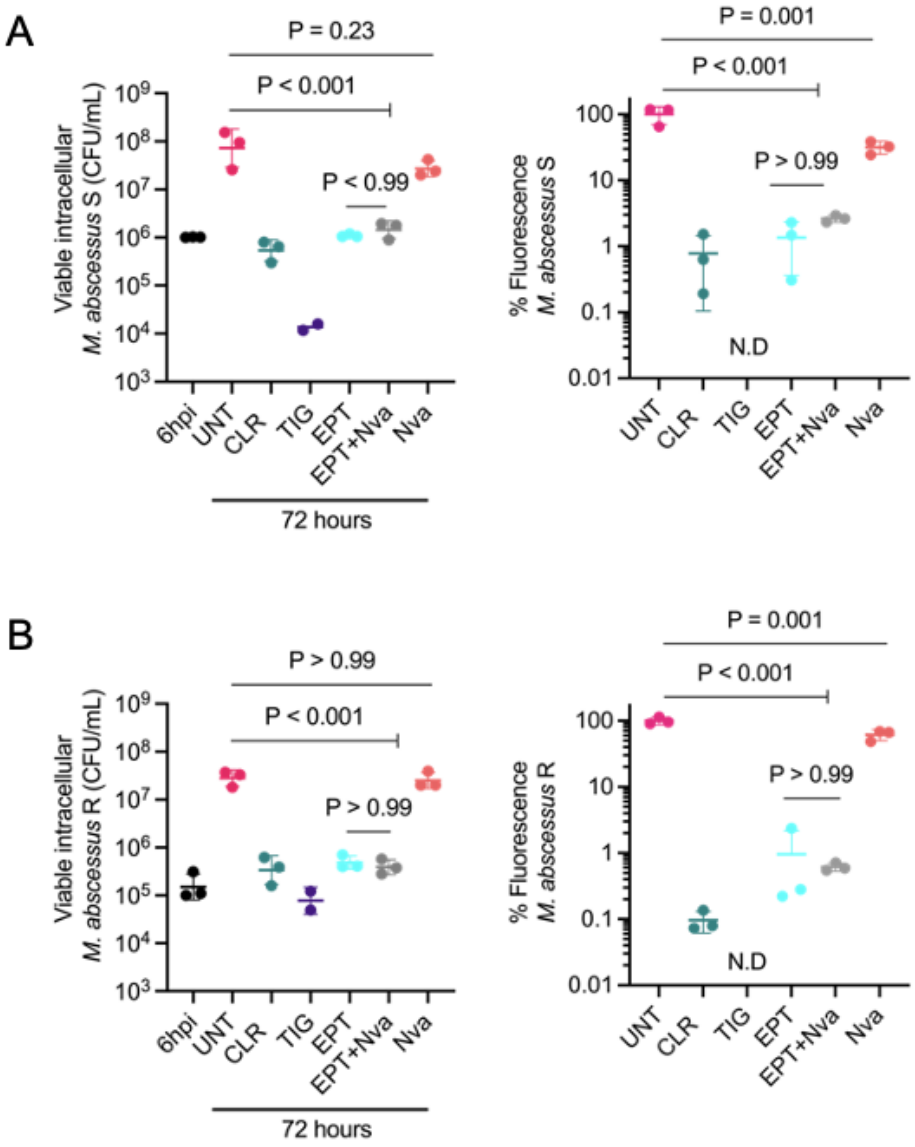

FIGURE 5.1. Intracellular activity of epetraborole and norvaline against *M. abscessus*. THP-1 macrophages were infected with smooth (**A**) and rough (**B**) morphotypes of *M. abscessus* tdTomato at MOI 1. Extracellular bacteria were killed with high dose amikacin (340 µM). Initial bacterial load was quantified 6 hours post-infection (hpi). Wells were washed and treated daily with PBS as untreated (UNT), 6.7 µM clarithromycin (CLR, 5X MIC), 43 µM tigecycline (TIG, 5X MIC), 1.5 μM epetraborole (EPT, 5X MIC), 3 mM norvaline (Nva, 5X MIC), or EPT+Nva (5X MIC). After 72 hours, cells were lysed with triton and plated for CFU counts. The fluorescence

(Ex550/Em590) of the cell lysate was measured with a TECAN M200. Data shown is mean ± SD from biological triplicates. P values obtained from one-way ANOVA with Tukey's multiple comparisons test. N.D; not detectable above media background.

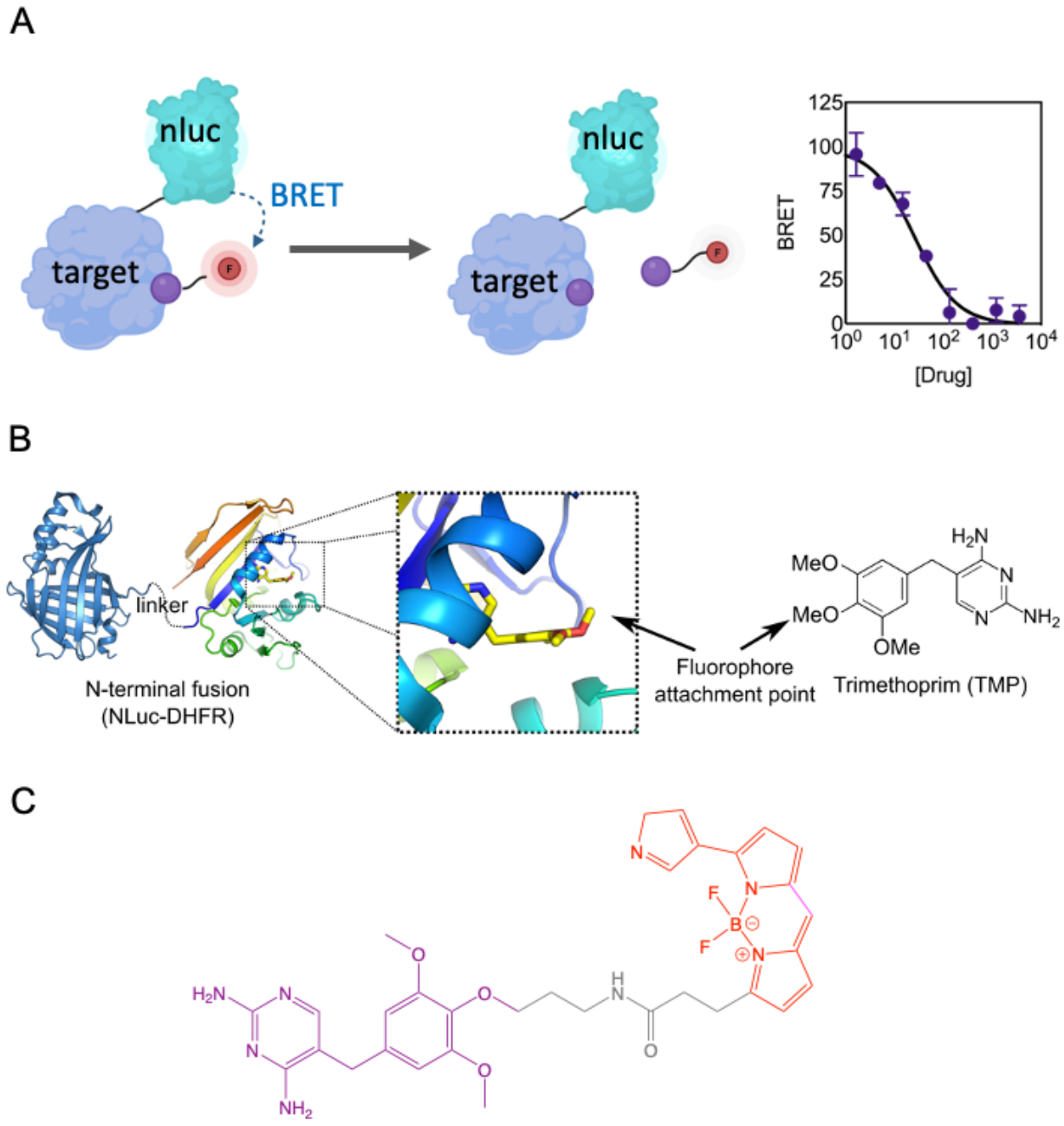

FIGURE 5.2. NanoBRET *in cellulo* target engagement assay. A Illustration of *in cellulo* target engagement assay. A fluorescent tracer binds to a target fusion protein with nano-luciferase (NLuc). Bioluminescence resonance energy transfer (BRET) is measured as the ratio of luminescence generated from NLuc and fluorescence emitted from the tracer (BRET = F_{Tracer}/Lum_{NLuc}). BRET is highest when the tracer is in dynamic equilibrium with the intracellular target and will decrease in a dose dependent manner from tracer displacement by the introduction

of other compounds with affinity for the target. Tracer cartoon is depicted with target specific moiety (purple) and fluorescent moiety (red). **B** NanoBRET proof of concept with dihydrofolate reductase (DHFR). The fusion protein of NLuc (PDB 5IBO, blue) and DHFR (PDB 6XG5, rainbow) connected with a flexible GSSG linker is modelled with the small molecule trimethoprim (TMP) bound in the DHFR active site. The binding of TMP positions the para-methoxy group in the appropriate orientation for the covalent addition of a linker and fluorescent BODIPY domain to minimize steric clashing. **C** Structure of the TMP-based (purple) BODIPY (red) tracer with short linker (grey).

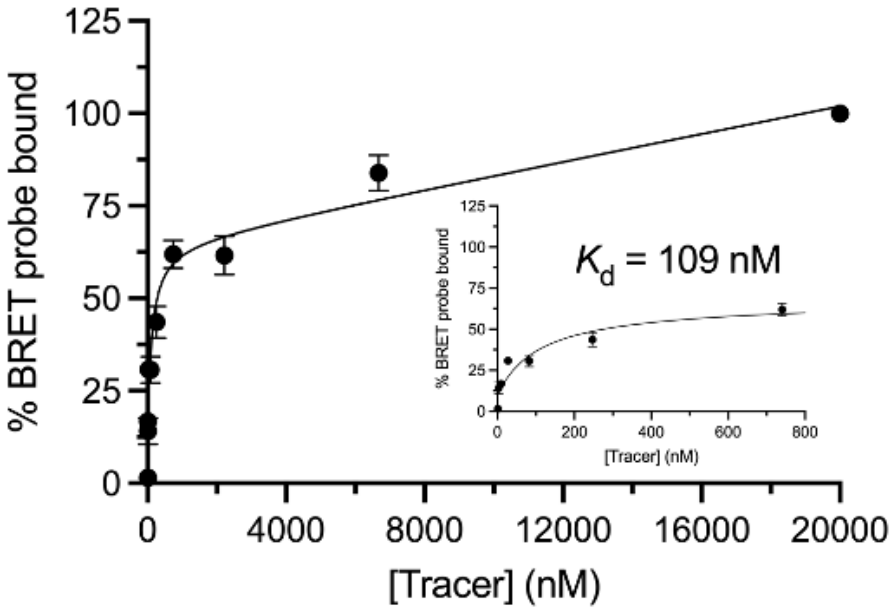

FIGURE 5.3. Target engagement with DHFR tracer *in cellulo*. Tracer saturation binding curve in *M. abscessus* expressing NLuc-DHFR. The dissociation constant (K_d) was obtained by non-linear fitting of experimental data points (mean ± SD of two independent experiments performed in triplicate) to the hyperbolic dose-response equation. Inset shows fit of data at low tracer concentrations.

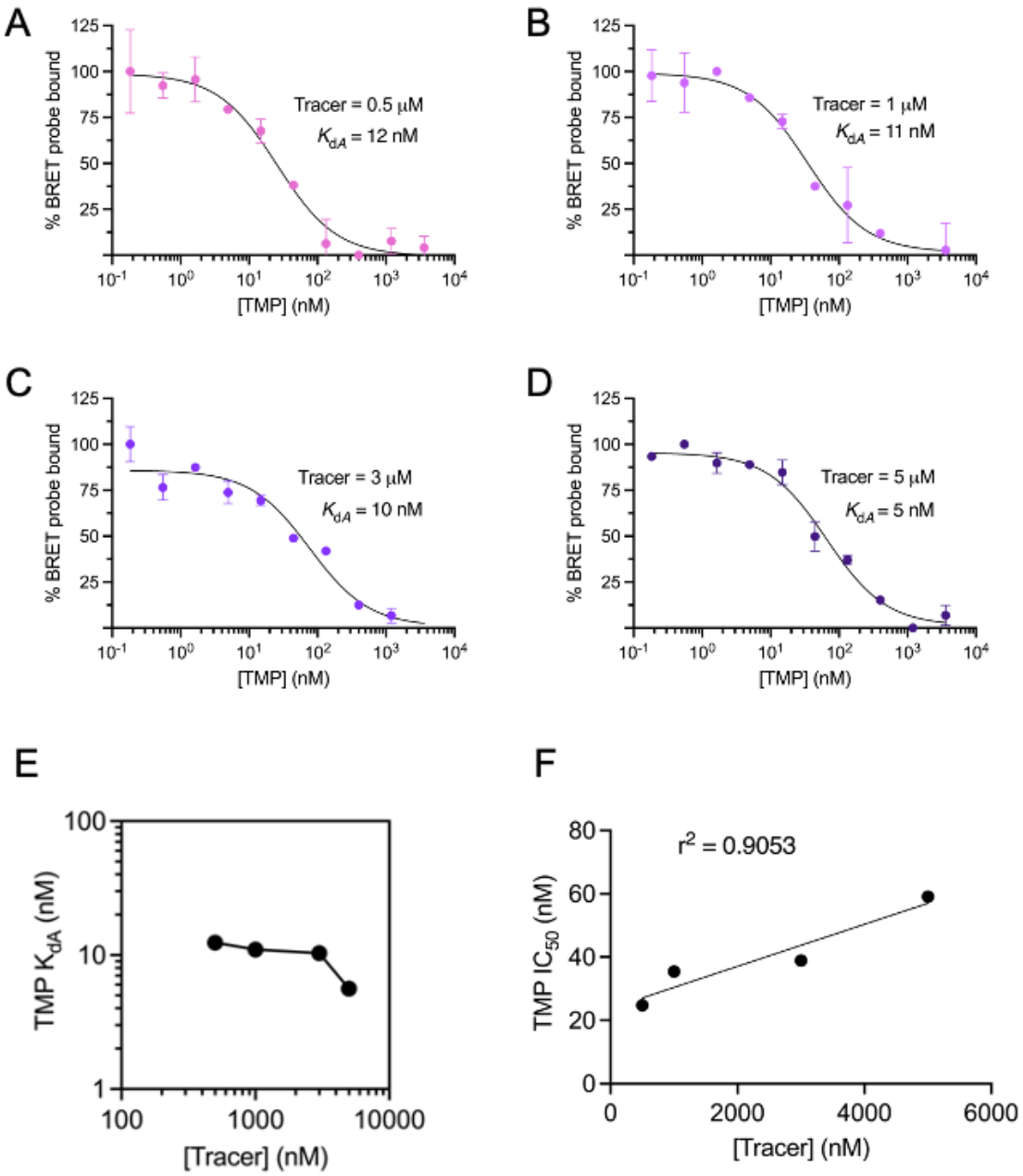

FIGURE 5.4. Competitive tracer displacement with TMP. A-D Tracer displacement at various concentrations with increasing TMP concentrations. Apparent dissociation constants (K_{dA}) were obtained by non-linear fitting of experimental data points (mean ± SD from a single experiment performed in triplicate) to a competitive one site model. **E** Tracer displacement by TMP is independent of tracer concentration. **F** Competitive inhibition between TMP and the tracer at the DHFR binding site. IC_{50} values for TMP were calculated using K_{dA} and the Cheng-Prusoff

equation. Linear relationship between IC_{50} of the displacing ligand and the the concentration of tracer indicates competitive inhibition.

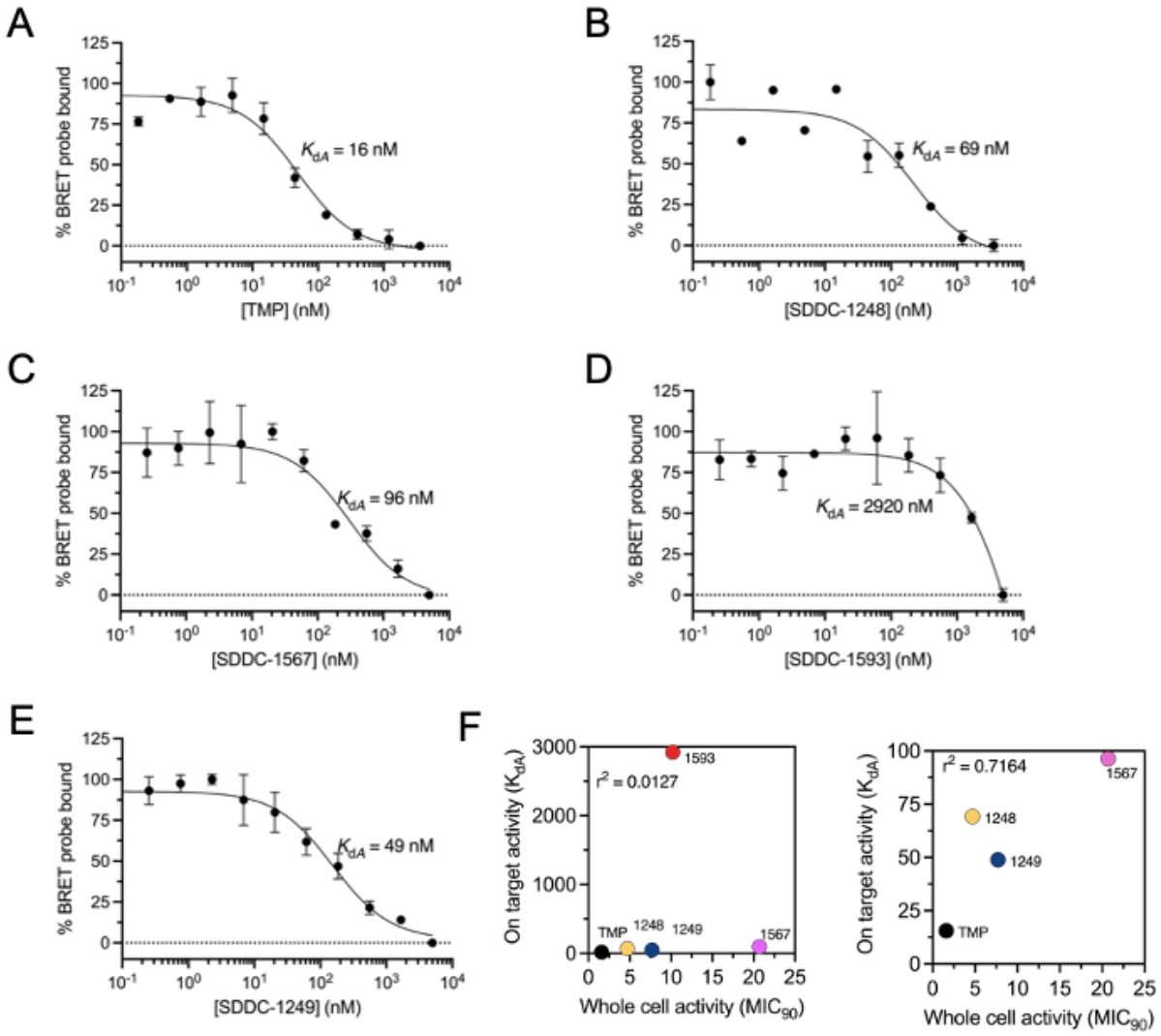

FIGURE 5.5. Target engagement assay to identify novel DHFR inhibitors. A-E Tracer displacement with new chemistries. TMP used as control with tracer at 1000 nM. K_{dA} was obtained by fitting the data (mean ± SD from a single experiment performed in triplicate) to a competitive one site binding equation. **F** BRET target engagement can identify off-target inhibitors. Correlation of *in cellulo* on-target activity to whole cell activity with novel DHFR inhibitors improves when the outlier DHFR inhibitor 1593 is removed. DHFR inhibitor 1593 with whole cell activity against *M. abscessus* no longer retains on-target DHFR activity.